Bridging the gap between genes and fungal natural products: Functional heterologous expression of the genes from the lichen *Cladonia uncialis*

by

Harman Gill

A Thesis submitted to the Faculty of Graduate Studies of
The University of Manitoba
in partial fulfilment of the requirements for the degree of

DOCTOR OF PHILOSOPHY

Department of Chemistry
University of Manitoba
Winnipeg

Abstract

Fungi, with an estimated 5 million species, constitutes the second most diverse kingdom on Earth. However, only about 10% of these species have been identified, highlighting the vast, untapped potential for discovering bioactive natural products. This thesis focuses on two main objectives: (1) exploring the chemical diversity of fungal natural products and (2) heterologous expression of biosynthetic gene clusters (BGCs) from the lichenized fungus *Cladonia uncialis*.

The first objective involved the isolation, characterization, and bioactivity profiling of secondary metabolites (SMs) from *Aspergillus fumigatus* and *Penicillium sanguifluum*. Two compounds were characterized from the *A. fumigatus*: N-formyl-4-hydroxyphenyl-acetamide (compound **1**) and atraric acid (compound **2**), with the latter being the first instance of its production from a non-lichenized fungus. In addition, two compounds were identified from *P. sanguifluum*: dehydrocurvularin (compound **3**) and 11-hydroxycurvularin (compound **4**).

Despite the identification of over 1,000 SMs, establishing definitive connections between these SMs and their BGCs remains elusive. Our group identified and annotated 48 secondary metabolite BGCs from the fungal partner of *C. uncialis*. This thesis investigates the heterologous expression of two BGCs from this collection: the orsellinic acid (OA) BGC (*cu-nr-pks-5*) and the halogenated isocoumarin BGC (*cu-pks-4*) in *A. oryzae* NSAR1. The OA gene cluster contains two genes, one encodes for the PKS enzyme and the other for a post-PKS tailoring enzyme, decarboxylase. The heterologous expression of PKSs revealed that *A. oryzae* can successfully produce de-novo OA from non-lichen fungi (*Fusarium spp.*), but not from lichen fungus *C. uncialis*. The expression of the decarboxylase gene demonstrated reversible decarboxylation of OA, marking the first instance of a native lichen gene expression in a heterologous host.

Additionally, halogenated isocoumarin BGC was explored. The core PKS (*Cu*-A) showed similarity to TerA in *Aspergillus terreus*, suggesting it catalyzes similar condensation reactions to form 2,3-dihydro-6-hydroxymellein. Unique genes within the cluster, *Cu*-halo and *Cu*-OMT, are proposed to catalyze halogenation and O-methylation, respectively, to produce halogenated isocoumarin. The heterologous expression of the cluster, both at the individual gene level and as a complete BGC, resulting in the production of various compounds, confirming its functional activity and potential for novel metabolite synthesis.

Acknowledgements

There are many people to whom I owe the success of this research program, and I take this opportunity to express my heartfelt gratitude to everyone who has contributed to my journey thus far.

First and foremost, I would like to thank my supervisor, Dr. John Sorensen, for his unwavering support and guidance throughout my PhD journey. His mentorship encompassed not only academic guidance but also contributed significantly to my personal and professional development.

I am deeply indebted to my committee members, Dr. Sean McKenna, Dr. Ayush, and Dr. Ned Buddisa, for their invaluable insights and contributions. Their expertise and encouragement were instrumental in the successful completion of my research.

I would also like to acknowledge the special mentorship of Dr. April Johnson and Dr. Hamid, whose guidance and support have been invaluable. Words cannot express my gratitude to these remarkable individuals.

My deep thanks go out to my family and friends, whose love and encouragement have been my constant source of strength. I am especially grateful to the Sorensen family; this lab has truly been a second home to me, where I have shared countless emotions and experiences. I appreciate the unwavering companionship of my friends—April Didi, Randi, Navriti Didi, Dakshina, Dieu, Seid and Alex—who have always been there to lend a helping hand.

I extend my gratitude to my beloved family, whose unwavering support has been instrumental in my journey. Their faith in me, even during the most challenging times, has been a constant source of strength. I owe an immeasurable debt to my parents, Yodhvir, Jasmeen, and Tarnpreet for their unconditional love, understanding, and encouragement. Their belief in me has been the driving force behind my accomplishments.

I would also like to express my sincere appreciation to my friends, Dr. Shiv Dhiman, Eshaan Gupta, Panthveer, list goes on. Their laughter, friendship, and inspiration have been invaluable in brightening my days and providing a much-needed respite.

To all my uncles, aunts, and cousins, thank you for your constant support and encouragement. And to my special friends/sisters, Gopi (Gurpreet), Kamal, and Arun, words cannot express my gratitude for your presence in my life.

I want to express my deepest gratitude to my wonderful husband, Ajaypal Singh Attal, whose love and support have been essential to my journey from starting my PhD as Harman Gill to finishing as Harman Gill Attal. His unwavering encouragement and dedication have been a continuous source of inspiration, and I am incredibly fortunate to have him by my side.

Finally, I am profoundly thankful to God for the guidance and strength that have brought me to this significant milestone.

Dedication

I dedicate this thesis to my parents, Jaswinder Pal Singh and Rajwant Kaur.

Their endless prayers and unwavering support have always given me wings to fly.

Contribution of Authors

Chapter 1: *Non-applicable*

Chapter 2: *Non-applicable*

Chapter 3: This chapter has already been published, with me as the primary contributor. Ellen M. E. Sykes from the Department of Microbiology is the second author. My contributions include the isolation, identification, characterization, and performing antimicrobial assays. The antibacterial assays were conducted in Dr. Ayush's lab, where Ellen provided the bacterial strains and assisted with the antibacterial testing.

Chapter 4: The work described in this chapter was conducted in collaboration with Dr. Georg Hausner and Dr. Ayush Kumar research group at the Department of Microbiology, University of Manitoba, Winnipeg, Canada. In this project, my role (Harman Gill) focused on fermenting fungi, screening, purifying, and characterizing compounds, and conducting antifungal assays. Aamer Kurdi, a PhD student, Department of Microbiology, identified the fungus and performed antibacterial and checkboard assays. The manuscript is currently in preparation for publication.

Chapter 5: I am the primary contributor of the presented work within this chapter. The manuscript is currently in preparation for publication.

Chapter 6: I am the primary contributor of the presented work within this chapter.

Chapter 7: I am the primary contributor of the presented work within this chapter.

Chapter 8: *Non-applicable*

Table of Contents

List of Figures

Most of the figures are created with BioRender.com

List of Tables

List of Supporting Information

Abbreviations

Abbreviation	Meaning
6-HMS	6-Hydroxymellein synthase
ACP	Acyl Carrier Protein
AT	Acyltransferase
ATP	Adenosine Triphosphate
B+E	Buffer + Enzyme
BGC	Biosynthetic Gene Cluster
BT	Beta Tubulin
$CDCl_3$	Deuterated chloroform (for NMR spectroscopy)
***Cu*-A**	PKS from isocoumarin BGC in *Cladonia uncialis*
***Cu*-B**	PKS-like protein with KR-DH domain in *Cladonia uncialis*
***Cu*-D**	FAD-binding Monooxygenase in *Cladonia uncialis*
***Cu*-oas**	Orsellinic acid synthase from *Cladonia uncialis*
***Cu*-OMT**	O-Methyltransferase from *Cladonia uncialis*
DCM	Dichloromethane
DH	Dehydratase
DMAPP	Dimethylallyl Pyrophosphate
ESB	Enzyme + Substrate + Buffer
EtOAc	Ethyl Acetate
FIC	Fractional Inhibition Concentration
HPLC	High-Performance Liquid Chromatography
IP	Isopentenyl Pyrophosphate
ITS	Internal Transcribed Spacer
KS	Ketosynthase
KRDH	Ketoreductase-dehydratase-like protein
LC-MS	Liquid Chromatography-Mass Spectrometry
MEOD	Deuterated Methanol (for NMR spectroscopy)
MeOH	Methanol
MIC	Minimum Inhibitory Concentration
MRSA	Methicillin-resistant *Staphylococcus aureus*
NMR	Nuclear Magnetic Resonance

NP	Natural Product
NSAR1	Refers to *A. oryzae* strain: ΔniaD, ΔsC, ΔadeA, ΔargB
nr-PKS	Non-reducing PKS
OA	Orsellinic Acid
PBS	Phosphate Buffered Saline
PCR	Polymerase Chain Reaction
PDA	Potato Dextrose Agar
PDB	Potato Dextrose Broth
PKS	Polyketide Synthase
RNA Pol	RNA Polymerase Gene
SAH	S-adenosyl-L-homocysteine
SAM	S-adenosyl-L-methionine, also known as AdoMet
S+B	Substrate + Buffer
SAT	Starter Unit: Acyltransferase (May also be referred to in the literature as "starter unit-acyl carrier protein transacylase" (SAT))
SDS	Sodium Dodecyl Sulfate
SM	Secondary Metabolite
TE	Thioesterase
VPS	Vacuolar Protein Sorting

Chapter 1

Introduction

1.1. Natural products- historical overview

Nature harbors a rich reservoir of structurally diverse molecules known as natural products (NPs), which have played an integral part in human life for millennia. The historical use of NPs has been found in ancient civilizations. The Mesopotamians (2600 BC) described approximately 1000 plants and plant-derived products, such as cedar oils from *Cedrus* species and poppy seed extracts from *Papaver somniferum*. Similarly, the Egyptian Ebers Papyrus (550 BC) contains over 800 medicinal prescriptions using aloe vera and castor oil from *Ricinus communis* (Borchardt, 2002). In 1985, according to the World Health Organization (WHO), around 60% of the human population relied on traditional medicine in the form of natural products to treat various ailments (Farnsworth et al., 1985). These bioactive compounds and their structural analogs have been a continuous source of new lead molecules in the pharmaceutical industry. They exhibit a broad spectrum of biological activities, such as antibiotic: erythromycin A (Kibwage et al., 1985), antifungal: nystatin (Michel, 1977), anticancer: doxorubicin (Arcamone, 1981), and hypolipidemic: lovastatin (Alberts, 1988) **(Figure 1)**. This makes them invaluable resources for drug exploration and development. Between 2014 and 2016, the FDA approved 12 new orally active natural product-derived drugs. Of these, six were for treating hepatitis C virus (HCV), four were antitumor agents, one was for managing chemotherapy-induced nausea, and one was for cardiovascular treatment (Newman & Cragg, 2020). Many years of exploration of NPs have resulting in the discovery of ~300,000 secondary metabolites from almost all living organisms, including prokaryotes (bacteria and cyanobacteria) and eukaryotes (fungi, plants, and animals) (Bérdy, 2005; Mahajan & Balachandran, 2015; Newman & Cragg, 2020).

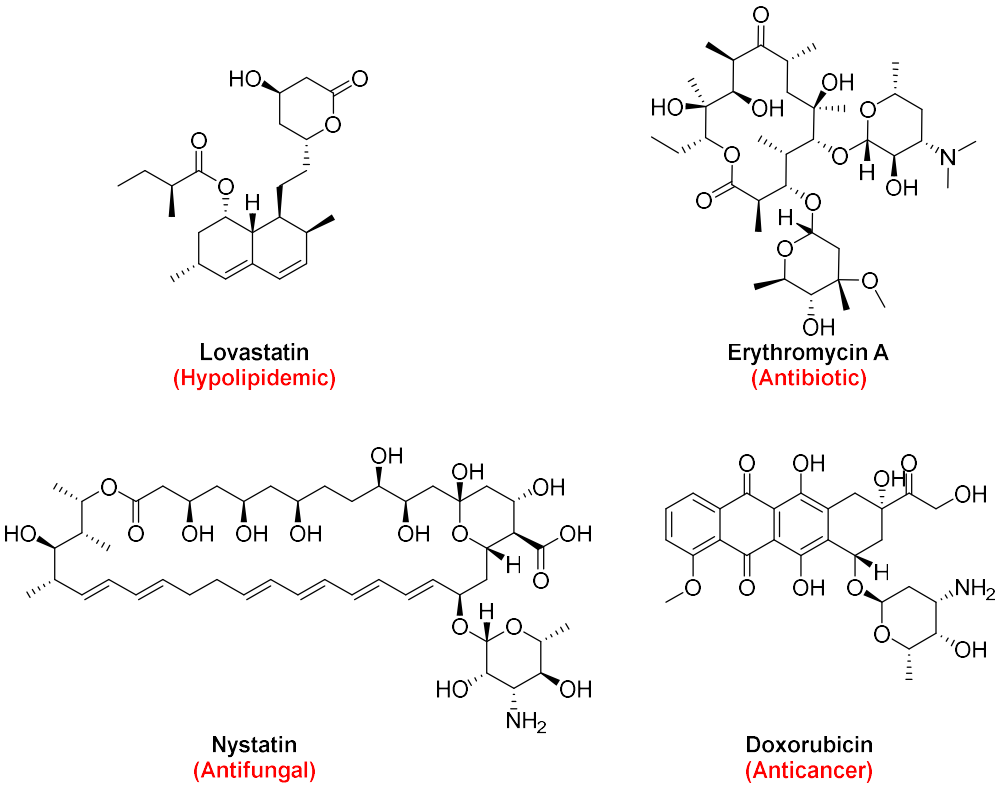

Figure 1: Natural products isolated from different species of bacteria, fungi and plants, and their biological properties (Arcamone, 1981; Endo, 2002; Farzam et al., 2024; Michel, 1977).

1.2. Fungal natural products

Fungi gained significant interest in 1928 with the discovery of the revolutionary antibiotic penicillin, which was isolated from *Penicillium notatum*. Its subsequent development into medicine in the 1940s laid a foundation for exploring these fungal communities. To date, fungi are known to produce almost 9000 compounds with various bioactivities, including antibiotic (griseofulvin), antifungal (ergokonin A), anticancer (taxol), antitumor (enniatin A), antiepileptic (alternarin A), and cholesterol-lowering (lovastatin) properties (Zhgun, 2023). In addition, fungi produce immunosuppressant compounds like cyclosporin A (G. Weber et al., 1994), widely used to prevent organ rejection in transplant surgery.

With an estimated 5 million species distributed across various ecosystems, ranging from terrestrial to aquatic and endophytic environments, fungi are the second most diverse kingdom on Earth (Blackwell, 2011; Grube et al., 2009). However, only a modest fraction, around 10%, of these ubiquitous organisms have been identified by researchers (Hawksworth & Lücking, 2017), highlighting the vast potential for exploration and discovery within this rich reservoir of bioactive natural products. These are heterotrophic organisms, and based on their modes of nutrition, they are classified into three classes: saprophytic, parasitic, and symbiotic. Symbiotic fungi are further divided into two subclasses **(Figure 2)**: mycorrhizal and lichenized fungi (Bahram & Netherway, 2022). My research focuses on fungal natural products, specifically lichenized fungal compounds.

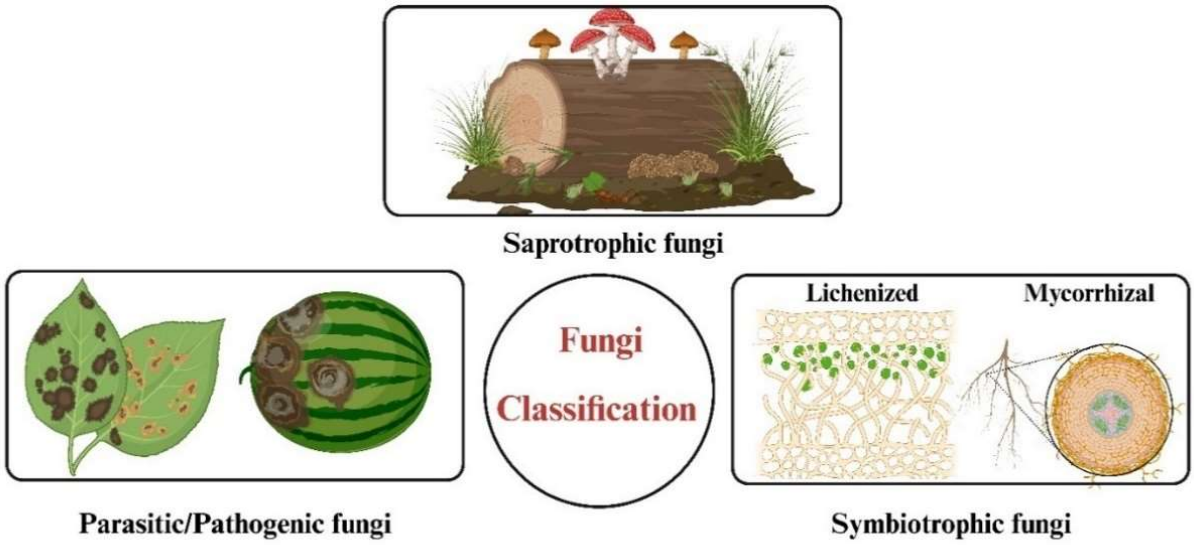

Figure 2: Classification of fungal species based on nutritional modes. Fungi can be categorized into three main groups: parasitic, symbiotrophic (lichenized and mycorrhizal), and saprotrophic, each reflecting distinct ecological strategies for obtaining nutrients. Created using BioRender.

1.3. Lichenized fungi

Historically, lichens were defined as slow-growing, dual organisms formed by a mutual relationship between a fungi (mycobiont) and an algae and/or cyanobacteria (photobiont) (Lutzoni & Miadlikowska, 2009) **(Figure 3)**. Typically, the taxonomic name of the mycobiont refers to the whole structure. For example, the name *Cladonia uncialis* refers to the lichenized fungus alone or in association with the photobiont algae. With recent advancements in science, it has been found that lichens are miniature ecosystems, as the lichen thallus (and its surface) hosts a complex and primarily specific microbiota of bacteria (Bates et al., 2011; Grube et al., 2009; Sierra et al., 2020) and so-called lichenicolous fungi (Spribille et al., 2016), which can either contribute to the symbiosis for nutrient acquisition and stress resistance (Grube et al., 2009, 2015; Sigurbjörnsdóttir et al., 2015) or behave as lichen pathogens (Diederich et al., 2018; Merinero & Gauslaa, 2018)

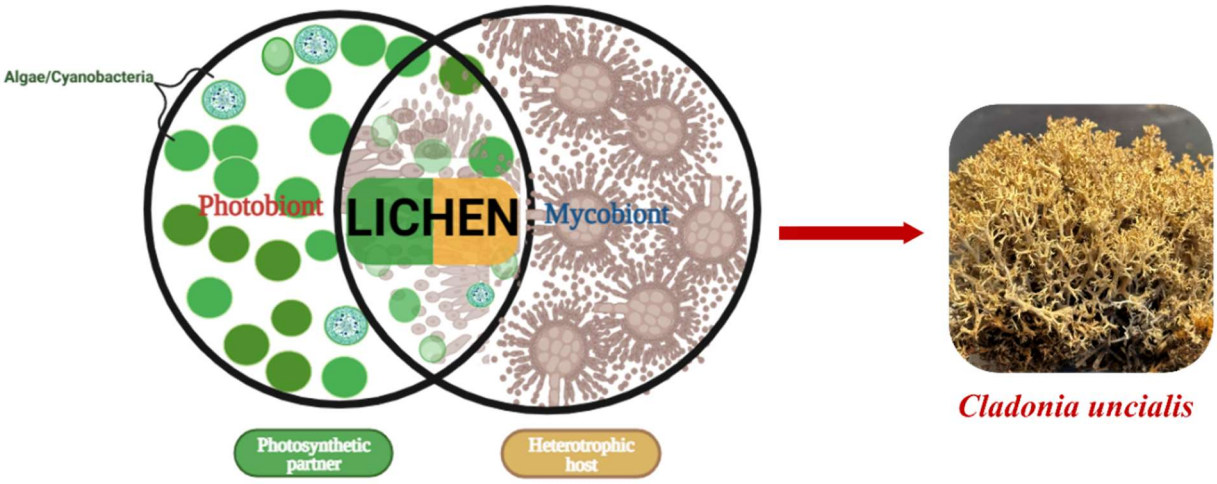

Figure 3: A representation of the symbiotic relationship between a photosynthetic partner (algae or cyanobacteria) and a heterotrophic host (fungus/mycobiont) forming a lichen, exemplified by the image of the lichen *Cladonia uncialis*. This illustration was prepared using BioRender and image credit for *Cladonia uncialis*: Harman Gill.

These unique communities have colonized all terrestrial habitats on earth, from the mildest conditions in our home gardens to the extremely harsh environmental conditions found in the arctic tundra or desert. Such adaptation to extremely diverse environmental conditions has occurred even though they are poikilohydric organisms, *i.e.,* they lack the ability to maintain homeostasis of cells and tissues (Matos et al., 2015). Due to industrialization and subsequent pollution, many lichens have been pushed to extinction, or their geographical distribution has been highly restricted (Pescott et al., 2015). They are commonly used as bioindicators to monitor air pollution, sulfur dioxide deposition, global warming and for the sensitive detection of metals and radionuclides (Bačkor & Loppi, 2009; Matos et al., 2015; Ohmura et al., 2013). Lichenized fungi are found scattered in several taxonomic classes, but the lecanoromycetes class comprises most of the described mycobiont species, including the well-studied *Cladonia* species, *Usnea florida* and *Xanthoria parietina*. Lichenologists have employed various techniques to measure thallus growth and have reported an average growth of 0.5-8 mm per year, depending on the species and environmental conditions (Hale, 1973). Because of this slow growth rate and difficulties in reconstituting the partnership under controlled conditions, lichens are challenging to study, and little is known about how these communities are established and sustained in diverse habitats.

1.4. Secondary metabolites from lichen mycobionts

Lichens produce a plethora of low-molecular-weight aliphatic and aromatic compounds derived from both primary and secondary metabolism. Primary metabolites encompass intracellular molecules necessary for basic life functions, spanning various chemical classes such as amino acids, polysaccharides, proteins, lipids, carotenoids, and vitamins (Nayaka & Haridas, 2020). In contrast, secondary metabolites are found outside the cells and exhibit unique and often complex

structures. These compounds are synthesized through specific biochemical pathways, where the simpler structures of primary metabolites undergo a series of enzymatic transformations, forming more intricate and specialized secondary metabolites (Nayaka & Haridas, 2020). Within lichen symbiosis, both the mycobiont and photobiont partners contribute to primary metabolite production, while SMs are primarily synthesized by lichenized fungi (Ranković, 2019). These SMs generally account for 5- 20% of the dry thallus weight (Molnár & Farkas, 2010). The major classes of secondary metabolites produced by lichen include depsides, steroids, xanthones, terpenes, anthraquinones, and chromones, which contribute to the chemical diversity **(Figure 4)** and ecological functions of lichens. Yet, their specific roles within the symbiotic relationship and ecosystem remain areas of ongoing research. For example, usnic acid is commonly produced by lichens from the *Usnea* and *Cladonia* genera, and this SM and semisynthetic derivatives have been well studied because of their diverse biological activities (Araújo et al., 2021).

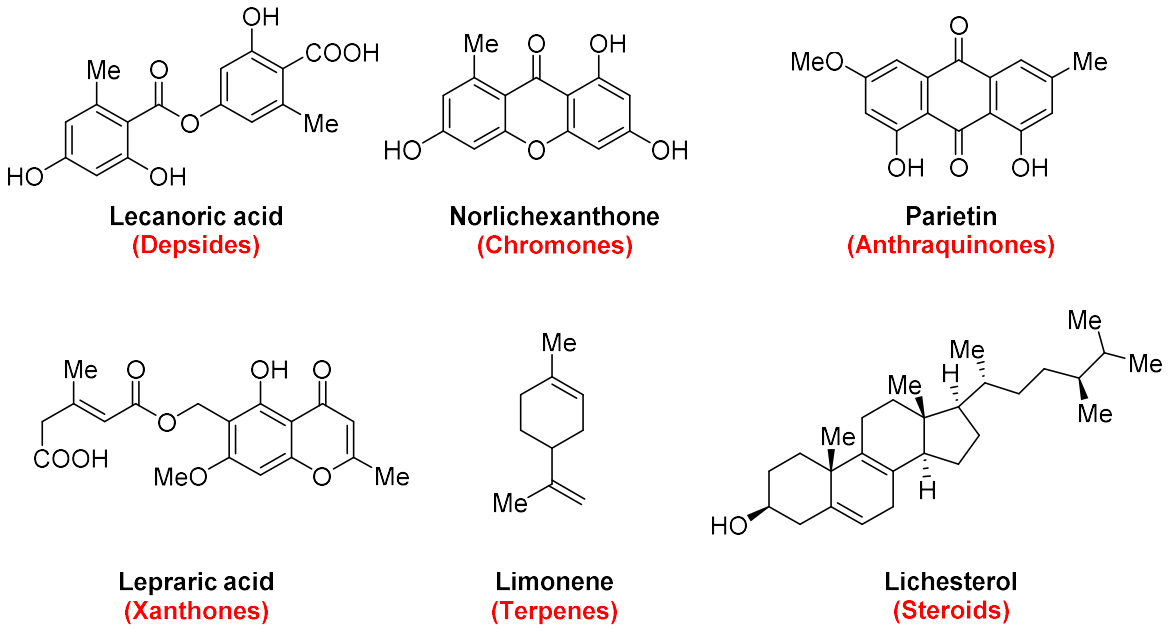

Figure 4: Major classes of secondary metabolites produced by lichen fungi.

1.5. Structural organization of the lichen thallus

The organization of the lichen thallus is not random, and each partner and compartment exhibit complementary functions. The mycobiont forms a cortical layer of dense fungal hyphae, which provides the photobiont partner with mechanical stabilization and shelter (Honegger, 1997). The photobiont in the medulla layer provides carbon nutrients to other partners through photosynthesis (Honegger, 1997). Cyanobacteria in some lichens are responsible for nitrogen fixation (Seneviratne & Indrasena, 2006). In addition, the lichen microbiome is also not homogenous, with differences between the center and edges of the lichen (Mushegian et al., 2011) and vertically between the surface and substrate (Noh et al., 2020). Algae predominantly dictate the phenotype of most lichens, whereas fungi are primarily responsible for producing secondary metabolites. Secondary metabolites produced by mycobiont or lichenicolous fungi exhibit a specific localization that is likely related to their biological functions, for example, metabolites produced in the lichens *Ophioparma ventosa* (Le Pogam et al., 2016) and *Peltigera* (Garg et al., 2016) **(Figure 5)** with the colored squares indicating their localization.

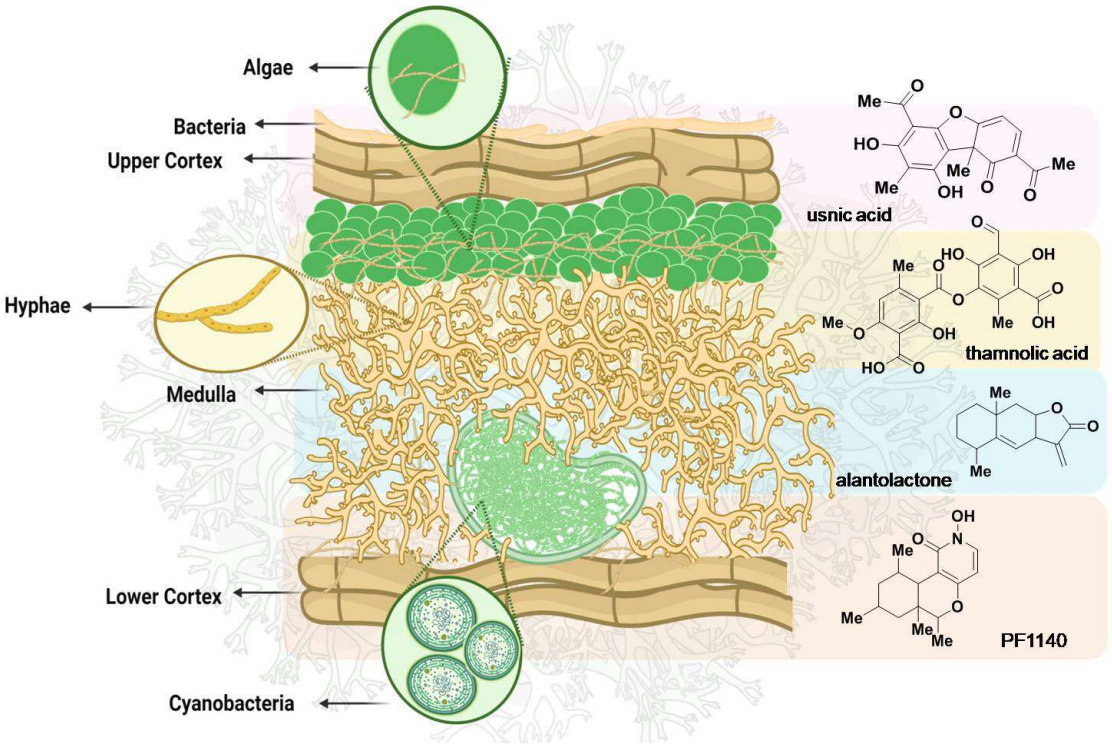

Figure 5: Intricate Structure of the Lichen Thallus: Lichens represent symbiotic partnerships between photosynthetic (photobiont) and heterotrophic (mycobiont) organisms. Additionally, lichens harbor a diverse microbiome comprising bacteria, lichenicolous fungi, and Basidiomycota yeasts. The picture is adapted from (Gill, Sorensen, et al., 2023).

1.6. Spatial distribution of the mycobiont secondary metabolites

Some biological functions can be deduced from biological activities like antibiotic or antifungal properties. SMs with such bioactivity are most likely involved in colonizing or protecting an ecological niche from other competing microbes. However, hints about biological functions can also be obtained by determining where specific SMs are produced in the thallus **(Figure 5)**. Reconstituted communities will be very useful, but methods like mass spectrometry imaging (MSI) allow SM localization to be studied in natural ecosystems. The spatial organization of SMs in a lichen using MSI was first reported in *O. ventosa* (Le Pogam et al., 2016). SMs show clear, distinct localization within the thallus, with the polyketide haemoventosin located on the

surface of the apotheciate thallus (red pigment found in the fruiting bodies), thamnolic acid found in the upper cortex and medulla, and divaricatic and miriquidic acids accumulating in the lower medulla and at the lichen/rock interface. Usnic acid appears to be vertically distributed equally across the thallus but is detected on the edges of the lichen and accumulates above the photobiont layer. SM spatial organization has also been investigated in the lichen *Peltigera* (Garg et al., 2016). This study employed an untargeted metabolomics approach relying on molecular networking. As expected, comparing the community to isolated partners (mycobiont, photobiont, and bacteria) showed little overlap in the metabolic profile, confirming that studying the whole community is particularly important. While this study used the Global Natural Product Social (GNPS) database to dereplicate known molecules rapidly, very few structures could be assigned to the novel metabolites detected in these extracts. Nevertheless, MSI of three different layers of *Peltigera*, sun-exposed top layer, middle layer, and bottom layer, revealed different metabolite distributions. For example, the fungal pyridone alkaloid PF1140 was found to be most abundant in the bottom layer, while asperphenamate and sesquiterpene lactones were mostly found in the middle layer. Although a promising approach, MSI remains challenging to employ for unknown molecules, and the strategy of using heterologous expression to identify SMs produced by mycobiont will provide the necessary information to perform targeted MSI (refer to section 1.18 for more details on heterologous expression).

1.7. Lichen secondary metabolites: understanding ecological functions

It is difficult to study lichens, so assigning their SMs to a function in their ecosystem is not trivial. A few functions have been reported. The most well-documented and validated function of fungal SMs is certainly protection from UV light, desiccation, and extreme temperatures provided by pigments through light absorption or reflection (Galanty et al., 2021; Noh et al., 2020; Ranković,

2019). Lichens appear particularly resistant to light, and the production of photoprotective SMs contributes to their high resistance to harsh environments (Nguyen et al., 2013). In *L. pulmonaria*, melanin production is responsive to light and likely protects against UV light (McEvoy et al., 2007). However, the production of depsidones in this lichen is not regulated by light, and a role in protection against herbivores has been suggested.

In contrast to melanin and parietin, which absorb light, it was found that the depside atranorin instead protects the lichen from UV light through reflection (Solhaug et al., 2010). Different SMs protect lichens from different light wavelengths, and they exhibit synergistic properties as antioxidants to protect the lichen thallus and photosystem of the photobiont, as demonstrated with vulpinic acid, pinastric acid and usnic acid in *Vulpicida pinastri*, and *Letharia vulpine* (Legouin et al., 2017; Phinney et al., 2019). Because of these properties, lichen SMs are also prospected for new natural photoprotective agents.

Another function of lichen secondary metabolites is to protect the lichen ecosystem from herbivorous predators (Pöykkö et al., 2005). However, this function is not clear, as the ability of the predator to defend itself against lichen SMs seems to play a more significant role than the presence of SMs (Gauslaa, 2005). Similarly, nutrient availability appears to be more important as to whether snails eat the lichen *Usnea taylorii* than the presence of SMs (Gadea et al., 2019). Thus, it remains unclear if protection from herbivorous predators is a primary biological function of lichen SMs. Other functions are related to heavy metal tolerance and allelopathy, as lichen SM extracts inhibit the growth of mosses (Goga et al., 2017; Molnár & Farkas, 2010).

1.8. Biological activities of lichen secondary metabolites

More than 1,000 SMs are known from lichenized fungi and possess diverse biological activities (Araújo et al., 2021), many of which are exclusively found in lichens (Shrestha & St. Clair, 2013), for instance, usnic acid. Metabolomic studies have suggested that lichenized fungi in the *cladoniaceae* (lecanoromycetes, ascomycota) class exhibit a unique chemical space compared to other non-lichenized fungal classes (Robey et al., 2021). For example, *Evernia prunastri* and *Pseudevernia furfuracea* are known as 'perfume lichens' which are extensively used in the fragrance industry (Calchera et al., 2019; Lutzoni & Miadlikowska, 2009). They are also used as preservatives and photoprotectants in cosmetics (Galanty et al., 2021). Indeed, lichen SMs have been extensively screened **(Figure 6)**, for example, for antimicrobial (fumarprotocetraric acid), antiprotozoal (usnic acid), antifeedant (vulpinic acid), antifungal (lecanoric acid), or antioxidant (atranorin) activities (Molnár & Farkas, 2010). The lichen SMs virensic acid, norlobaric acid, salazinic acid, parellic acid, and physodic acid have been reported for anti-HIV activity (Neamati et al., 1997), while pannarin, 10-chloropannarin, and sphaerophorin are known for their high cytotoxic potential against rat lymphocytes as compared to colchicines (Correche et al., 2005). These examples show the great potential of lichen SMs in diverse applications.

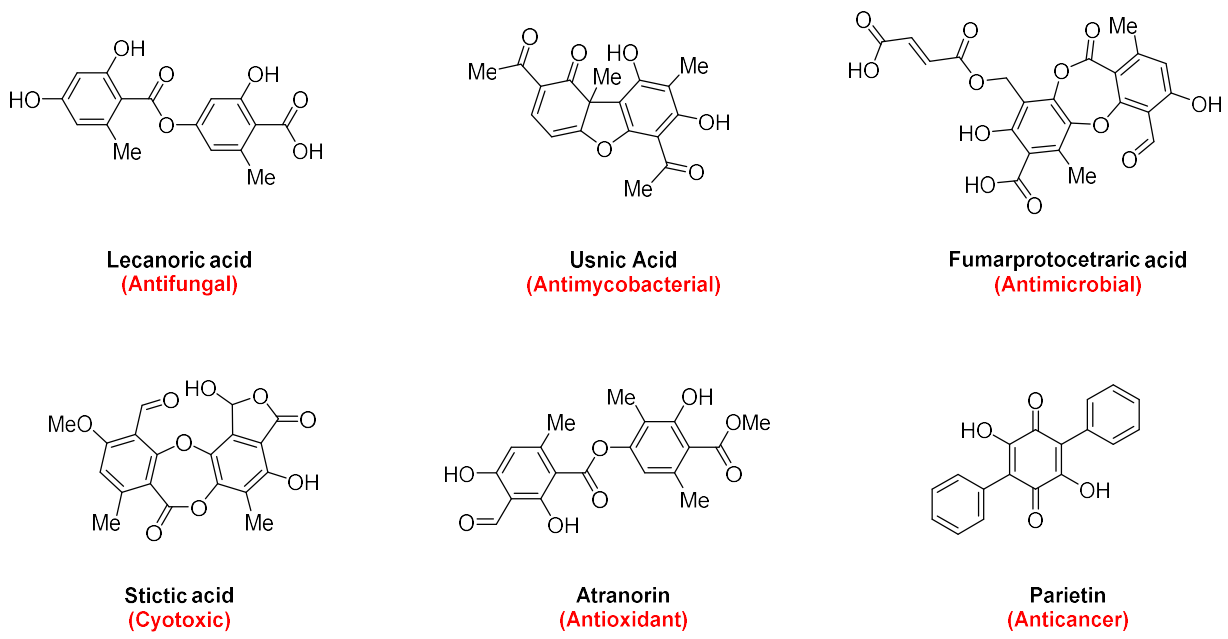

Figure 6: Examples of lichen secondary metabolites and reported bioactivities (Molnár & Farkas, 2010).

1.9. Biosynthetic pathways of SMs production by lichen mycobionts

The carbon source in lichens originates from a photobiont, either cyanobacteria or algae, which undergoes photosynthesis to produce carbohydrates. These carbohydrates, classified as primary metabolites, are subsequently transferred to the fungal partner (mycobiont). Within the mycobiont, the conversion of these primary metabolites into secondary metabolites (SMs) occurs, a metabolic process outlined by Mosbach (Mosbach, 1969). Biosynthesis refers to the synthesis of structurally diverse organic molecules, the SMs, catalyzed by specific enzymes encoded by genes within the microorganism's genome. Biosynthetic pathways leading to the production of SMs are differentiated into three types **(**

Figure 7), based on various starter units: acetyl CoA and malonyl CoA for the polyketide pathway, acetyl and mevalonate for the terpene pathway, and erythrose-4-phosphate and phosphoenolpyruvate for the shikimate pathway (Mosbach, 1969).

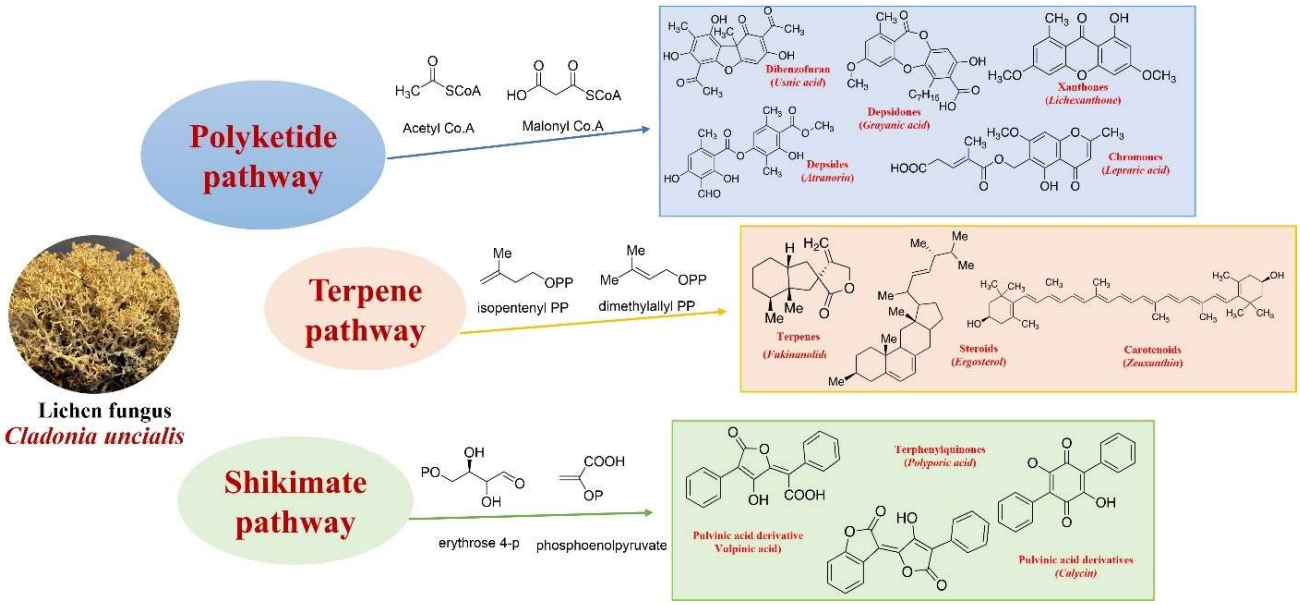

Figure 7: Illustration of three biosynthetic pathways: polyketide, terpene, and shikimate for secondary metabolite production in lichen mycobionts.

1.10. Polyketide synthases (PKSs)

Polyketides are polymers of acyl units assembled to form phenolic or aliphatic structures. They are structurally and functionally diverse family of bioactive NPs that can be found in bacteria, fungi, and plants (Hertweck, 2009). These polyketonic structures are synthesized by multifunctional mega-synthases, known as polyketide synthases (PKSs). PKSs exhibit significant structural and sequence similarities with fatty acid synthases (FASs) and employ a similar catalytic mechanism in the biosynthesis of polyketide natural products (Weissman, 2009).

1.11. Domain architecture and PKSs pathway

Polyketide synthases are multidomain enzymes, with each domain serving a specific catalytic function. The basic process of polyketide assembly by PKSs involves several catalytic modules: loading, extending, reducing, and terminal modules, each comprising various domains necessary for polyketide biosynthesis (Keating & Walsh, 1999). In the loading module, the acyl carrier

protein (ACP) domain is flexible within the PKS superstructure and features a phosphopantetheine "arm" responsible for shuttling intermediates to and from other catalytic domains (**Figure 8**). Additionally, the acyltransferase (AT) domain functions as a 'gatekeeper' facilitating the recruitment of the appropriate priming or extension unit to the KS and ACP domains (H. Park et al., 2014). In the extending module, the ketosynthase (KS) domain plays a crucial role in catalyzing the carbon-carbon bond formation via Claisen condensation reaction in polyketide biosynthesis (Staunton & Weissman, 2001).

To initiate polyketide biosynthesis, the PKS must first be 'primed'. The acyltransferase (AT) domain recruits a starter unit, acetyl CoA, to the ketosynthase (KS) domain. Subsequently, an extension unit, malonyl CoA, is recruited by the AT domain to the acyl carrier protein (ACP) domain. Within the extending module, the KS domain catalyzes decarboxylative Claisen condensation, extending the polyketide chain by two carbon atoms. This intermediate is then transferred to the KS domain, allowing the AT domain to recruit another malonyl CoA to the ACP. This iterative process can be repeated multiple times, elongating the backbone chain by two carbon atoms per cycle (Cox et al., 2018). Although not strictly necessary for chain elongation, extra reducing domains present within a PKS facilitate chemical modifications. These include ketoreductase (KR), dehydratase (DH), and enoyl reductase (ER) domains, which sequentially reduce a carbonyl group to a fully reduced carbon (**Figure 8**) (Akey et al., 2010; Ames et al., 2012; Keatinge-Clay & Stroud, 2006).

Another optional domain, the C-methyltransferase (MT) domain (**Figure 8**), which is responsible for adding methyl groups to the α-carbons of the polyketide backbone, utilizes S-adenosyl methionine (SAM) as a methyl group donor (Skiba et al., 2016)**.**

Once the polyketide is fully extended, the reaction requires termination and release of the product. Three terminal domains that help in releasing products are the thioesterase (TE), reductase (R), and Claisen cyclase (CLC or CYC) domains (Du & Lou, 2010). The TE domain (**Figure 8**) is the most common, which hydrolyzes the polyketide from the ACP domain, leaving a terminal carboxylic acid. Alternatively, an R domain may be employed, using NADPH to produce an aldehyde. Less commonly, a Claisen cyclase (CLC or CYC) domain cleaves and cyclizes polyketides via Claisen condensation (Korman et al., 2010). The diverse termination methods offer the potential to produce diverse molecules from the same substrate by varying folding patterns (Du & Lou, 2010).

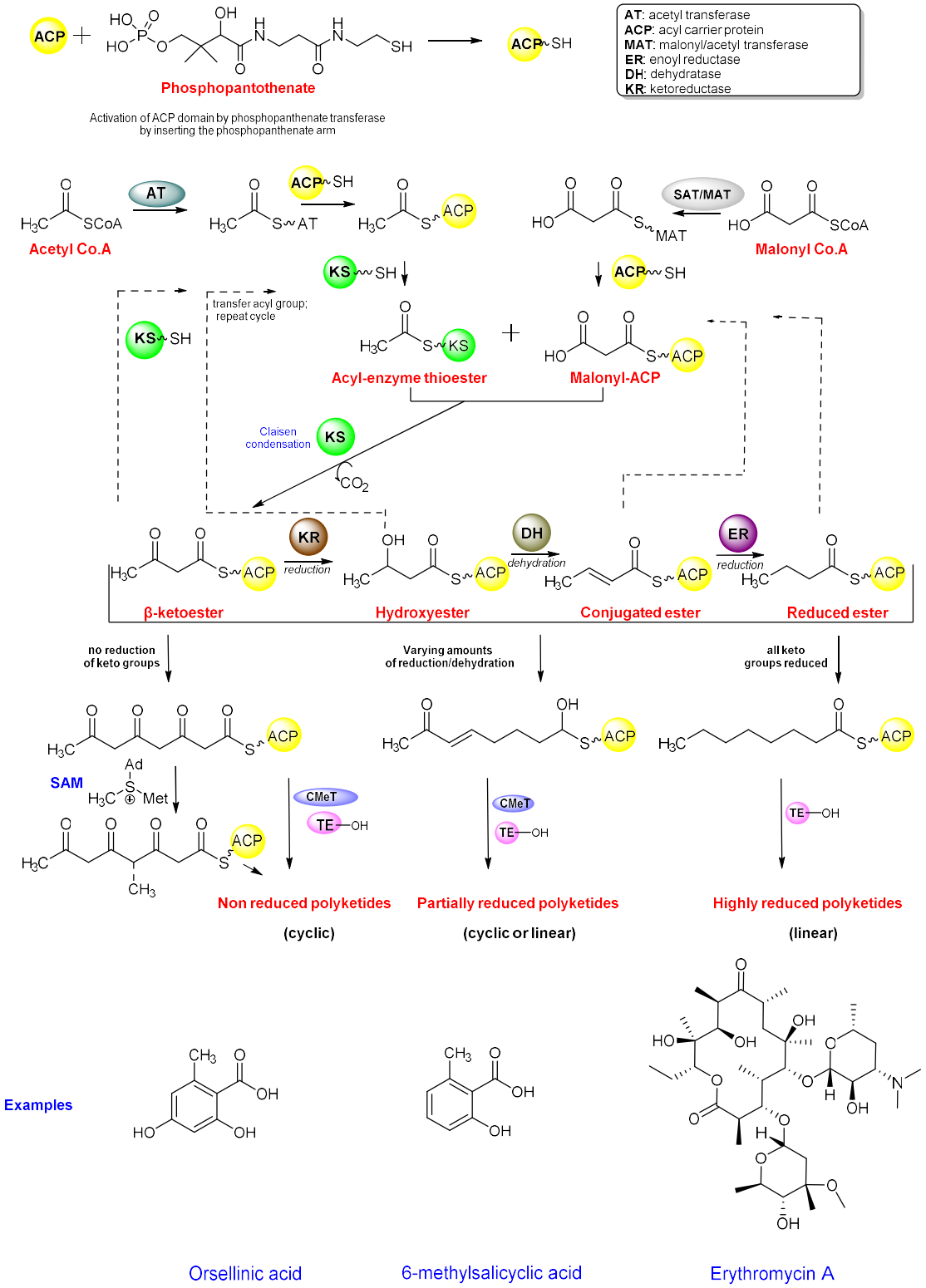

Figure 8: A detailed overview of reduced, partially reduced, and highly reduced polyketides biosynthesis with examples from each class.

1.12. Classification of polyketide synthases (PKSs)

The mechanistic nature of these domains categorizes PKSs into three main types: type I, type II, and type III. Type I PKSs are often known as 'megasynthases' and encompass all or most catalytic domains within a single protein. They are prevalent in bacteria and fungi. Type I PKSs can be subdivided into two types: Iterative (iPKSs), found in fungi, and modular PKSs (mPKSs), found exclusively in bacteria. Modular type I PKSs biosynthesize polyketides akin to an assembly line employing multiple catalytic modules, whereas iterative type I PKS repeatedly utilize the same set of domains from a single module throughout polyketide biosynthesis (Cox et al., 2018; Staunton & Weissman, 2001; Weissman, 2009).

Based on the domain architecture of type I iterative PKSs, they are grouped into three categories depending on how much they reduce the poly-β ketone chain: highly reducing (hr-PKS), partially reducing (pr-PKS), and non-reducing (nr-PKS) polyketide synthases (**Figure 8**). Highly Reducing PKSs (hr-PKSs) can reduce all poly-β-ketone intermediates to saturated carbon-carbon bonds, facilitated by the presence of KR, DH, and either a trans- or cis-acting ER. For example, erythromycin A (**Figure 8**). Partially reducing PKSs (pr-PKSs) contain a KR or DH domain and can generate polyketides harboring hydroxyl groups through the reduction of specific β-ketone groups, for example, 6- methylsalicylic acid (6-MSA) (Scott et al., 1971). Non-reducing (nr-PKSs) lack KRs or ERs, resulting in the synthesis of extended poly-β-ketone intermediates that undergo cyclization to yield heterocyclic aromatic compounds such as orsellinic acid (Cox & Skellam, 2020).

Type II PKSs are comprised of a complex of monofunctional proteins exclusive to bacteria. They resemble type II FASs in that they consist of discrete dissociative enzymes that operate in trans

to generate polyketides iteratively (Hertweck et al., 2007). Lastly, Type III PKSs are homo-dimeric proteins that utilize coenzyme A esters instead of ACPs to produce polyketide intermediates. These PKSs employ a single active site to catalyze a sequence of decarboxylation, condensation, cyclization, and aromatization reactions (Yu et al., 2012). They are also referred to as chalcone-synthase-like PKSs and can be isolated from plants, bacteria, and fungi. Type III PKSs utilize cinnamoyl-CoA as a starter unit for chain extension, resulting in the formation of flavonoids and stilbenes (Yu et al., 2012). Most bioactive compounds produced by aromatic polyketides derived from the polyketide pathway lichen are aromatic, and belong to type 1 PKS, therefore my research is particularly focused on type 1 iterative PKSs.

1.13. Lichen polyketide synthases

Most lichen SMs are aromatic polyketides derived from the polyketide pathway. These compounds are unique to lichens and are formed by linking two aromatic units (orcinol and p-orcinol) through ester, ether, and C-C bonds. Examples are depsides, depsidones, and dibenzofurans. Xanthones, chromones, and anthraquinones are some more interesting examples of lichen polyketides **(Figure 9)**. Single aromatic rings are classed as orcinol-type, with orsellinic acid being the primary example of this class.

The carbon core of the SMs is formed by the PKS and typically contains a single aromatic ring with orsellinic acid being a common product. The higher oxidation states such as depsides, depsidones and dibenzofurans are the result of transformations of the PKS product by accessory or tailoring enzymes such as cytochrome P_{450} or methyltransferases. Related depsides, such as lecanoric acid, feature one (or more) aromatic ring(s) joined by a simple ester linkage. The depsidones, such as salazinic acid and grayanic acid, feature a biphenyl ether linkage in addition

to an ester bond, forming a central seven-membered ring. Other structural classes of SM's are dibenzofurans, with usnic acid being the most well-known of this class, originates from the oxidative coupling of phloroacetophenone **(Figure 9)**. All other colored pigments, like anthraquinones, xanthones, and chromones, are produced by intramolecular condensation followed by aromatization of polyketide units rather than an oxidative coupling step. Quinones such as parietin, and diphenyl butenolides, exemplified by vulpinic acid (Nayaka & Haridas, 2020), are also among the common structural classes encountered. The aromatic phenolic core, with a pattern of alternating oxygenation **(Figure 9)**, suggests that most lichen SMs belong to the polyketide chemical family.

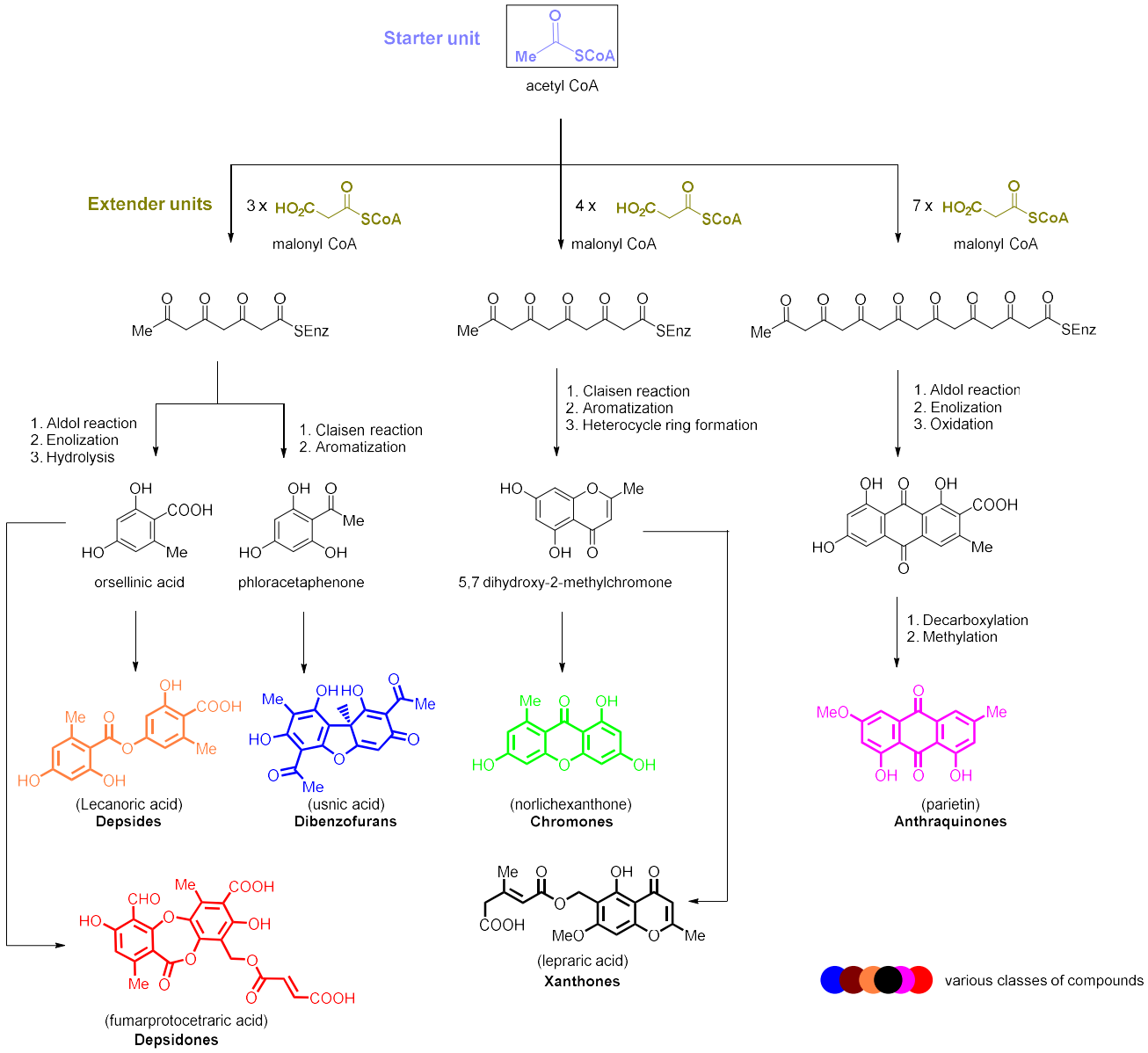

Figure 9: Polyketide pathway illustrating the biosynthesis of various classes of polyketide.

Aromatic polyketides produced through this route differ by the number of malonyl CoA molecules incorporated and the type of cyclization. Additional modifications, including dimerization, increase the diversity of the lichen compounds. Other lichen SMs are synthesized by the mevalonate terpene and the shikimic acid pathways (Goga et al., 2018)

1.14. Terpene and shikimate pathway

The terpene pathway, also known as the mevalonate or HMG-CoA reductase pathway, leads to the production of isopentenyl pyrophosphate and dimethylallyl pyrophosphate, which serve as the precursors for the higher terpenes, such as carotenoids, and steroids. In this pathway, two acetyl CoA molecules undergo a Claisen condensation followed by the addition of a third acetyl CoA *via* an aldol reaction to yield an HMG-CoA **(Figure 10)**. Next, mevalonic acid is formed by the reduction of the thioester which after the introduction of the pyrophosphate, undergoes decarboxylative elimination to isopentenyl pyrophosphate (IPP) and dimethylallyl pyrophosphate (DMAPP). Both IPP and DMAPP act as precursors for the terpene class of compounds such as limonene (Kahriman et al., 2011), phytol (Rajab et al., 1998), lutein (Czeczuga & Czeczuga-Semeniuk, 2003), and lichesterol (Safe et al., 1975). Each of these terpenes have been reported in lichen fungi; however, a specific role has yet to be elucidated.

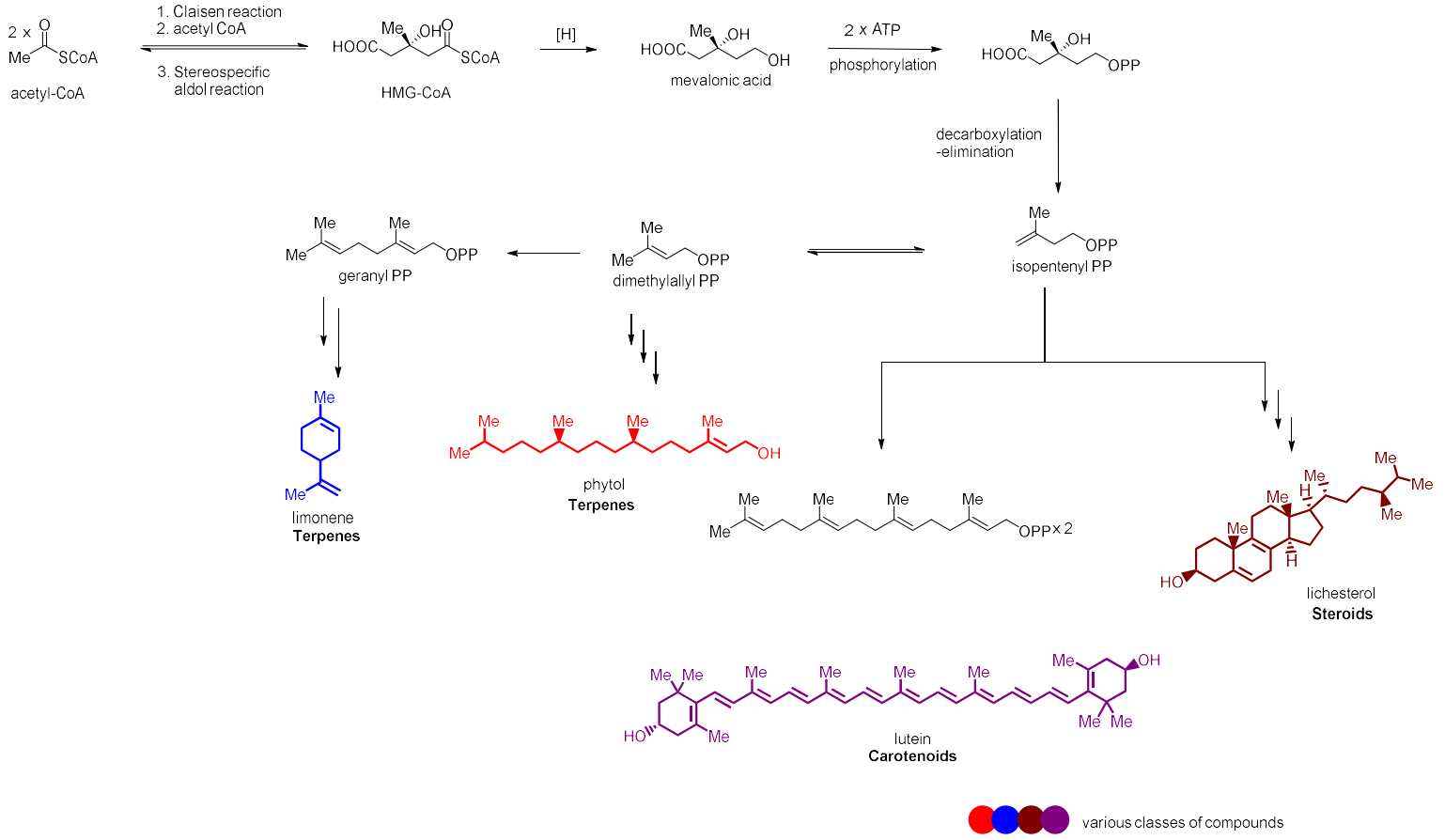

Figure 10: Biosynthesis of lichen secondary metabolites via the terpene pathway, terpenes, carotenoids, and steroids are synthesized from isoprene units isopentenyl pyrophosphate and dimethylallyl pyrophosphate.

The shikimic acid/shikimate pathway involves seven biosynthetic steps that form aromatic amino acids and folates. Shikimic acid is formed by the fusion of phosphoenolpyruvate (PEP) and erythrose-4-phosphate via an aldol reaction and subsequent elimination and reduction. A second PEP is condensed onto shikimate acid via chorismic acid and a Claisen rearrangement that generates the aromatic amino acids L-tyrosine and L-phenylalanine. Tryptophan is also a shikimate-derived amino acid with extra carbons from glyceraldehyde 3-phosphate. The known lichen SM's polyporic acid and the theleporic acid are derived from L-phenylalanine and belong to the triphenyl quinone class of natural products. A more ubiquitous natural lichen product,

pulvinic acid, is produced by further oxidative modification of polyporic acid **(Figure 11)**. Secondary Metabolites produced by the shikimate pathway are widely found in the *Stictaceae* family of lichens.

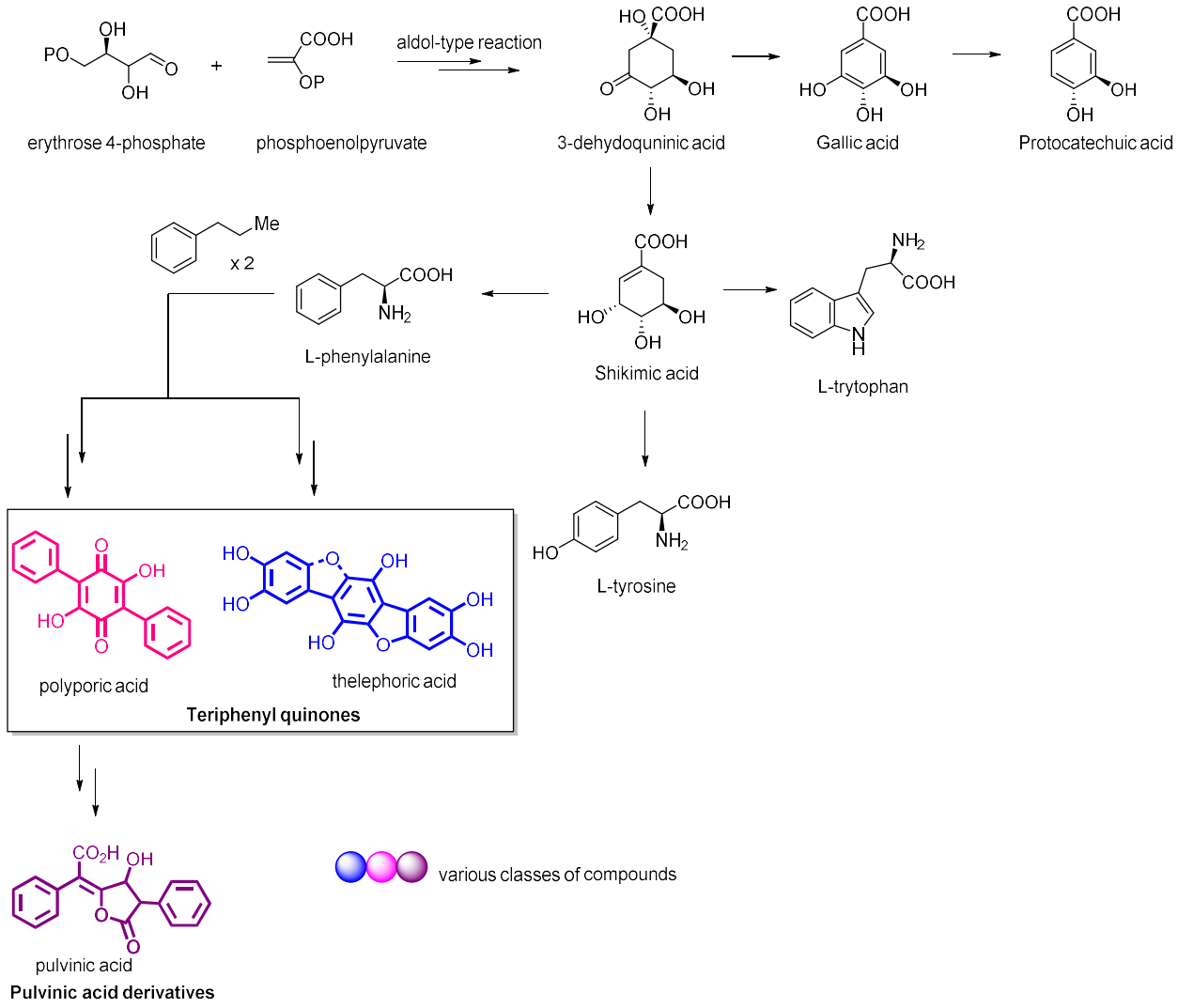

Figure 11: The biosynthesis of lichen secondary metabolites via the shikimic acid pathways, terphenyl quinones, and pulvinic acid derivatives, is synthesized from L-phenylalanine.

1.15. Abundance of polyketide biosynthetic pathways

In fungi, SM biosynthetic pathways are controlled by genes that are often located at the same genomic locus and are co-regulated, defining a biosynthetic gene cluster (BGC) organization (Keller, 2019). These BGCs are organized around a core gene that encodes the enzyme responsible for the first raw stable intermediate. These core enzymes are classified into four major groups: polyketide synthases (PKSs), non-ribosomal peptide synthetases (NRPSs), terpene cyclases (TCs) and dimethylallyl tryptophan synthetases (DMATs). Analysis of mycobiont genomes has revealed that lecanoromycetes are particularly enriched in polyketide pathways (Mosunova et al., 2022). Thus, the genomic information is consistent with the observation that most of SMs identified from lichens are polyketides. However, most reported compounds are aromatic, typically synthesized by non-reducing PKSs, while reducing PKSs usually produce linear polyketides. Comparative genomics of lecanoromycetes and lichenized fungi show their genomes are as rich in non-reducing PKSs (Calchera et al., 2019). Such an abundance in PKSs suggests that many more lichen polyketides await to be discovered. Surrounding the core gene in BGCs are ancillary genes, such as decarboxylase, methyltransferase, P450 oxidases, and other predicted functions, that catalyze tailoring reactions and thus contribute to chemical and structural modification of these SMs (Bertrand et al., 2018a; Martinet et al., 2019).

1.16. The genomes of lichenized fungi have revealed a unique potential for polyketide production

Despite the large number of SMs isolated from lichen and the examination of their medicinal properties and potential applications, conclusive links between chemical structures and the corresponding biosynthetic gene clusters remain very limited. This is largely due to the

challenges with cultivating the lichen assemblage or the corresponding mycobiont in the laboratory. This limits the ability to perform the function assignment using gene deletions to examine the effect on SM profiles and production. The application of next-generation sequencing has represented a significant advance in our ability to examine SM production in lichen fungi. Whole genome sequencing for many lichens has been carried out, and openly available online software such as antiSMASH has facilitated the annotation of SM biosynthetic gene clusters (BGCs). These efforts have revealed that the number of BGCs present in the genome is often far greater than the metabolite profiles detected by chromatographic methods such as HPLC and LC-MS. This diversity of BGCs suggests that the full potential of lichen SM's has yet to be fully revealed. Most cryptic gene clusters have a gene that codes for a PKS as the core carbon assembly step. However, there is a significant amount of variability in the accessory genes that flank the PKS, suggesting a high degree of structural diversity in the metabolites structures.

1.17. Linking biosynthetic gene clusters to known lichen compounds

Phylogenetic analyses of fungal PKSs have revealed that enzymes belonging to the same monophyletic clade tend to share the same enzymatic activities and produce the same polyketide backbone. Phylogenetic analyses of core enzymes are thus a very useful approach to investigate the chemical diversity of fungal polyketides. In addition, the large diversity of chemical structures and biological activities is further enhanced by tailoring genes located next to the PKS gene. Phylogenetic analyses of PKSs, comparative genomics, and transcriptomics studies have identified candidate BGCs for several well-known lichen polyketides.

Grayanic acid was the first compound linked to a BGC in the genome of *C. grayi*. Due to the correlation between grayanic acid production and expression of the CgrPKS16 gene (Armaleo

et al., 2011). In addition, the predicted BGC comprises genes encoding an *O*-methyltransferase and a cytochrome P_{450} which exhibit enzymatic activities consistent with the grayanic acid structure. This BGC was also conserved in *C. uncialis* (Bertrand et al., 2018b), *E. prunastri* and *P. furfuracea* (Calchera et al., 2019). Resequencing of two different chemotypes of *P. furfuracea* from metagenomes indicated that the homologue of the PKS assigned to grayanic acid is likely responsible for producing olivetoric and physodic acids in this lichen (Singh et al., 2021).

Another important lichen polyketide due to its potential applications is usnic acid. The genome of *C. uncialis* was sequenced with the specific aim to identify the BGC involved in the production of usnic acid (M. Abdel-Hameed et al., 2016b; Bertrand et al., 2018a). Chemical studies indicated that a non-reducing PKS produces usnic acid with a carbon methylation domain and a single tailoring enzyme that is required for oxidative dimerization (M. Abdel-Hameed et al., 2016b). The genome of *C. uncialis* contains a single candidate BGC consistent with the predicted requirements, which was found to be expressed in the lichen thallus where usnic acid is detected (M. Abdel-Hameed et al., 2016b). This candidate BGC was also found in *E. prunastri* and *P. furfuracea* (Calchera et al., 2019). A more recent comparative genomic analysis of lichenized fungi found a correlation between this BGC and usnic acid production (Pizarro et al., 2020). The correlation between transcriptomics and usnic acid production in *Nephromopsis pallescens* suggested that the Nppks7 PKS is responsible for the production of this SM (Y. Wang et al., 2018).

Similarly, the mycobiont *Cladonia macilenta* was sequenced to identify the BGC involved in the production of biruloquinone, an acetylcholinesterase inhibitor that is a promising candidate to prevent Alzheimer's disease (Park et al., 2013). A recent transcriptomics approach enabled the

assignment of this compound to a BGC which comprising PKS21, a close homolog of the cercosporin *CTB1* gene, and five other genes (Kim, Jeong, et al., 2021). This BGC is fully conserved in *Cladonia borealis* and *Cladonia metacorallifera*. While the genome of *C. metacorallifera* was released in 2014 (S.-Y. Park et al., 2014), it has only recently been used to search for the BGC involved in the production of the red pigment cristazarin (Jeong et al., 2021). Unfortunately, 27 out of 30 PKS genes were differentially regulated when cristazarin is produced and it was impossible to assign any of them to this pigment. The *Stereocaulon alpinum* genome was compared to *Cladonia* genomes to identify a candidate BGC for atranorin biosynthesis (Kim, Liu, Woo, Kang, Park, Yu, Ha, Oh, Yang, Kim, et al., 2021). A comparative genomics and biosynthetic gene clustering approach determined the set of PKSs common to these mycobionts and the ones most likely involved in producing depsides and depsidones. This approach identified the Pks23 BGC in *S. alpinum* and *C. rangiferina* as candidates to produce atranorin because this SM was only reported in these two lichens. The gene composition of the predicted BGC was also consistent with the chemical structure of atranorin, which has an unusual methoxycarbonyl group. This BGC is also present in the genomes of 5 other mycobionts, which can produce atranorin (Kim, Liu, Woo, Kang, Park, Yu, Ha, Oh, Yang, Kim, et al., 2021). A phylogenetic analysis of the PKS showed that Pks23 belongs to a new group of non-reducing PKSs. This BGC was fully validated with functional analyses (refer to section 1.20).

In addition to linking BGCs to compounds isolated from lichen thalli, genome analyses allow one to predict the production of other SMs. For example, the combination of *C. uncialis* genome and expression data suggested that one BGC encoding a PKS homologous to the polyketide synthase from terrein (*A. terreus)* produces halogenated derivatives of 6-hydroxymellein (M. Abdel-Hameed et al., 2016a). Other BGCs appear highly conserved with the betaenone BGC in

Phomabetae, patulin BGC in *Aspergillus clavatus*, azaphilone BGC in *Monascus pilosus*, and emodin-derived anthraquinone BGCs, suggesting that *C. uncialis* can also produce these kinds of SMs. However, they have not been reported yet (Bertrand et al., 2018b).

The different genome analyses that focused on lichen SM pathways not only linked candidate BGCs to known lichen molecules, but they also revealed a much larger and diverse biosynthetic production potential than previously known, which may lead to the identification of new chemical backbones and new biological roles in lichen communities. Functional analyses of these candidate BGCs will be key to understanding their biological roles further.

1.18. Heterologous expression as a strategy to elucidate lichen biosynthetic pathways

The difficulty in reconstituting lichen communities in the laboratory and their slow growth make functional studies very difficult. Another challenge is that laboratory conditions are often not suitable to produce SMs from the lichen mycobiont. Indeed, it is well-known that SMs are produced under very specific conditions that are difficult to determine and reproduce in the laboratory, resulting in cryptic biosynthetic pathways or silent BGCs (Keller, 2019). Therefore, it is important to find a reliable strategy to link genes to compounds. One approach that is widely implemented to elucidate fungal biosynthetic pathways is heterologous expression in a fungal host where gene expression can be controlled. Surrogate hosts like *Aspergillus oryzae* (NSAR1), *Aspergillus nidulans,* or *Saccharomyces cerevisiae* are routinely used to characterize BGCs from non-lichenized fungi and have been used for a few lichen pathways. However, successful heterologous expression of PKSs from lichenized fungi has been reported for only a very limited number (three) of cases **(Table 1)**, and each of these achievements represents a significant breakthrough in lichen research.

Table 1: Heterologous expression of polyketide synthases (PKSs) from lichen mycobionts.

PKS's	Native hosts	Surrogate hosts	Molecules	References
PFUR17_02294	*Pseudevernia furfuracea*	*Saccharomyces cerevisiae*	Lecanoric acid	(Kealey et al., 2021)
Pks23	*Endo carponpusillum*	*Saccharomyces cerevisiae*	Naphthalene pyrone	(Harvey et al., 2018)
Atr1	*Stereocaulon alpinum*	*Ascochyta rabiei*	Atranorin	(Kim, Liu, Woo, Kang, Park, Yu, Ha, Oh, Yang, Kim, et al., 2021)
MPAS	*Cladonia uncialis*	*Aspergillus oryzae* NSAR1	No production	(Bertrand & Sorensen, 2019)
6-MSAS	*Cladonia uncialis*	*Aspergillus oryzae* NSAR1	No production	(Bertrand & Sorensen, 2019)
OAS	*Cladonia uncialis*	*Aspergillus oryzae* NSAR1	No production	(Bertrand & Sorensen, 2019)
UlPks6	*Usnea longissima*	*Aspergillus oryzae* NSAR1	No production	(Yi et al., 2016)
CgrPks2	*Cladonia grayi*	*Aspergillus oryzae* NSAR1	No production	(Armaleo et al., 2011)
ScPks1	*Solorina crocea*	*Aspergillus oryzae* NSAR1	No production	(Gagunashvili et al., 2009)
XsePks1	*Xanthoparmelia semiviridis*	*Aspergillus nidulans*	No production	(Chooi et al., 2008)

MPAS: methyl phloroacetophenone synthase; **6-MSAS**: 6-methylsalicylic acid synthase; **OAS**: orsellinic acid synthase.

1.19. Successful expression of lichen polyketide synthases in *Saccharomyces cerevisiae*

Heterologous expression of lichen depside PKS has been recently reported in yeast (Kealey et al., 2021). Expression of codon-optimized *PFUR17_02294* from the perfume lichen *P. furfuracea* was performed in a yeast strain that was engineered to contain a copy of the *Bacillus subtilus sfp* gene which encodes a phosphopantetheinyl transferase needed to activate the acyl carrier protein (ACP) domain of the PKS. Transformants produced an orsellinic acid dimer that was identified as the depside, lecanoric acid. It is unusual that a PKS can synthesize lecanoric acid, which is a depside. The presence of orsellinic acid was also observed after prolonged culture fermentation, resulting from the hydrolysis of the ester linkage (Kealey et al., 2021). How this dimerization is performed by the PKS requires an in-depth investigation at the mechanistic level and may suggest that lichen mycobionts exhibit more diverse enzymatic capabilities.

Harvey and colleagues (Harvey et al., 2018) have also developed a *S. cerevisiae* strain for heterologous expression of various fungal BGCs. In this work, 41 cryptic BGCs (28 PKSs and 13 TCs) were selected from diverse Ascomycota and Basidiomycota species, and 22 of them yielded detectable SMs. One of the successful expression trials involved the Pks23 from the lichenized fungus *Endocarpon pusillum*. Pks23 produced two related naphthalene pyrones, which are known precursors of phenalenone in *Penicillium herquei* in which the biosynthetic pathway was elucidated through gene deletions and heterologous expression in yeast (Gao et al., 2016). However, the BGC does not seem to be fully conserved and *E. pusillum* most likely produces related but different compounds.

1.20. Successful expression of a lichen gene cluster in *Ascochyta rabiei*

Kim and coworkers (Kim, Liu, Woo, Kang, Park, Yu, Ha, Oh, Yang, Kim, et al., 2021) have recently published an article demonstrating the first successful functional heterologous expression of a novel lichen polyketide BGC from the lichen mycobiont *Stereocaulon alpinium*. The presence of methoxycarbonyl within the 3-methyl orsellinic acid makes it a unique molecule among other depsidones and depsides. The BGC is comprised of genes encoding three enzymes (Atr1: PKS; Atr2: P450 monooxygenase; Atr3: O-methyltransferase) and a transporter (Atr4). They chose to express Atr1, Atr2 and Atr3 in a strain of the plant pathogenic fungus, *Ascochyta rabiei*, in which the BGC for solanapyrone production was removed (Kim, Liu, Woo, Kang, Park, Yu, Ha, Oh, Yang, Kim, et al., 2021). Genes were cloned from the genomic DNA of *S. alpinum*. 4-O-demethylbarbatic acid was observed after the successful expression of Atr1 (Pks23), consistent with the biosynthesis of atranorin. Similarly to lecanoric acid, 4-O-demethylbarbatic acid is a dimer produced by the PKS, indicating that lichen PKSs commonly produce dimeric SMs **(Figure 12)**. Transformants co-expressing Atr1 with either Atr2 or Atr3 yielded different intermediates (proto atranorins) and a shunt product (baeomycesic acid), while co-expression of all three genes resulting in the production of atranorin **(Figure 12)**. This study represents a breakthrough in the study of lichen SMs because it demonstrated the the efficiency of comparative genomics and phylogeny to select candidate BGCs and resulting in the first full elucidation of a lichen biosynthetic pathway.

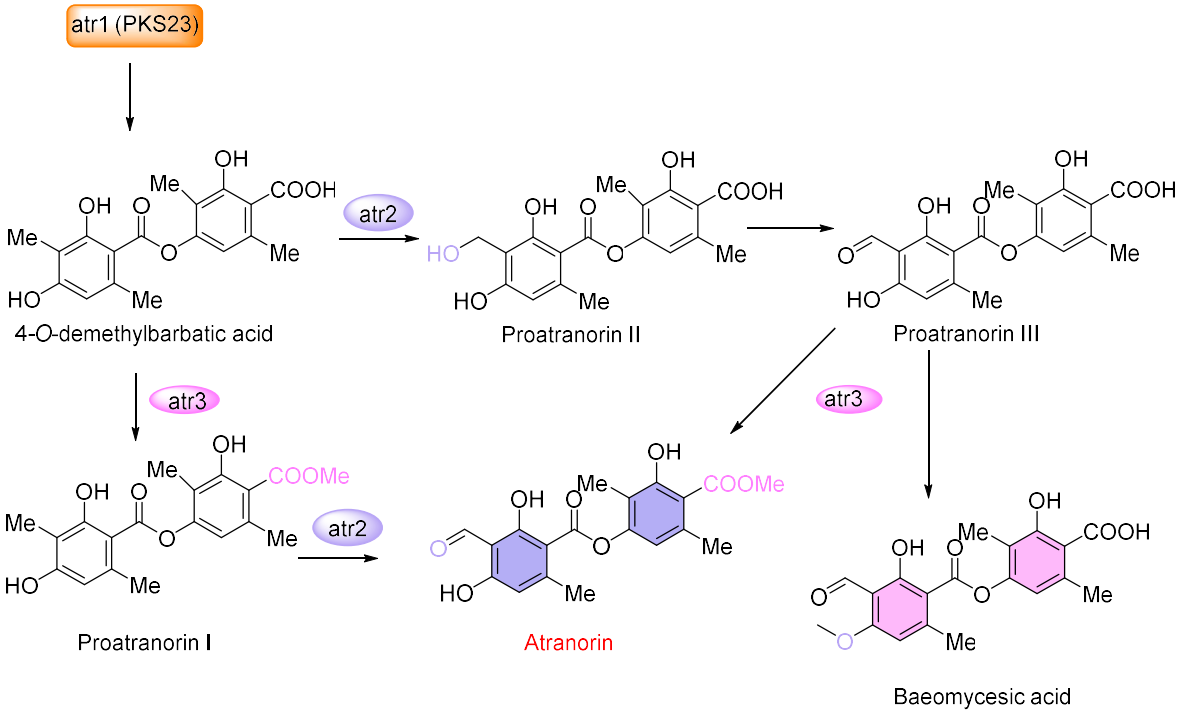

Figure 12: Biosynthesis of atranorin by the lichen mycobiont *Stereocaulon alpinium* in *Ascochyta rabiei*.

1.21. Problems associated with heterologous expression of lichen polyketide synthases in *Aspergillus oryzae*

Although *A. oryzae* has a proven record as an amenable host for the functional analysis of fungal PKSs, successful expression in this host of PKSs from lichenized fungi is still a daunting task. To date, various heterologous expression attempts in *A. oryzae* have been reported with non-reducing PKSs **(Table 1)**. Unfortunately, in all the reported cases, no corresponding metabolite could be detected in fermentation culture extracts. Transcription of the PKS genes was observed in each case, and the transcripts were consistent with the expected gene structure, (Bertrand & Sorensen, 2019). The ketosynthase domain of *C. uncialis* PKSs was further investigated for functionality, and they did not show any particular features compared to non-lichenized PKSs (M. E. Abdel-Hameed et al., 2018).

Moreover, they were successfully produced in *Escherichia coli*, suggesting that at least partial lichen PKSs can be translated accurately (Abdel-Hameed et al., 2018). Thus, the reasons for the absence of metabolite production remain unclear, although it may be linked to the translation of the full-length PKS. For example, expressing the lecanoric acid or atranorin PKSs in *A. oryzae* would inform about whether the PKS or the host is the limiting factor.

Conversely, expressing in yeast or *A. Rabiei* the PKS genes that failed to produce compounds in *A. oryzae* could represent an interesting alternative. Although the KS domain was successfully produced in *E. coli*, one hypothesis could be that *A. oryzae* degrades lichen PKSs after translation. An *A. oryzae* strain lacking the PepE and tripeptidyl peptidase genes produced high-titers of recombinant human lysozyme and bovine chymosin proteins (Jin et al., 2007). Similarly, autophagy and vacuolar protein sorting (VPS) degrade accumulated, misfolded or unfolded proteins. Finally, other issues could be related to missing precursors for the PKS or missing tailoring enzymes to release the polyketide chain.

1.22. Possible solution to heterologous expressing of lichen polyketide synthases in *Aspergillus oryzae*

The heterologous expression of lichen PKSs in *NSAR1 A. oryzae* offers an intriguing strategy for producing complex polyketides. However, achieving efficient expression can be challenging due to differences in codon usage between the native lichen and the fungal host. Although lichen genes from *C. uncialis* transcribe effectively, no translation or secondary metabolite production was observed after fermentation (Bertrand & Sorensen, 2019). Enumeration of the codon composition of protein-encoding genes exhibits preferences for certain codons within synonymous sets to encode an amino acid. These preferences reflect the bioavailability of complementary tRNA (Hanson & Coller, 2018; Quax et al., 2015). The PKS genes of *C. uncialis*

also show codon biases (Bertrand et al., 2015). For instance, when a gene from one organism has codon biases that do not match the tRNA pools of the host organism, different organisms may have distinct codon biases.

This problem is widely addressed by chemically synthesizing a gene with synonymous codons optimized for the host's translation system, thereby enhancing the expression of heterologous genes (Feng et al., 2021; Kealey et al., 2021). Codon optimization involves modifying the DNA sequence of the lichen PKS genes. This modification aligns them with the preferred codon usage of *A. oryzae* without altering the amino acid sequence of the encoded proteins.

To achieve this, the Sorensen group has established a collaboration with Dr. Jerome Collemore from the Westerdijk Fungal Biodiversity Institute in Holland. This collaboration secured ~ 635 kb of codon-optimized genes from the Joint Genomic Institute (JGI) in Berkeley, California. We received a collection of PKSs and tailoring genes from JGI, that are used in the project.

1.23. Summary of research project objectives

This thesis explores the chemical diversity of fungal natural products. It involves the isolation, characterization, and profiling of secondary metabolites produced by various fungal strains, explicitly focusing on bioactive compounds from *Aspergillus fumigatus*, *Penicillium sanguifluum* and lichenized fungi, *C. uncialis*. The slow growth rate of lichens has made the direct isolation of their secondary metabolites challenging. Therefore, this research emphasizes the heterologous expression of biosynthetic gene clusters (BGCs) responsible for valuable secondary metabolite production, particularly polyketide synthases (PKSs) and accessory genes. The study also involves the development and application of codon-optimized BGCs to improve expression efficiency. This would, in turn, provide the methodological groundwork for the mass

production and commercialization of interesting secondary metabolites from lichens. The main hypothesis of this study is that fungal species, including both lichenized and non-lichenized fungi, possess untapped biosynthetic gene clusters (BGCs) capable of producing novel and bioactive secondary metabolites, and these BGCs can be functionally expressed in heterologous hosts to explore and harness their chemical diversity.

The goals of my doctoral research are summarized into the following three objectives.

Objective 1: Exploring the Chemical Diversity of Fungal Natural Products from *Aspergillus fumigatus* and *Penicillium sanguifluum.*

Objective 2: Heterologous expression of orsellinic acid BGC (*cu-nr-pks-5*) from mycobiont *C. uncialis.*

Objective 3: Heterologous expression of halogenated isocoumarin BGC (*cu-pks-4*) from mycobiont *C. uncialis*

Chapter 2

Materials and methods

2.1 Materials and methods related to chapter 1

Not applicable.

2.2 Materials and methods related to chapter 2

For a list of primers used in all chapters, refer to **Table S1**. All the media components used in the study are detailed in **Table S2**.

2.3 Materials and methods related to chapter 3

This chapter has been published (Gill, Sykes, et al., 2023a) with me as the primary contributor. I acknowledge Dr. Ayush Kumar for providing bacterial strains, Dr. Georg Hausner for providing fungal strains for antimicrobial testing, and Ellen M. E. Sykes (2nd author) for helping with antibacterial testing.

2.3.1 Sample collection and fungal isolation

The soil sample was collected, along with a sample of lichen thallus, on the McGillivray Trail (latitude 49.8053, longitude −95.2374), Southeast Manitoba, in June 2020. The soil sample was incubated on potato dextrose agar (PDA) for seven days at 28°C. One (S4) of the fungal isolates showed inhibition of the neighboring fungi growth on the same Petri plate. Therefore, we selected S4 for further investigation by subculturing on PDA plates to obtain a monospore culture of the fungus putatively labeled S4.

2.3.2 Identification of fungus

Approximately 100 mg of the mycelia from the active S4 fungal strain was extracted using an isolation kit (E.Z.N.A.® Fungal DNA Mini Kit). Taxonomic identification was achieved by DNA amplification and sequencing of the internal transcribed spacer (ITS) region using the ITS1F and ITS4R primers **(Table S1)**. Sequencing was performed at the Cancer Care Manitoba Research Institute, University of Manitoba. A homology search of the sequencing results (with primers removed) was performed using BLASTn against the NCBI GenBank database. The reference strain sequences with the highest identity and query coverage score were downloaded from the NCBI database. A phylogenetic tree was constructed using the Neighbor-Joining (NJ) method in MEGA 7.0 software with 1000 bootstrap repeats (Kumar et al., 2016). The isolated fungus (S4) was identified as a strain of *Aspergillus fumigatus.*

2.3.3 Fermentation and extraction of *Aspergillus fumigatus* culture

The monospore culture of *Aspergillus fumigatus* strain SL-2203 was cultured on PDA at 28°C for seven days. Four pieces of mycelial agar plugs (0.5 cm × 0.5 cm) were inoculated into two separate 2 L Erlenmeyer flasks, each containing 1L potato dextrose broth (PDB). The culture was shaken at 28°C at 200 RPM for seven days. The culture broth (2 L) was filtered to remove mycelia, acidified with HCl (pH < 2), and extracted twice with an equivalent volume of ethyl acetate (*EtOAc)***.** The combined organic layers were dried (Na_2SO_4), filtered, and evaporated under reduced pressure to obtain a crude extract (650 mg), which was used in subsequent steps.

2.3.4 Isolation and identification of metabolites

The crude extract (650 mg) was fractionated by passing through a pre-packed normal-phase spherical silica (10g, 60µm) flash chromatography column (Biotage ® Sfär Silica) using the

Biotage Isolera Prime 3.3.0 apparatus. The flow rate was set at 10 mL/min, and UV-VIS detection was recorded at 264 and 245 nm. A gradient of dichloromethane (DCM): methanol (MeOH) (100:0 to 80:20) was used. In this run, pure compound **1** was eluted in a mixture of DCM: MeOH (95:5) and pure compound **2** was eluted in DCM: MeOH (90:10) to yield ~234 mg and ~36 mg of compounds, respectively. The identities of the compounds were confirmed by nuclear magnetic resonance (NMR) and liquid chromatography-mass spectroscopy (LC-MS). The complete characterization data is provided in chapter 3.

2.3.5 Antimicrobial activities

Four multi-drug-resistant (MDR) clinically isolated bacterial and five environmental fungal strains **(Table 2)** were chosen to evaluate the antimicrobial activities of compounds **1** and **2**.

Table 2: Test organisms used for antimicrobial activities.

S. No	Bacterial test organism	Source
1	*Acinetobacter baumannii* (RND) efflux pump deficient strain	AB258
2	*Acinetobacter baumannii* wild type strain	ATCC17978
3	*Pseudomonas aeruginosa (RND)* efflux pump deficient strain	PAO750
4	*Staphylococcus aureus* subsp. *aureus* Rosenach; methicillin-resistant	ATCC43300
	Fungal test organism	
1	*Aspergillus oryzae*	NSAR1
2	*Aspergillus spp.*	SL-2201*
3	*Ganoderma lucidum*	WIN(M)1804#
4	*Pleurotus ostreatus*	WIN(M)1803#
5	*Trichoderma citrinoviride*	SL-2202*

* University of Manitoba isolated laboratory strains, species were confirmed via sequencing.

The fungal strains WIN(M) was obtained from Winnipeg collection at University of Manitoba.

2.3.6 Preliminary assay of the crude extract

The antimicrobial activity of the crude extract was determined using the well diffusion method

(Magaldi et al., 2004). The crude extract (200 µg) was screened *in vitro* for antimicrobial activity against bacterial and fungal strains. Bacterial and fungal plates were incubated at 37°C for 24 and 28°C for 72 h, respectively. The zone of inhibition was determined by measuring the clear zone around each disk, and the average diameter was calculated in millimeters (mm). The assay was performed in triplicates.

2.3.7 Antimicrobial susceptibility testing of isolated compounds

Compounds **1**, **2** and their synergistic effect was tested using the disk diffusion method according to Clinical Laboratory Standard Institute (CLSI) guidelines (Wayne, 2010). In summary, a single bacterial colony was grown overnight in Luria broth (LB) and sub-cultured (1:100) in fresh LB. Strains were grown for 5 hours with shaking at180 RPM and 37°C. Then the culture was diluted in 0.85% sterile saline to achieve 0.5 McFarland standard using the Densichek (Biomerieux, Canada). A sterile cotton swab was immersed in bacterial suspension, and excess fluid was removed. The bacterial swab was further streaked in three directions on Mueller-Hinton agar (MHA) plates to obtain confluent bacterial growth. The media surface was allowed to dry, followed by placing the sterile paper disks and adding compound **1** (50 µg/mL, 100 µg/mL, 150 µg/mL, and 200 µg/mL in methanol), compound **2** (50 µg/mL, 100 µg/mL, 150 µg/mL, and 200 µg/mL in methanol) and compound **1**+**2** (25 µg/mL, 50 µg/mL, 100 µg/mL each in methanol) on the disks. Ciprofloxacin was used as a positive control; methanol was used as a negative control. The plates were incubated at 37°C for 16-20h, depending on the bacterial strain, and the zone of inhibition was recorded in millimeters (mm). Three independent biological replicates were performed.

2.3.8 Minimum inhibitory concentration (MIC) of isolated compounds

The MIC of broth micro-dilution method was performed according to the CLSI guidelines (Wayne, 2010). In brief, single colonies of bacterial cultures were grown overnight in 10mL of LB and then sub-cultured (1:100) in fresh LB with further incubation at 37°C with shaking at 180 RPM for 5 hours. Cultures were then diluted in 0.85% sterile saline solution to achieve 0.5 McFarland standard using the Densichek (Biomerieux, Canada). The diluted bacterial culture was further diluted 1:50 in Mueller-Hinton broth (MHB) for inoculation to obtain approximately 5×10^5 colony-forming units per milliliter (CFU/mL). The tested bacteria were 2-fold serially diluted in MHB and incubated at 37°C for 16-20 h, depending on the bacterial strain. Tests on compound **1**, **2**, and **1**+**2** (synergy effect) were performed from a minimum of 16 µg/mL to 512 µg/mL concentration. Ciprofloxacin and methanol were used as positive and negative controls, respectively. The assay was performed with three biological replicates.

2.3.9 Antifungal assay of the isolated compounds

The antifungal activity of compounds **1** and **2** isolated from *A. fumigatus* were tested using a disk diffusion method (Sadeghian et al., 2016). Briefly, paper disks (5 mm diameter) with varying concentrations (100 µg/mL, 200 µg/mL, 300 µg/mL, and 500 µg/mL in methanol) of compounds on each disk were inoculated at four symmetrical points on the PDA plate. A fungal disk (5 mm in diameter) was placed in the center of the plate. The plates were incubated at 28°C until the control fungal mycelium covered the plate. Mycelia plugs cultured on PDA without any added compounds, were utilized as controls to calculate mycelial inhibition **(Figure 13)**. The assay was performed in triplicates. The negative control disk was treated with a solvent in which the compound was dissolved for validation.

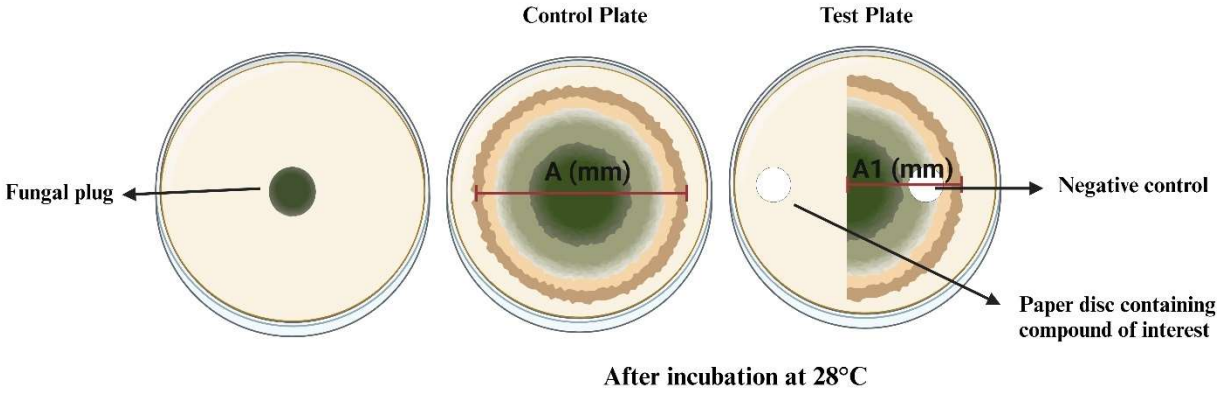

Figure 13: Illustration of the antifungal disk diffusion method.

After incubation at 28°C, the control plate showed fungal mycelium growth (A mm), whereas the test plate showed a zone of inhibition (A1 mm) around the disk containing the compound of interest. Antifungal activity was evaluated by measuring the inhibition zone using the following formula:

$$\textit{Growth inhibition percentage} = [(A\text{-}A1)/A] \times 100$$

- A is the fungal growth diameter in control plates (mm).
- A 1 is the fungal growth diameter in test plates (mm).

2.4 Materials and methods related to chapter 4

This work was conducted in collaboration with Dr. Georg Hausner and Dr. Ayush Kumar at the Department of Microbiology, University of Manitoba, Winnipeg, Canada, as part of the Wawatay project with Indigenous students. Aamer Kurdi, a PhD student in the Department of Microbiology at the University of Manitoba, performed the experiments described in sections **2.4.1 to 2.4.4** and **2.4.9**. My role in this project focused on the fermentation of fungi, the screening, purification, and characterization of compounds, and the conduct of antifungal assays.

2.4.1 Sample collection and fungal cultivation*

Soil samples were collected from Falcon Beach (49°41'06.3"N 95°19'20.1"W) located in Manitoba, Canada, and stored in plastic bags. To isolate individual fungal strains, 100 mg of the soil sample was dissolved in 10 mL of sterile distilled water. This soil suspension was then incubated at room temperature for 1 h. Subsequently, 100 µL of the suspension was spread onto malt extract agar (MEA) plates **(Table S2)** supplemented with rose Bengal solution **(Table S2)** and chloramphenicol (100 µg/mL) (Kramer & Pady, 1961). Duplicate plates were prepared, sealed with parafilm, and incubated at 22ºC and 37ºC for three to five days, respectively. Once fungal colonies appeared, individual colonies were aseptically transferred to fresh MEA plates and incubated at 22ºC for five-seven days. For long-term storage pure fungal strains were maintained on MEA slants at 4ºC.

2.4.2 Assay using agar plugs and bacterial strains*

Each fungal isolate was screened for antibacterial activity using the agar plug assay (Uzma & Chowdappa, 2017), which was performed against seven bacterial strains (Table 3). Initially, a single bacterial colony was cultured overnight in luria broth (LB) and subsequently sub-cultured at a 1/100 ratio in fresh LB. After a 5-hours incubation period with shaking at 180 RPM at 37°C, the bacterial strains were diluted in saline solution (0.85% NaCl concentration) and cell densities were adjusted to 10^8 CFU/mL using a 0.5 McFarland turbidity standard (BioMerieux, Durham, NC, USA). The diluted bacterial cultures were then evenly spread on LB agar plates using cotton swabs. A circular plug of fungal agar culture was then carefully placed onto the LB

* This part of the project **(2.4.1- 2.4.4)** involves collaboration with Aamer Kurdi, a PhD student in the Department of Microbiology at the University of Manitoba. He performed these experiments.

agar plates containing the bacteria. Subsequently, these plates were incubated for 16 to 20 hours at 37°C. Fungal isolates exhibiting zones of inhibition were selected and stored in triplicate at 4°C on MEA slants for further analysis.

2.4.3 Nucleic acid extraction*

The fungal culture was grown on MEA plates and incubated in the dark at 20 °C for up to four weeks. Two Erlenmeyer flasks (250 mL), each containing 100 mL of PYG broth (**Table S*2*),** were inoculated with 10 agar blocks (2 mm × 2 mm × 1 mm) and then placed in dark at 20 °C for up to ten days. The fungal mycelium from the liquid media was harvested via vacuum filtration. Afterwards, the mycelium was ground using a prechilled mortar and pestle along with acid-washed sand, and DNA for next-generation sequencing was extracted and prepared by using previously described methods (Wai & Hausner, 2021).

2.4.4 Fungal identification by using galaxy platform*

The paired-end reads for the whole genome of strain 111-12 were uploaded onto the Galaxy platform (The Galaxy Community et al., 2022) for genome assembly using Spades. The aim of this study was to identify molecular markers suitable for fungal identification. Queries were made using sequences from the *Penicillium citrinum* strain, including ITS, Beta tubulin, elongation factor, and calmodulin. The NCBI BLAST search tool was used to retrieve nuclear markers for strain 111-12. Additionally, putative biosynthetic gene clusters were identified using antiSMASH version 7.0 (Blin et al., 2023).

* This part of the project **(2.4.1- 2.4.4)** involves collaboration with Aamer Kurdi, a PhD student in the Department of Microbiology at the University of Manitoba. He performed these experiments.

2.4.5 Fermentation and extraction of *Penicillium sanguifluum* culture

The fungal strain *Penicillium sanguifluum* was cultured on potato dextrose agar (PDA) for seven days at 28°C. Four mycelial agar plugs (0.5 cm × 0.5 cm) were taken and inoculated into two separate 2 L Erlenmeyer flasks, each containing 1 L of potato dextrose broth (PDB). Flasks were incubated for 7 days at 28°C at 200 RPM. The resultant 2L culture broth was filtered using cheesecloth to remove the mycelia and acidified (pH <2) with hydrochloric acid (HCl) and extracted twice using an equivalent volume of ethyl acetate (EtOAc). The organic layers obtained from the extractions were combined, dried with sodium sulfate (Na_2SO_4), and concentrated under reduced vacuum pressure to obtain a crude extract (1.3 g). The crude extract is then used in the next steps.

2.4.6 Purification and characterization of the metabolites

The crude extract (1.3g) was fractionated by passing through a pre-packed normal-phase spherical silica (Biotage® Sfär Silica) column (10 g, 60 µm) using a flash chromatography system (Biotage Isolera Prime 3.3.0). The flow rate was adjusted to 10 mL/min, and UV/VIS detection was monitored at 245 and 264 nm. A gradient of DCM: MeOH (100:0 to 80:20) was used. Compound **3** was eluted in a mixture of DCM: MeOH (95:5), while compound **4** was eluted in a mixture of DCM: MeOH (80:20). Both compounds were characterized by nuclear magnetic resonance (NMR) and liquid chromatography-mass spectrometry (LC-MS). For the characterization data, refer to chapter 4.

2.4.7 Minimum inhibitory concentration (MIC) test

Bacterial strains **(Table 3**) were used to determine the minimum inhibitory concentration (MIC) of compounds **3** and **4**, following CLSI guidelines (Wayne, 2010), which are described in detail

in section **2.4.2**. In general, an overnight culture was diluted to a 0.5 McFarland standard and then further diluted to inoculate the wells of a 96-well plate with 5x10^5 cells each. In control wells, cells were not treated with the test compounds. The plate was incubated statically at 37°C for 24 hours, and the MIC was determined by examining the plates for growth.

Table 3: Bacterial strains used in this study.

S. No	Bacterial test organism	Source
1	*Acinetobacter baumannii* Clinical isolate and multi drug resistant	AB030
2	*Acinetobacter baumannii* efflux pump deficient strain	AB258
3	*Acinetobacter baumannii* Wild type	ATCC17978
4	*Pseudomonas aeruginosa* Clinical isolate and multi drug resistant	PA82
5	*Pseudomonas aeruginosa* efflux pump deficient strain	PA0750
6	*Pseudomonas aeruginosa* Wild type	PA01
7	*Staphylococcus aureus* Rosenach; methicillin-resistant	ATCC43300

2.4.8 *In-vitro* evaluation of antifungal assay

The well diffusion method (B. Wang et al., 2022) was used to evaluate the antifungal activity of compounds **3** and **4** isolated from *Penicillium sanguifluum*. A mycelial plug (0.5 cm × 0.5 cm) of the target organism *Ophiostoma novoulmi* subspecies *americana* (CBS108928) and *Cryphonectria parasitica* (ATCC 38755) fungi was inoculated at the center of each PDA plate. The plates were then perforated at equidistant points from the fungal plug using a sterile borer. Various concentrations of the compounds (50 µg/mL, 100 µg/mL, 250 µg/mL, 500 µg/mL, 700 µg/mL, and 1000 µg/mL) were added to the wells. The growth of mycelial plugs on a PDA plate without any compounds was used as a control to measure the degree of mycelial inhibition (Gill, Sykes, et al., 2023b). The plates were incubated at 28°C until the fungal mycelium in the control plate covered the entire plate **(Figure 14)**. To ensure reproducibility the test was performed in duplicate, and the growth diameter was measured to evaluate antifungal activity.

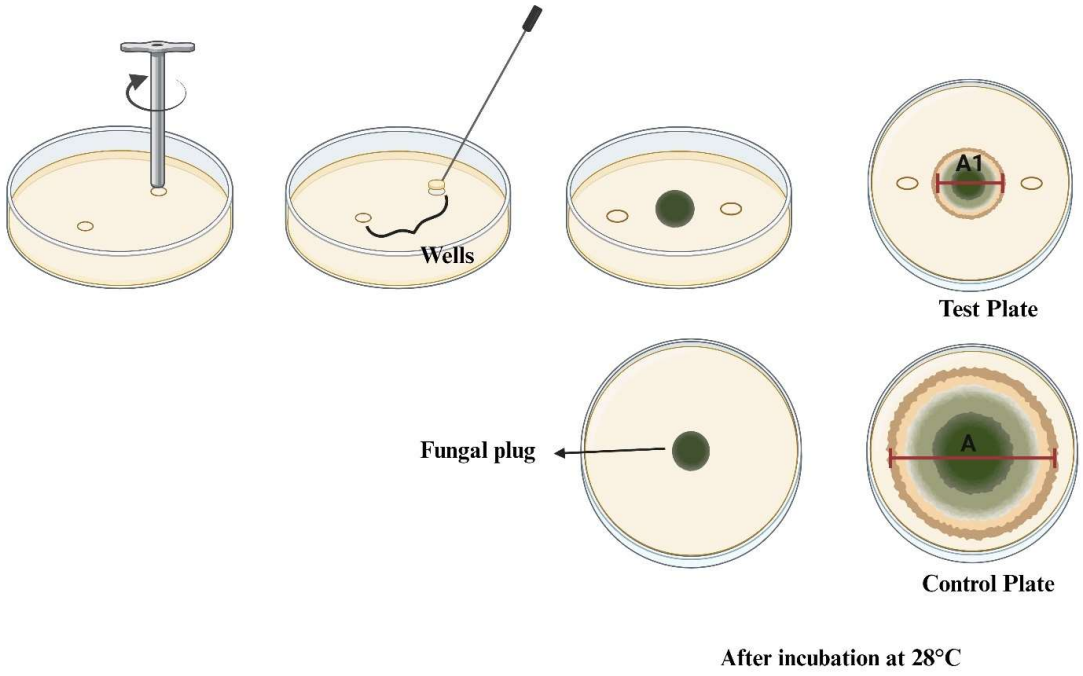

Figure 14: Illustration of the antifungal well diffusion method. Wells were created and compounds of interest were added to the wells.

After incubation at 28°C, the control plate displayed fungal mycelium growth (A mm) while, the test plate showed inhibition (A1 mm) in growth. The formula used to calculate the percentage of growth inhibition is:

$$\textit{Percentage of growth inhibition} = [(A - A1)/A] \times 100$$

- A is the fungal growth diameter in control plates (mm).
- A 1 is the fungal growth diameter in test plates (mm).

2.4.9 Checkboard assay*

The assay was conducted in 96-well plates, following a previously established procedure

* This part of the project involves collaboration with Aamer Kurdi, a PhD student in the Department of Microbiology at the University of Manitoba. He performed these experiments.

(Domalaon et al., 2019) targeting *Acinetobacter baumannii* and *S. aureus* (MRSA) infections (Brown et al., 2021; Maragakis & Perl, 2008; Özgür & Aksaray, 2014). The inoculum was prepared as described earlier for the MIC test (section 2.4.7), and assays were carried out to evaluate the susceptibility of the antibiotic of interest and isolated compounds **3** and **4**. Subsequently, working solutions were prepared in MHB by doubling (2X) the concentration of the antibiotic and quadrupling (4X) the concentration of compounds. The antibiotic was serially diluted two-fold along the x-axis, while compound of interest was serially diluted two-fold along the y-axis of the well plate, creating a matrix of combinations at varying concentrations. Wells containing MHB with or without bacterial cells served as positive or negative controls, respectively. The 96-well plate was then incubated at 37°C for 18 hours and then MIC was determined by assessing the turbidity in the wells to evaluate bacterial growth. Meropenem was selected to test against *A. baumannii* AB258 (efflux deficient), while oxacillin, ampicillin, and clindamycin were selected for testing against methicillin-resistant *Staphylococcus aureus* (MRSA), both alone and in combination with compounds **3** and **4**.

The fractional inhibition concentration (FIC) index was calculated using the following formula:

$$\boldsymbol{FIC\ index} = (\boldsymbol{MIC\ A\ in\ Combination}\ /\boldsymbol{MICA}) + (\boldsymbol{MIC\ B\ in\ Combination}/\boldsymbol{MIC\ B})$$

- MIC A: represents the minimum inhibitory concentration (MIC) of the antibiotic alone.
- MIC A in Combination indicates the antibacterial activity of the antibiotic when combined with the adjuvant in the same well.
- MIC B denotes the MIC of the adjuvant when tested alone.
- MIC B in Combination refers to the antibacterial activity of the adjuvant when combined with the antibiotic in the same well.

FIC index values of ≤0.5 were interpreted as synergistic, values between 0.5 and 4 as indifferent, and values ≥4 as antagonistic.

2.5 Materials and methods related to chapter 5

This is the first report of the successful functional heterologous expression of a native lichen gene in *E. coli*. I am the primary contributor to this chapter. To provide the necessary background and introduce the project, I included sections 2.5.1 to 2.5.5, originally conducted by former group members of our lab Dr. Mona Abdel-Hameed and Dr. Robert Bertrand.

2.5.1 Sampling, cDNA synthesis, and taxonomic identification of the lichen *C. uncialis*

Lichen sample of *C. uncialis*, with voucher number Normore 8774, housed in the Herbarium of the University of Manitoba, was collected in October 2008 from Northern Manitoba, Canada. The collection site was (N 54°42′24.7″; W 101°33′53.1) a south-facing granite ridge predominantly populated by Jack Pine trees. The sample's identity as *C. uncialis* was confirmed by ITS amplification of the DNA, which showed that a DNA sequence matched other entries for *C. uncialis* with >95% sequence identity and 0% gaps. Total RNA extraction (from ~100mg lichen thallus) was carried out using the RNeasy Plant Mini kit (Qiagen), followed by DNase treatment to remove DNA contamination. Reverse transcription of mRNA was performed using the RevertAid H Minus First Strand cDNA Synthesis Kit (ThermoScientific) with the Oligo (dt)18 primers. Detailed protocols for these procedures can be found in a study by Mona Abdel Hameed (M. Abdel-Hameed et al., 2016b).

2.5.2 De novo genome sequencing and BGC analysis of the *C. uncialis* mycobiont

The genome of the *C. uncialis* mycobiont was de novo sequenced at MICB DNA sequencing services (Manitoba Institute of Cell Biology, Cancer Care Manitoba, University of Manitoba) using an Illumina MiSeq sequencer with a MiSeq Micro V2 sequencing kit. After sequencing, contigs were assembled and submitted to antiSMASH 3.0 (T. Weber et al., 2015). In total, 48 secondary metabolite biosynthetic gene clusters were identified (Bertrand et al., 2018a, 2018b).

2.5.3 Annotation and domain analysis of *cu-nr-pks-5*, BGC from the *C. uncialis*

The biosynthetic gene cluster *cu-nr-pks-5* comprises two genes: orsellinic acid synthase (polyketide synthase) and decarboxylase (an accessory gene). Orsellinic acid synthase (*Cu-oas*) is presumed to be the primary enzyme responsible for biosynthesis of orsellinic acid. Meanwhile, decarboxylase was predicted to convert orsellinic acid to orcinol. Polyketide synthase (*Cu-oas*) was annotated using antiSMASH version 7.1.0 (Blin et al., 2023) by submitting nucleotide sequences at https://fungismash.secondarymetabolites.org/#!/start. Functional analysis of proteins, entailing classification into families and prediction of domains, was carried out using InterPro 99.0 (Paysan-Lafosse et al., 2023) on protein sequences to confirm domain presence.

2.5.4 Phylogenetic analysis of *cu-nr-pks-5*, BGC from the *C. uncialis*

This work was performed and explained in detail by previous Sorensen laboratory student Dr. Robert Bertrand (Bertrand et al., 2018a, 2018b).

2.5.5 Plasmid Preparation

Plasmids (pAdeA) containing the orsellinic acid synthase gene, from *C. uncialis* (*Cu-oas*) and *Fusarium sp.* (*Fu-oas*) (Bertrand & Sorensen, 2019) were used in this project. These plasmids were prepared by Robert Bertrand so, I obtained these from the Sorensen laboratory.

2.5.6 Transformation of the orsellinic acid synthase gene in *A. oryzae* NSAR1

To prepare protoplasts, spores of the *A. oryzae* NSAR1 were inoculated into 20 mL of DPY media and incubated in a sterile baffled 500 mL Erlenmeyer flask on a shaking incubator at 30°C/160 RPM for three to four days. The *A. oryzae* tissue was pressed through a cotton-packed sterile syringe, and the pellet was transferred into 10 mL of TF1 **(Table S2)** solution. This mixture was then incubated at 30°C/160 RPM for 2 hours, after which the tissue was once again pressed through a cotton-packed sterile syringe to extract the protoplasts within the supernatant. The protoplast-containing solution was centrifuged at 1500 RPM for 10 minutes, and the supernatant was discarded. The pellet was resuspended in 10 mL of prewarmed TF2 **(Table S2)** solution followed by another centrifugation at 1500 RPM for 10 minutes, with subsequent removal of the supernatant. The protoplast containing pellet was then resuspended in 1-2 mL of TF2 solution, and 200 µL of this protoplast solution was added to 15 mL centrifuge tubes.

For transformation: Each transformation plasmid (pAdeA) containing *Cu*-oas and *Fu-oas* (1000 ng/µL) was added to a volume of 10 µL per 200 µL of protoplast solution and incubated at room temperature for 30 minutes. Successively and gradually, 250 µL, 250 µL, and 850 µL aliquots of TF3 **(Table S2)** solution were added to the protoplast solution and left at room temperature for 30-minute. Then, 5 mL of TF2 solution was added to each protoplast solution,

which was further centrifuged for 10 minutes at 1500 RPM, supernatant was discarded. The resulting pellet was resuspended in 500 µL of TF2 solution.

To prepare two-layer agar plate, a bottom layer **(Table S2)** plate was first prepared and solidified. The 500 µL of protoplast suspension was then mixed with 5 mL of a liquid top layer **(Table S2),** which have identical composition to the bottom layer, except the agar concentration, which was adjusted to 8 g/L. This mixture was poured onto the solidified bottom layer and allowed to solidify. The plates were incubated upside-down at 30°C for four to seven days until *A. oryzae* colonies appeared. Spores from transformant colonies were then inoculated into bottom layer agar plates lacking sorbitol using an inoculating loop. These plates were also incubated upside-down at 30°C for another four to seven days.

The bottom layer was prepared ahead of the transformation day and stored at 4°C.

2.5.7 Fermentation of *Cu-oas* and *Fu-oas A. oryzae* NSAR1 transformants

Transformed *A. oryzae* NSAR1 colonies were inoculated into Czapek-Dox media supplemented with starch* in five 500 mL baffled Erlenmeyer flasks (100 mL in each flask). The culture was then incubated at 30°C/160 RPM for five days. Similarly, control culture (200 mL) with untransformed *A. oryzae* NSAR1 was also incubated.

* To dissolve the starch, approximately 800 mL of water was added to a boil. Then, a starch-water slurry was prepared in cold water and slowly added to boiling water while stirring. Once the solution had turned clear, all other ingredients were added, and the final volume of the solution was adjusted to 1 L.

2.5.8 Extraction of the fermentation culture

The combined 500 mL culture broth of transformed *A. oryzae* NSAR1 was filtered using cheesecloth to remove mycelia. The broth was then acidified (pH < 2) with concentrated HCl and extracted twice with an equal volume of ethyl acetate. The organic layers were dried with sodium sulfate and evaporated on a rotary evaporator to obtain a crude extract. The same procedure was replicated for extraction of untransformed *A. oryzae* NSAR1 cultures. Crude extracts obtained from both transformed and untransformed cultures were used for further characterization.

2.5.9 Characterization of the crude extract of *Cu-oas A. oryzae* NSAR1 transformants

The crude extracts from the transformed and untransformed cultures were subjected to analysis using an HPLC system (Waters HPLC Separations Module 2695 paired with a PDA Detector Model 2996). Chromatographic separation was performed with μBondapak® Waters C18 column (3.9 X 300 mm) with a particle diameter ranging from 15 to 20 μm and pores of 125 Å. The flow rate was 1 mL/min, and the eluent was continuously monitored at 210-600 nm. The separation was conducted using the usnic acid 60 min TFA method stored in the HPLC system. In this method, the elution process began with a mobile phase consisting of 20% methanol and 80% water containing 0.1% formic acid for the initial 10 minutes. Subsequently, a linear gradient was applied, increasing the methanol concentration to 100% for 10 minutes and this composition was held constant for 20 minutes. Subsequently, a linear gradient was employed back to the initial mobile phase of 20% methanol over 10 minutes and maintained for a final 10 minutes. The total chromatographic run was 60 minutes.

The presence of orsellinic acid in the crude extracts was confirmed using HPLC analysis. A reference sample of orsellinic acid for comparison was purchased from Biosynth Carbosynth (Catalog No. F067708).

Heterologous Expression of decarboxylase in *A. oryzae* NSAR1

2.5.10 Isolation and Cloning of the putative decarboxylase gene from the *C. uncialis*

The accessory gene, decarboxylase, was cloned from the *cu-nr-pks-5* biosynthetic gene cluster of the *C. uncialis* genome using primers (Table S1). The transformation plasmid pUSA was linearized through restriction digestion with the FastDigest Kpn1 enzyme (ThermoScientific). Subsequently, the linearized plasmid (pUSA) was purified and concentrated using agarose gel electrophoresis. The amplified decarboxylase gene was integrated into the pUSA (linearized plasmid) using In-Fusion technology (Takara). The transformant plasmid construct (decarboxylase-pUSA) was transformed into Stellar *E. coli* cells and screened via plating them on LB + ampicillin (50 µg/mL) plates followed by overnight incubation at 37°C. Colonies were then selected from the plates and inoculated into liquid LB supplemented with ampicillin (50 µg/mL), allowing overnight growth at 37°C/180 RPM. The plasmid was extracted from overnight grown *E. coli* culture using the GenJet Plasmid Miniprep Kit (ThermoScientific), following the manufacturer provided guidelines. The extracted plasmid (decarboxylase-pUSA) was confirmed through DNA sequencing (Eurofins MWG Operon). This work was performed by Dr. Robert (ex-PhD student) in the Sorensen laboratory.

2.5.11 Plasmid transformation in *A. oryzae* NSAR1

A similar transformation protocol was followed as outlined above in section 2.5.6 except the plasmid used was pUSA, with methionine as a selection marker. Transformed *A. oryzae* NSAR1 colonies were inoculated into Czapek-Dox media supplemented with starch for induction (refer section 2.5.7) in five baffled Erlenmeyer flasks (500 mL), with 100 mL media dispensed in each flask. Two additional cultures were grown in 500 mL baffled Erlenmeyer flasks containing 100 mL of media but without starch. All cultures were incubated at 30°C/160 RPM for five days. As controls, two untransformed cultures **(Figure 15)**, each containing 100 mL of media, were incubated under the same conditions.

2.5.12 Bioassay of whole-cell decarboxylase for converting orsellinic acid to orcinol

10 mg of orsellinic acid (Biosynth Carbosynth) was dissolved in 2 mL of DMSO. This DMSO solution containing orsellinic acid (2 mL) was added to 100 mL of five-day old transformant of *A. oryzae* NSAR1 from 2.5.11. Orsellinic acid was also added in control cultures **(Figure 15)**. The cultures were then fermented for another two days at 30°C/160 RPM. After seven days, the cultures **(Figure 15)** were extracted, and the metabolites were characterized. For details on the extraction, refer to section 2.5.8. The samples were analyzed by ^{1}HNMR .

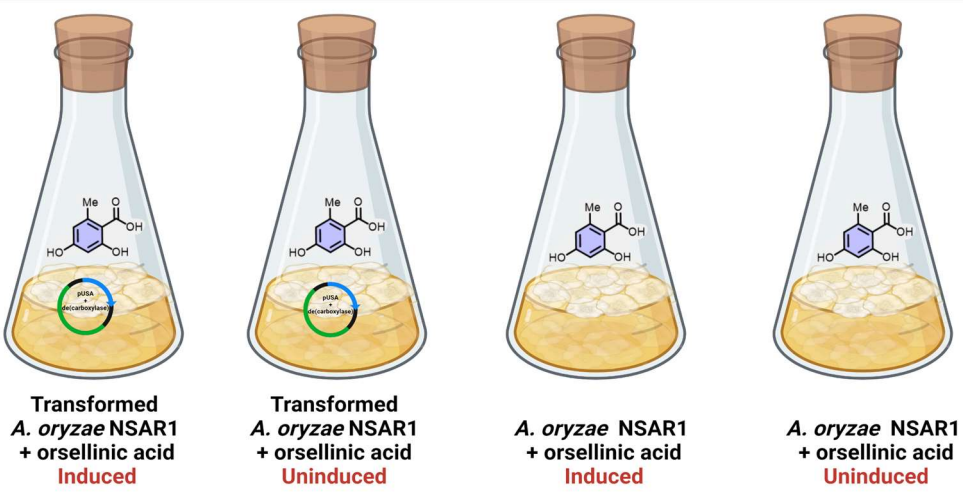

Figure 15: Representation of transformed (with pUSA-decarboxylase) and untransformed *A. oryzae* NSAR1, both in the presence and absence of orsellinic acid under similar experimental conditions for a whole-cell bioassay study.

2.5.13 Cloning of a putative decarboxylase gene in *E. coli*

The 963 bp decarboxylase gene from the pUSA vector (containing decarboxylase) gene from *C. uncialis* was amplified using DreamTaq PCR Master Mix 2X (Thermo Scientific). The forward and reverse primer used in this study are listed in (Table S1). The amplification reaction was performed using an Eppendorf Mastercycler personal (Eppendorf AG, Hamburg, Germany). The reaction was set as follows: 95°C for 2 min; 30 cycles of 94°C for 15 s, 60°C for 20 s, and 68°C for 30 s; and a final extension at 68°C for 5 min. The PCR product was purified using a NucleoSpin® Gel and PCR Clean-up kit (Macherey-Nagel, Germany) and then ligated into the pQE80L vector using a Gibson assembly® cloning kit (New England Biolabs). The resultant ligated plasmid was chemically transformed into *E.coli* DH5α cells (Thermo Fischer Scientific). Following confirmation of integration of the correct insert via counter selection on agar using ampicillin (25 ug/mL) and PCR, the plasmid was retransformed into *E. coli* BL21(DE3) cells

(Sigma-Aldrich). The inserted gene sequence was confirmed using Sanger sequencing (Eurofins Genomics).

2.5.14 Heterologous expression of the decarboxylase gene in *E. coli*

A single bacterial colony was used to inoculate 20 mL of LB medium containing ampicillin (100 µg/mL) and incubated overnight at 37°C with shaking at 250 rpm. This overnight culture was transferred to 2 L (OD_{600} 0.05) of Luria broth with 100 µg/mL ampicillin and fermented at 37 °C with shaking at 250 rpm until the optical density of the culture at 600 nm reached an absorbance of approximately 0.6 AU. The culture was then induced with isopropyl-β-D-thio-galactopyranoside (IPTG) at a final concentration of 1 mM, and fermentation was continued at 35°C for an additional 16 h.

2.5.15 Cell lysis and protein purification from *E. coli*

2.5.15.1 Cell Lysis

The bacterial cells were collected by centrifugation at 5,000 × g (Thermo Scientific TM Sorvall TM) for 10 min at 4 °C. The obtained pellet was analyzed via 10% SDS-PAGE electrophoresis to check target protein expression. Subsequently, the pellet was resuspended in cold H1 buffer (20 mM Tris-HCL, 200 mM NaCl, and 0.02% Na3N, pH=8.0), followed by the addition of 1.0 mM phenyl methyl sulfonyl fluoride (PMSF) to protect the expressed proteins from being broken down by proteolytic enzymes. The resuspended cells were placed on ice, and the cell membrane was lysed by sonication (50% amplitude, 20s pulses at 45s intervals for 12 cycles) using an ultrasonic homogenizer (Branson model 150T). A second centrifugation step was performed at

30,000 × g (Thermo Scientific TM Sorvall TM) for 30 min at 4 ◦C. The cell debris was discarded, and the supernatant was filtered with a 0.22 μm filter before purification.

2.5.15.2 Protein purification

For enzyme purification, all procedures were performed in a cold room at 4 °C. The protein was purified with an AKTA pure (GE Healthcare) using a HisTrap HP 1 mL column (GE Healthcare, Chicago, IL, USA). The supernatant was loaded onto the column, and stepwise elution was carried out at a flow rate of 1 mL min–1 using the following eluents: 25 mL of eluent A (20 mM potassium phosphate, 50 mM imidazole, and 500 mM NaCl [pH 7.5 adjusted by HCl]) for washing out unbound proteins, and 25 mL of eluent B (20 mM potassium phosphate, 500 mM imidazole, and 500 mM NaCl [pH 7.0 adjusted by HCl]) for elution of His-tagged decarboxylase. The fractions were analyzed via 10% SDS-PAGE electrophoresis to confirm protein purification. Protein concentration was determined using a Coomassie (Bradford) protein assay (Bradford, 1976).

2.5.16 Homology modeling of decarboxylase gene

2.5.16.1 Protein Homology Recognition Engine V 2.0 (Phyre2) analysis of decarboxylase gene

The predicted protein sequence of the decarboxylase enzyme from *C. uncialis* (A0A1Z1C438) was submitted to the Phyre2 protein homology and analogy recognition engine (Kelley et al., 2015). The resulting 3D protein model of the decarboxylase enzyme was visualized using Jmol. The family lineage prediction generated by Phyre with high confidence was subsequently submitted to the Scope-Structural Classification of Proteins database. This database compares

the decarboxylase enzyme's family lineage against a repository of known protein structures in a protein database bank (PDB) determined by X-ray crystallography.

2.5.16.2 Phylogenetic analysis of the putative decarboxylase gene

To identify the structural similarity of the gene encoding decarboxylase, the amino acid sequences of proteins with known structural characteristics, pertinent to the decarboxylase function were retrieved from the UniProt database. These sequences were selected based on their assignment to the SCOPe database. The retrieved protein sequences were used to construct phylogenetic tree using MEGA 11 (v. 7.0) (Tamura et al., 2021) software, employing the Maximum Likelihood method and the JTT matrix-based model (Jones et al., 1992). The transferase family-domain containing protein (A0A5N6TQ87) of *Aspergillus avenaceus* was used as an out-group. The branch confidence was estimated using 1000 bootstrap replicates of the interior branch test (Dopazo, 1994; Rzhetsky & Nei, 1992).

2.5.16.3 Metal-binding site identification of the decarboxylase gene

A multiple sequence alignment of the decarboxylase gene from *C. uncialis* was performed with structurally related decarboxylases from *Rhodopseudomonas palustris*, *Pseudomonas fluorescens*, and *Rhizobium spp.* using the UniProt database. This database helped identify the amino acid sequences of the protein binding sites within these decarboxylases. To further investigate metal coordination with these amino acids, the sequence was visualized using UCSF Chimera (Pettersen et al., 2004). The metal binding site was annotated based on its highest sequence similarity with the decarboxylase of *Rhizobium sp*. This analysis provided insights into the metal-ion interactions with these decarboxylases.

2.5.17 Enzyme-catalyzed decarboxylation reactions

A reaction mixture (final volume, 300 μL) containing 10 mM substrate, 100 μg mL–1purified enzyme, and 0.067M HyClone™ Phosphate Buffered Saline (PBS) (pH 7.0), with and without 10 mM zinc chloride, was placed into a microtube, and the mixture was incubated at 30°C or at 4°C for 16 h with shaking (250 rpm). In addition, a series of negative control reactions, such as substrate + buffer (SB), buffer + enzyme (BE), and buffer only (B), using water (H_2O) instead of phosphate buffer, were performed to confirm the enzyme activity.

To understand the enzyme's substrate specificity, we initially focused on phenolic benzoates, particularly orsellinic acid, 2,4-dihydroxybenzoic acid, and anthranilic acid. Our results, summarized in **Figure 44**, show that the enzyme efficiently decarboxylates orsellinic acid to orcinol. To explore the reaction's reversibility, we tested if orcinol and resorcinol could be converted back to their corresponding benzoic acids.

2.5.18 Enzyme-catalyzed carboxylation reactions

A reaction mixture (final volume, 300 μL) identical to that described in the section above has an amount of 3 M KHCO3 added to the mixture. Following the addition of an equal amount of 5 M HCL, the reaction mixtures were centrifuged at 4°C, 12,000 × g, 20 min, and then a volume of 50 μL of the resulting supernatant was analyzed by HPLC as described below. Negative control reactions (no enzyme) were carried out by substituting water for the phosphate buffer under the same conditions.

2.5.19 Analytical analysis of samples

Analysis of the enzyme assay was carried out on a Waters HPLC Separations Module 2695 system equipped with a PDA Detector Model 2996 by injecting 50 µL of the supernatant using an autosampler. The column was a µBondapak® Waters C18 (3.9 X 300 mm) with a particle diameter of 15-20 µm with 125 Å pores. A gradient of Milli-Q water and methanol was used as the mobile phase (solvent A was distilled water with 0.1% formic acid, and solvent B was methanol) at a flow rate of 1 ml/min. The UV signal was monitored at 250 nm, and spectra were collected from 200 to 400 nm.

Standards 2,4-dihydroxybenzoic Acid (Alfa Aesar), resorcinol (Thermo Fischer Scientific), orcinol (Sigma-Aldrich), orsellinic acid (Biosynth Carbosynth), anthranilic acid (Sigma-Aldrich), and aniline (Sigma-Aldrich) were used for comparison.

2.6 Materials and methods related to chapter 6

2.6.1 Preliminary experiments using the native 6-hydroxymellein synthase (6 hms) gene

In this study, genomic DNA was extracted from *C. uncialis* using standard procedures (M. Abdel-Hameed et al., 2016a). The KS domains were amplified using four sets of degenerate primers targeting putative PKS genes from *C. uncialis*. Four putative PKS genes, designated as *cu-pks-1* to *cu-pks-4*, were successfully amplified. Total mRNA was then extracted and reverse transcribed to construct a cDNA library, which was screened for transcriptionally active PKS genes using the same degenerate primers. Only one gene fragment, corresponding to *cu-pks-4*, (later encoded as 6 hms) showed amplification, confirmed by control experiments to exclude DNA contamination. The Rapid Amplification of cDNA Ends (RACE) technique was employed to

identify both 3′ and 5′ ends of *cu-pks-4*, This nucleotide sequence was used to design a new set of primers that allowed for the amplification of the adjacent fragment of the cDNA. The process was continued in an iterative fashion until the full-length gene spanning 6150 bp was sequenced. Subsequent bioinformatics analysis was performed to annotate the sequence for homology, conserved domains, and potential functional annotations (M. Abdel-Hameed et al., 2016a).

2.6.2 Bioinformatics analysis of *cu-pks-4* BGC

The domain architecture of *cu-pks-4* was established using two approaches: initially, BLAST homology searches targeting the 6 hms gene, followed by domain analysis using antiSMASH version 3.0 (T. Weber et al., 2015). Subsequently, the already sequenced genome of *C. uncialis* was scrutinized to locate the genomic contig containing *cu-pks-4*, facilitating its precise identification and localization within the contig. This enabled the identification of post-PKS tailoring genes associated with *cu-pks-4*. Moreover, phylogenetic analysis was conducted to assess the evolutionary relatedness of *cu-pks-4* and its associated genes with other organisms (Ascomycota), particularly *Aspergillus terreus*.

When I started this project, thanks to a gene synthesis grant from the Joint Genomics Institute, we received 79 codon-optimized genes (55 PKSs, 24 tailoring genes). In this collection, we also received an entire codon-optimized biosynthetic gene cluster, *cu-pks-4*, containing PKS (*Cu*-A) along with tailoring genes (*Cu*-B, *Cu*-D, *Cu*-halo, *Cu*-OMT) from *C. uncialis*. Details are provided in chapter 6.

2.6.3 Secondary metabolic analysis of *cu-pks-4* BGC

The nucleotide sequence of the *Cu*-A (PKS) gene from *cu-pks-4* BGC was formatted in FASTA format, ensuring accuracy and completeness without gaps or errors. The formatted sequence was

submitted to the antiSMASH version 7.0 (Blin et al., 2023). During submission, default parameters, including known Cluster blast, mibiG cluster comparison, and cluster Pfam analysis features, were selected. The results were analyzed upon completion of the run.

2.6.4 Gateway cloning of *Cu*-A gene in the pTYGSade expression vector

In general, Gateway cloning (LR) reactions were performed in a single microfuge to construct an expression vector containing the gene of interest **(Figure 16)**. The reaction mixture (final volume, 10 µL) was prepared by mixing 1-7 µL (50–150 ng) of an entry plasmid (pEYA) containing the desired genes, 1 µL of a destination (*Cu*-A pTYGSade) plasmid (150 ng/µL), and up to 8 µL of TE buffer at pH 8.0. After this, LR Clonase™ II enzyme mix (Thermo Fischer Scientific) was thawed on ice for approximately 2 minutes, followed by two 2-second vortex cycles. Subsequently, 2 µL of LR Clonase™ II enzyme mixture was added to the sample mixture and thoroughly mixed by vortexing. The reaction mixture was then incubated overnight at 25°C. The remaining enzyme mix was stored at either –20°C or –80°C (Although the protocol recommends 1 hour of incubation, overnight incubation was found to be successful during optimization.) pENTR™gus (an entry clone containing the Arabidopsis thaliana β-glucuronidase (gus) gene was used as a positive control in the LR reaction provided by the manufacturer.

To terminate the reaction, 1 µL of Proteinase K solution was added to each sample, followed by vortexing and incubation at 37°C for 10 minutes.

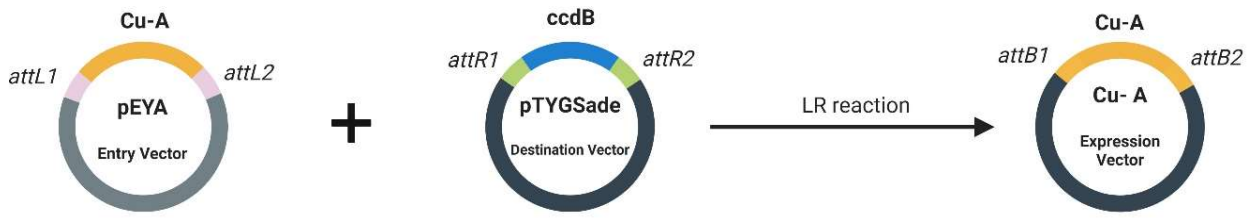

Figure 16: Schematic illustration of LR cloning of *Cu*-A gene using pEYA as the entry vector and pTYGSade as the destination vector. The expression vector is pTYGSade.

2.6.5 Transformation of the *Cu*-A pTYGSade expression vector in *E. coli*

In general, One Shot® ccdB Survival™ 2 T1R chemically competent cells (Thermo Fisher, Cat. no. A10460) were thawed on ice. Then, 1-5 µL (10 pg to 100 ng) of a Gateway mixture (from section 2.6.4) was added to each vial of competent cells for transformation. As a positive control, 1 µL (10 pg) of pUC19 was added to a separate vial of cells and gently mixed. The vials were then incubated on ice for 30 minutes. Subsequently, the cells were subjected to heat shock for 30 seconds at 42°C without shaking, followed by a 2-minute incubation on ice. Afterward, 250 µL of pre-warmed S.O.C. media was added to each vial, and the mixture was incubated at 37°C for 1 hour at 225 RPM. Finally, 25–100 µL of the transformation mixture were plated onto selective pre-warmed LB media supplemented with ampicillin (50 µg/mL), and the plates were incubated overnight at 37°C.

2.6.6 Isolation of *Cu*-A pTYGSade plasmid from *E.coli*

After overnight incubation, colonies that appeared on selective plates were picked (minimum 4 colonies) and inoculated into LB media with ampicillin (100 µg/mL). The cultures were then grown overnight at 37°C with shaking at 225 RPM. The *Cu*-A pTYGSade plasmid was then extracted from the overnight grown *E. coli* suspension using a GeneJET Plasmid Midiprep Kit

(Thermo Fisher Scientific) in accordance with manufacturer's guidelines. Positive transformants were screened via colony PCR using specific primers to confirm the presence of the desired DNA inserts. Once confirmed, the plasmid was sent for sequencing Genewiz, Azenta to validate the integrity and accuracy of the inserted DNA sequences.

2.6.7 Transformation of the *Cu*-A pTYGSade plasmid in *A. oryzae* NSAR1

Detailed in section 2.5.6.

2.6.8 Fermentation, extraction and characterization of metabolites produced by *Cu*-A pTYGSade transformants

After double selection of the *Cu*-A pTYGSade plasmid containing the *Cu*-A gene on Czapek-Dox media plates supplemented with amino acids (according to the plasmids), transformed *A. oryzae* NSAR1 colonies were sequentially inoculated into DPY media. This was performed in five baffled Erlenmeyer flasks (1000 mL), each containing 500 mL of media. The cultures were incubated at 30°C/160 RPM for seven days. As a control, untransformed *A. oryzae* NSAR1 was grown in two baffled Erlenmeyer flasks (1000 mL), each with 500 mL of media. For details on extraction, refer to sections 2.5.8.

2.6.9 Characterization of compounds produced by *Cu*-A pTYGSade transformants

The crude extract (~880 mg) was fractionated by passing through a pre-packed normal-phase spherical silica (Biotage® Sfär Silica) column (10 g, 60 μm) using a flash chromatography system (Biotage Isolera Prime 3.3.0). The flow rate was adjusted to 10 mL/min, and UV/VIS detection was monitored at 245 and 264 nm. A gradient of DCM: MeOH (100:0 to 80:20) was used. Compound **5** was eluted in a mixture of DCM: MeOH (98:2), while compound **6** was eluted

in a mixture of DCM: MeOH (90:10). These compounds were characterized by nuclear magnetic resonance (NMR). For the characterization data please refer to chapter 6.

2.6.10 Construction and transformation of pTYGSade and pTYGSmet plasmids

LR reactions (detailed in the section 2.6.4) were used to construct the three-gene plasmid (*Cu*-A_*Cu*-D_*Cu*-OMT pTYGSade plasmid) and the two-gene plasmid (*Cu*-B_*Cu*-halo pTYGSmet plasmid. Three gene plasmid (*Cu*-A_*Cu*-D_*Cu*-OMT pTYGSade) was then transformed into *A. oryzae* NSAR1 (as described in section 2.5.6). Positive transformants were selected by growing them on Czapek-Dox media plates (lacking adenine). Positive *A. oryzae* NSAR1 transformants were inoculated into DPY media. This procedure was performed in five baffled Erlenmeyer flasks (1000 mL), each containing 500 mL of media. The cultures were incubated at 30°C/160 RPM for seven days. As a control, untransformed *A. oryzae* NSAR1 was grown in two baffled Erlenmeyer flasks (1000 mL), each with 500 mL of media. For details on the extraction and characterization of metabolites, please refer to sections 2.5.8 and 2.5.9.

2.6.11 Co-transformation of pTYGSade and pTYGSmet plasmids

Plasmid co-transformation involved the transformation of three gene plasmid (*Cu*-A_*Cu*-D_*Cu*-OMT pTYGSade) and the two-gene plasmid (*Cu*-B_*Cu*-halo pTYGSmet) into *A. oryzae* NSAR1. These plasmids possess distinct origins of replication and selection markers. Initially, both plasmids were simultaneously transformed into *A. oryzae NSAR1* (for methodology refer section 2.5.6) and selected on double selection media plates lacking adenine and methionine. However, this approach was unsuccessful. Subsequently, protoplast of the *A. oryzae NSAR1* transformant containing the three-gene plasmid pTYGSade (*Cu*-A, *Cu*-D, and *Cu*-OMT) was prepared. Protoplasts derived from these transformants were then used for the second

transformation, wherein the pTYSGmet plasmid (*Cu*-B and *Cu*-halo) was transformed into the existing transformants containing three genes pTYGSade transformant **(Figure 17)** following the same procedure outlined in section 2.5.6, except here the selective media plates lack adenine and methionine for double selection of the transformant having both plasmids with 5 genes (*cu-pks-4*, BGC) in total. The plates were incubated upside down at 30°C for four to seven days until the *A. oryzae NSAR1* colonies appeared. Spores from transformant colonies were then inoculated into plates lacking sorbitol using an inoculating loop. These plates were also incubated upside down at 30°C for another four to seven days.

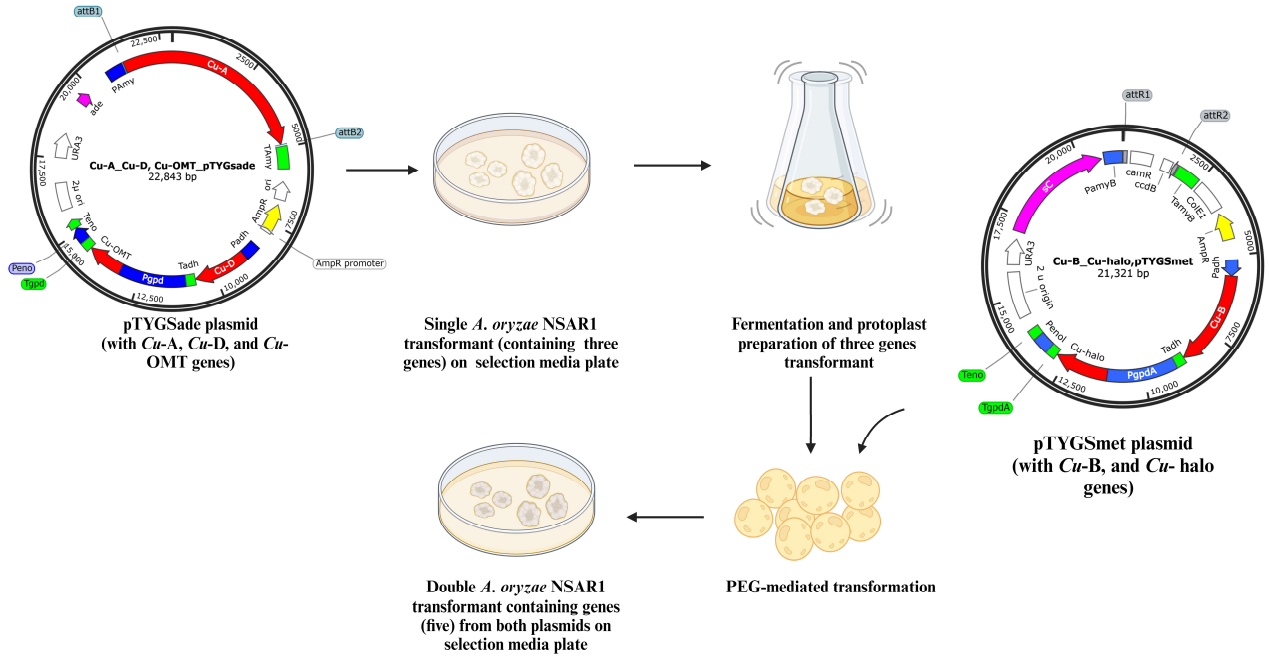

Figure 17: Schematic workflow representation of the co-transformation of two plasmids: pTYGSade (left), carrying *Cu*-A, *Cu*-D, and *Cu*-OMT genes, and pTYGSmet (right), carrying *Cu*-B and *Cu*-halo genes, into *A. oryzae* NSAR1. For clear visualizations of the plasmid maps, please refer to **Figure 53**.

2.6.12 Confirmation of integration of genes into *A. oryzae* NSAR1 genome

Three colonies were randomly selected and each of them was inoculated into 100 mL of DPY at 30°C for four days. Following incubation, the culture broth was filtered, and approximately 0.05 g of tissue was used for gDNA isolation. Mycelia were first frozen in liquid nitrogen and then pulverized into fine powder using a pestle and mortar. The E.Z.N.A. fungal DNA mini kit (Omega) was used for gDNA extraction, following the manufacturer guidelinesF. The ground mycelia were then divided into microfuge tubes and stored at -80°C for future use. Out of that, one microfuge tube was used for PCR **(Figure 18).**

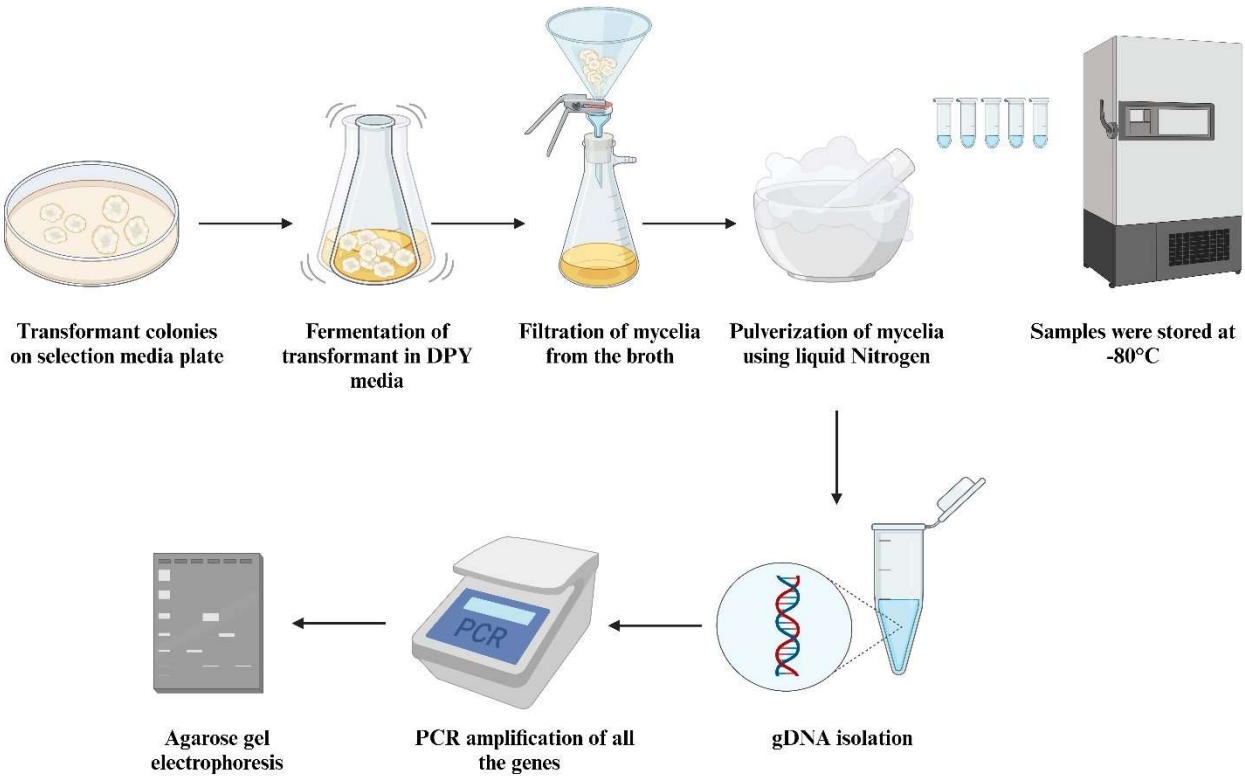

Figure 18: Illustration of workflow to confirm the chromosomal integration of genes in the *A. oryzae* NSAR1 transformant.

To confirm the chromosomal integration of individual genes, gene-specific primers listed in **(Table S1)** were used to amplify approximately 800 bp of both the promoter and gene sequences. The primers used for each gene were as follows: *Cu*-A (Amy-for/TerA-rev), *Cu*-B (padh-for/TerB-rev), *Cu*-D (padh-for/TerD-rev), *Cu*-OMT (pgpdA-for/OMT-rev), and *Cu*-halo (pgpdA-for/Halog-rev). All PCR reactions were performed using Dream Taq DNA polymerase and reagents (ThermoScientific). The reagents for each 25 µL reaction volume included: 2.5 µL of 10X DreamTaq Buffer (containing 20 mM $MgCl_2$), 2.5 µL of 2 mM dNTP mix, 1 µL of 10 µM forward primer, 1 µL of 10 µM reverse primer, template DNA (variable concentration), 0.2 µL of 1.25 U DreamTaq DNA polymerase, and nuclease-free water to make the volume to 25 µL.

PCR was performed using a Bio-Rad thermocycler under the following conditions: initial denaturation at 95°C for 2 minutes, followed by 35 cycles of denaturation at 95°C for 30 seconds, annealing at 55-65°C (3-5°C below primer Tm) for 30 seconds, and extension at 72°C for 30 seconds per KB, with a final extension at 72°C for 10 minutes and an indefinite hold at 4°C. Amplicons were electrophoresed on a 1% agarose gel containing 2 µL of SYBR Safe DNA gel stain (Invitrogen) and run for approximately 45 minutes using a Bio-Rad gel box and a VWR powerpack set to 230 mA and 200 V. The amplicons were visualized using a transilluminator.

2.6.13 Real-time quantitative reverse transcription polymerase chain reaction (RT-qPCR)

RNA was isolated from the samples prepared in section 2.6.12 using E.Z.N.A. fungal RNA mini kit (Omega), by following the manufacturer's protocol. Total RNA was first transcribed into complementary DNA (cDNA) using reverse transcriptase. The cDNA was then used as the template for quantitative PCR (qPCR), with the amount of amplification measured in each PCR

cycle using SYBR fluorescence. RT-qPCR was performed in a single-step microfuge tube using SYBR green super mix (iTaq Universal) in one step. For a 20 µL reaction volume, the mixture included 10 µL of 2X master mix with SYBR (iTaq Universal), 5 µL of RNA template, 0.25 µL of reverse transcriptase (iTaq universal), 0.6 µL of 10 µM forward primer, 0.6 µL of 10 µM reverse primer, and 3.6 µL of high-purity H_2O. The PCR conditions were as follows: initial denaturation at 50°C for 10 minutes, 95°C for 3 minutes followed by 35 cycles of denaturation at 95°C for 5 seconds, annealing at 60°C for 1 minute, and a melt curve was analyzed at the end.

2.6.14 Fermentation and Extraction of metabolites produced by co-transformants

The transformant containing the complete biosynthetic gene cluster (BGC) *cu-pks-4*, which includes five genes, was selected for cultivation. It was grown in DPY media at 30°C with shaking at 160 RPM for seven days. The genes in pTYSade and pTYGSmet constructs are regulated by constitutive promoters: *Cu*-A by the amy (amylase) promoter, *Cu*-D and *Cu*-B by the adh (alcohol dehydrogenase) promoter, and *Cu*-OMT and *Cu*-halo by the gpd (glyceraldehyde-3- phosphate dehydrogenase) promoter. After the seven-day incubation, the culture was homogenized using a blender and then filtered through cheesecloth. The resulting filtrate was transferred to a separating funnel, and the pH was adjusted to 3 by adding 6 M HCl. An equal volume of ethyl acetate was added to the broth, and the mixture was stirred for 20 minutes. The filtrate was then transferred into a separating funnel and shaken twice to separate the aqueous and organic phases. After complete separation, the water phase was re-extracted twice and dried by adding anhydrous $NaSO_4$. This was removed by filtration. The organic extract was dried under a vacuum on a rotary evaporator.

2.6.15 Characterization: Biotage purification, NMR and, LC-MS of metabolites produced by co-transformants

The crude extract (550 mg) was fractionated using a pre-packed normal-phase spherical silica (10 g, 60 μm) flash chromatography column (Biotage ® Sfär Silica) with a Biotage Isolera Prime 3.3.0 apparatus. The flow rate was maintained at 10 mL/min, and UV-VIS detection was performed at 264 and 245 nm. A gradient of DCM: MeOH was employed, beginning with 100% DCM and progressing to DCM: MeOH (7:3). Fractions were collected in test tubes and analyzed by thin-layer chromatography (TLC). Test tubes containing similar compounds were pooled together. The waste containing non-UV active compounds was also collected and dried under vacuum using a rotary evaporator. The compounds were then characterized by nuclear magnetic resonance (NMR) and liquid chromatography-mass spectrometry (LC-MS).

2.7 Materials and methods related to chapter 7

In Chapter 6, we observed that nr-PKS *Cu*-A from *C. uncialis* shares significant homology (~60%) with nr-PKS TerA from *Aspergillus terreus*. In a recent publication, Dr. Russel Cox's research group demonstrated that the heterologous expression of TerA in *Aspergillus niger* results in the production of triketide lactone, 6,7-dihydroxymellein, and orsellinic acid as a shunt metabolite (Kahlert et al., 2021). However, in our heterologous expression of *Cu*-A in *A. oryzae* (please refer to chapter 6), we did not observe the formation of 6,7-dihydroxymellein or orsellinic acid. This led us to hypothesize that the role of PKS may differ in *C. uncialis*. To further investigate the role of the O- methyl transferase (OMT) enzyme within the same BGC, we performed following feeding experiments with an *A. oryzae* OMT transformant with orsellinic acid and orsellinic acid methyl ester **(Figure 19)** to investigate whether the OMT enzyme catalyzes the methylation of the oxygen atom of orsellinic acid or methyl orsellinate.

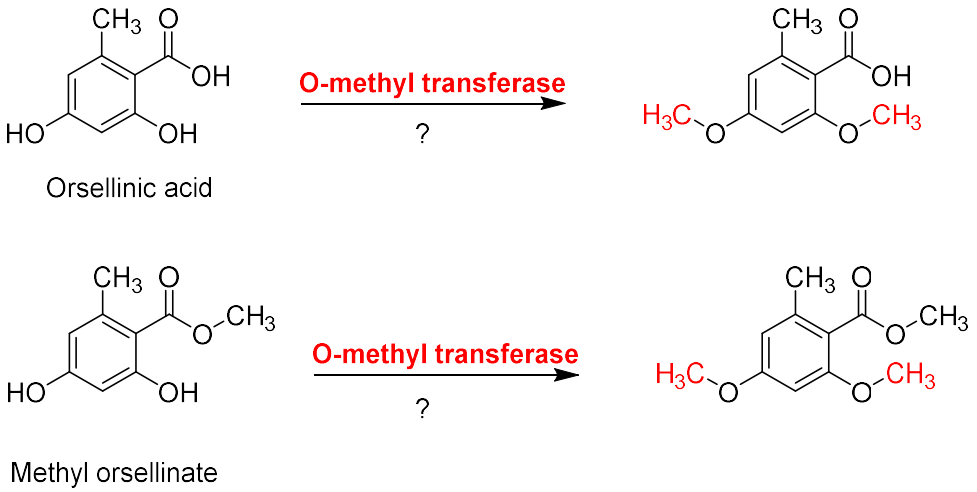

Figure 19: Potential methylation of orsellinic acid and its methyl ester by O-methyl transferase enzyme from *C. uncialis*.

2.7.1 Transformation of *Cu*-OMT pTYGSade plasmid into *A. oryzae* NSAR1

The pTYGSade plasmid containing the codon-optimized O-methyl transferase (*Cu*-OMT) gene was transformed into *A. oryzae* NSAR1 using the protocol described in the section 2.5.6. The transformants were selected by culturing them on Czapek-Dox media plates lacking adenine twice.

2.7.2 Feeding the transformants with orsellinic acid

The *A. oryzae* NSAR1 transformants carrying the *Cu*-OMT gene from section 2.7.1 were cultured in DPY media in five baffled Erlenmeyer flasks (500 mL) each containing 100 mL of media. The cultures were incubated at 30°C with shaking at 160 RPM for five days. For control untransformed *A. oryzae* NSAR1 was grown in two baffled Erlenmeyer flasks (500 mL) with 100 mL of media. After five days, 10 mg of orsellinic acid (Biosynth Carbosynth) was dissolved in DMSO and added to five *A. oryzae* NSAR1 transformant flasks and one untransformed *A. oryzae* NSAR1 control flasks. The cultures were then incubated at 30°C with shaking at 160

RPM for an additional two days. After seven days, the cultures were extracted; refer to sections 2.5.8. The crude extract was obtained through ethyl acetate extraction from all cultures and was analyzed using NMR to assess the presence of additional methyl group.

2.7.3 Feeding the transformants with methyl orsellinate

Methyl orsellinate (10 mg) was fed to *A. oryzae* NSAR1 transformants **(Figure 20)** carrying the *Cu*-OMT gene from section 2.7.1. The experiment mentioned above in section 2.7.2 was repeated, the only change was substrate. The cultures were incubated for 7 days, yielding a total of 170 mg of crude extract from *Cu*-OMT transformants. The crude extract (170 mg) was further fractionated by flash chromatography column (Biotage ® Sfär Silica). A gradient of dichloromethane (DCM): methanol (MeOH) (100:0 to 80:20) was used. This eluted partial pure compound **10** in a mixture of DCM: MeOH (97:3). The identity of compound **10** was confirmed by nuclear magnetic resonance (NMR) and liquid chromatography-mass spectroscopy (LC-MS). The complete characterization data is provided in chapter 7.

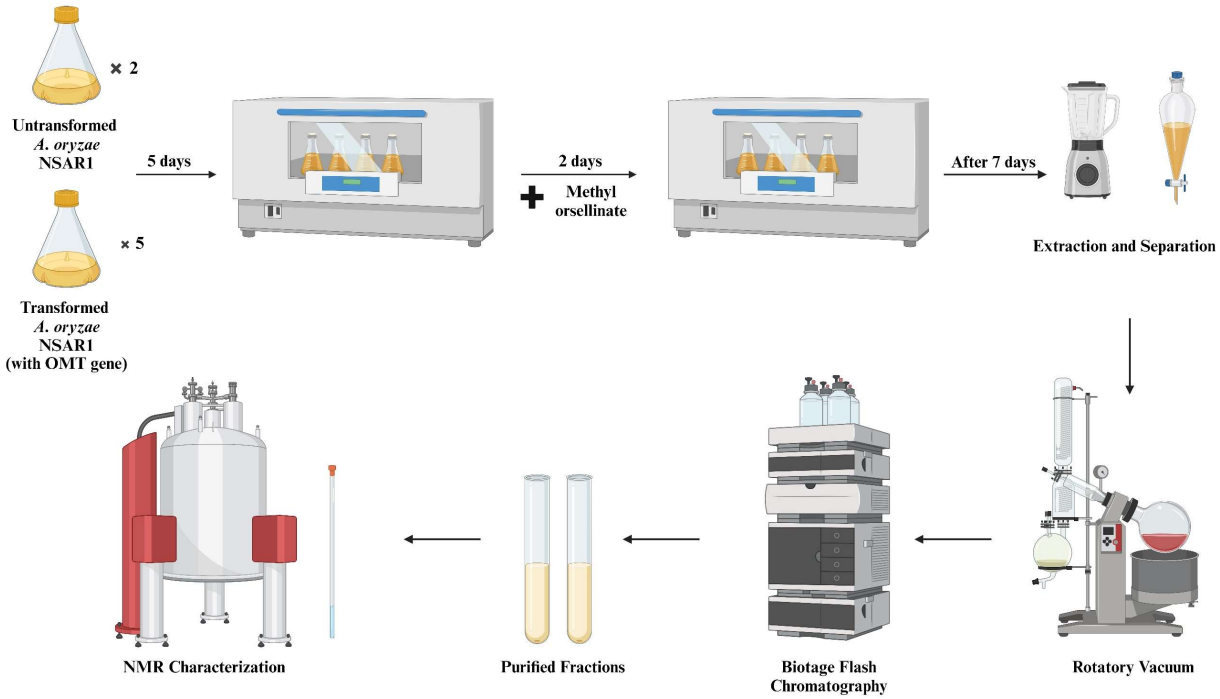

Figure 20: Schematic representation of a feeding experiment conducted on *A. oryzae* transformants using methyl orsellinate.

2.7.4 Feeding with ^{13}C-labeled sodium acetate

The *A. oryzae* NSAR1 transformants carrying the *Cu*-OMT gene from section 2.7.1 were cultured in DPY media in four baffled Erlenmeyer flasks, untransformed *A. oryzae* NSAR1 in three baffled Erlenmeyer flasks (500 mL), each with 100 mL of media, and one media control. The cultures were incubated at 30°C with shaking at 160 RPM for five days. After five days, 10 mg of methyl orsellinate was added along with 5mM ^{13}C-labeled sodium acetate (Cambridge Isotope Labs) in one flask. The controls are detailed in **Figure 21.**

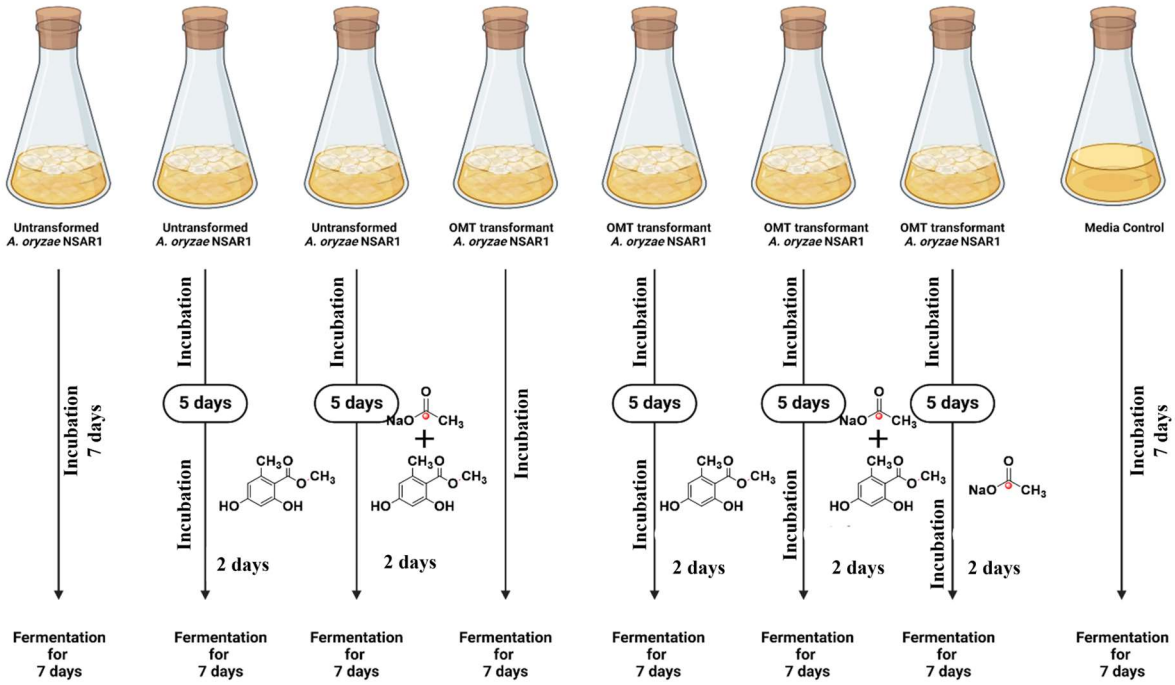

Figure 21: Experimental setup for isotope labeling with ^{13}C-labeled sodium acetate and methyl orsellinate as substrate. A. oryzae NSAR1 cultures and controls were cultured for five days. Substrates were then added to selected flasks, and incubation continued for an additional two days, making a total fermentation of seven days.

Chapter 3

Isolation of Bioactive Metabolites from Soil Derived Fungus- *Aspergillus fumigatus*

This chapter is already published. I am the primary contributor to this work. I acknowledge Dr. Ayush Kumar for providing bacterial strains, Dr. Georg Hausner for fungal strains to perform antimicrobial testing, and Ellen M. E. Sykes (2nd author) for helping with antibacterial testing.

Gill, H., Sykes, E. M. E., Kumar, A., & Sorensen, J. L. (2023). Isolation of Bioactive Metabolites from Soil Derived Fungus-*Aspergillus fumigatus*. *Microorganisms*, *11*(3), Article 3. https://doi.org/10.3390/microorganisms11030590.

3.1 Introduction

Naturally occurring bioactive compounds produced by microorganisms and their structural analogs have been a continuous source of new lead molecules in the pharmaceutical industries. There are almost 22,500 bioactive secondary metabolites from almost all living organisms, including eukaryotes (fungi, plants, and animals) and prokaryotes (bacteria and cyanobacteria)(Bérdy, 2005; Mahajan & Balachandran, 2015). Fungi are the second most diverse (3-5 million species) kingdom on earth; almost 9000 bioactive compounds ranging from anti-microbial, -cancer, -allergic, and -oxidant are produced by fungi (Manganyi & Ateba, 2020). The most prolific producers of natural products are ascomycetes fungi (*Aspergillus*, *Fusarium*, and *Penicillium*)(Manganyi & Ateba, 2020).

Aspergillus is one of the largest and most intensively investigated taxon of fungi. There are more than 180 species in this genus, including *A. fumigatus*, *A. flavus*, *A. niger*, and *A. terreus* (W.-Y.

Zhao et al., 2022). *Aspergillus fumigatus*, a ubiquitous fungus, is widely distributed ranging from air, soil, and even on the International space station (Blachowicz et al., 2019; Knox et al., 2016). It plays an essential ecological role as a decomposer of carbon and nitrogen sources (Dagenais & Keller, 2009; Tekaia & Latgé, 2005) and biological role by producing a broad array of secondary metabolites (Wiemann et al., 2013). In total, *A. fumigatus* has demonstrated the potential to produce at least 226 bioactive molecules (Frisvad et al., 2009) and of these 36 chemical structures have been putatively linked to biosynthetic gene clusters (BGCs) in the *A. fumigatus* genome (Bignell et al., 2016; Lind et al., 2017). A single BGC has the potential to produce structurally and functionally diverse bioactive compounds (Fischbach & Clardy, 2007). For example, the production of ferroverdins and bagremycins, two classes of metabolites with distinct bioactivities, comes from the same BGC. It has been observed that the activation of this biosynthetic pathway is determined by the availability of iron (Martinet et al., 2019). This is an example of how BGCs can form "superclusters" that function to biosynthesize two or more similar molecules (Martinet et al., 2019). Thus, it provides an opportunity to explore the chemical space of *A. fumigatus*.

In our continuing investigation of bioactive secondary metabolites, a strain of *A. fumigatus* was obtained from a soil sample collected underneath a lichen thallus in Manitoba. The crude extract of this fungus displayed antimicrobial activity in preliminary bioassays. Bioassay-guided fractionation of the extract resulting in the isolation and identification of two compounds (**Figure 22**), N-formyl-4-hydroxyphenyl-acetamide **1**, and atraric acid **2** with a yield of ~117 mg/L and ~18 mg/L, respectively. The structures of these compounds (**1** and **2**) were elucidated using spectroscopic analysis. Additionally, antimicrobial evaluation of these compounds revealed that these compounds exhibited significant antifungal activity against five selected fungal strains and

modest antibacterial activity against multi-drug-resistant bacterial strains. To the best of our knowledge, this is the first report of these compounds from *A. fumigatus*. Previous reports on N-formyl-4-hydroxyphenyl-acetamide (Compound **1**) have only been from two sources (in unknown marine-derived fungus (X. Li et al., 2006) and *Penicillium chrysogenum* (An et al., 2013)), with yields of ~1-3 mg/L. Herein, *A. fumigatus* showed significantly higher yields of ~117 mg/L. More significantly, this appears to be the first report of atraric acid **2** being isolated from a non-lichen fungal strain. In this chapter, we describe the results and discussion of production, isolation, structural elucidation, and bioactive profiling of these compounds (**1** and **2)**.

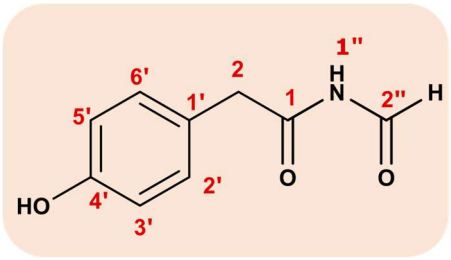

Compound **1**

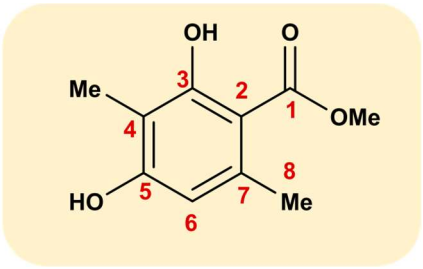

Compound **2**

Figure 22: Chemical structures of N-formyl-4-hydroxyphenyl-acetamide **1** and atraric acid **2**.

3.2 Fungal isolation and preliminary selection

In total, six fungal isolates with different morphologies were successfully isolated from underneath the soil sample of the lichen thallus. One out of six isolates were observed stunting the growth of neighboring fungi on the PDA plate **(Figure 23 b)**. Therefore, the crude extracts of all isolates were screened for antagonistic activities against bacterial (*Acinetobacter baumannii* RND efflux pump deficient strain AB258, *Acinetobacter baumannii* wild type ATCC 17978, *Pseudomonas aeruginosa* RND efflux pump deficient strain PAO750, MRSA

ATCC43300) and fungal strains (*Trichoderma citrinoviride* strain *SL-2202*, *Aspergillus oryzae* NSAR1, *Aspergillus spp.* strain SL-2201, *Ganoderma lucidum* strain WIN(M)1804, and *Pleurotus ostreatus* strain WIN(M)1803). The crude extract, from the S4, (the fungus that inhibited the growth of surrounding fungi) exhibited antibacterial activity, especially against MRSA and *Acinetobacter baumannii* RND efflux pump deficient strain AB258 with 19 mm and 16 mm zone of inhibition **(Figure 23 d, e)**, respectively. Similarly, the crude extract showed strong antifungal activity with a larger zone of inhibition (36 mm) against *Aspergillus spp.* strain SL-2201 **(Figure 23 f)**. Therefore, the strain, S4, was selected and analyzed for further experiments.

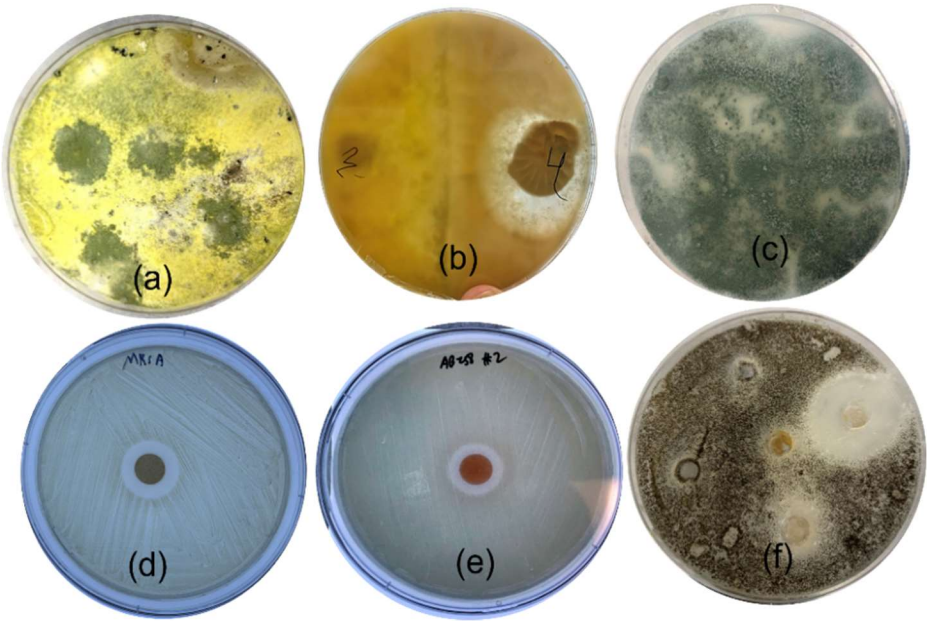

Figure 23: (a) Growth of fungi from soil sample (b) Inhibition of neighboring fungus by fungus S4 (c) Monospore subculture of sample S4 fungus (*Aspergillus fumigatus* strain SL-2203) (d) Activity of crude extract against MRSA, (e) Activity of the crude extract against *Acinetobacter baumannii* AB258, and (f) Antifungal activity of the crude extract against *Aspergillus spp*. strain SL-2201.

3.3 Identification of fungus

To identify fungal strain S4, DNA barcoding was used. The ITS fragment of approximately 600 bp was amplified and sequenced. NCBI BLAST analysis showed that the query sequence shared a high degree of homology with *Aspergillus fumigatus* (accession number: MT529131.1), with 99% query coverage and 98.51% sequence similarity **(Figure S 7)**. A phylogenetic tree was constructed using the fungal strain S4 ITS region, along with a few closely related species like *Aspergillus ruber*, *Aspergillus fischeri*, *Aspergillus flavus*, *Aspergillus niger* and other reference sequences **(Table 4)** obtained from GenBank. *Penicillium sp.* was used as an out-group

Table 4: Reference fungal isolates used in the phylogenetic analysis of present study and their GenBank accession numbers.

S. No	Species	GenBank Accession
1	*Aspergillus fumigatus*	MT529131.1
2	*Aspergillus flavus*	NR_111041.1
3	*Aspergillus niger*	OM802854.1
4	*Aspergillus terreus*	MT436785.1
5	*Aspergillus ruber*	NR_131286.1
6	*Aspergillus fischeri*	NR_137479.1
7	*Penicillium sp.*	KY930467.1

Phylogenetic analysis further confirmed that query sequence S4 clustered monophyletically with *Aspergillus fumigatus* MT529131.1 **(Figure 24)** using 100 bootstrap support. Based on these results **(Figure 24)**, the isolated strain S4 was identified as *Aspergillus fumigatus* strain SL-2203.

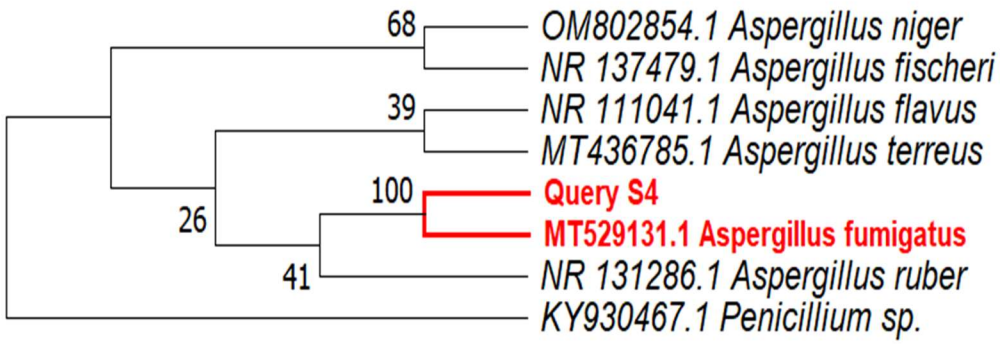

Figure 24: Phylogenetic tree showing the relationship between the ITS sequence of strain S4 and other fungal strains retrieved from GenBank based on a BLASTn search. The tree was constructed using the neighbor joining (NJ) method with MEGA 7.0 using *Penicillium sp*. as an outgroup. Bootstrap values are based on 1000 replicates.

3.4 Fermentation, extraction, and isolation of compounds

A. fumigatus S4 was grown in 2 L of PDB at 28 ± 2°C for 7 days. The ethyl acetate extraction from 2L culture broth yielded 650 mg of the crude extract. The chromatographic fractionation of the crude extract yielded two main compounds **1** (~117 mg/L) and **2** (~18mg/L).

3.5 Structure Identification

The structures of compounds **1** and **2** were identified by nuclear magnetic resonance (NMR) and liquid chromatography-mass spectroscopy (LC-MS). In addition, the data **(Figure S 1** to **Figure S 6)** were compared with the literature (X. Li et al., 2006; Mun et al., 2020).

Compound **1** (N-formyl-4-hydroxyphenyl-acetamide): Colorless crystals; ^{1}H NMR (MeOD, 500 MHz) δ_H 9.06 (1H, s, H-2”), 7.11 (2H, d, J = 8.1 Hz, H-2’, 6’), 6.76 (2H, d, J = 8.1 Hz, H-3’, 5’), 3.57 (2H, s, H-2), ^{13}CNMR (MeOD, 125 MHz); δ_C 173.5 (C-1), 163.4 (C-2”),156.3 (C-4’), 130.0 (C-2’,6’), 124.1 (C-1’), 115.0 (C-3’, 5’), 41.6 (C-2); HMBC correlations: H-2/C-1’,-2’/-6’, -2”,-1; H-2’/C-2, -3’, -4’; H-3’/C-1’, -2’, -5’, -4’.The molecular formula of compound **1** (**Figure 25**)

is $C_9H_9NO_3$, a molecular ion of [M-H] 178.0581 (179.0582 calculated) was observed with negative ion mode of LC-MS.

Compound **2** (atraric acid): Colorless oil; ^{1}HNMR (MeOD, 500 MHz); δ_H 6.13(1H, s, H-6), 3.78(3H, s, H-10), 2.27(3H, s, H-8), 1.96 (3H, s, H-9), 11.92 (ArOH-3), ^{13}CNMR (MeOD , 125 MHz); δ_C 172.5 (C-1), 162.5 (C3), 159.7 (C-5), 139.6 (C-7), 110.2 (C-6), 108.4 (C-4), 103.5 (C-2), 50.6 (C-10), 22.9 (C-8), 6.7 (C-9). LC-MS was identical to the literature (Mun et al., 2020).

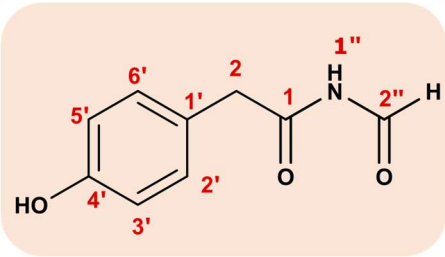

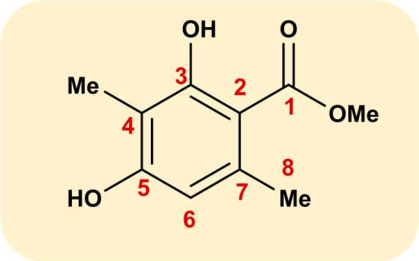

(1) **(2)**

Figure 25: Chemical structures of N-formyl-4-hydroxyphenyl-acetamide (**1**) and atraric acid (**2**).

3.6 Antimicrobial activities

3.6.1 Antibacterial activities

Compounds **1**, **2**, and an equimolar mixture of **1** and **2** (Synergistic effect), as well as the crude extract were tested for their antibacterial activity against *Acinetobacter baumannii* RND efflux pump deficient strain AB258, *Acinetobacter baumannii* wild type ATCC17978, *Pseudomonas aeruginosa* RND efflux pump deficient strain PAO750, and MRSA. The results showed that compounds **1** and **2** inhibited RND efflux pump deficient bacterial strains (*Acinetobacter baumannii*, *Pseudomonas aeruginosa*) with a concentration between 50µg/mL to 200µg/mL. The synergistic effect of compounds **1** and **2** is almost similar to those observed when these

compounds were tested individually, meaning that no synergism between compounds **1** and **2** was observed. The maximum zones of inhibition for compounds **1** and **2** (19.1 mm and 10.2 mm) **(Figure 26)** were reported against *Acinetobacter baumannii* AB258 at a concentration of 200 µg/mL. Although a zone of inhibition (19 mm) was observed for the crude extract against MRSA, the isolated compounds did not exhibit any activity against the same bacteria. The positive control ciprofloxacin (25 µg/mL) exhibited the maximum zone of inhibition (26.9 mm) against *Pseudomonas aeruginosa*. No zone of inhibition was observed for the negative control (methanol), for any bacterial strains.

Further, the minimum inhibition concentration (MIC) values were evaluated. The MIC values of Compounds **1**, **2, 1**+**2** (Synergistic effect), and crude extract was > 100 µg/mL. However positive control (ciprofloxacin) showed MIC 10 µg/mL.

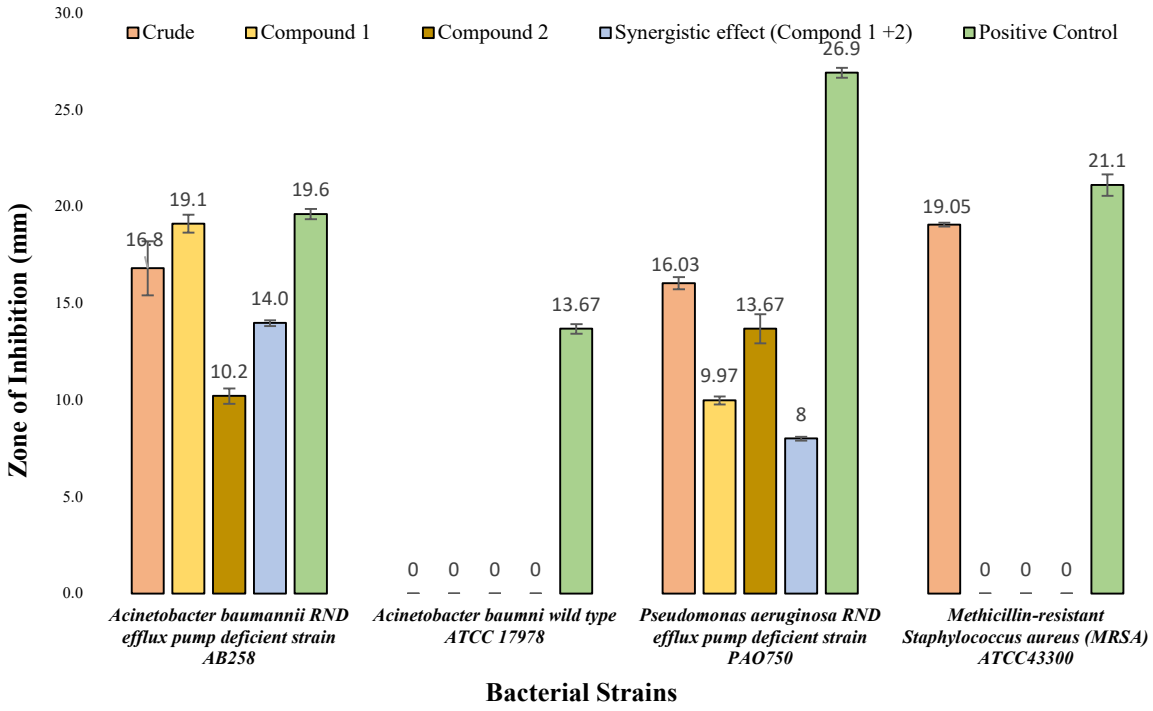

Figure 26: Average diameter of zone of inhibition (mm) of crude extract, compound **1**, compound **2**, synergistic effect of compounds **1** and **2**, and a positive control (ciprofloxacin) against four clinical

isolates of multi-drug-resistant bacterial strains. Data is presented as mean ± SD from three independent experiments, with a significance level of $p < 0.05$. versus the control group.

3.6.2 Antifungal activities

The evaluation of the inhibitory effect of compounds **1** and **2** against five selected fungal strains was performed at a concentration of 100 μg/mL, 200 μg/mL, 300 μg/mL, and 500 μg/mL. This was performed by comparing the average diameters (mm) of mycelial growth in plates with and without (control) compounds **(Figure 28)**. The control group consisted of mycelia grown without any added compounds. Results showed that compared to control compound **2** displayed strong inhibition against all the selected strains, with inhibition ratios ranging from 13% to 87% **(Figure 27)**. In contrast, compound **1** exhibited mycelial inhibition only against *Aspergillus oryzae* NSAR1 (~14%), *Ganoderma lucidum* strain WIN(M)1804 (~20%), and *Pleurotus ostreatus* strain WIN(M)1803 (~80%).

Furthermore, the highest inhibitory effect was observed against *Pleurotus ostreatus strain* WIN(M)1803 **(Figure 27)**, with inhibitory ratios of 79% and 88% for compounds **1** and **2**, respectively.

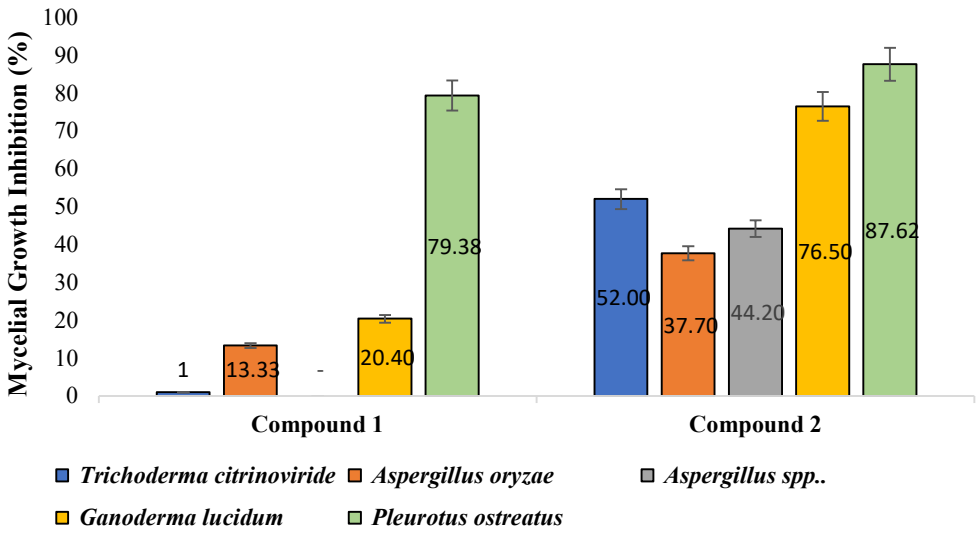

Figure 27: The percentage of mycelial growth inhibitions of compounds **1** and **2** against five fungal strains, as compared to a control growth plate. The inhibition was calculated as mean ± SD (n=3) and were considered significant at $p < 0.05$ in comparison to the control group.

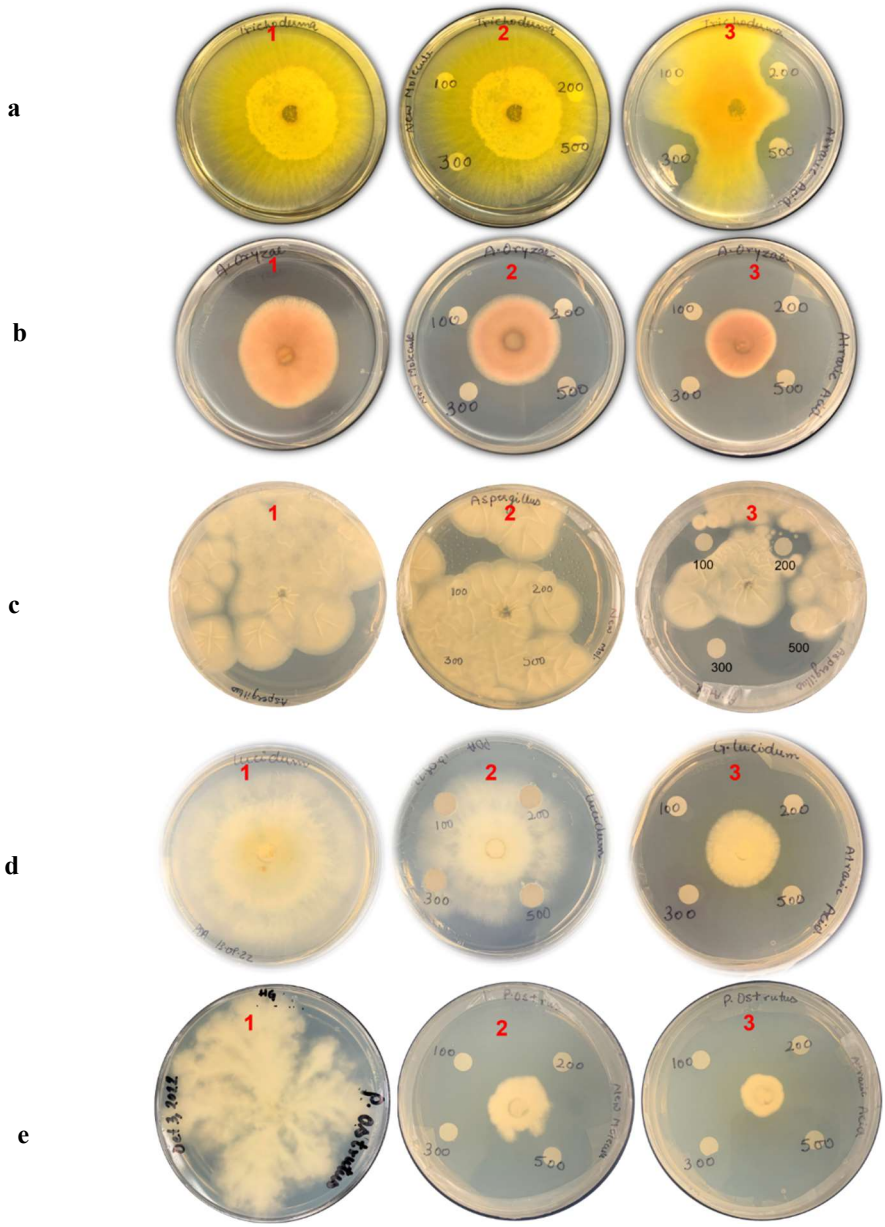

Figure 28: The antifungal activity of compounds **1** and **2** at a concentration of 100 µg/mL, 200 µg/mL, 300 µg/mL, and 500 µg/mL on the mycelium growth of different fungal strains (a) *Trichoderma citrinoviride* strain SL-2202, (b) *NSAR1 Aspergillus oryzae*, (c) *Aspergillus spp.* strain SL-2201, (d) *Ganoderma lucidum* strain WIN(M)1804, (e) *Pleurotus ostreatus* strain WIN(M)1803, (1) Control; (2) Compound **1**; (3) Compound **2**.

3.7 Discussion

Aspergillus is a diverse genus of fungi that are known as prolific producers of structurally diverse classes of compounds (X. Zhang, Li, et al., 2018), such as alkaloids (Shi et al., 2015; Song et al., 2012; W. Y. Zhao et al., 2010) anthraquinones (D.-H. Li et al., 2016; Y. Zhang et al., 2012), drimane sesquiterpene lactone (Felix et al., 2013), sterigmatocystin analogs (Song et al., 2014), and many more. Several natural products produced by *Aspergillus* are well-known for their pharmaceutical values such as lovastatin as a cholesterol-lowering drug (Boruta & Bizukojc, 2017), butenolide derivatives as an anti-inflammatory agents (M. Liu et al., 2018), 3′-(3-Methylbutyl)-butyrolactone II as antifungal (Cazar et al., 2005), and aurasperone H as an anticancer drug (D.-H. Li et al., 2016). These compounds have great medicinal applications, while *Aspergillus* species also have been reported to produce mycotoxins such as aflatoxins, ochratoxin A, and fumonisins (Perrone & Gallo, 2017). Despite this, scientists are actively investigating the potential benefits of compounds produced by these species.

In this study, a single strain of *Aspergillus fumigatus* strain SL-2203 was successfully sub-cultured from a soil sample that was fortuitously collected with a sample of lichen thallus. After applying the soil sample to a PDA plate, it was observed that one of the fungal strains present appeared to inhibit the growth of other fungal strains present on the plate. This suggested that this specific fungal strain was producing some antifungal natural products that warranted further investigation. This strain of fungus (*S4)* was selected to screen for potential antimicrobial metabolites. Subculturing of this fungus from the original soil plate and subsequent sequencing of the ITS region and construction of a phylogenetic tree revealed that this fungus (S4) shared ~99% sequence similarity (100 bootstrap value) with *Aspergillus fumigatus* (MT529131.1).

To investigate the bioactive metabolites produced by this strain of *A. fumigatus,* a large scale (2 L) fermentation culture in PDB was prepared. The crude EtOAc extracts displayed prominent bioactivity against MRSA and *Acinetobacter baumannii* AB258 (19 mm and 16 mm zone of inhibition, respectively). Similarly, the crude extract showed strong antifungal potential with a zone of inhibition (36 mm) against a stock strain of an environmentally isolated *Aspergillus spp.* strain SL-2201.

Subsequent bioassay (antifungal) guided fractionation of this crude EtOAc extract over silica gel afforded two pure molecules, compound **1** (~ 117 mg/L) and compound **2** (~18 mg/L). The structures of compounds **1** and **2** were successfully identified using NMR and LC-MS, and the results were compared with literature data to confirm their accuracy. The spectroscopic characterization of these two isolated metabolites revealed that compound **1** was N-formyl-4-hydroxyphenyl-acetamide and compound **2** was atraric acid.

The bioactivity profile of compounds **1**, **2**, and a mixture of both (**1**+**2**) was evaluated against a panel of four clinically isolated multi-drug-resistant bacterial strains and five non-pathogenic fungal strains **(Table 1)**. The maximum zones of inhibition for compound **1** and **2** (19.1 mm and 10.2 mm) **(Figure 26)** was reported against *Acinetobacter baumannii* AB258. These findings showed that compounds **1** and **2** has exhibited inhibition only against RND efflux pump deficient bacterial strains but not *Acinetobacter baumannii* wild type ATCC 17978, suggesting that efflux might be an important method for the removal of these molecules from bacterial cells. The synergistic effect of compounds **1** and **2** was similar to when tested individually. A zone of inhibition (19 mm) was also observed for the crude EtOAc extract against MRSA; however, neither **1** nor **2** displayed any inhibitory activity against this same strain of bacteria. This suggests

that there were additional compounds present in the crude extract that was not recovered in the subsequent purification process.

We also observed the antifungal activity of **1** and **2** when assayed against a series of fungal strains. It was observed that atraric acid **2** displayed excellent bioactivity in inhibiting fungal growth and that compound **1** (N-formyl-4-hydroxyphenyl-acetamide) exhibited moderate activity. The mycelial growth of the five fungal strains that we assayed were significantly inhibited by compound **2**, ranging from 37% to 87% inhibition of fungal growth depending on which strain was assayed. The inhibitory effect of compounds **1** and **2** against *Pleurotus ostreatus* strain WIN(M)1803 was the highest, with an inhibition ratio of 79.38 % and 87.62 %, respectively. The antifungal activity of **2** may provide some rationale for the biosynthesis of this molecule by both lichen and non-lichen fungi as competition for resources against other fungi in the environment would be a significant challenge.

There have been only two previous reports of N-formyl-4-hydroxyphenyl-acetamide **1** being isolated as a natural product. Compound **1** has been described as being produced by a strain of an unknown marine-derived fungus and was assayed for radical scavenging (X. Li et al., 2006) where it displayed strong activity. A second report of the isolation of **1** was from a strain of *Penicillium chrysogenum* where it displayed moderate cytotoxicity against Du145, A-549, and HeLa cell lines (An et al., 2013).To the best of our knowledge, these are only two reports of the isolation of compound **1**. In these previous reports the yield of **1** was observed in a range of 1 -3 mg / L, however our strain of *A. fumigatus* was producing considerably higher yields of ~ **120 mg/L** in unoptimized growing conditions. The reasons for this high level of production of **1** are not immediately apparent but may be linked to the unique ecological niche from which this strain

of *A. fumigatus* was isolated. The production of compound **1** may be an adaptation mechanism to being in soil underneath a lichen thallus that produces an array of secondary metabolites.

Atraric acid **2**, has been previously reported as a metabolite in lichen fungi (Mun et al., 2020) and it has been reported that **2** can exhibit anti-cancer activity against prostate cancer, act as an antagonist of androgen receptor (Hessenkemper et al., 2014), and possesses antioxidant and antimicrobial (Güvenç et al., 2012) activities against Gram (+) microorganisms and *Candida dubliniensis* and *Candida krusei*. We observed an unoptimized production level of ~18 mg/L of atraric acid **2** from our strain of *A. fumigatus*. This report appears to the first observation of atraric acid **2** being produced in a non-lichen fungus. The production of **2** by this strain of *A. fumigatus*, isolated from beneath a lichen thallus, may represent a horizontal gene transfer event from lichen to non-lichen fungi. This type of gene transfer could result in the acquisition of new traits or abilities by the recipient fungi, such as increased tolerance to environmental stressors or the ability to produce novel secondary metabolites. However, there is limited research on the occurrence and effects of horizontal gene transfer between lichen and non-lichen fungi. Further studies are needed to fully understand the mechanisms and implications of this phenomenon. However, conclusive proof of that hypothesis is beyond the scope of this thesis.

3.8 Conclusion

In summary, this study describes the isolation, full-structure elucidation, and bioactivity profiling of compounds **1** and **2**. We observed a significant production of compound **1, (**~ 120 mg / L) from our strain of *A. fumigatus*. Both compounds **1** and **2** showed modest antibacterial activity but did show potentially promising antifungal activity. This is the first report we are aware of on the production of these metabolites from *A. fumigatus* and the first report of **2** from a non-lichen

fungus. It is possible that this specific strain of *Aspergillus fumigatus* strain SL-2203 has the potential to increase the production of certain metabolites, which could make it useful for the industrial production of natural antimicrobials. However, more research would be needed to confirm this and determine the feasibility of large-scale production.

Chapter 4

Penicillium sanguifluum as a source of dehydrocurvularin and its antifungal and antibacterial properties

The work described in this chapter was conducted in collaboration with Dr. Georg Hausner and Dr. Ayush Kumar research group at the Department of Microbiology, University of Manitoba, Winnipeg, Canada. In this project, my role (Harman Gill) focused on fermenting fungi, screening, purifying, and characterizing compounds, and conducting antifungal assays. Aamer Kurdi, a PhD student, Department of Microbiology, identified the fungus and performed antibacterial and checkboard assays. The manuscript is currently in preparation for publication.

4.1 Introduction

Antimicrobial resistance (AMR) refers to the failure of drugs to effectively kill or inhibit the growth of microbes, such as bacteria, parasites, viruses, and fungi. Resistance can either be intrinsic, present across all isolates of a particular species, or acquired over time. For instance, Gram-positive bacteria are inherently resistant to Aztreonam, and Gram-negative bacteria are resistant to glycopeptides (Barker, 1999). Acquired resistance, which develops through mutations over time, includes rifampicin resistance in all species, fusidic acid and quinolone resistance in *staphylococcus spp*. (Barker, 1999).

In 2019, the World Health Organization (WHO) identified AMR as one of the top ten global health threats. It already imposes substantial social burden and is responsible for approximately 25,000 deaths annually in Europe alone (O'Neill, 2016). Studies suggest that without

intervention, microbial resistance could result in more than 10 million deaths by 2050, surpassing the number of deaths caused by cancer (Tang et al., 2023).

Species of particular concern are the 'ESKAPE' pathogens (*Enterococcus faecium*, *Staphylococcus aureus*, *Klebsiella pneumoniae*, *Acinetobacter baumannii*, *Pseudomonas aeruginosa* and *Enterobacter spp.*), which are relevant to nosocomial infections, *Mycobacterium tuberculosis*, *Enterobacteriaceae* (e.g. *E. coli*), and *Neisseria gonorrhoeae* (Rice, 2008).

AMR is on the rise amid a dwindling pipeline for new antibiotic development. Within just eight decades of antibiotic use, bacterial infections that were once easily treatable are becoming resistant to existing treatments. This underscores the urgency for researchers to explore novel therapeutic drugs from various sources. Since the discovery of penicillin, fungal secondary metabolites have been intensively studied for their potential bioactive properties (Alberts, 1988).

Fungi are well-known to produce secondary metabolites during active cell growth (Hawksworth & Lücking, 2017). Many fungi are known for their capability to produce a broad range of bioactive and currently clinically used metabolites, including antibiotics, immune suppressants, and cholesterol-lowering drugs (Devi et al., 2020).

In this study, fungi were isolated from Manitoba soil and screened against Gram positive and Gram-negative bacteria. Among the 12 isolates, one fungal isolate, labeled 111-12, showed antibacterial activity against both methicillin-resistant *S. aureus* (MRSA) and wild-type *A. baumannii* . This fungal isolate (111-12) was identified as *Penicillium sanguifluum*, a species belonging to the *Penicillium* section *Citrina*.

The primary goal of this study was to isolate and evaluate the antibacterial activity of bioactive compounds from *Penicillium sanguifluum*. Additionally, bioactive compounds **3** and **4 (Figure 29)** were evaluated for their adjuvant potential to currently available antibiotics. Compounds **3** and **4** were also tested against two plant pathogens, *Ophiostoma novo-ulmi* and *Cryphonectria parasitica*, which are responsible for dutch elm disease (DED) and chestnut blight disease (CBD), respectively, in North America.

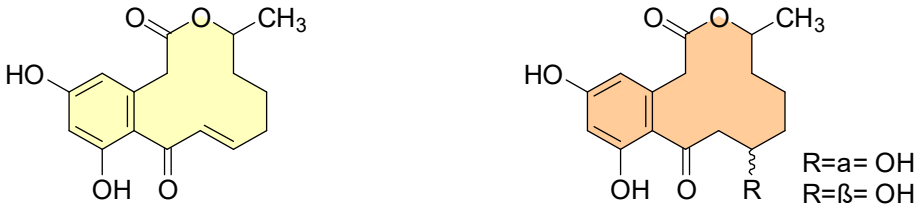

Compound 3 **Compound 4**

Figure 29: Chemical structures of compounds **3** and **4**.

4.2 Preliminary screening of fungal isolates

In this study, a total of 12 fungal isolates were obtained and evaluated for preliminary screening for antibacterial activity against Gram- negative and positive bacteria. The Gram-negative bacteria included *P. aeruginosa* PA01 (wild type), *P. aeruginosa* PA82 (clinical isolate), *P. aeruginosa* PA0750 (efflux deficient), *A. baumannii* ATCC17978 (wild type), *A. baumannii* AB030 (clinical isolate), and *A. baumannii* AB258 (efflux pump deficient). The Gram-positive bacteria tested was methicillin-resistant *S. aureus* (MRSA). All 12 fungal isolates exhibited antibacterial activity against efflux-deficient (*P. aeruginosa* PA0750, *A. baumannii* AB258) strains. However, none of the isolates showed activity against the clinical isolate (*A. baumannii* AB030, *P. aeruginosa* PA82) and wild type (*P. aeruginosa* PA01, *A. baumannii* ATCC17978) strains. Eleven out of twelve fungal strains did not show activity against Gram-positive bacteria.

During preliminary screening, one fungal isolate (111-12), *Penicillium sanguifluum*, exhibited antibacterial activity against Gram-negative, *P. aeruginosa* PA0750 (efflux deficient), *A. baumannii* AB258 (efflux deficient), and Gram-positive, methicillin-resistant *S. aureus* (MRSA), bacteria. Therefore, it was selected for further study.

4.3 Fungal identification and antiSMASH analysis

From the whole genome sequence four nuclear markers were extracted to determine the identity of the fungal isolate. The phylogenetic analysis of these four nuclear markers (ITS, β-tubulin, Calmodulin , RNA polymerase II gene) is shown in **Figure S 8**. The **Table 5** shows that strain 111-12, based on four markers, consistently matched with available NCBI sequences of other *P. sanguifluum* strains. Three of the four markers also group *P. sanguifluum* sequences with *Penicillium roseopurpureum* **(Figure S 8).** However, the beta-tubulin dataset separates *P. sanguifluum* from *P. roseopurpureum* . Previous reports have shown that multiple markers are usually required to resolve species within the *Penicillium* section *citrina* (Houbraken et al., 2010; Pangging et al., 2019; Visagie et al., 2014).

Table 5: Blastn results for sequences recovered (Accession numbers) of four nuclear markers from fungal strain 111-12.

Strain number	Nuclear markers	Query coverage	Identity percentage	Accession numbers	Species name
111-12	ITS	100%	100%	MH858377.1	*P. sanguifluum*
	β-tubulin	100%	96.96%	KY469187.1	*P. sanguifluum*
	Calmodulin	100%	98.67%	JN606543.1	*P. sanguifluum*
	RNA polymerase II gene	100%	98.62%	MN969135.1	*P. sanguifluum*

The genomic sequence of *P. sanguifluum* 111-12 was submitted to the antiSMASH (Blin et al., 2023) database to identify possible gene clusters associated with the production of secondary metabolites. Forty-two gene clusters were identified and can be classified into six categories: type 1 polyketide, NRPS (non-ribosomal polyketides), NRPS-like (non-ribosomal polyketides like), terpene, siderophore, and betalactone. One contig (identified as 13.1 region) appears to harbor a gene cluster that could be responsible for the synthesis of dehydrocurvularin **(Figure 30)**. The characterization of the secondary metabolites produced by *Penicillium sanguifluum* confirmed that it indeed produces dehydrocurvularin.

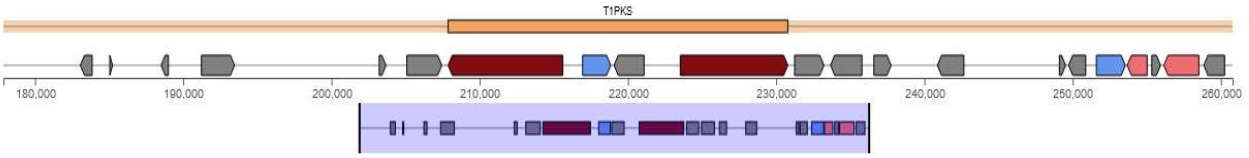

Figure 30: Predicted gene cluster for dehydrocurvularin in *Penicillium sanguifluum*, as identified using antiSMASH analysis.

The gene cluster identified in the13.1 region of *P. sanguifluum* 111-12 has 50% similarity with the corresponding gene cluster found in *Aspergillus terreus* **(Figure 31)**. A fungal species that has also been reported to produce dehydrocurvularin (Xu et al., 2013).

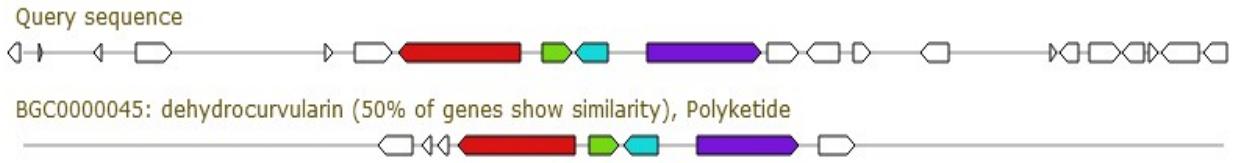

Figure 31: The query sequence (based on strain 111-12) in the top row represents the region found in *Penicillium sanguifluum*. BGC0000045 in the bottom row is the MIBiG accession number for the gene cluster responsible for dehydrocurvularin synthesis in *Aspergillus terreus*.

4.4 Fermentation and extraction

Penicillium sanguifluum was grown in 2 L of PDB, at 28◦C, for 7 days. The ethyl acetate extraction from 2 L culture broth yielded 1.3 g of the crude extract. The chromatographic fractionation of the crude extract yielded two main compounds (**3** and **4**), dehydrocurvularin (~120 mg/L) and 11-hydroxycurvularin (~70 mg/L) respectively **(Figure 32)**.

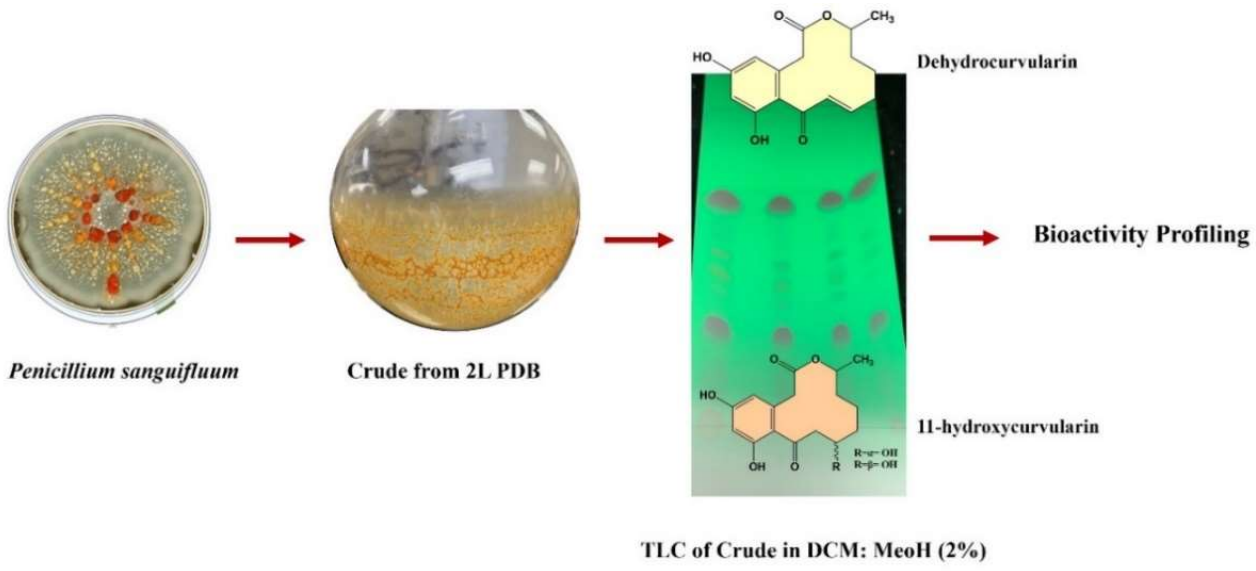

Figure 32: *Penicillium sanguifluum* fungus grown at a 2L scale (left). Thin layer chromatography (TLC) image showing the two main compounds, dehydrocurvularin and 11-hydroxycurvularin, using a DCM 2% solvent system (right).

4.5 Characterization of the metabolites

Compound **3** (dehydrocurvularin): White crystals; ^{1}H NMR ($CDCl_3$, 500 MHz): δ_H 3.53 (1H, d, J = 17.6 Hz, H-2), 4.04 (1H, d, J = 17.6 Hz, H-2), 6.26 (1H, d, J = 2.4 Hz, H-4), 6.22 (1H, d, J = 2.4 Hz, H-6), 6.64 (1H, d, J = 15.5 Hz, H-10), 6.61 (1H, ddd, J = 15.5 Hz, 8.9 Hz, 4.0 Hz, H-11), 2.33 (1H, m, H-12), 2.49 (1H, m, H-12), 1.67a (1H, m, H-13), 1.97 (1H, m, H-13), 1.66a (1H, m, H-14), 1.90 (1H, m, H-14), 4.88 (1H, m, H-15), 1.26 (3H, d, J = 6.4 Hz, H-16).

[a] Overlapped resonance signals.

^{13}C NMR ($CDCl_3$, 125 MHz): δ_C 19.8 (C-16, CH_3), 24.05 (C-13, CH_2), 32.71 (C-12, CH_2), 33.95 (C-14, CH_2), 43.94 (C-2, CH_2), 73.02 (C-15, CH), 103.31 (C-6, CH), 113.62 (C-4, CH), 114.41 (C-8, qC), 131.48 (C-10, CH), 137.61 (C-3, qC), 148.23 (C-11, CH), 160.98 (C-5, qC), 166.28 (C-7, qC), 171.93 (C-1, qC), 196.28 (C-9, qC). The molecular formula of compound **3** is $C_{16}H_{18}O_5$, a molecular ion of [M-H] 290.315 (291. 521 calculated) was observed in the negative ion mode of LC-MS.

Compound **4** (enantiomeric mixture of 11-hydroxycurvularin): an enantiomeric mixture, encompassing (11R, 15S)-11-hydroxycurvularin and (11S, 15S)-11-hydroxycurvularin; light yellow crystals; ^{1}H NMR (MeOD, 500 MHz): δ_H 6.30 (1H, d, J=2.24 Hz, H-4), 6.24 (1H, d, J=1.64 Hz, H-6), 4.99 (1H, m, H-15), 4.1 a (1H, m, H-11), 3.98 (1H, d, J=15.9Hz, H-2), 3.61 (1H, d, J=15.9 Hz, H-2), 3.24 a (1H, dd, J=2.3 Hz, J=8.7 Hz, H-10), 2.85 a (1H, dd, J=11.8 Hz, J=22 Hz, H-10), 1.65 a (2H, m, H-14), 1.25 a (1H, m, H-13), 1.46 a (2H, m, H-14), 1.38 a (m, 2H, H-12), 1.15 (3H, J=3.36 Hz, H-16).

In the same proton NMR δ_H 6.24 (2H, dd, 2.27 Hz, H-4), 4.83 (1H, m, H-15), 4.1 a (1H, m, H-11), 3.89 (1H,d, 15.4Hz, H-2), 3.24 a (1H, dd, 2.3Hz, 8.7 Hz, H-7), 2.85 a (1H, dd, 11.8Hz, 22.Hz, H-7), 1.65 a (2H, m, H-13), 1.25a (1H, m, H-13), 1.46 a (2H, m, H-14), 1.38 a (m, 2H, H-12), 1.14 (3H, 3.46Hz, H-16). [a] Overlapped resonance signals.

^{13}C NMR (MeOD, 125 MHz): δ_C 205.15, 204.28 (C-9, qC), 171.32, 171.08 (C-1, qC), 160.45 160.21 (C-5, qC), 159.37, 158.46 (C-7, qC), 136.72, 135.96 (C-3, qC), 119.15, 118.65 (C-8, qC), 111.23, 110.81 (C-4, CH), 101.50, 101.39 (C-2, CH), 73.45, 70.91 (C-15, CH), 67.29, 66.29 (C-11, CH), 53.41, 52.18 (C-10, CH2), 39.78, 38.83 (C-2, CH2), 34.10, 33.52 (C-12, CH2), 31.25, 30.90 (C-14, CH2), 21.68, 20.10 (C-13, CH2), 17.81, 17.75 (C-16, CH3).

The data provided above matches with literature (Greve et al., 2008) confirmed the characterization of these molecule.

4.6 Minimum inhibitory concentration (MIC) of purified compounds

The minimum inhibition concentration (MIC) values for purified compounds **3** and **4** were evaluated against three bacterial strains: *A. baumannii* AB258, methicillin-resistant *S. aureus* (MRSA), and *A. baumannii* ATCC17978 **(Table 6)**. Compound **3** (dehydrocurvularin) had MICs values of 32 µg/mL, 64 µg/mL against *A. baumannii* AB258 and *S. aureus* MRSA respectively. In contrast, compound **4** (11-hydroxycurvularin) exhibited extremely high MIC values (>120 µg/mL) against all tested bacterial strains. *A. baumannii* ATCC17978 displayed an MIC value of 2048 µg/mL for both compounds **3** and **4**, indicating significant resistance.

Table 6: Minimum inhibitory concentrations (MIC) of compounds **3** and compound **4** against *A. baumannii* AB258, methicillin-resistant *S. aureus* (MRSA), and *A. baumannii* ATCC17978 bacterial strains.

S. No	Strains	MIC values in µg/mL	
		Compound 3	Compound 4
1	*A. baumannii* AB258	64	128
2	*S. aureus* MRSA	32	128
3	*A. baumannii* ATCC17978	2048	2048

4.7 In-vitro evaluation of antifungal assay

The evaluation of the inhibitory effect of compounds **3** and **4** on two plant pathogenic strains *Ophiostoma novoulmi* subspecies *americana* (CBS108928) and *Cryphonectria parasitica* (ATCC 38755) was performed by comparing the average diameters (mm) of mycelial growth of the plates with and without (control) compounds. The control group included mycelia grown without added compounds. The results showed that, in comparison to the control, compound **3** displayed strong inhibition against both selected strains, with inhibition ratios ranging from 9% to 59% **(Figure 33)**. In contrast, compound **4** exhibited weak mycelial inhibition against *C. parasitica* (~8%) and *Ophiostoma novoulmi* (~2%) at 1000 µg (~8%).

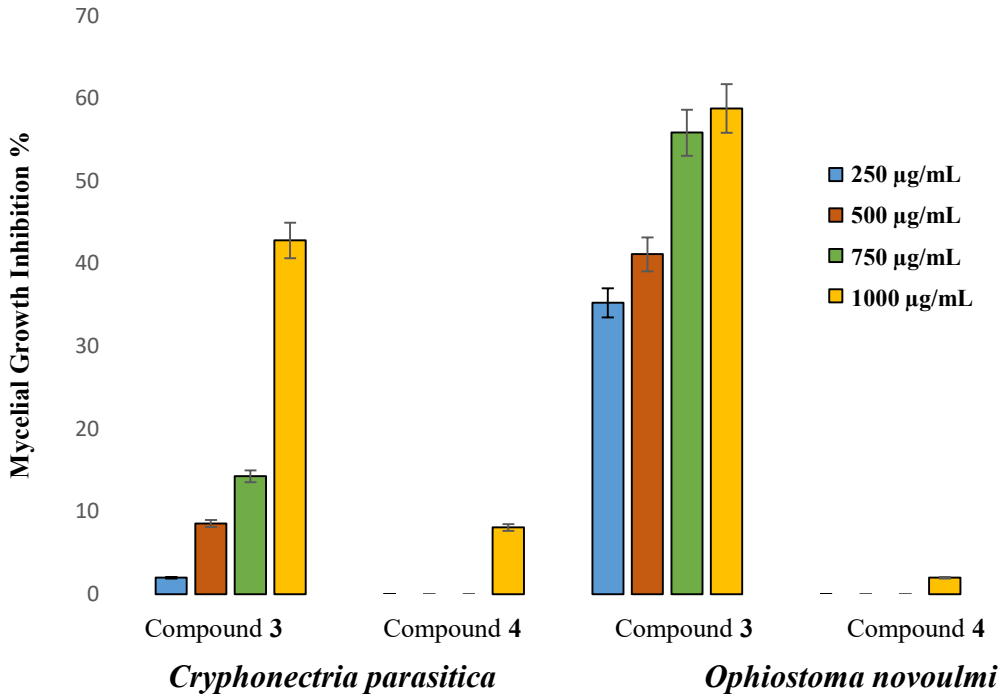

Figure 33: The percentage of mycelial growth inhibition of compounds **3** and **4** against *Cryphonectria parasitica* and *Ophiostoma novoulmi* fungal strains, as compared to a control growth plate. The inhibition rates were calculated as mean ± SD (n = 3) and were considered significant at $p < 0.05$ in comparison to the control group.

4.8 Checkerboard assay

The combination of compounds **3** and **4** with meropenem significantly lowered the MIC of meropenem against *A. baumannii* AB258 (meropenem 32 µg/mL to 8 µg/mL with compound **3**, and 16 µg/mL with compound **4 (**

Figure 34) FIC value of 0.5. Compounds **3** and **4** were also tested for synergy against *A. baumannii* ATCC17978 (wild type) and *A. baumannii* AB030 (clinical isolate), but there was no

activity due to high resistance mechanisms in these strains.

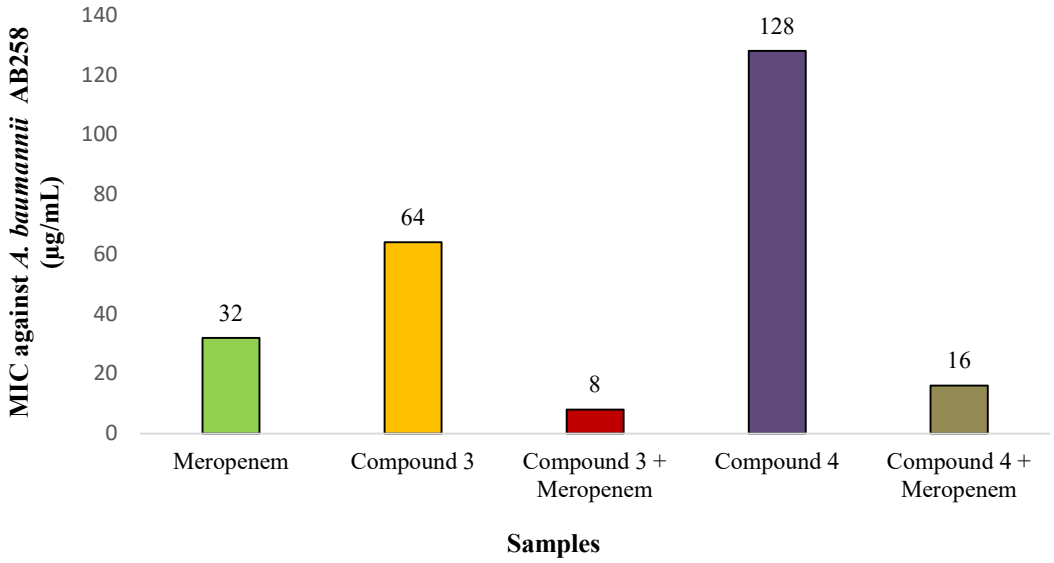

Figure 34: Antibacterial activities of compounds **3**, **4**, and meropenem against *A. baumannii* AB258, both individually and in combination.

When compounds **3** and **4** were combined with clindamycin against methicillin-resistant *S. aureus* (MRSA), the MIC value of clindamycin significantly dropped from 1024 µg/mL to 1 µg/mL with compound **3** and to 2 µg/mL with compound **4**. The FIC value for the combination of compound **3** and clindamycin was 1, indicating an additive effect without synergism. In contrast, compound **4** had an FIC value of 0.5, indicating synergism with clindamycin.

When these compounds were tested in combination with oxacillin, the MIC decreased from 128 µg/mL to 64 µg/mL (FIC 1) with compound **3** and to 16 µg/mL (FIC 0.1) with compound **4**. This result demonstrates that compound **4** works synergistically with both oxacillin and clindamycin. Additionally, compound **3** lowered the MIC of ampicillin from 256 µg/mL to 128 µg/mL (FIC 0.5) **(Figure 35).**

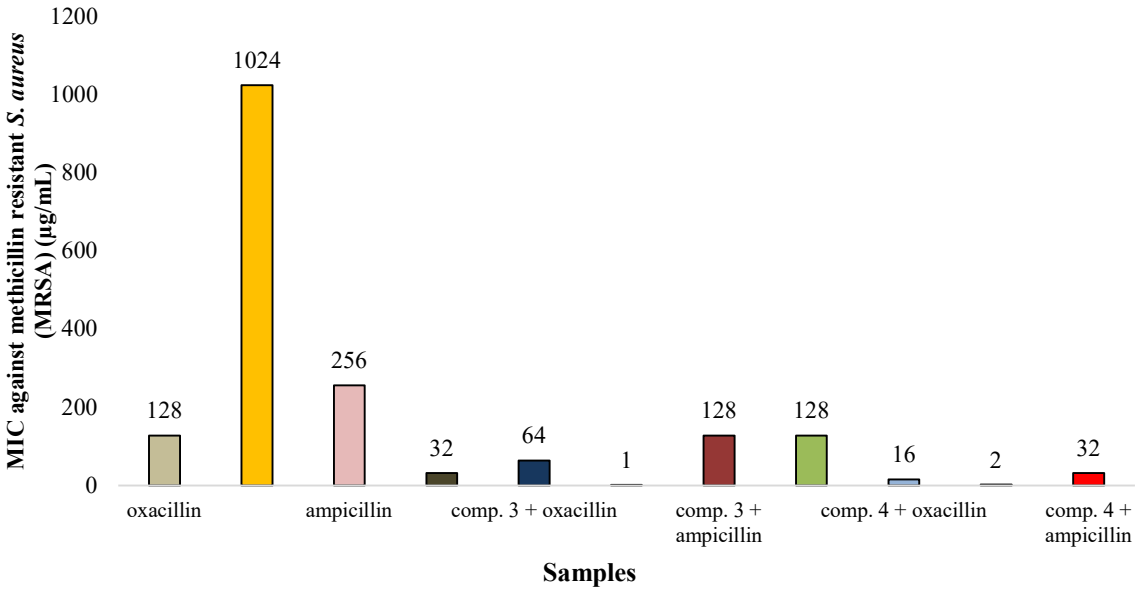

Figure 35: Antibacterial activities of compounds **3** and **4**, oxacillin, ampicillin, and clindamycin against *S. aureus* (MRSA), individually and in combination of antibiotics and compounds.

4.9 Discussion

Antimicrobial resistance in bacteria is a critical global health concern (Arnold et al., 2024; Parker et al., 2024). Addressing resistance requires the discovery of new antimicrobial compounds and adjuvants for existing antibiotics. This study underscores the potential of fungi as a source of novel antimicrobial compounds. Our screening of fungal strains identified *P. sanguifluum* (111-12) as a promising candidate for producing bioactive compounds inhibit the growth of *A. baumannii* AB258 and *S. aureus* MRSA. The strain was confirmed as *P. sanguifluum* through phylogenetic analysis of ITS, beta-tubulin, RNA polymerase, and calmodulin sequences and belongs to the *Penicillium* section *Citrina* which is known for its rich production of natural products (J. Houbraken et al., 2011; Pangging et al., 2019).

Fermentation of *P. sanguifluum* (111-12) yielded two bioactive compounds: dehydrocurvularin (**3**) and 11-hydroxycurvularin (**4**). These compounds, previously isolated from various fungi such

as *Aspergillus welwitschiae*, *Curvularia intermedia*, and *Aspergillus terreus* (Jeon, 2009; Meepagala et al., 2016; Xu et al., 2013), have been shown to exhibit antibacterial activity against *Escherichia coli*, as well as activity against tumor cell lines, and they can act as phytotoxins (Meepagala et al., 2016; Xiang et al., 2020; Xu et al., 2013). Another study showed that (S)-dehydrocurvularin inhibits the formation of appressorium in *Magnaporthe oryzae* during rice blast disease (Jeon, 2009). Recently (S)-dehydrocurvularin antifungal activity was reported for *Candida auris* and *Candida albicans* by interfering with their adhesion to epithelium cells (Kamauchi et al., 2022). Cell adhesion plays a very important role in candidiasis facilitating invasion of the human body and developing resistance to antifungals by promoting biofilm formation (Kamauchi et al., 2022). Dehydrocurvularin also exhibits antifungal activity against *Candida spp.* by interfering with cell adhesion, a critical factor in candidiasis and biofilm formation (Kamauchi et al., 2022).

This study presents the first data on the activities of dehydrocurvularin (**3**) and 11-hydroxycurvularin (**4)** against *S. aureus* MRSA and the Gram-negative pathogens *A. baumannii* AB258 and *P. aeruginosa*. The MICs of compounds **3** and **4** were 64 µg/mL, 128 µg/mL against *A. baumannii* AB258 (efflux pumps deficient), and 32 µg/mL, 128 µg/mL against *S. aureus* MRSA, respectively. These low MIC values indicate potent antibacterial activity with minimal side effects (Kowalska-Krochmal & Dudek-Wicher, 2021). The potential synergistic effects of these compounds with known antibiotics were also examined. Compound **3** reduced the MIC of meropenem against *A. baumannii* from 32 µg/mL to 8 µg/mL, whereas compound **4** reduced it to 16 µg/mL. Both compounds exhibited synergism with ampicillin against *S. aureus* MRSA, lowering the MICs from 256 µg/mL to 128 µg/mL and 32 µg/mL, respectively. However, only compound **3** showed synergy with oxacillin, reducing the MIC from 128 µg/mL to 64 µg/mL.

Additionally, the antifungal properties of these compounds were assessed against pathogens that cause Dutch Elm Disease (*ophiostoma novoulmi* subspecies americana) and Chestnut Blight Disease (*cryphonectria parasitica*). Compound **3** exhibited significant mycelial growth inhibition ~50 % in *Cryphonectria parasitica* and *Ophiostoma novoulmi* at a concentration of 1000 µg/mL, whereas compound **4** showed weak inhibition (<10 %). Further research is required to elucidate the underlying mechanisms of their antifungal properties.

The genome sequencing of *P. sanguifluum* (111-12) revealed forty-two gene clusters associated with secondary metabolite production, highlighting its potential as a source of bioactive compounds and confirming its potential to produce compounds **3** and **4**.

4.10 Conclusion

This study highlights the urgent need for new antibiotics and adjuvants due to the emergence of antibiotic resistance in *A. baumannii* and *S. aureus* MRSA. The promising antibacterial activity of P. *sanguifluum* (111-12) derived bioactive compounds dehydrocurvularin (**3**) and 11-hydroxycurvularin (**4**) against these resistant strains offers a potential solution. These compounds showed bioactivity on their own and demonstrated synergistic potential when combined with various antibiotics (ampicillin, oxacillin, and clindamycin). Despite being known compounds with weak activities, our findings provide new insights into their bioactivities and potential as strong adjuvants to revive antibiotics that have lost efficacy. Additionally, the *P. sanguifluum* genome contains forty-two biosynthetic gene clusters, suggesting that various methods can enhance the production and yield of valuable natural products. These findings support the further exploration of fungal-derived compounds as viable alternatives in combating antibiotic resistance.

Chapter 5

Functional heterologous expression of the reversible decarboxylase from the lichen, *Cladonia uncialis*

I am the primary contributor to this chapter. The manuscript is currently under preparation for publication. To the best of our knowledge, this is the first report of the successful functional heterologous expression of a native lichen gene in *E. coli*.

5.1 Introduction

Lichen are slow-growing, complex miniature ecosystems formed by the mutual assemblage between a fungal partner (mycobiont) and an algal and/or cyanobacterial partner (photobiont) (Grimm et al., 2021; Lutzoni & Miadlikowska, 2009). They have colonized and adapted to diverse ecological niches ranging from the mildest conditions of home gardens to extremely harsh conditions, such as Arctic tundra or desert regions (Matos et al., 2015). The exploration of lichen mycobiont-derived secondary metabolites (SMs) has resulting in the discovery of over 1,000 compounds; however, conclusive links between these SMs and biosynthetic genes remain elusive. Recent advances in next-generation sequencing technology, annotation tools, and synthetic biology have expedited the identification and putative linkage of biosynthetic gene clusters (BGCs) to the chemical structures of SMs. These studies have revealed that there are more BGCs in lichen genomes than there are known SMs from lichenized fungi. This hidden metabolic potential provides the motivation to link putative genes with their functions through

heterologous expression in a heterologous host. Some of the host organisms used to characterize BGCs from lichenized fungi include *Escherichia coli* (*E. coli*), *Aspergillus oryzae* NSAR1, and *Saccharomyces cerevisiae* (Armaleo et al., 2011; Gill et al., 2023; Kealey et al., 2021; Kim et al., 2021; Yi et al., 2016).

These approaches have met with limited success with only two instances in which depside polyketide synthases (PKSs) were functionally expressed in heterologous systems (Kealey et al., 2021; Kim et al., 2021). The direct functional expression of genes from the lichen genome remains elusive. One previous example of success with a tailoring gene was the heterologous expression of the pyrG gene from the lichen *Solorina crocea*, which encodes an orotidine 5'-monophosphate decarboxylase, in *Aspergillus nidulans* (Sinnemann et al., 2000), resulting in a uridine-independent strain.

This study demonstrated the feasibility of expressing a lichen gene in a heterologous host, but functional in vitro protein expression has yet to be achieved. The biosynthesis of SMs are controlled by genes that are often located at the same genomic locus are co-regulated, (Yang et al., 2022) and are organized around a core gene, such as polyketide synthases (PKS). The core gene in turn is flanked by various ancillary genes, such as decarboxylase, methyltransferase, P450 oxidases, and other tailoring reactions that contribute to the structural modification of this core product of the PKS (Bertrand et al., 2018a; Gill, Sorensen, et al., 2023; Martinet et al.,

2019). One of the commonly observed tailoring genes encodes for enzymes that belong to the decarboxylases family. These tailoring enzymes play a crucial role in catalyzing the removal of a carboxyl group from various phenolic compounds. Intriguingly, it has been observed that some decarboxylases can exhibit reversible catalytic activity placing a carboxylate group on an appropriate substrate. This reversible catalytic activity has been extensively explored in bacteria (Ishii et al., 2004; Kino et al., 2020; Kirimura et al., 2010; Wuensch et al., 2014, 2015; Yoshida et al., 2007), but remain unexplored in lichens.

Using a homology searching approach, our group showed the taxonomic identification, de-novo sequencing, and annotation of various biosynthetic gene clusters from *C. uncialis* (Bertrand et al., 2018a, 2018b). Among these clusters, we identified a BGC named *cu-nr-pks-5*, consisting primarily of two genes: a gene that encodes for a polyketide synthase (PKS) that appears to produce orsellinic acid and an accessory gene that encodes for a decarboxylase **(Figure 36)**. The PKS gene *cu-nr-pks-5* (AUW31139) appears to be a type I non-reducing polyketide synthase, lacking any observable reducing domains. The tailoring gene was annotated as encoding for a decarboxylase enzyme that was predicted to convert orsellinic acid to orcinol (Bertrand et al., 2018a). Homology mapping indicated the possibility for the reversible role of the decarboxylase gene based on a comparison with a previously reported enzyme identified in a species of *Rhizobium* Gram-negative bacteria (Yoshida, 2004 et al.).

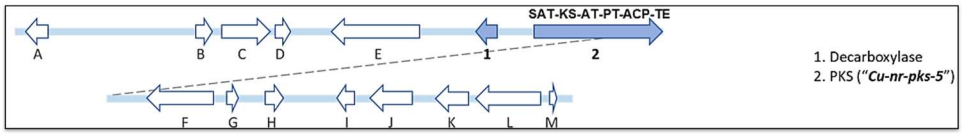

Cu-nr-pks-5 type 1 non reducing polyketide synthase (PKS) gene cluster in the ***C. uncialis.***

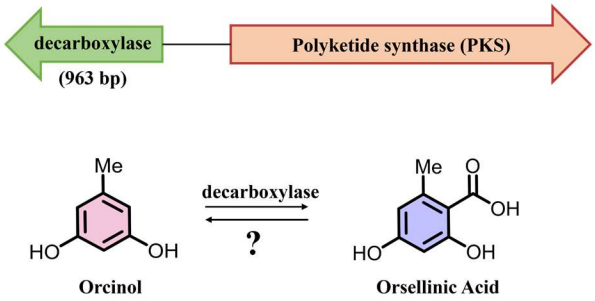

Figure 36: Gene clusters (*cu-nr-pks-5*) that contain a type 1 non-reducing polyketide synthase (PKS) in *C. uncialis*. This cluster comprises two genes: a PKS gene predicted for orsellinic acid biosynthesis and a tailoring gene, decarboxylase, predicted to facilitate the conversion of orsellinic acid to orcinol.

Previous arduous attempts at heterologous expression in *A. oryzae* of the *cu-nr-pks-5* gene encoding the PKS from this cluster were unsuccessful (Bertrand & Sorensen, 2019). In the present study, we investigated the expression of the lichen accessory gene decarboxylase in *E. coli*, along with its potential to catalyze enzymatic reactions involving aromatic phenols.

We here report the successful expression of this decarboxylase in *E. coli* and demonstrate the reversible carboxylation of aromatic phenols. This enzyme catalyzes a reaction with great commercial potential as we discuss below. To the best of our knowledge, this is the first report of the successful functional heterologous expression of a native lichen gene in *E. coli* and the production of a catalytically active protein.

5.2 Characterization of the crude extract of orsellinic acid synthase (*Cu-oas* and *Fu-oas*) transformants

Ethyl acetate extracts from transformants carrying the *Fu-oas* gene, *Cu-oas* gene, and the *A. oryzae* NSAR1 control were analyzed via HPLC to assess de novo orsellinic acid production **(Figure 37)**. The HPLC analysis showed that the orsellinic acid standard had a retention time of 35.43 minutes with UV absorption maxima at 213, 258, and 295 nm **(Figure 37 A)**. In contrast, the *A. oryzae* strain containing the *Cu-oas* gene did not exhibit a peak at this retention time, though a peak at 17.23 minutes was detected. The retention time and UV spectrum of this peak did not match those of orsellinic acid **(Figure 37 B)**. No peaks were observed in the control *A. oryzae* NSAR1 strain at the expected retention time **(Figure 37 D)**.

The *A. oryzae* strain transformed with the *Fu-oas* gene showed a peak at 33.13 minutes, with UV absorption maxima at 212, 259, and 293 nm, closely matching the orsellinic acid standard **(Figure 37 C)**. These results validate the potential of the *A. oryzae* NSAR1 system to express exogenous polyketide synthase (PKS) genes and suggest it could be utilized in future experiments to produce a broader range of metabolites.

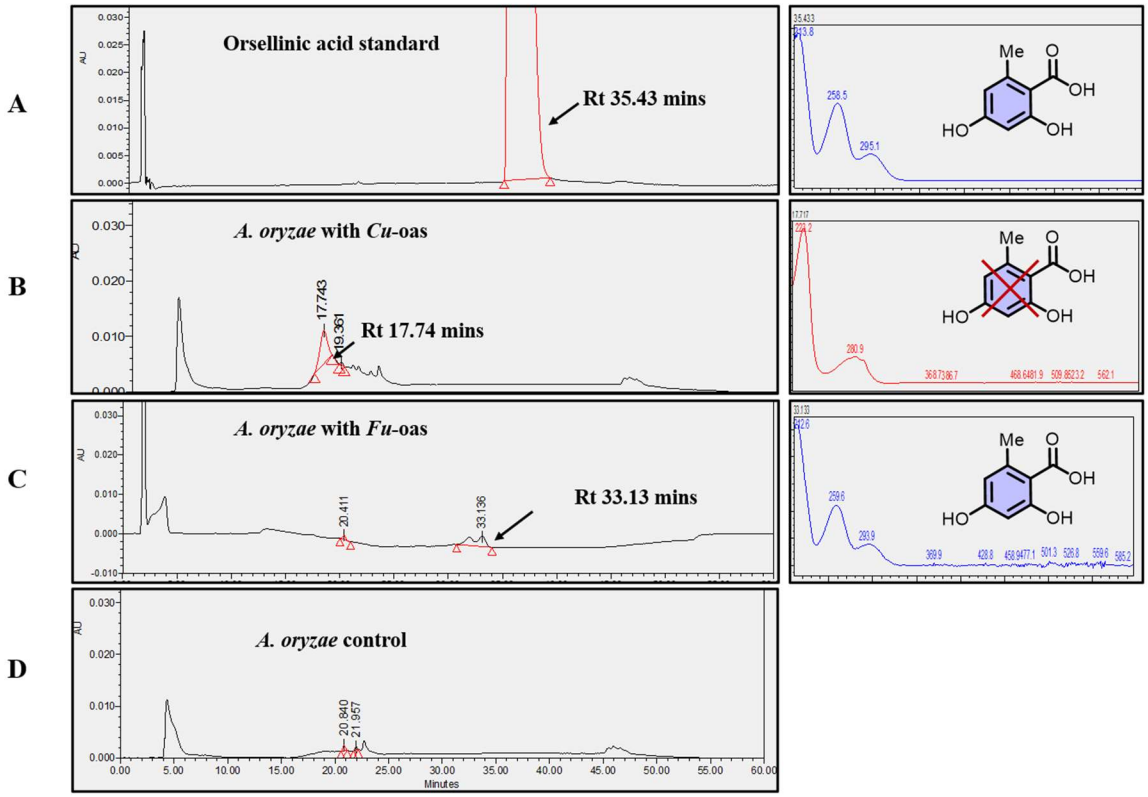

Figure 37: HPLC trace and UV spectrum at 250 nm of *A. oryzae* NSAR1 transformed with *Cu*-oas and *Fu*-oas genes. (A) Orsellinic acid standard (B*) A. oryzae* NSAR1 transformed with *Cu*-oas gene (C) *A. oryzae* NSAR1 transformed with *Fu*-oas gene (D) Native *A. oryzae* NSAR1.

5.3 Functional expression of decarboxylase gene from the lichen *C. uncialis* in *A. oryzae*

The ^{1}HNMR spectra of standard orsellinic acid and orcinol were recorded as: orsellinic acid (MeOD, 500 MHz): δ_H 6.18 (1H, d, J = 2.8 Hz), 6.12 (1H, d, J = 2.8 Hz), 2.47 (3H, s); Orcinol (MeOD, 500 MHz): δ_H 6.10 (2H, d, J = 2.6 Hz), 6.05 (1H, t, J = 2.8 Hz), 2.15 (3H, s), **Figure S 9 , Figure S 10**.

The ethyl acetate extracts from induced and uninduced decarboxylase transformants, as well as from the control cultures of *A. oryzae* NSAR1 was extracted. The ^{1}HNMR spectra of these extracts revealed characteristic peaks for both orsellinic acid and orcinol. As illustrated in **Figure**

38, the crude extract from the induced decarboxylase transformant showed signals at δ_H 6.04, 6.10, and 2.47, corresponding to orsellinic acid, and signals at δ_H 6.10, 6.04, and 2.15, consistent with orcinol. Similarly, in the uninduced transformants **(Figure S 11)**, peaks at δ_H 6.27, 6.24, and 2.47 were attributed to orsellinic acid, while δ_H 6.12, 6.18, and 2.15 corresponded to orcinol. Indeed, the detection of orcinol signals in the control, **Figure S 12**, led to the inconclusive results, suggesting the possibility of spontaneous conversion.

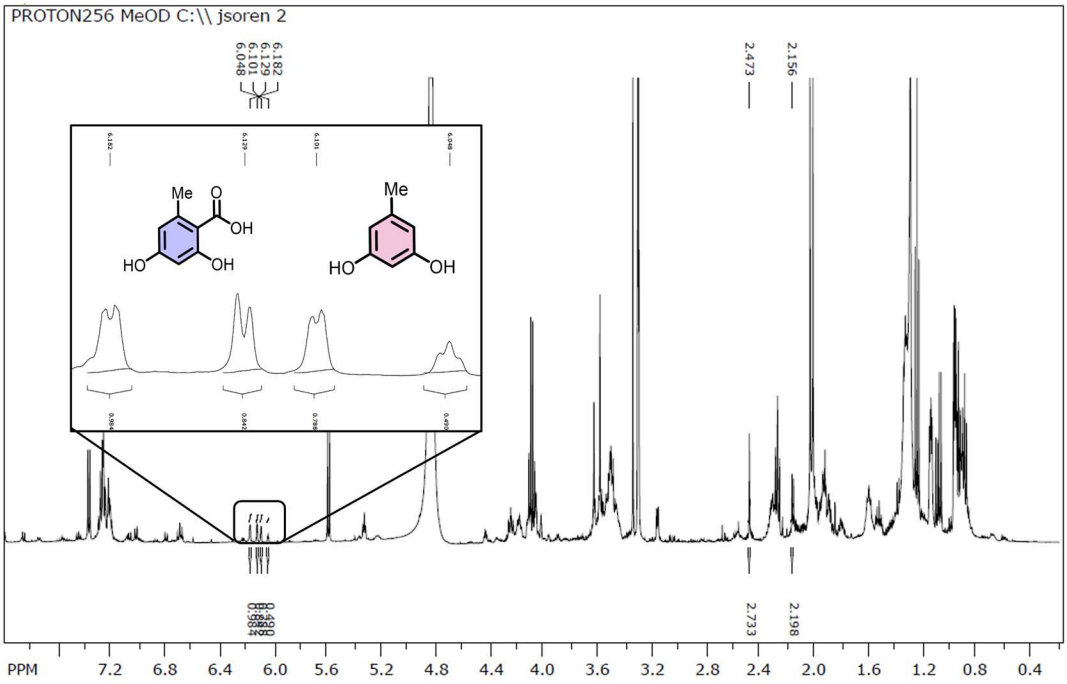

Figure 38: [1]H NMR spectrum of the crude extract from induced decarboxylase *A. oryzae* NSAR1 transformants, supplemented with orsellinic acid, was recorded in MeOD at 500 MHz.

Therefore, to resolve this ambiguity we decided to switch to a different surrogate host and perform in vitro assays using purified protein.

5.4 Cloning of the decarboxylase gene from the lichen *C. uncialis*

The gene that appears to have high homology with a decarboxylase from the biosynthetic gene cluster (*cu-nr-pks-5*) were amplified from *C. uncialis* gDNA using the PCR method described in the Materials and Methods. This gene was then placed into the fungal expression plasmid, pUSA ,using a recombination cloning method (Bertrand et al., 2018a). The 963 bp decarboxylase gene was amplified from the expression plasmid and cloned into the bacterial expression plasmid pQE80L **(Figure S 13)** using Gibson assembly. Sanger sequencing of the recombinant pQE80L-His-DeCO2 plasmid confirmed that the lichen gene, decarboxylase, was correctly inserted into the plasmid without the introduction of mutations during the PCR or Gibson assembly reactions.

5.5 Expression of the decarboxylase gene from the lichen *C. uncialis*

The bacterial expression vector pQE80L-His-DeCO$_2$ containing a T5 promoter regulated by IPTG and an N-terminal His$_6$ tag upstream of the decarboxylase gene was transformed into the *E. coli* strain BL21. The induced cells were harvested by centrifugation, incubated with SDS loading buffer, and subjected to SDS-polyacrylamide gel electrophoresis (SDS-PAGE) to reveal an overexpression protein band with a molecular mass of ~35 kDa **(Figure 39)**. The protein band was consistent with the molecular mass (~33.4 kDa) deduced from the translated amino acid sequence of the decarboxylase gene which also includes the 0.84 kDa from the His$_6$ tag. Then, the soluble fraction was subjected to Ni^{2+} affinity chromatography using the AKTA pure system using imidazole to elute the bound protein. Fractions containing the decarboxylase protein **(Figure S 14)** were combined and dialyzed with 10 mM potassium phosphate buffer (pH 7.0) and then concentrated using an Amicon Ultra-2 Centrifugal Filter, 10 kDa MWCO (MilliporeSigma™). The enzyme solution was stored at -20 °C until use.

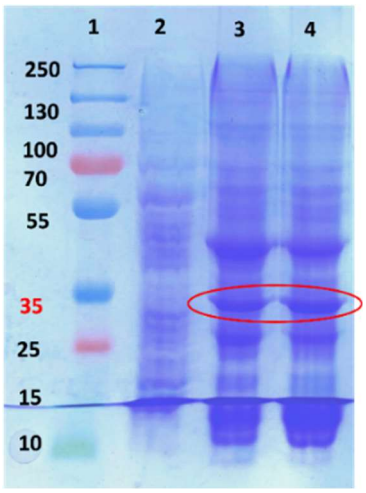

Figure 39: SDS-PAGE (10%) analysis of decarboxylase protein. Lane 1: protein ladder (kDa); lane 2: uninduced cells; lanes 3 & 4: induced cells. Cells were induced with 1mM IPTG, revealing a protein band with a molecular mass of ~35 kDa in lane 3 and 4. The predicted molecular mass of the decarboxylase protein was 35 kDa.

5.6 Homology modeling

The software package Phyre2 was used to identify other proteins that were similar to our expressed protein and to generate a predicted 3-dimensional folding structure. The results revealed that the predicted 3D structure exhibited 34% identity with 100% confidence with the metallo-dependent hydrolase superfamily and the PP1699/LP2961-like family (**Figure S 15A**). A homology search of the PP1699/LP2961-like family through the Scope database showed that it matches with three structurally known proteins, 2 amino-3-carboxymuconate 6-semialdehyde decarboxylase NbaD (Q83V25), 4-oxalomesaconate hydratase LigJ (Q6NOR4), thermophilic reversible gamma-resorcylate decarboxylase (Q60GU1), and two putative hydrolases (Q88M75, and Q88TJ2) (**Figure S 15B**). The predicted protein structure has a TIM beta/alpha barrel fold **(Figure 40)** that is consistent with this superfamily of proteins.

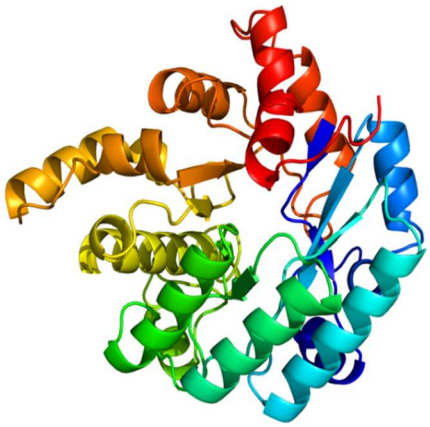

Figure 40: Phyre2 generated predicted protein structure of the decarboxylase enzyme based on the translated amino acid sequence.

5.7 Phylogenetic tree analysis

We next elected to construct a phylogenetic tree to place the sequence of our enzyme in the evolutionary context and to further confirm the homology results generated above. We used, as a comparator set, a series of proteins with some previous structural studies that have been conducted. This list included 2-amino-3-carboxymuconate 6-semialdehyde decarboxylase NbaD from *Pseudomonas fluorescens* (Q83V25), 4-oxalomesaconate hydratase LigJ from *Rhodopseudomonas palustris* (Q6NOR4), and thermophilic reversible gamma-resorcylate decarboxylase from *Rhizobium sp*. Our text sequence was the gene that encodes the decarboxylase enzyme that was identified in the genome of the lichen *C. uncialis* (A0A1Z1C438). The analysis revealed that the decarboxylase enzyme from lichen *C. uncialis* shares 71% similarity with the thermophilic reversible gamma-resorcylate decarboxylase from *Rhizobium spp.* **(Figure 41)**.

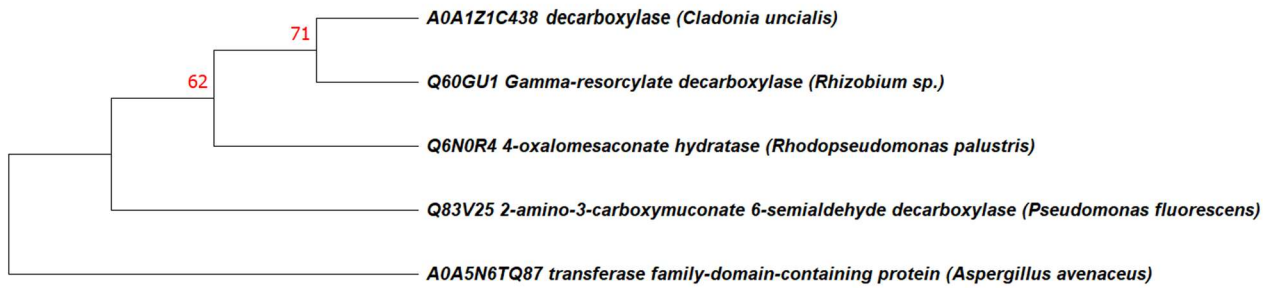

Figure 41: Phyre generated predicted protein structure of the decarboxylase enzyme based on the translated amino acid sequence. Evolutionary history was constructed using Maximum Likelihood method and JTT matrix-based model.

5.8 Metal binding site analysis

Based on the reported activity of other decarboxylase enzymes we expected to observe a metal binding site in our lichen decarboxylase. In order to confirm the presence of a metal binding site in our decarboxylase we used multiple sequence alignment using the software package UniProt. The thermophilic reversible gamma-resorcylate decarboxylase (*Rhizobium sp.*) was visualized using the UCSF Chimera software. In the native enzyme, a single Zn^{2+} ion is liganded by Glu8, His10, His164, Asp287, and a water molecule at the active site center (T. Li et al., 2006). Multiple sequence alignment revealed that Glu8, His10, His164, and Asp287 residues of gamma-resorcylate decarboxylase (*Rhizobium sp.*) corresponded to the binding sites Glu5, His7, His150, and Asp274 **(Figure 42 A)** in the decarboxylase enzyme from *C. uncialis*. This alignment facilitated the proposal of the putative structural model **(Figure 42 B)** for a decarboxylase enzyme from *C. uncialis*.

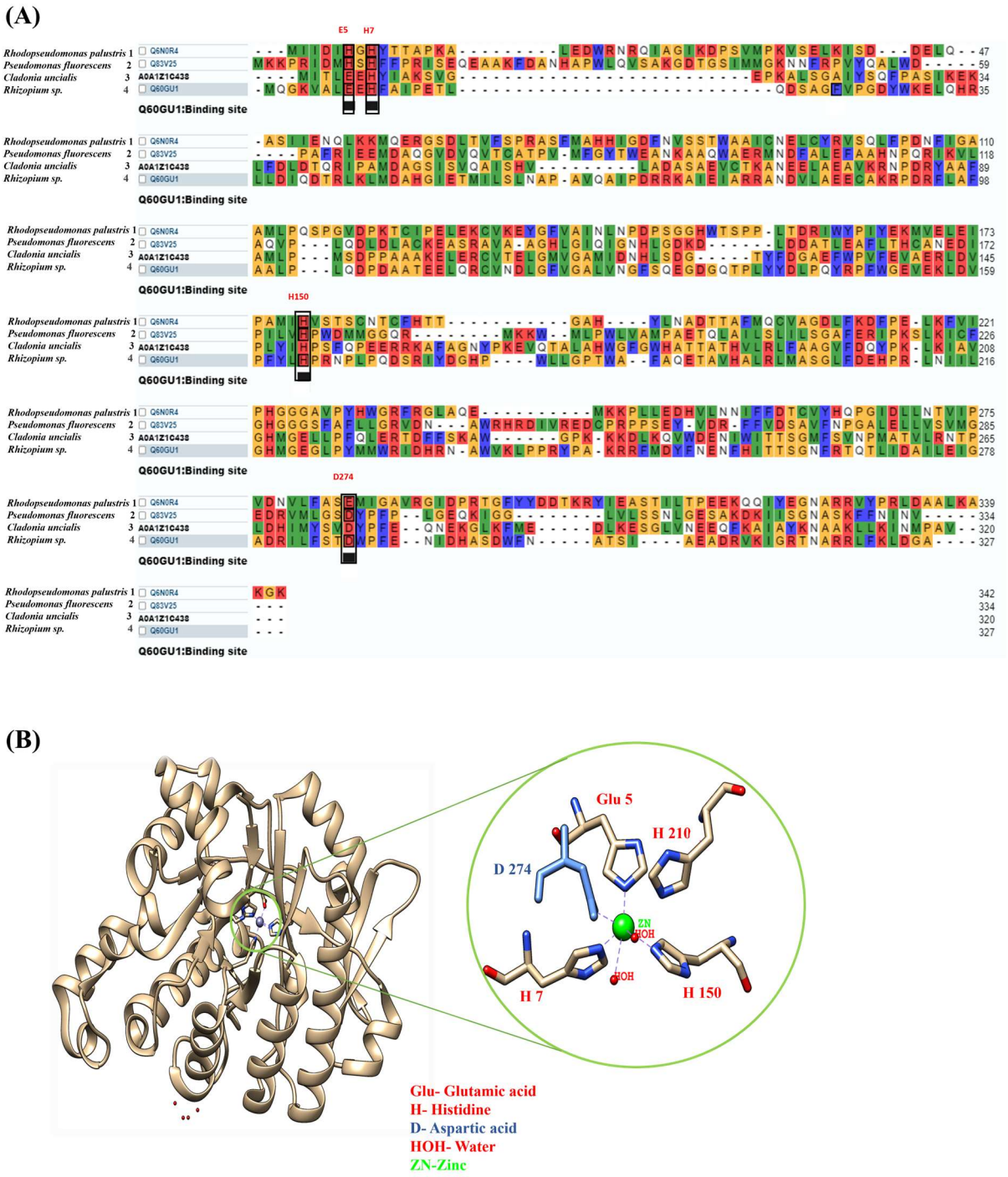

Figure 42: (A) Multiple sequence alignment of structurally known genes from 1. *Rhodo pseudomonas palustris* 2: *Pseudomonas fluorescens*, 3: *Cladonia uncialis* 4: *Rhizobium sp.* (B) Putative Zn^{2+} metal ion binding site in decarboxylase from *C. uncialis* based on multiple sequence alignment matching with thermophilic reversible gamma-resorcylate decarboxylase (*Rhizobium spp.*).

5.9 Substrate specificity

5.9.1 Decarboxylation

We initially sought to determine the substrate scope of the decarboxylation reaction catalyzed by this enzyme. We observed the gene that encodes for this enzyme co-localized with a polyketide synthase that appears to encode for orsellinic acid biosynthesis. We therefore carried out a very limited substrate scope focusing on a series of related phenolic benzoates. We examined the decarboxylation reaction of orsellinic acid, 2,4-dihydroxybenzoic acid, and anthranilic acid (**Figure S 16** to **Figure S 20**). The results from this experiment are summarized in **Figure 44** and reported as the area under the curve for the peak generated by HPLC analysis of the enzyme assays. Our initial results indicated that the enzyme readily catalyzed the decarboxylation of orsellinic acid to orcinol. This conversion was significantly enhanced by the addition of zinc at 30 °C, achieving approximately 82% conversion compared to only 8% without zinc **(Figure 43 A)**. We could also observe the enzyme catalyzed decarboxylation of 2,4-dihydroxybenzoic acid to resorcinol but only in the presence of zinc and with a considerably lower yield (~6%) **(Figure 43 B)**. No conversion could be detected in the absence of zinc or at 4 °C either with or without zinc added. Control experiments were also performed in which phosphate buffer was replaced with water to evaluate the conversion. However, no activity was observed when water was used in place of the phosphate buffer. Additionally, spontaneous conversion of orsellinic acid to orcinol occurred in controls at 30 °C, but at a slower rate of approximately 5%, with no spontaneous conversion observed at 4 °C **(Figure 43 A)**. Anthranilic acid, in contrast to the other substrates, did not undergo any detectable decarboxylation under the experimental conditions, even with the addition of zinc or temperature variations **(Figure S 20)**.

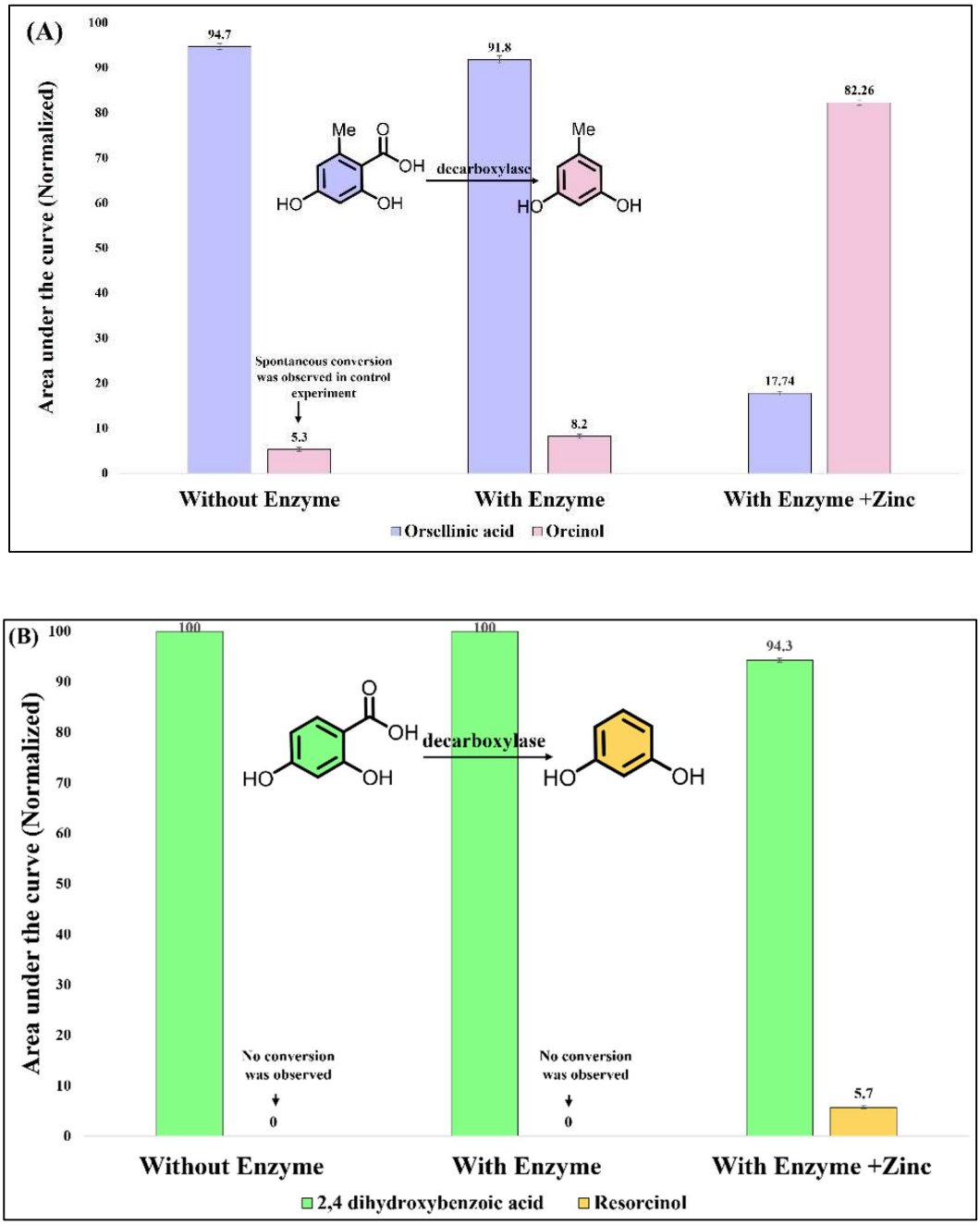

Figure 43: Analysis of enzyme catalysis for the conversion of orsellinic acid to orcinol at 30°C (A), and 2,4-dihydroxybenzoic acid to resorcinol at 30°C (B). The enzyme catalysis reactions were analyzed by comparing the area under the curve for the product peaks in the HPLC chromatograms obtained with and without the addition of zinc. The chromatograms were recorded at a wavelength of 250 nm.

5.9.2 Carboxylation

We then sought to examine the reversible nature of the chemical reaction catalyzed by this enzyme. We used the aromatic phenols orcinol and resorcinol to determine if these substrates could be converted into the corresponding substituted benzoic acid. In order to provide a source for the carboxylate group we chose to add 3 M potassium bicarbonate ($KHCO_3$) to the assay buffer. Based on our observation of a metal binding site in the enzyme structure we also set out to determine the effect of exogenous zinc on the carboxylation reaction. To our satisfaction we observed conversion of orcinol to orsellinic acid with ~ 7% yield in the presence of both enzyme and zinc at 4 °C **(Figure 44 A)**. We did observe a very small conversion (< 2%) of orcinol to orsellinic acid in the presence of both enzyme and zinc when we helped the reaction at 30 °C (**Figure S 24**). The absence of zinc in the enzyme assay completely abolished any trace of orsellinic acid production. A control experiment with substrate in buffer with no enzyme also resulting in no detectable orsellinic acid production **(Figure 44 A)**. We could also observe the conversion of resorcinol to 2,4-dihydroxybenzoic acid in the presence of this enzyme. In contrast to the orsellinic acid, we observed the highest yield of product (~ 25% conversion) when the assay was held at 30 °C when zinc was added to the enzyme **(Figure 44 B)**. When the assay with both zinc and enzyme present was held at 4 °C only a trace of 2,4-dihydroxybenzoic acid was observed (Figure S6 B). Interestingly in the absence of exogenous zinc we could observe ~ 12 % conversion of resorcinol to 2,4-dihydroxybenzoic acid **(Figure 44 B).** In the absence of enzyme, no product could be detected at either temperature **(Figure S 21 and Figure S 22)**. We also attempted the carboxylation of aniline to anthranilic acid **(Figure S 25)**, however under all conditions tested we could observe no conversion to product.

These results are significant as they demonstrate the reversible nature of this enzyme and suggest that it might be an effective catalyst for the synthesis of substituted carboxylic acids. This is a particularly meaningful result as the laboratory synthesis of orsellinic acid from orcinol involves multiple steps with air and moisture sensitive reagents. The use of this enzyme can achieve the same outcome in a single step with bicarbonate as the main reagent.

The results in **(Figure 44)** demonstrates the substrate specificity of decarboxylase, with zinc playing a pivotal role as a cofactor of the enzyme's catalytic efficiency.

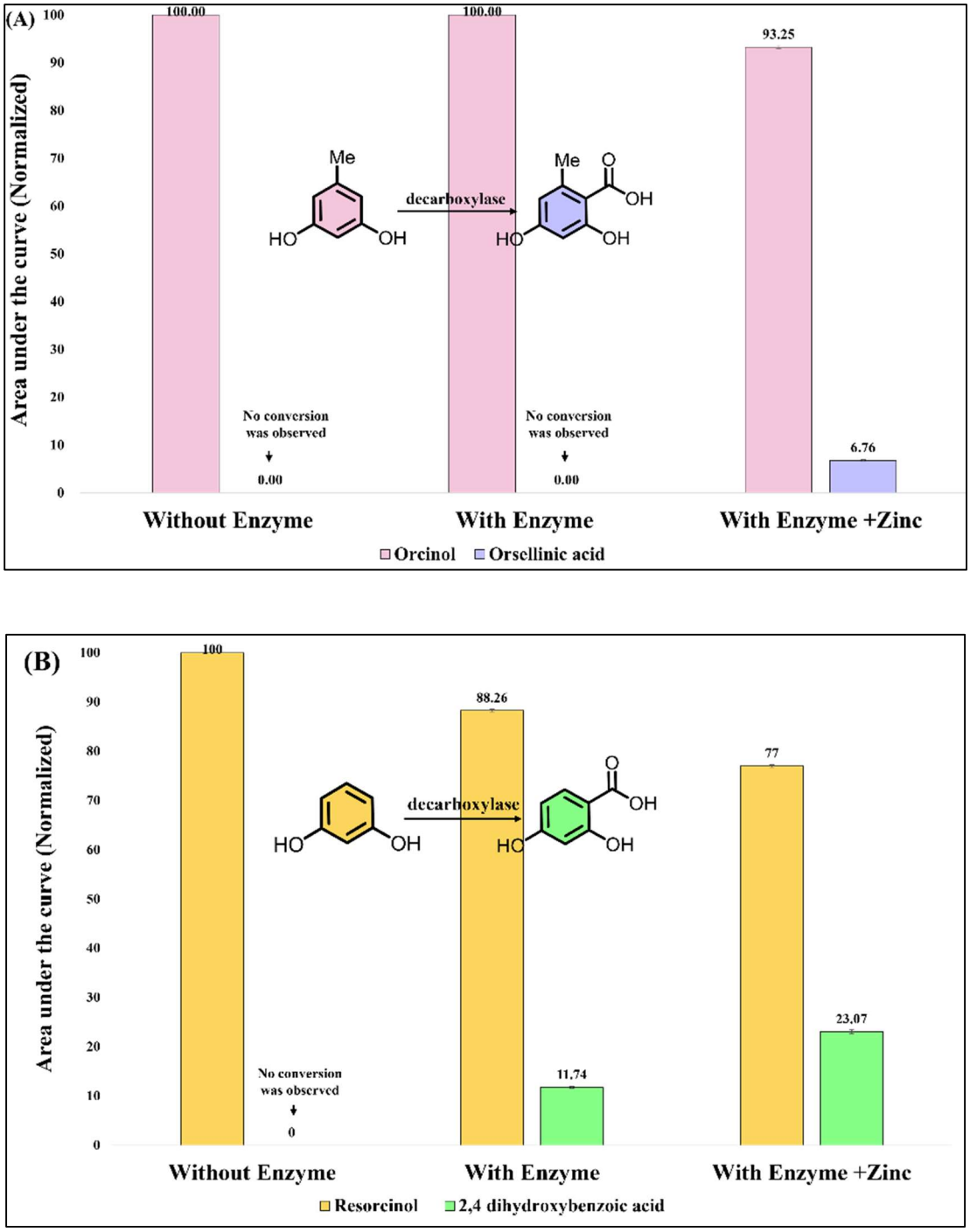

Figure 44: Comparative analysis of enzyme catalysis for conversion of (A) orcinol to orsellinic acid at 4°C and (B) resorcinol to 2,4-dihydroxybenzoic acid at 30°C. The enzyme catalysis reactions were analyzed by comparing the area under the curve in the HPLC chromatograms obtained with and without the addition of zinc. The chromatograms were recorded at a wavelength of 250 nm.

5.10 Proposed mechanisms for reversible decarboxylase

5.10.1 Proposed mechanism of decarboxylation

We have speculated that the mechanism of the decarboxylation reaction would require the zinc atom to play a pivotal role in facilitating the catalytic process **(Figure 46)**. Based on the crystal structure of the closely related sequence of reversible 2,6-dihydroxybenzoate (gamma-resorcylate) decarboxylase from Rhizobium sp. (Goto et al., 2006) with decarboxylase of *C. uncialis*, we predict that the divalent zinc ion in *C. uncialis* decarboxylase coordinates with the active site residues Glu5, His7, and His150. The zinc ion would potentially form an ion pair with the carboxylate of the substrate. We also speculate that the carboxylate of Asp274 would play a role as a proton shuttle during the tautomerization of the phenol group ortho to the carboxylate. We also suggest that the imidazole group of His210 might sit in a position to act as a general acid in this process with a water molecule acting as a proton shuttle. This step is summarized in step (**1**) in **(Figure 45)**. This results in the formation of the tautomer shown in structure (**2**), which undergoes decarboxylation, re-aromatization, and protonation to yield orcinol as shown in structure (**3**). This also leaves an open valence on the zinc that would be ready to accept another molecule of substrate. The proton of this carboxylic acid of the substrate would potentially be used to reprotonate the nitrogen atom of His210, possibly using the water molecule as a proton shuttle.

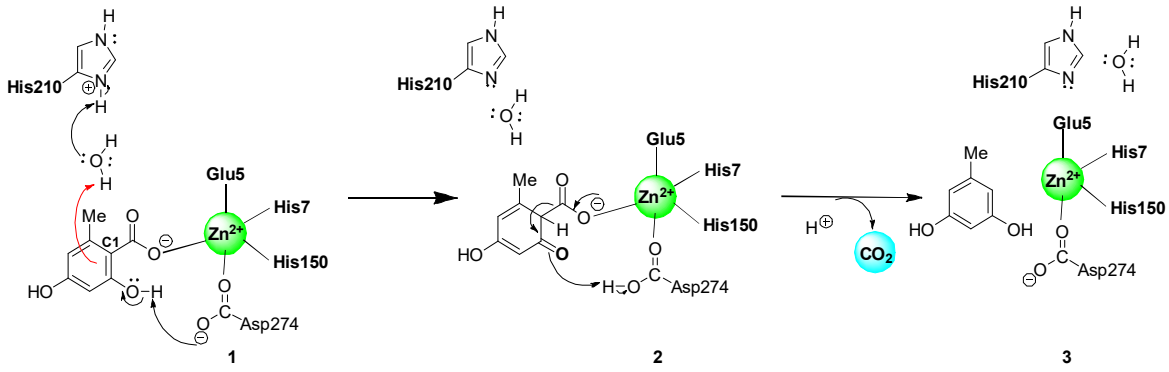

Figure 45: Proposed mechanism for the decarboxylation of an ortho-acid by the decarboxylase enzyme from *C. uncialis*.

5.10.2 Proposed mechanism of carboxylation

We also speculated on the mechanism of the carboxylation process catalyzed by this decarboxylase enzyme. In particular we sought to explain the necessary interaction between the carbonate molecule and the divalent zinc. We proposed that after binding of the phenolic substrate (**1**), in this case orcinol, the carbonate can potentially displace the carboxylate of Asp274 on the zinc as shown in structure (**2**). This would set up an interaction that would facilitate the attack on the carbonyl of the carbonate via a tautomerization of the ortho phenol group as described in structure (**3**). We speculate that re-aromatization would be rapid (**4**) and with the transfer of a proton to the tetrahedral intermediate (**5**). Collapse of this tetrahedral intermediate would form the carboxylic group (**6**) with concomitant release of a molecule of water. Release of the final product could be facilitated by protonation of the ortho phenol (**7**) resulting in the formation of orsellinic acid (**8**) (**Figure 46)**. Full confirmation of this mechanism would require a separate detailed mechanistic study.

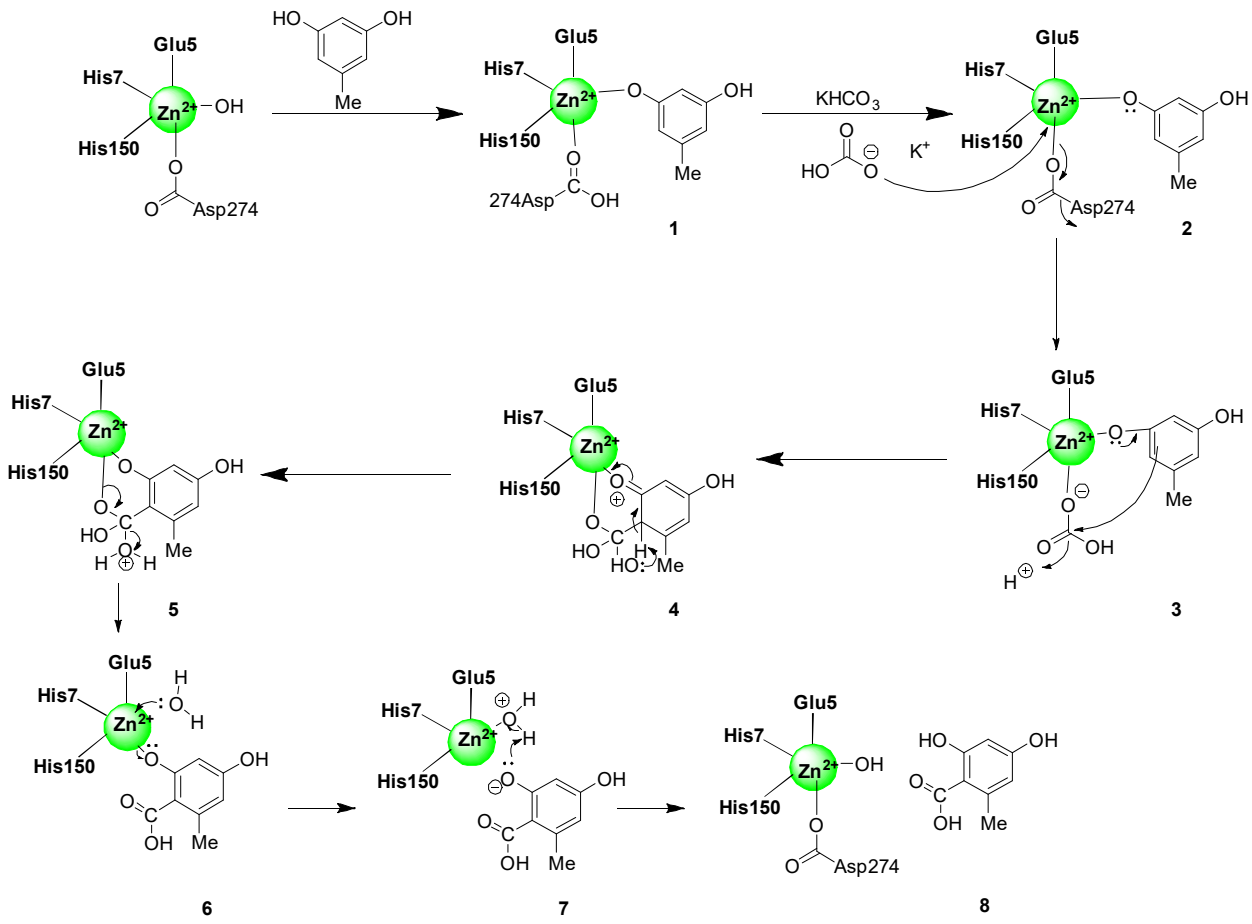

Figure 46: Proposed Mechanism for Carboxylation by the decarboxylase enzyme from *C. uncialis.*

5.11 Discussion

Several lichen genes have been indirectly linked to their tentative function through genome mining strategies such as comparative homology mapping, transcriptional profiling, and phylogenetic analyses. However, attempts to validate these associations through heterologous expression in *Aspergillus spp.* or *E. coli* have met with only limited success. There have been only two recent reports where polyketide synthases (PKSs) have been successfully expressed in heterologous systems. One study demonstrated the heterologous expression of a codon-optimized gene, *pfur17-0229*, from the perfume lichen *Pseudevernia furfuracea* in *Saccharomyces cerevisiae* (Kealey et al., 2021) resulting in the production of lecanoric acid.

Another report by (Kim et al., 2021) demonstrated the functional heterologous expression of a novel lichen polyketide biosynthetic gene cluster (BGC) from the lichen mycobiont *Stereocaulon. alpinium* in a plant pathogenic fungus, *Ascochyta rabiei* resulting in the production of detectable amounts of atranorin.

We previously reported (Bertrand et al., 2019) on the attempted expression of the polyketide synthase at the core of his gene cluster (*cu-nr-pks-5*), which we predicted to be responsible for orsellinic acid biosynthesis. In this previous work we observed transcription of the gene but no detectable natural product formation, for reasons that still do not appear apparent. Despite this failure we sought to explore the function of the adjacent gene that appeared to encode for a decarboxylase. This gene was only 963 bp in length giving a predicted size of the resulting protein of 35 kDa. Furthermore, the lack of observable introns led us to speculate that this gene might be amenable to expression in *E. coli* using standard techniques. To that end, we amplified and cloned this gene into the pQE80L expression plasmid, chosen for its T5 lac promoter, which allows moderate expression levels, making it a better choice for potentially toxic proteins. Since it was unknown whether the produced protein would be toxic to *E. coli*, the plasmid's inclusion of the *lacIq* gene helps repress foreign gene expression until induced by IPTG. Additionally, the N-terminal His6 tag facilitates purification (The QIA *expressionist*-fifth edition).

We were able to successfully induce the expression of the decarboxylase gene with IPTG and subsequent purification using NTA Ni2+ affinity chromatography at 4 °C yielded a protein with an observed approximate molecular mass of 35 kDa as determined by SDS-PAGE chromatography. We observed protein degradation when we attempted protein purification at 30 °C, as analyzed by SDS-PAGE **(Figure S 14)**. Literature reports on the purification of reversible

resorcylate decarboxylase from *Rhizobium sp.* (Yoshida et al., 2004) and reversible 2,3-dihydroxybenzoic acid decarboxylase from *Fusarium oxysporum* (X. Zhang, Ren, et al., 2018) were also carried out at 4 °C, suggesting that lower temperatures may help in maintaining protein stability during purification.

The predicted 3D structure of the purified protein revealed a TIM beta/alpha barrel fold, suggesting homology with the metallo-dependent hydrolase superfamily. The construction of a phylogenetic tree revealed that the decarboxylase from *C. uncialis* shares 71% similarity (1000 bootstrap value) with a thermophilic reversible gamma-resorcylate decarboxylase from *Rhizobium sp.* (Yoshida et al., 2004). The homology modeling with reversible gamma-resorcylate also predicted the presence of a metal binding site, most likely an atom of zinc based on previous observations (Goto et al., 2006)

This enzyme was part of a small biosynthetic gene cluster that had at the core a gene that encoded for a PKS that was predicted to produce orsellinic acid. We therefore set out to determine if this decarboxylase enzyme could catalyze the decarboxylation of orsellinic acid. We observed that, indeed, the decarboxylation of orsellinic acid was accelerated in the presence of both enzyme and zinc **(Figure S 17)**. We did also observe some background spontaneous decarboxylation of orsellinic acid, but the presence of both enzyme and zinc resulting in a considerable increase in the production of orcinol under the same conditions. We also observed that this enzyme was capable of the decarboxylation of 2,4-dihydroxybenzoic acid, a substrate that did not undergo any observable spontaneous reactions. Perhaps unsurprisingly this enzyme had a requirement for an atom of zinc to be present for fully efficient catalysis, an observation consistent with other known decarboxylases.

Most significant, we observed that the reverse reaction could be efficiently catalyzed by this enzyme, with resorcinol being converted to 2,4-dihydroxybenzoic acid as well as orcinol being converted to orsellinic acid. We also observed an interesting in the temperate where this enzyme was most effective in carrying out this reaction. We observe the highest yield of orsellinic acid when the reaction was run at 4°C but a higher temperature of 30°C has the best yield of 2,4-dihydroxybenzoic acid. One possible explanation for the lack of observable orsellinic acid at 30°C is that any product formed might be readily decarboxylated back to orcinol at this temperature.

While we were disappointed to not observe any reaction with anthranlic acid or aniline, it was not entirely unexpected. These results are consistent with previous work, which suggests that the presence of a phenolic hydroxyl group (OH) is essential for carboxylation or decarboxylation metallo-dependent enzymatic reactions (Bierbaumer et al., 2023). Based on these results, we proposed a mechanism for enzymatic decarboxylation (**Figure 45**) that involves a tautomerization to the keto form of the phenol which provides an electron sink for the decarboxylation. The mechanism of carboxylation (**Figure 46**) also invokes the involvement of the phenolic OH group, again via a keto-enol tautomerization. We also speculate that the *ortho*-OH group is involved in directing the substrate to bind to the zinc atom in a way to facilitate the capture of an enzyme-bound carbonate. The confirmation of these mechanisms for this particular decarboxylase would require a detailed mechanistic study, but we suggest that they are consistent with previous reports (Liu et al. 2024)

This is the first report of a reversible decarboxylase from a lichen-forming fungus, although such enzymes have been extensively reported from bacteria (Ishii et al., 2004; Kino et al., 2020;

Kirimura et al., 2010; Wuensch et al., 2014, 2015; Yoshida et al., 2007). This suggests the possibility of horizontal gene transfer from bacteria to lichenized fungi, which may have enabled the acquisition of new capabilities, such as the production of novel secondary metabolites (SMs). However, reports of gene transfer between bacteria and lichenized fungi remains limited, and further research will be needed to elucidate these mechanisms and implications.

The gene coding for this decarboxylase appears in the genome of *C. uncialis* flanking a gene that encodes for a polyketide synthase that is predicted to produce orsellinic acid. Since orcinol is a well-known lichen natural product (Huneck, 1973; Papadopoulou et al., 2007; Ranković, 2019) our results may suggest that there is a dedicated decarboxylase that has a role in biosynthesis. It appears that although orsellinic acid can undergo spontaneous decarboxylation it may not be an efficient enough process for the lichen fungi. Lichen have adapted to thrive in cold and harsh environments and part of the discussion is how these fungi can operate metabolism under these conditions. The use of dedicated enzymes to accelerate reactions that, under other conditions would be spontaneous, may be one of the adaptation mechanisms.

This is also the first report of the functional expression of a decarboxylase enzyme from a lichen-forming fungus. Additionally, this is also the first report of the functional expression of a post-PKS tailoring enzyme from a lichen. This report may suggest that there would be utility in pursuing the functional expression of other tailoring genes that have been observed in the lichen genome (Bertrand et al. 2018b). These tailoring enzymes may be a source of effective biocatalysts that have some commercial potential. For example, orcinol is effectively a commodity chemical readily available with costs on the order of a few cents per milligram, Orsellinic acid on the other hand is considerably more expensive with costs on the order of a

dollars per milligram. The use of an enzyme catalyzed reaction to produce orsellinic acid therefore has considerable commercial potential. The conversion of orcinol to orsellinic acid using conventional organic synthesis techniques involves several steps involving air and moisture sensitive reagents.

This decarboxylase enzyme might also have applications beyond the synthesis of orsellinic acid. For example, the Kolbe-Schmitt is a well-known conventional carboxylation reaction of salicylic acid derivatives with extensive industrial applications (Glueck et al., 2010). However, the chemical reaction is a highly energy-consuming and requires strong basic conditions with high temperature/pressure (Gilman et al., 1940). In contrast, the enzymatic addition and removal of the carboxyl group could provide the best solution to accelerate such reactions. Moreover, the lack of regioselectivity in these synthetic reactions leads to the formation of numerous by-products, posing practical challenges in product separation (Gilman et al., 1940). The best alternative for attaining high regioselectivity and eco-friendly carboxylation of phenolic compounds would be the use of decarboxylase enzymes.

In conclusion, the successful cloning, expression, and characterization of the decarboxylase gene from *C. uncialis* provide valuable insights into the biosynthesis of orcinol in lichen. Future research should focus on elucidating the enzymatic mechanisms and regulatory pathways associated with decarboxylase activity in lichens. Exploring the genetic organization of biosynthetic gene clusters and conducting feeding experiments with labeled substrates could elucidate the intricate processes of lichen SMs biosynthesis. Additionally, investigating the potential applications of decarboxylase and other enzymes in the biotechnology and

pharmaceutical industries may lead to the development of novel biocatalysts that can accomplish difficult to achieve reactions.

5.12 Conclusion

This study achieved the cloning, expression, and characterization of the decarboxylase gene from *C. uncialis*, shedding light on the BGC of orsellinic acid in *C. uncialis*. The substrate specificity of the enzyme, along with its potential role in catalyzing the reversible conversion of orsellinic acid to orcinol and 2,4-dihydroxybenzoic acid to resorcinol, was investigated. Indeed, the reversible decarboxylation between orcinol and orsellinic acid suggests the possibility of synthesizing orsellinic acid from orcinol. Further research is needed to fully understand the enzymatic mechanisms and regulatory pathways associated with decarboxylase role in lichens.

Chapter 6

Functional heterologous expression of a halogenated isocoumarin biosynthetic gene cluster from the lichen, *Cladonia uncialis*

6.1 Introduction

The advent of next-generation sequencing (NGS) has revolutionized natural product research, particularly in the identification of biosynthetic gene clusters (BGCs) within lichen genomes. NGS expedites genome-guided research by sequencing millions of DNA fragments simultaneously, resulting in significant decreases in time and cost. Before the development of NGS, alternative approaches were used to identify genes associated with natural products biosynthesis. One such method was primer fishing, which involves conducting PCR reactions using degenerate primers on cDNA generated from the total mRNA of an organism. By targeting and amplifying these transcriptionally active genes, researchers could then sequence the amplified products using traditional Sanger sequencing methods, allowing for the identification and study of specific biosynthetic genes (M. Abdel-Hameed et al., 2016a).

Dr. Mona Abdel-Hameed, a former Ph.D. student in the Sorensen group, conducted preliminary work on *cu-pks-4* BGC. In early experiments that were designed to identify the biosynthetic gene cluster associated with usnic acid production in *C. uncialis*, she generated the cDNA sequence of a transcriptionally active polyketide synthase (PKS). Surprisingly, the amplified sequence lacked the typical MT domain, typically found in the usnic acid gene cluster, also contained a TE domain instead of the predicted CYC domain. This discrepancy with the predicted sequence of the usnic acid PKS gene prompted the question: if the PKS does not produce usnic acid, what

was it synthesizing? The genome assembly provided the first clue, revealing that this PKS was associated with four tailoring genes which is not consisted with the single tailoring gene expected for usnic acid biosynthesis. This new PKS gene appeared to anchor a distinct BGC called *cu-pks-4* (M. Abdel-Hameed et al., 2016a).

6.2 What is the function of this PKS?

The Sorensen group previously reported a putative identification of the *cu-pks-4* gene cluster in *C. uncialis* which appears to code for a halogenated isocoumarin compound (Abdel-Hameed et al., 2016). This biosynthetic gene cluster (BGC) consists of five genes, with the core gene being a polyketide synthase (PKS) named as *Cu*-A **(Figure 47)**. This PKS gene has a high homology with a PKS gene reported from *Aspergillus terreus* that is responsible for producing intermediates of the mycotoxin terrein (Kahlert et al., 2021).

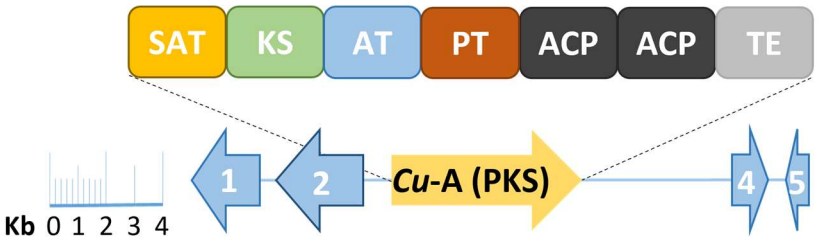

(1): Monooxygenase (*Cu*-D) **(2)**: Protein with KR-DH-like features (*Cu*-B) **(4)**: Halogenase (*Cu*-halo) **(5)**: O-methyltransferase (*Cu*-OMT)

Figure 47: The biosynthetic gene cluster *cu-pks-4* identified in *C. uncialis*. The legends in red color (in brackets) represent abbreviations for gene names that are referenced in the next section.

Surrounding *Cu*-A (PKS) there are four tailoring genes (**Figure 47**). These four genes are associated within the *cu-pks-4* cluster are: an upstream FAD-binding monooxygenase (*Cu*-D), an upstream PKS-like gene featuring ketoreductase and dehydratase (KR-DH) domains (*Cu*-D),

a downstream halogenase (*Cu*-halo), and a downstream O-methyltransferase (*Cu*-OMT). These functional assignments were made based on their homology with known genes from related biosynthetic clusters available in GenBank (M. Abdel-Hameed et al., 2016a).

Heterologous expression of *terA*, the PKS gene from *A. terreus* that has high homology to *cu-pks*-4 in *A. oryzae* NSAR1 resulted in the formation of the non-reduced pentaketide 2,3-dehydro-6-hydroxymellein, along with orsellinic acid and 4-hydroxy-6-methylpyranone as shunt products. This non-reduced pentaketide is further reduced by a separately encoded KR-DH peptide (TerB) to yield 6-hydroxymellein **(Figure 48)**. The collaborative functions of TerA and TerB were recently confirmed through functional expression in *A. oryzae* NSAR1 (Kahlert et al., 2021), which led to the production of 6-hydroxymellein **(Figure 48)**. Lichens have been a rich source of various halogenated molecules with significant biological properties (Ranković, 2019). These include halogenated anthraquinones such as 2-chloroemodin (Cohen & Neil Towers, 1996); depside, chloroatranorin (Türk et al., 2006), fluoroatranorin (Bauri et al., 2024), 10-chloropannarin (Correche et al., 2002), chloroatranol, and buellin (Millot et al., 2009). Additionally, novel chlorinated amides such as cladoniamides (A, B, D-G) were isolated from mycobiont partner of *Streptomyces uncialis* (Williams et al., 2008).

In our previous studies, we identified a homolog of TerA and TerB in the *C. uncialis* genome. We hypothesize that the homologs of TerA and TerB encoded as *Cu*-A and *Cu*-B in the *C. uncialis* genome perform a similar function.

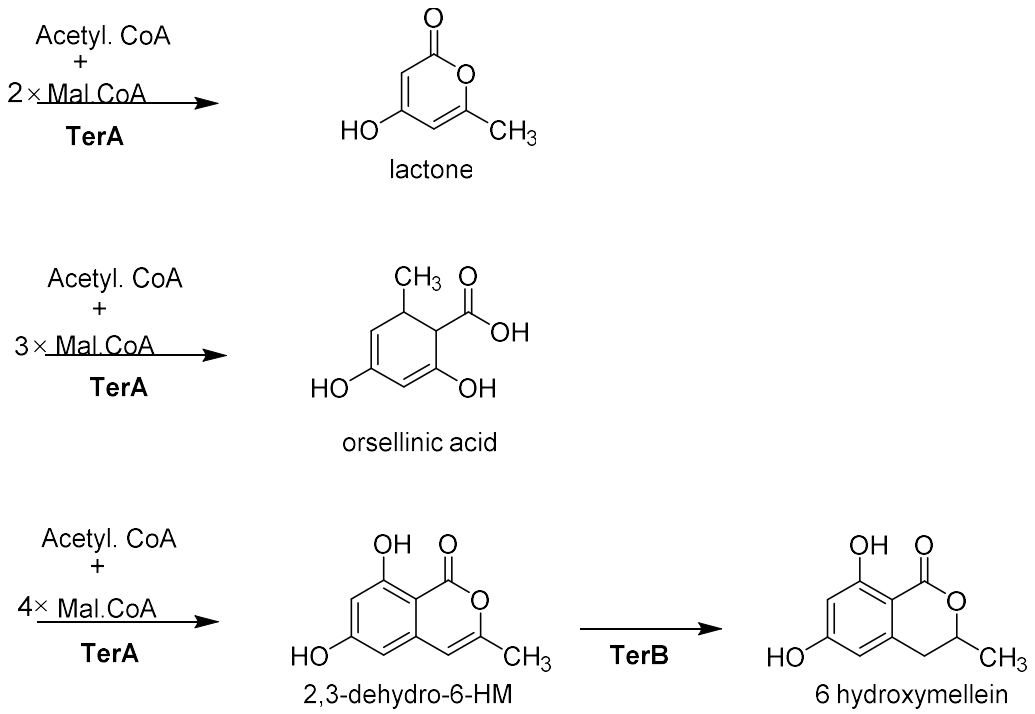

Figure 48: Biosynthesis of 6-hydroxymellein with collaborating expression of TerA and TerB from *A. terreus* in *A. oryzae* NSAR1 (Kahlert, Villanueva, et al., 2021).

In our previous studies, we identified a homolog of TerA and TerB in the *C. uncialis* genome. We hypothesize that the homologs of TerA and TerB encoded as *Cu*-A and *Cu*-B in the *C. uncialis* genome perform a similar function. In addition to these homologs, the annotated biosynthetic gene cluster in *C. uncialis* also includes genes, identified by homology, that encode for an FAD monooxygenase, O-methyltransferase, and halogenase **(Table 7)**. Based on this, we propose that 6-hydroxymellein is converted into a halogenated isocoumarin (M. Abdel-Hameed et al., 2016a), as illustrated in **Figure 49**.

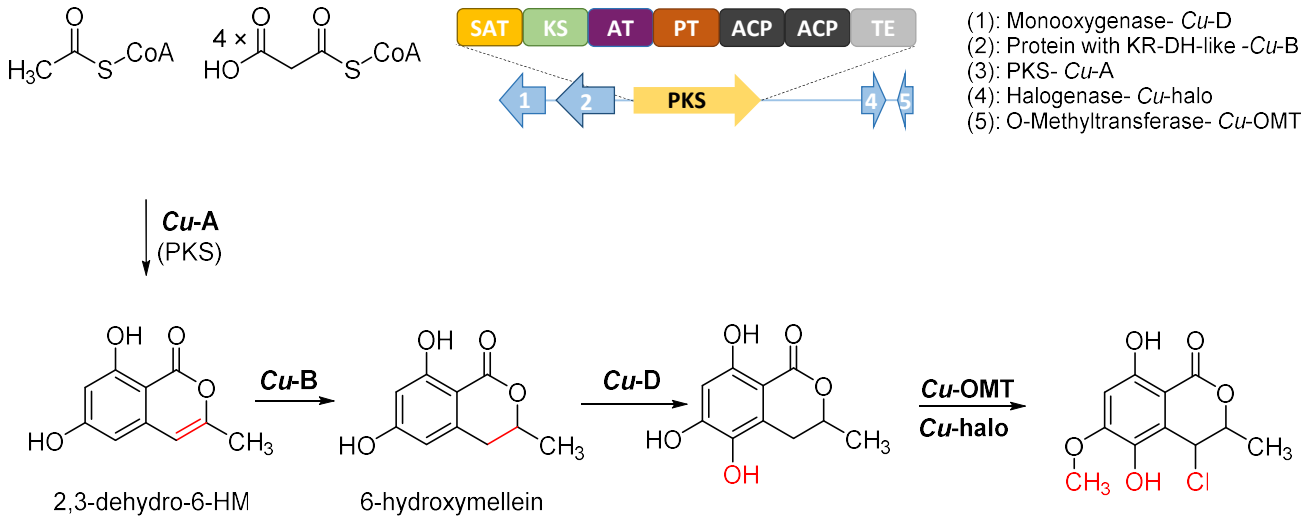

Figure 49: Proposed biosynthetic pathway and domain architecture of the halogenated isocoumarin biosynthetic gene cluster (*cu-pks-4*) isolated from *C. uncialis*.

To identify potential lichen metabolites similar to the hypothesized end products we conducted an extensive search of the Dictionary of Natural Products. Three similar compounds were identified **(Figure 50)**. Compounds A and B were isolated from *Lachnum papyraceum* (Stadler & Anke, 1995), while compound C was isolated from *Graphis sp.*(Takenaka et al., 2011). None of these compounds have been observed in *C. uncialis*. Although each of these isolated metabolites exhibits only two of the three proposed modifications (hydroxylation, O-methylation, and halogenation), the presence of molecules resembling the hypothesized end-product supports the plausibility of the proposed structure. Based on these molecules, a halogenated isocoumarin **(Figure 49)** was proposed.

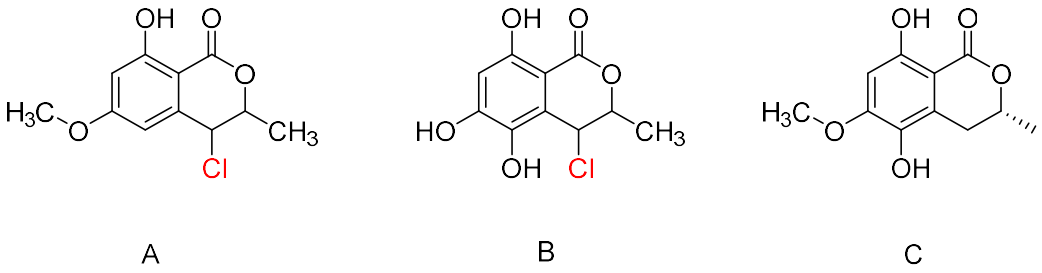

Figure 50: Three lichen-derived molecules structurally similar to the hypothesized end-product of the proposed biosynthetic pathway: (A) 4-chloro-6-methoxymellein, (B) 4-chloro-5,6-dihydroxymellein, (C) 5-hydroxy-6-methoxymellein.

In **chapter 5**, previous attempts at heterologous expression of the gene from *C. uncialis* coding for an orsellinic acid synthase (OAS) in *A. oryzae* NSAR1 was unsuccessful in producing orsellinic acid. However, when the OAS gene from *Fusarium* spp., a non-lichen fungal species, was expressed under similar conditions, the production of orsellinic acid was observed.

Therefore, we decided to investigate codon-optimized lichen, *C. uncialis*, genes for expression in *A. oryzae* NSAR1. With the support of a gene synthesis grant from the Joint Genomics Institute, we received a collection of codon-optimized genes (PKSs and tailoring genes). Among these, we received a complete BGC, *cu-pks-4*, from *C. uncialis*. This cluster comprised of the PKS gene (*Cu*-A) and four tailoring genes (*Cu*-B, *Cu*-D, *Cu*-halo, and *Cu*-OMT).

6.3 Bioinformatics analysis of *cu-pks-4* BGC

In a previous study, total mRNA from a fungal sample of *C. uncialis* was extracted and reverse-transcribed into a complete cDNA library. The full-length sequence (6150 bp) was annotated using antiSMASH (V.1) (Medema et al., 2011), revealing that *cu-pks-4* is an iterative type I PKS containing a ketosynthase (KS), an acyl transferase (AT), two acyl carrier proteins (ACP), and a terminal thioesterase (TE) domain. Further manual BLAST analysis and updated annotation

using antiSMASH (V.3.0) (T. Weber et al., 2015) identified post-PKS tailoring genes within a 54,157 bp contig. This analysis identified four genes associated with *cu-pks-4*, including an upstream FAD-binding monooxygenase, an upstream PKS-like motif with ketoreductase and dehydratase (KR-DH) domains, a downstream halogenase, and a downstream O-methyltransferase. These functions were assigned based on their homology with characterized genes in related biosynthetic clusters in GenBank (M. Abdel-Hameed et al., 2016a).

Phylogenetic analysis revealed a close homology between the *Cu*-A, *Cu*-B, and *Cu*-D genes from the *cu-pks-4* cluster and their counterparts, TerA, TerB, and TerD, respectively, found in the terrein biosynthetic gene cluster of *A. terreus* (**Table 7**). This suggests a conserved functional role for these genes in polyketide biosynthesis. The amino acid sequence of the codon-optimized *Cu*-A gene was submitted to UniProt for analysis. The results revealed that *Cu*-A has a high sequence similarity of 58.1% with the TerA gene from *A. terreus* and 46.8% similarity with a polyketide synthase gene from *Alternaria burnsii* **(Figure S 26)**. InterPro analysis further supported the functional similarity between *Cu*-B and TerB, as both proteins contain similar domain architectures, including DH, C-Met, and KR domains **(Figure S 28)**.

While *Cu*-halo and *Cu*-OMT do not have counterparts in the terrein gene cluster, manual BLAST analysis identified homologous genes in other organisms. *Cu*-halo showed 56% similarity to a gene from *Staphylococcus borealis* (ESZ96411), suggesting a potential role in halogenation reactions. Similarly, *Cu*-OMT exhibited 77% similarity to a gene from *Philocephala scopiformis*, indicating a potential role in O-methylation reactions. These findings suggest that the *cu-pks-4* cluster may encode a unique biosynthetic pathway for the production of halogenated isocoumarins in *C. uncialis* (M. Abdel-Hameed et al., 2016a).

Table 7: Genes in *cu-pks-4* biosynthetic gene cluster from *C. uncialis*

S. No	Genes names	Genes Abbreviation	Terrein pathway homolog	Putative function
1	Monooxygenase	*Cu*-D	TerD	oxidation
2	Protein with KR-DH like features	*Cu*-B	TerB	reduction
3	Polyketide Synthase	*Cu*-A	TerA	2,3-dehydro-6-hydroxymellein synthesis
4	Halogenase	*Cu*-halo	N/A	halogenation
5	O- methyl transferse	*Cu*-OMT	N/A	o-methylation

6.4 Secondary metabolic analysis of *cu-pks-4* BGC

With the support of a gene synthesis grant from the Joint Genomics Institute, we acquired the complete codon-optimized biosynthetic gene cluster (BGC) for the halogenated isocoumarin (version of *C. uncialis*). I began the project by analyzing the gene sequences, submitted for both antiSMASH (V.7.1) (Blin et al., 2023) and InterPro analysis (Paysan-Lafosse et al., 2023), https://www.ebi.ac.uk/interpro/, for comprehensive domain identification. The antiSMASH results identified key domains present within the cluster, including the SAT, KS, AT, DH, PT, ACP, and TE domains, with a specific emphasis on the dehydratase (DH) domain detected within the cluster **(Figure 51)**.

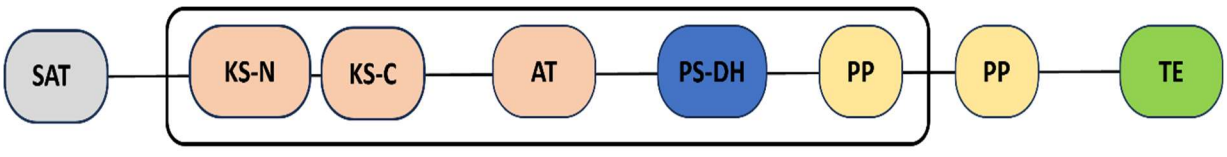

Figure 51: Pfam domain annotation of *cu-pks-4* BGC isolated from *C. uncialis* via antiSMASH analysis, highlighting key biosynthetic domains, including the dehydratase (DH) domain.

This observation was further validated by InterPro analysis **(Figure 52)**, which revealed high degree of homology between the PT and DH domain **(Figure S 27)**. The combined analysis confirmed the presence of the SAT, KS, AT, DH, PT, ACP, ACP, and TE domains within *cu-pks-4* BGC.

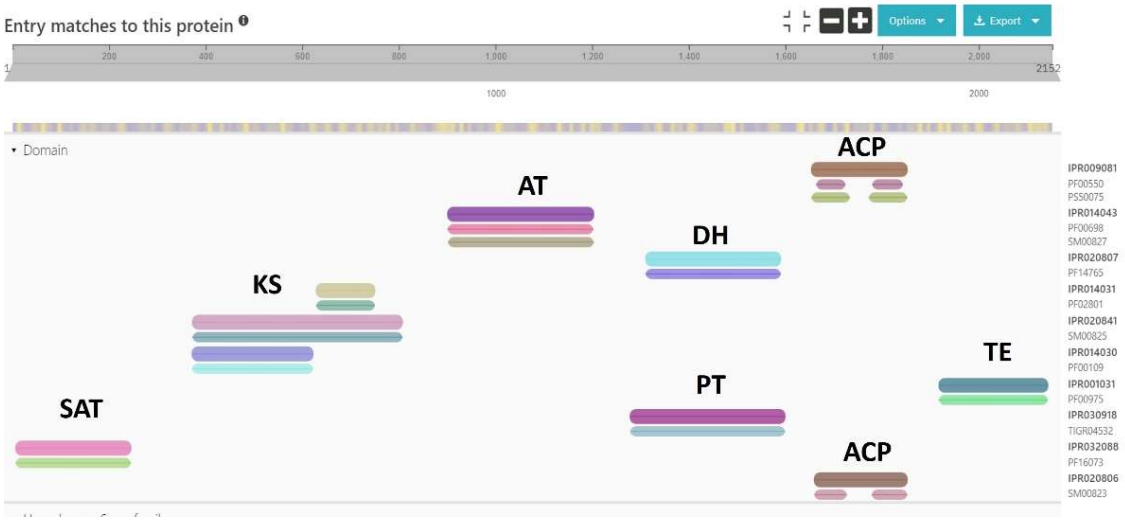

Figure 52: InterPro analysis of *Cu*-A from *C. uncialis* identified the SAT, KS, AT, DH, PT, ACP, ACP, and TE domains. The labels were manually added, and the corresponding InterPro identifier codes are presented on the right side of the figure.

6.5 Gateway cloning of isocoumarin BGC genes in expression vectors

Three plasmids were constructed for the expression of the isocoumarin BGC: (1) *Cu*-A pTYGSade, which contains the 6,459 bp *Cu*-A gene regulated by an amylase promoter; (2) *Cu*-A_*Cu*-D_*Cu*-OMT pTYGSade, harbors the *Cu*-A gene (6,459 bp) under the control of an amylase promoter, along with the *Cu*-D gene (1,788 bp) under the adh promoter and the *Cu*-OMT gene (1,197 bp) under the control of a gpd promoter. Both plasmids have the pTYGSade backbone and utilize adenine as a selection marker, (3) *Cu*-B_*Cu*-halo pTYGSmet includes the *Cu*-B gene (3,012 bp) under the adh promoter and the *Cu*-halo gene (1,689 bp) under the gpd

promoter. This plasmid uses the pTYGSmet backbone and methionine as selection markers. Detailed descriptions of these plasmids are provided in **Table 8** and **Figure 53**.

Table 8: Plasmid names, sizes (bp), key genes, promoters, and backbones in halogenated isocoumarin BGC

S. No	Plasmid Name	Size (bp)	Genes	Promoters*	Backbone
1	*Cu*-A-pTYGSade	20,015	*Cu*-A (6459 bp)	Pamy	pTYGSade
2	*Cu*-A_*Cu*D_*Cu*-OMT pTYGSade	22,843	*Cu*-A (6459 bp) *Cu*-D (1788 bp) *Cu*-OMT (1197 bp)	Pamy Padh Pgpd	pTYGSade
3	*Cu*-B_*Cu*-halo pTYGSmet,	21,321	*Cu*-B (3012 bp) *Cu*-halo (1689 bp)	Padh Pgpd	pTYGSmet

***Pamy**: promoter amylase, **Padh**: promoter alcohol dehydrogenase, **Pgpd**: promoter glyceraldehyde-3-phosphate dehydrogenase.

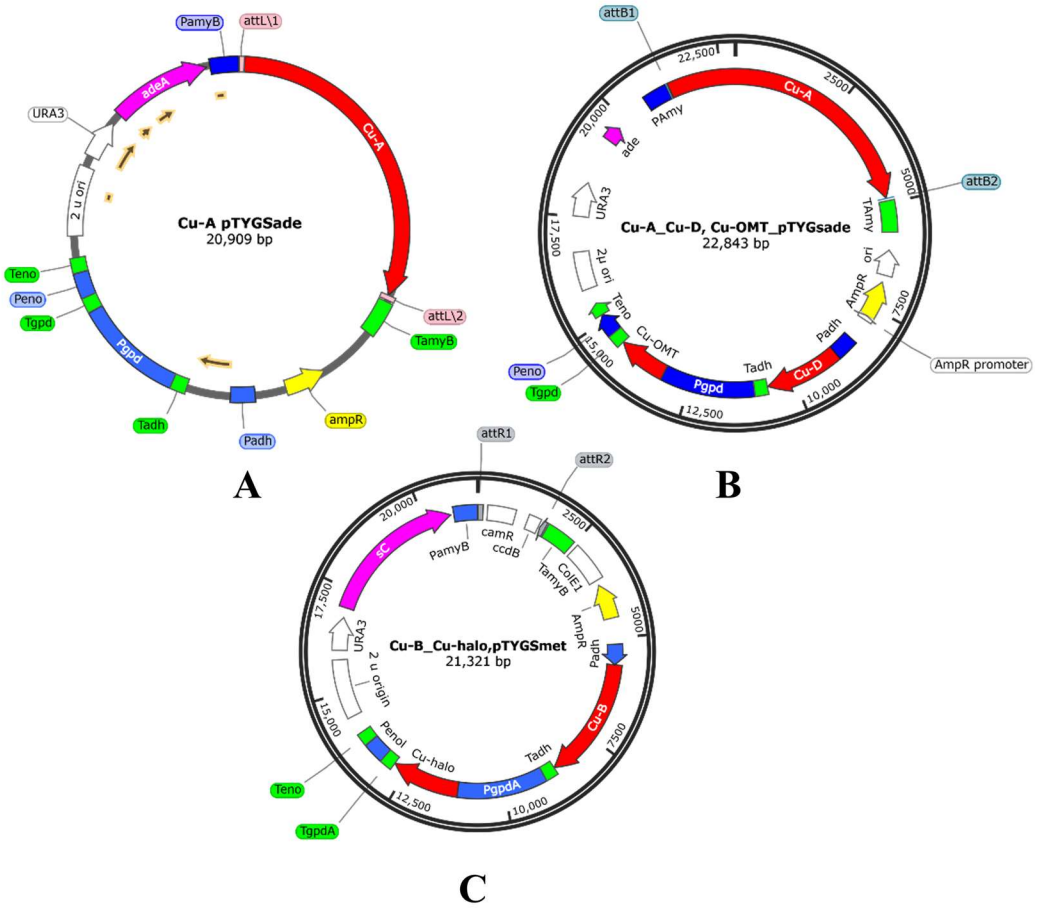

Figure 53: Three expression plasmids were constructed for the isocoumarin, *cu-pks-4*, BGC. (A) *Cu*-A-pTYGSade (adenine-based selection), (B) *Cu*-A_*Cu*-D_*Cu*-OMT pTYGSade (adenine-based selection), and (C) *Cu*-B_*Cu*-halo pTYGSmet (methionine-based selection). Genes are highlighted in red, promoters in blue, and terminators in green. The selection markers adenine (ade) and methionine (sC) are indicated in pink. The ampicillin resistance gene (AmpR), depicted in yellow, facilitates the shuttling of initial plasmid constructs through *E. coli*.

6.6 Fermentation, extraction, and characterization of compounds produced by *Cu*-A pTYGSade transformant

Positive transformants of *A. oryzae* NSAR1 with *Cu*-A were grown in 2.5 L of DPY media at 30°C for 7 days. Ethyl acetate extraction from 2.5 L culture yielded ~880 mg of crude extract.

6.7 Characterization of compounds 5 and 6 produced by *Cu*-A pTYGSade transformants

The chromatographic fractionation using biotage flash chromatography of the crude extract yielded two main compounds **5** (~220 mg) and **6** (~10 mg). The structures of compounds **5** and **6 (Figure 54)** were identified by NMR and LC-MS. The data is as follows:

Compound **5** (Pyrone): White crystals; ^{1}H NMR (MeOD, 500 MHz) δ_H 7.94 (1H, s, H-6), 6.48 (1H, s, H-3), 4.29 (2H, s, H-7). ^{13}CNMR (MeOD, 125 MHz); δ_C 175.43 (C-2), 169.00 (C-5),145.95 (C-4), 139.56 (C-6), 109.31 (C-3), 59.75 (C-7); HMBC correlation: C-2/H-6, C-5/H-6, C-5/H-3, C-5/H-7, C-4/H-3, C-4/H-6, C-3/H-7. The molecular formula of compound **5** is $C_6H_6O_4$ and a molecular ion of [M-H] 141.05 (142.11 calculated) was observed in the negative ion mode of LC-MS.

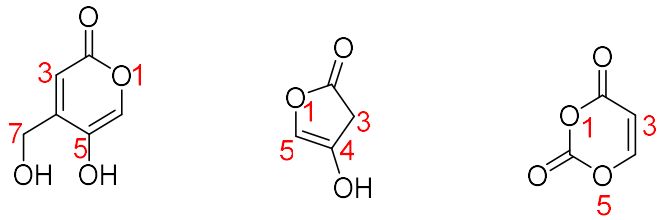

Compound **5** Compound **6** Compound **7**

Figure 54: Chemical structures of compounds **5, 6** and **7**.

Compound **6** (Tetronic Acid): Creamy powder; ^{1}H NMR (MeOD, 500 MHz) δ_H 6.74 (1H, s, H-5), 2.55 (2H, s, H-3), ^{13}CNMR (MeOD, 125 MHz); δ_C 174.80 (C-2), 28.41 (C-3), 166.66 (C-4), 133.76 (C-5); HMBC correlations: H-5/C-4, H-3/C-2.The molecular formula of compound **5** is $C_4H_4O_3$ and a molecular ion of [M-H] 99.80 (100.07 calculated) was observed with negative ion mode of LC-MS.

6.8 Characterization of the metabolites produced by three gene plasmid transformants

The transformant of *A. oryzae* NSAR1, which contains three introduced genes (*Cu*-A, *Cu*-D, and *Cu*-OMT), was cultivated in 2 L of DPY media at 30°C for 7 days. The ethyl acetate extraction from the 2 L culture resulted in ~670 mg of the crude extract. Chromatographic fractionation of this crude extract yielded four major compounds: **5** (~20 mg), **6** (<5 mg), **7** (<5 mg), and **8** (<5 mg).

The characterization data for compound **7 (Figure 54)** is as follows:

Compound **7**: (Pleurone): white powder; ^{1}H NMR (MeOD, 500 MHz) δ_H 8.54 (1H, d, J = 9.86 Hz, H-4), 5.79 (1H, d, J = 9.86 Hz, H-3), ^{13}CNMR (MeOD, 125 MHz); δ_C 165.86 (C-2), 150.19 (C-6), 148.26 (C-4), 97.53 (C-3). Data is similar to literature (Lee et al., 2011).

6.9 Confirmation of integration of BGC genes into the *A. oryzae* NSAR1 genome

Genomic DNA was extracted from an *A. oryzae* NSAR1 transformant containing five gene BGC. This DNA was used as a template for amplifying the *Cu*-A, *Cu*-B, *Cu*-D, *Cu*-OMT, and *Cu*-halo genes. The agarose gel electrophoresis results showed bands for the amplified fragments: *Cu*-A-frag (719 bp), *Cu*-B-frag (814 bp), *Cu*-D-frag (828 bp), *Cu*- OMT-frag (841 bp), and *Cu*- halo-frag (854 bp) **(Figure 55)**. These findings confirm the successful integration of the entire five gene biosynthetic gene cluster into the *A. oryzae* NSAR1 genome.

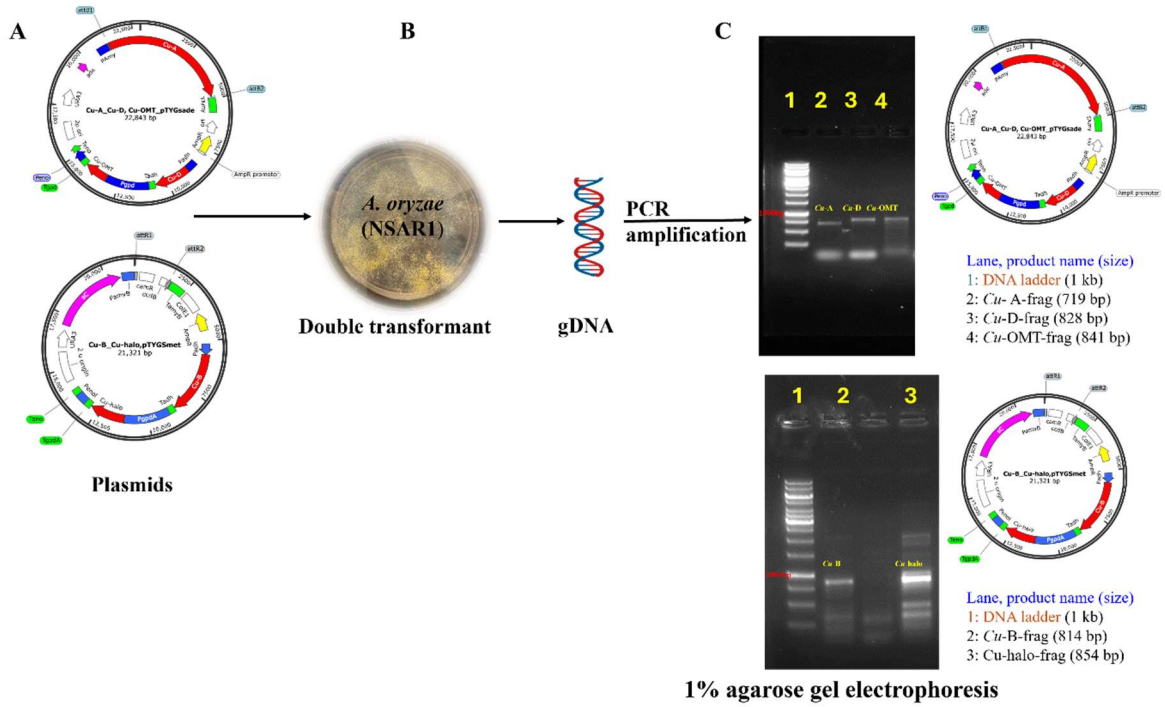

Figure 55: Confirmation of chromosomal integration of the five gene biosynthetic gene cluster (BGC) into *A. oryzae* NSAR1. (A) Schematic representations of the plasmid constructs used for transformation, showing the arrangement of *Cu*-A, *Cu*-B, *Cu*-D, *Cu*-OMT, and *Cu*-halo genes along with their respective promoters and terminators (B) Image of *A. oryzae* NSAR1 transformant on a selection media plate. (C) Agarose gel electrophoresis results of PCR amplification using gene-specific primers. The gel images confirm the integration of the individual genes as indicated by the presence of specific bands: Lane 1: contains the DNA ladder, Lane 2 shows amplification of *Cu*-A (719 bp), Lane 3 shows *Cu*-D (828 bp), and Lane 4 shows *Cu*-OMT (841 bp). The lower gel image shows successful amplification of *Cu*-B (814 bp) and *Cu*-halo (854 bp) confirming their integration. A 1 kb ladder was used for size comparison, with the sharp band marked in red at 1000 bp. The names of the genes are annotated on the gel. For clear visualizations of the plasmid maps, please refer to **Figure 53**.

6.10 Real-time quantitative reverse transcription polymerase chain reaction (RT-qPCR)

mRNA was extracted from both transformed and untransformed *A. oryzae* NSAR1 samples, and gene expression levels were analyzed using RT-qPCR for five genes (*Cu*-A, *Cu*-OMT, *Cu*-D, *Cu*-B, and *Cu*-halo) within the isocoumarin biosynthetic gene cluster (BGC). The expression levels in the transformed samples were compared with those in the untransformed control

(Figure 56). The transformed samples displayed Ct values of approximately 20 cycles for *Cu-A, Cu-OMT,* and *Cu-D,* indicating higher expression of these genes **(Figure 56)** whereas the untransformed controls showed minor background amplification, effectively close to zero. This highlights that *Cu*-A, *Cu*-OMT, and *Cu*-D are actively expressed in transformed *A. oryzae* NSAR1. In contrast, the *Cu-B* and *Cu-halo* genes exhibited minimal or undetectable expression, with Ct values exceeding 30 cycles.

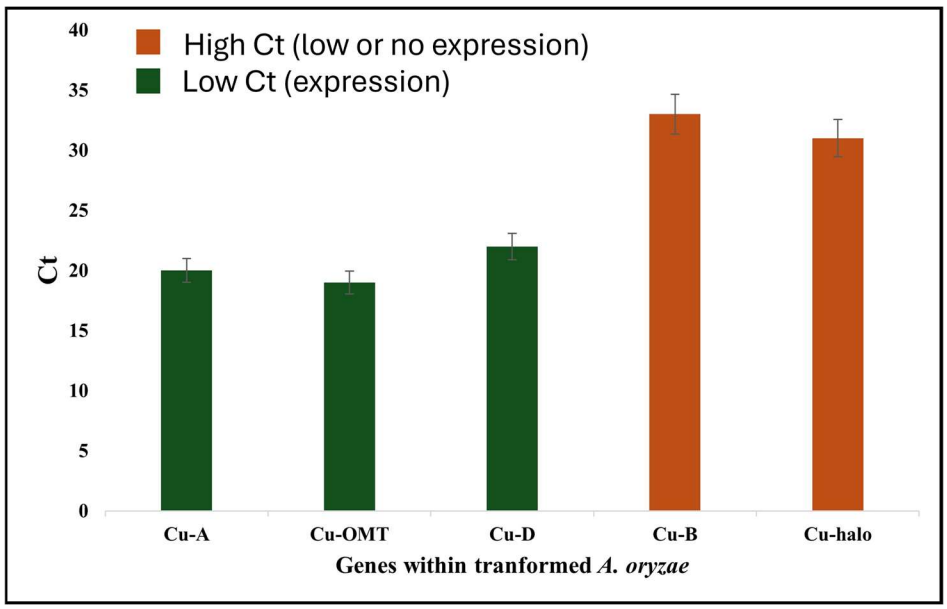

Figure 56: RT-qPCR analysis of gene expression levels for five genes (*Cu*-A, *Cu*-OMT, *Cu*-D, *Cu*-B, *Cu*-halo) in the *cu-pks-4* BGC in transformed *A. oryzae* NSAR1.

6.11 Characterization of the metabolites produced by whole BGC transformant

The transformant of *A. oryzae* NSAR1, which contains whole BGC genes (*Cu*-A, *Cu*-D, *Cu*-OMT, *Cu*- halo and *Cu*-B), was cultivated in 2.5 L of DPY medium at 30°C for 7 days. Ethyl acetate extraction from 2.5 L culture resulted in ~800 mg of the crude extract. Chromatographic fractionation of this crude extract yielded three major compounds: **5** (~20 mg), **6** (<5 mg) and

compound **8** (~200 mg). The non-UV detected compound **8** was collected in a separate container. The purification of this crude sample resulted in ~200 mg of compound **8**.

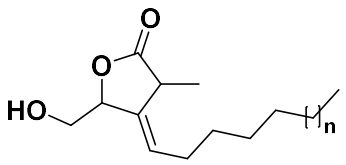

Figure 57: Chemical structure of compound **8**.

6.12 LC-MS analysis

The crude extracts of *A. oryzae* NSAR1 transformants- including a single transformant with *Cu*-A, a triple transformant with *Cu*-A, *Cu*-D, and *Cu*-OMT, and a five gene transformant containing the complete BGC- were analyzed using LC-MS, alongside a 6-hydroxymellein standard and control samples of native *A. oryzae* broth and mycelia.

LC-MS analysis of these crude extracts did not showed the presence of 6-hydroxymellein ($[M-H]^-$ = 193.05). However, a distinct peak was observed at a retention time of approximately 5.4 minutes in the triple transformant (*Cu*-A, *Cu*-D, and *Cu*-OMT), with a corresponding mass of $[M-H]^-$ at 367.35 **(Figure 58)**.

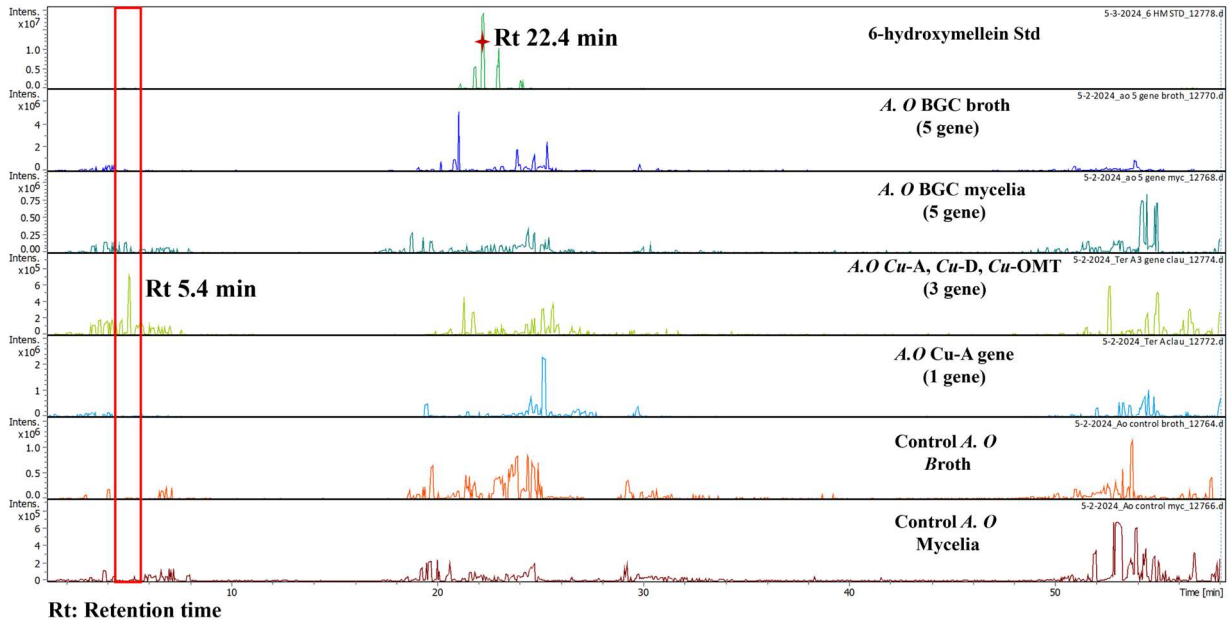

Figure 58: Total ion chromatogram (TIC) analysis of *A. oryzae* NSAR1 transformants. A distinct peak at a retention time (Rt) of 5.4 minutes, corresponding to a mass of $[M-H]^-$ = 367.35, was observed only in transformants containing *Cu*-A, *Cu*-D, and *Cu*-OMT.

The extracted ion chromatogram for m/z 367 confirmed that this distinct peak was found only in these samples. Based on the molecular weight of the expected product 2,3-dehydro-6-hydroxymellein base ion peak at $[M-H]^-$ at191.333, these results suggest the plausible biosynthesis of a Glycosylated Isocoumarin, likely compound **9** (M.W 368.338, expected $[M-H]^-$ 367.338 observed $[M-H]^-$=367.335 **(Figure S 30)**. Compound **9**, identified as 6-(4'-O-methyl-beta-glucopyranosyl)-8-hydroxy-3-methylisocoumarin, has been reported from the fungus *Torrubiella tenuis* BCC 12732 (Kornsakulkarn et al., 2009).

Further validation through NMR analysis is necessary to confirm the structure of the produced compound. This is the first successful observation of heterologous expression of a lichen PKS.

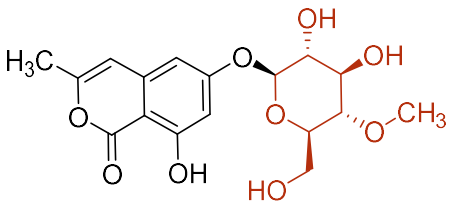

Figure 59: Chemical structure of compound **9**, glycosylated isocoumarin.

6.13 Discussion

A gene cluster encoding a halogenated isocoumarin, which includes trans-PKS-like domains and a halogenase, was identified in the genome of *C. uncialis*. This cluster comprises five genes, three of which share significant genetic similarity with genes in the terrein BGC of *A. terreus*. However, the *C. uncialis* cluster uniquely contains a halogenase (*Cu*-halo) and an O-methyltransferase (*Cu*-OMT), which are absent in the terrein BGC. Based on the known biosynthetic role of the core polyketide synthase (PKS) TerA in the terrein pathway of *A. terreus* and the similarity between TerA and *Cu*-A, it is proposed that *Cu*-A catalyzes similar condensation reactions, leading to the formation of a pentaketide scaffold, 2,3- dihydro,6-hydroxymellein **(Figure 49)**. The inclusion of unique genes in *C. uncialis*, such as *Cu*-halo and *Cu*-OMT, which are absent in the terrein pathway, suggests that the intermediate undergoes additional modifications, specifically O-methylation and halogenation. This hypothesis is supported by the isolation of molecules from lichens with structures similar to the predicted end-product **(Figure 50).**

Bioinformatics analyses using antiSMASH version 7.0 and InterPro revealed key domains within PKS (*Cu*-A) of *cu-pks-4* BGC, including SAT, KS, AT, DH, PT, ACP, and TE. Importantly, the DH domain was not previously reported in previous studies using antiSMASH v1.0 (M. Abdel-

Hameed et al., 2016a). These domains are essential for the sequential synthesis and modification of the halogenated isocoumarin structure. The identification of homologous domains to those in the terrein biosynthetic pathway supports the hypothesis that the *cu-pks-4* cluster follows a similar mechanistic pathway, but with the distinct addition of a halogenase and an O-methyltransferase gene. These additional tailoring enzymes contribute to the diversification of biosynthetic products from *C. uncialis* compared to those from *A. terreus*. The amino acid sequence of the codon-optimized *Cu*-A gene was analyzed against UniProt, revealing a high sequence similarity of 58.1% with TerA from *A. terreus* and 46.8% similarity with a polyketide synthase gene from *Alternaria burnsii*.

PCR amplification using gene-specific primers demonstrated that all five genes of the isocoumarin BGC were successfully integrated into the genomic DNA of *A. oryzae* NSAR1. To assess the expression of these genes, RT-qPCR analysis was performed, revealing high expression levels of *Cu-A*, *Cu-D*, and *Cu-OMT*, whereas *Cu-B* and *Cu-halo* exhibited very low expression levels. One possible explanation for this observation is that *Cu-B* and *Cu-D* are regulated by the same promoter (adh), and *Cu-halo* and *Cu-OMT* are under the gpd promoter. Consequently, in each set, only one gene was highly expressed, whereas the other genes had lower expression levels. However, this hypothesis requires further research to confirm.

Fermentation of the transformants: (1) *Cu-A*; (2) *Cu-B*, *Cu-D*, *Cu-OMT*; (3) double transformant (with the entire BGC), resulting in the production of pyrone **5**. In the literate its reported that sugar-fermenting fungi, *A. flavus* and *A. oryzae* converts glucose to kojic acid via gluconic acid (Ola et al., 2019; Rasmey & Abdel-Kareem, 2021). However, we confirmed that compound **5** is different from kojic acid indeed a pyrone **(Figure 60)**, which is produced in the *Cu*-A gene

containing *A. oryzae* transformants. In control experiments in which untransformed *A. oryzae* was grown under the same conditions, compound **5** was not detected. Structural elucidation was performed using NMR and LC-MS. HMBC analysis revealed a strong correlation between C-5 and H-7, indicating a three-bond relationship characteristic of pyrone. In contrast, this correlation in kojic acid involves a five-bond relationship, which typically results in a weak or absent signal, confirming that compound **5** is distinct from kojic acid.

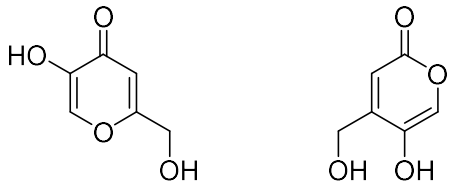

Kojic acid Compound **5**

Figure 60: Chemical structure of kojic acid and compound **5**.

LC-MS analysis of crude extracts from different *A. oryzae* NSAR1 transformants, including those containing the single, triple, and complete five gene BGC, did not detect the presence of 6-hydroxymellein ($[M-H]^-$ = 193.05). However, a distinct peak was observed at a retention time of approximately 5.4 minutes in the triple transformant (*Cu*-A, *Cu*-D, and *Cu*-OMT), with a corresponding mass of $[M-H]^-$ at 367.35 (**Figure 58**). This finding suggests the production of a compound **9** other than 6-hydroxymellein. The absence of 6-hydroxymellein in the transformants may be attributed to the minimal expression of *Cu*-B, which, according to the literature, is required along for the reduction of 2,3-dehydro-6-hydroxymellein (Kahlert, Villanueva, et al., 2021).

A. terreus related biosynthetic gene cluster (BGC) was also identified in the marine-derived fungus *Roussoella sp.* DLM33 (Kahlert, Bernardi, et al., 2021). Bioinformatics analysis revealed

homology between the *Roussoella* genes rslA and rslB and the TerA and TerB genes involved in terrein biosynthesis. Heterologous expression experiments confirmed that rslA and rslB are functionally similar to TerA and TerB, with both genes being necessary for the production of the compound 6-hm. Despite domain differences between TerB (containing DH, C-Met, and KR domains) and rslB (containing DH and KR domains), cross-species expression of gene combinations (rslA + TerB and TerA + rslB) still led to the successful production of 6-hm, indicating the possibility of gene swapping between species.

InterPro analysis of the *Cu*-B shares greater homology with TerB, containing similar KR, C-Met, and KR domains **(Figure S 28)**. Based on these findings, future experiments could test combinations such as *Cu*-A + *Ter*B and *Ter*A + *Cu*-B to evaluate their potential in 6-hm biosynthesis. Such experiments could not only validate the functional interchangeability of these genes but also optimize conditions for scalable biosynthesis of target metabolites.

6.14 Conclusion

The gene cluster from *C. uncialis* encodes a halogenated isocoumarin and shares similarities with the terrein BGC of *A. terreus*. However, the *C. uncialis* cluster includes unique genes such as a halogenase (*Cu*-halo) and an O-methyltransferase (*Cu*-OMT), suggesting additional modifications like halogenation and methylation of the intermediate pentaketide scaffold. Heterologous expression in *A. oryzae* confirmed the production of a pyrone compound distinct from kojic acid, and LC-MS analysis revealed a novel compound, possibly resulting from incomplete reduction due to low *Cu*-B expression. Future studies on cross-species gene combinations may optimize biosynthesis and validate functional gene interchangeability.

Chapter 7

Exploring O-Methyltransferase from the halogenated isocoumarin Biosynthetic Gene Cluster from the lichen, *Cladonia uncialis*

I am the primary contributor to this chapter. In this chapter we have provided intriguing insights into the O-methyl transferase enzyme, but much remains to be discovered about its function. I had the opportunity to present this work at the American Society of Pharmacognosy conference (2023) in Rockville, USA, where it received significant interest and constructive feedback for further study.

7.1 Introduction

S-adenosyl-L-methionine (also known as AdoMet) dependent methyltransferases (MTases) are ubiquitous biological enzymes that methylate various biomolecules, including DNA, proteins, and small-molecule secondary metabolites. MTases typically catalyze the transfer of a methyl group from AdoMet to the C, O, N, and S nucleophiles of an acceptor substrate. In this process, S-adenosyl-L-methionine (SAM) acts as a methyl donor, converting it into S-adenosyl-L-homocysteine (SAH) and producing a methylated substrate (Struck et al., 2012). Due to this function, these enzymes are commonly known as SAM-dependent methyltransferases.

MTases play a crucial role in the tailoring step of biosynthesis and post modification of natural products (NPs) structure. O-Methylation can alter the biological activity and pharmacological properties of compounds by shielding hydroxyl or carboxyl moieties (Liscombe et al., 2012; Y. Liu et al., 2022). For example, depsides such as gyrophoric acid, lecanoric acid, atranorin, anziaic acid, and 2'-O-methyl anziaic acid, along with the dibenzofuran compound usnic acid, have been

isolated from the lichens *Melanelia subaurifera* and *Melanelia fuliginosa* (Ristić et al., 2016). Among these, 2'-O-methyl anziaic acid exhibited the strongest antimicrobial activity. The dimethylated form of resveratrol, pterostilbene, is five times more effective than the unmethylated form in inhibiting fungal growth (Jeandet et al., 2002). Additionally, the methylation of flavonoids like chrysin and apigenin significantly enhances their liver stability and intestinal absorption (Walle, 2007)

In **Chapter 6**, we observed that nr-PKS *Cu*-A shares significant homology (~60%) with nr-PKS TerA from *Aspergillus terreus*. In a recent publication, Dr. Russel Cox's research group demonstrated that the heterologous expression of TerA in *Aspergillus niger* results in the production of triketide lactone, 6,7-dihydroxymellein, and orsellinic acid as a shunt metabolite (Kahlert et al., 2021). However, in our heterologous expression experiments of *Cu*-A in *A. oryzae* (please refer to chapter 6), we did not observe the formation of 6,7-dihydroxymellein or orsellinic acid. This led us to hypothesize that the role of PKS may differ in *C. uncialis*. To investigate the role of O-methyl transferase (OMT) within the same BGC, we fed *an A. oryzae* OMT transformant with orsellinic acid and methyl orsellinate **(Figure 61)** to investigate whether the OMT enzyme catalyzes the methylation of the oxygen atom of orsellinic acid or methyl orsellinate.

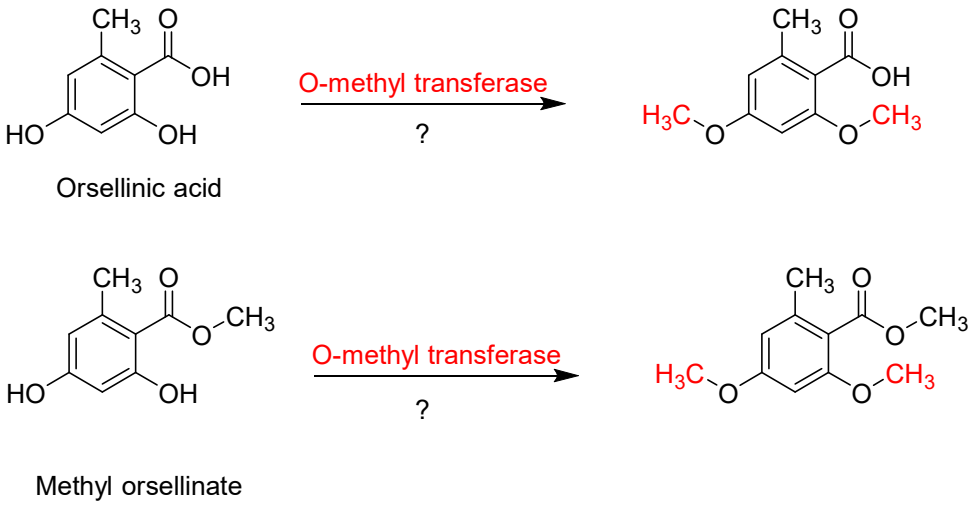

Figure 61: Predicted methylation of orsellinic acid and methyl orsellinate by O-methyl transferase from *C. uncialis*.

Aromatic polyketide and phenyl propanoid derivatives are abundant in plants, making plants a common source for identifying post-modifying enzymes, such as O-methyltransferases. O-methyltransferases, particularly those from fungi, exhibit high substrate specificity. For examle, in *Trichoderma hypoxylon*, two distinct O-methyltransferases, (TdaH and TdaO) selectively methylate two ortho-hydroxyl groups on the same phenyl ring of pretrichodermamide A, (Fan et al., 2023). Moreover, in *Aspergillus niger*, O-methyltransferase AdaD catalyzes the O-methylation at position C-9 of the tetracyclic compound TAN-1612, despite its precursor possessing different hydroxyl groups (Y. Li et al., 2011).

Therefore, the aim of this study was to determine the substrate specificity of O-methyltransferase and identify the exact position of methylation on orsellinic acid or methyl orsellinate.

7.2 Bioinformatic Analysis

The identity between *Cu*-OMT and *Philocephala scopiformis* (KUJ06291) has been reported as 77% (M. Abdel-Hameed et al., 2016a). Upon receiving the codon-optimized *Cu-OMT* gene, we initiated this project by conducting a BLAST search. The results of the protein sequence revealed a close genetic relationship between the *C. uncialis* OMT and fungal S-adenosyl-L-methionine-dependent methyltransferases **(Figure S 32)**. Specifically, as shown in **Table 9**, the BLAST results showed 80.76% identity with a methyltransferase from *Mollisia scopiformis* and 77.22% identity with *Stagonospora sp.* SRC1lsM3a with 99% query coverage.

Table 9: Blast statistics showing a genetic similarity between the codon-optimized O-methyltransferase from *C. uncialis* and its native counterpart in *C. uncialis*, as well as with known S-adenosyl-L-methionine-dependent methyltransferases from *Mollisia scopiformis* and *Stagonospora sp.* SRC1lsM3a.

Description	Max Score	Total Score	Query Cover	E value	Per. Identity	Accession no.
Putative -O-methyl transferase [*C. uncialis*]	777	777	100%	0.0	95.98%	AMM27732.1
S-adenosyl-L-methionine-dependent methyltransferase [*Mollisia scopiformis*]	665	665	99%	0.0	80.76	XP_018060646.1
S-adenosyl-L-methionine-dependent methyltransferase [*Stagonospora sp. SRC1lsM3a*]	636	636	99%	0.0	77.22	OAK96138.1

Next, we analyzed the conserved domains within *Cu*-OMT. The protein sequence of *Cu*-OMT was subjected to a conserved domain database (CDD). The results indicated that *Cu*-OMT likely functions as a methyltransferase belonging to the AdoMet_MTases superfamily, specifically Methyltransf_2 family (Pfam00891) **(Figure S 31)**, which includes a range of O-methyltransferases. This Methyltransf_2 domain spans residues are from 173-376 in the *Cu*-

OMT sequence, with an E-value of 8.35e-19 **(Table 10)**. This enzyme is predicted to catalyze the transfer of a methyl group to the oxygen atom of the substrate.

Table 10: Conserved domain hits of *Cu*-OMT from *C. uncialis*.

Name	Accession	Description	Interval	E-value
Methyltransf_2	Pfam00891	This family includes ranges of O-methyltransferases.	173-376	8.35e-19

InterPro analysis further corroborated these findings, classifying *Cu*-OMT as an S-adenosyl-L-methionine-dependent methyltransferase (SAM, PS51683), catechol-O-methyltransferase (COMT-like; IPR16461), and O-methyltransferase (O-mtase; PIRF005739) **(Figure 62)**. These findings conclusively indicate the role of *Cu*-OMT in methyl group transfer.

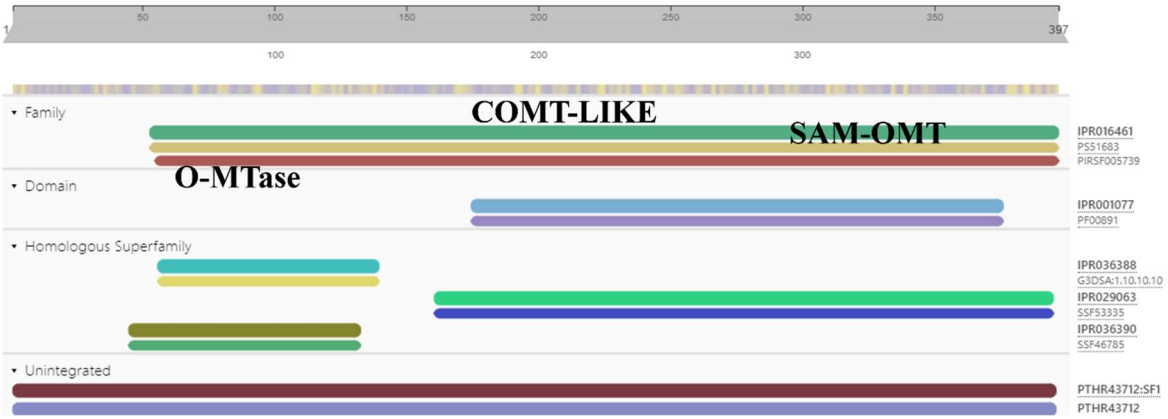

Figure 62: InterPro analysis of *Cu*-OMT, highlighting the identification of COMT-like, SAM-OMT, and O-methyltransferase (O-mtase) domains. The corresponding InterPro identifier codes are listed on the right side.

7.3 Feeding transformants with orsellinic acid

The crude extract was analyzed by NMR spectroscopy. The NMR analysis did not show any signals indicating the presence of additional methyl group.

7.4 Feeding transformants with methyl orsellinate

Compound **10** **(**$C_{12}H_{14}O_4$) was characterized using NMR and LC-MS and identified as 6,8-dimethoxy-3-methyl-3,4-dihydro-1*H*-isochromen-1-one ($C_{12}H_{14}O_4$, mass 222.09). The NMR data for the methyl orsellinate standard and Compound **10** are as follows:

Methyl orsellinate: white powder: ^{1}H NMR (MeOD, 500 MHz): δ_H 6.22 (1H, s), 6.18 (1H, s), 3.92 (3H, s), 2.47 (3H, s). Spectrum is provided in **Figure S 33**.

Compound **10** (6,8-dimethoxy-3-methyl-3,4-dihydro-1H-isochromen-1-one): oil: ^{1}H NMR (MeOD, 500 MHz): ^{1}H NMR (500 MHz; MeOD) δ_H 6.53 (1H, d, J = 2.09 Hz, 7-H), 6.46 (1H, d, J = 2.09 Hz, 5-H), 4.55–4.48 (1H, m, 3-H), 3.86 (3H, s,OCH_3), 3.86 (3H, s, OCH_3), 2.95–2.81 (2H, m, 4-H), 1.42 (3H, d, J = 6.24, 3-CH_3); ^{13}C NMR (125 MHz; MeOD) δ_C 165.2 (C1), 164.2, 163.1 (C-8, C-6), 144.4, 105.4 (C-8a, C-4a), 104.1 (C-5), 97.2 (C-7), 74.1 (C-3), 54.9, 54.7 (2×OCH_3), 35.5 (C-4), 19.3 (CH_3); EIC of 221.0 observed (expected 222.0892). Spectrum data is provided in supplementary information **(Figure S 34 to Figure S 36)**. The ^{1}H and ^{13}CNMR spectra of this compound compared well with the literature (van Otterlo et al., 2007).

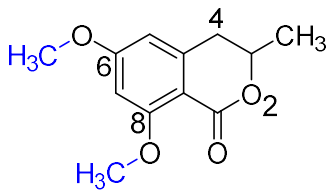

Compound **10**

Figure 63: Chemical structure of compound **10**.

7.5 Proposed biosynthetic pathway for compound 10

In the biosynthetic pathway, the methyl carbanion of methyl orsellinate performs a nucleophilic attack on the carbonyl carbon (C=O) of acetate derived from the host *A. oryzae*, forming an intermediate **3,** as shown in **Figure 64**. This intermediate is further reduced to intermediate **4**. The cyclization of intermediate **4** results in the formation of 6-hydroxymellein (intermediate **6**). Finally, an O-methyltransferase enzyme catalyzes the transfer of a methyl group to the oxygen at positions 6 and 8 of the aromatic ring, introducing methoxy groups at these positions and yielding the final product, 6,8-dimethoxy-3-methyl-3,4-dihydro-1H-isochromen-1-one, compound **10**.

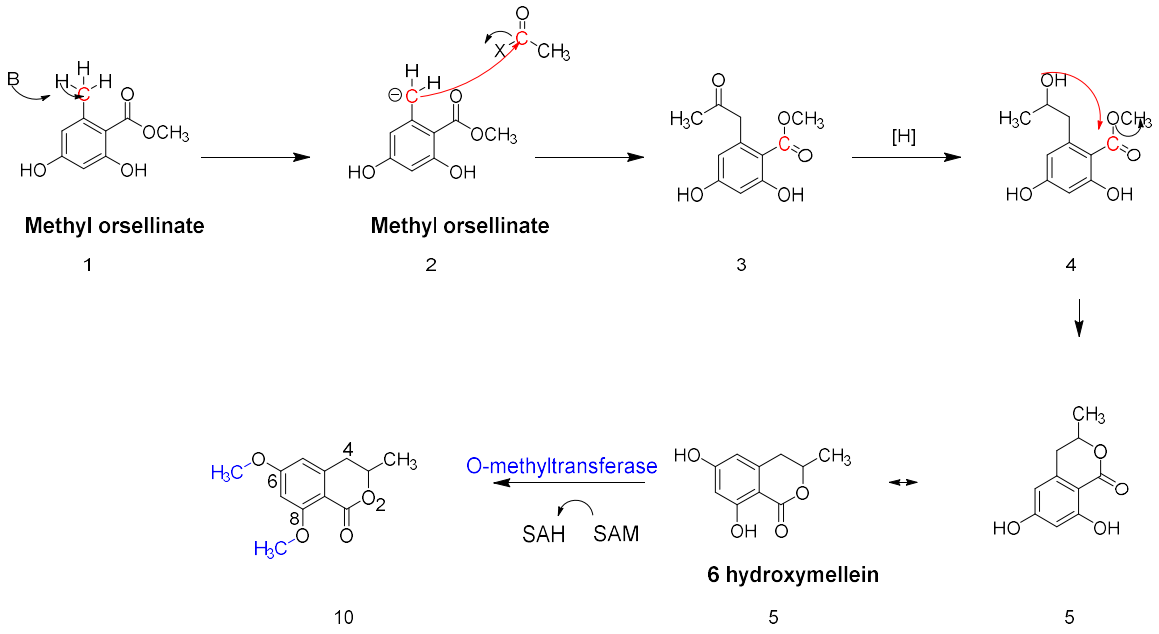

Figure 64: Proposed biosynthetic pathway for compound **10.**

7.6 Feeding experiment with ^{13}C-labeled sodium acetate

We anticipated that feeding the culture with labeled sodium acetate and methyl orsellinate would result in the synthesis of the expected product, as shown in **Figure 65**, compound **10** (6,8-Dimethoxy-3-methyl-3,4-dihydro-1H-isochromen-1-one).

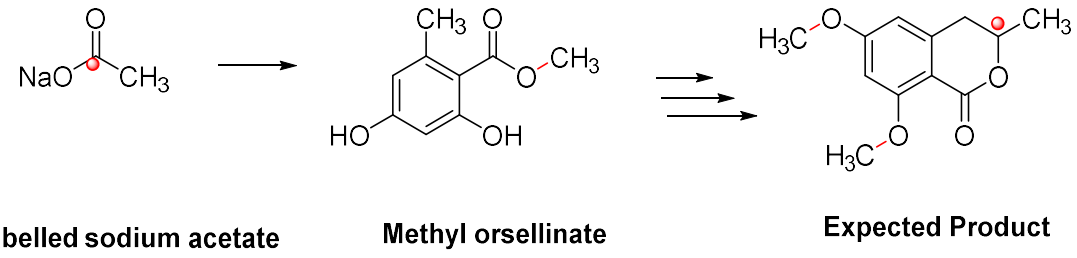

Figure 65: Proposed conversion of methyl orsellinate into methoxy mellein using ^{13}C-labeled sodium acetate.

However, instead of yielding 6,8-Dimethoxy-3-methyl-3,4-dihydro-1H-isochromen-1-one (compound **10**), the experiment results showed a new, uncharacterized product (< 1 mg,).

The ^{13}CNMR spectra is presented in **Figure 66**. Herein, the top spectrum (red) represents the culture supplemented with ^{13}C-labeled sodium acetate, and the bottom spectrum (black) corresponds to the culture with unlabeled sodium acetate. The observed differences in the spectral peaks, highlighted by arrows, indicate the successful incorporation of the ^{13}C isotope into the metabolite profiles. These spectral variations suggest that the labeled carbon atoms from the ^{13}C-labeled sodium acetate were integrated into the molecular skeleton of the newly synthesized metabolite. However, to fully elucidate the structure of this new compound, we need to repeat the experiment to obtain a higher yield of this product and perform further detailed structural analysis.

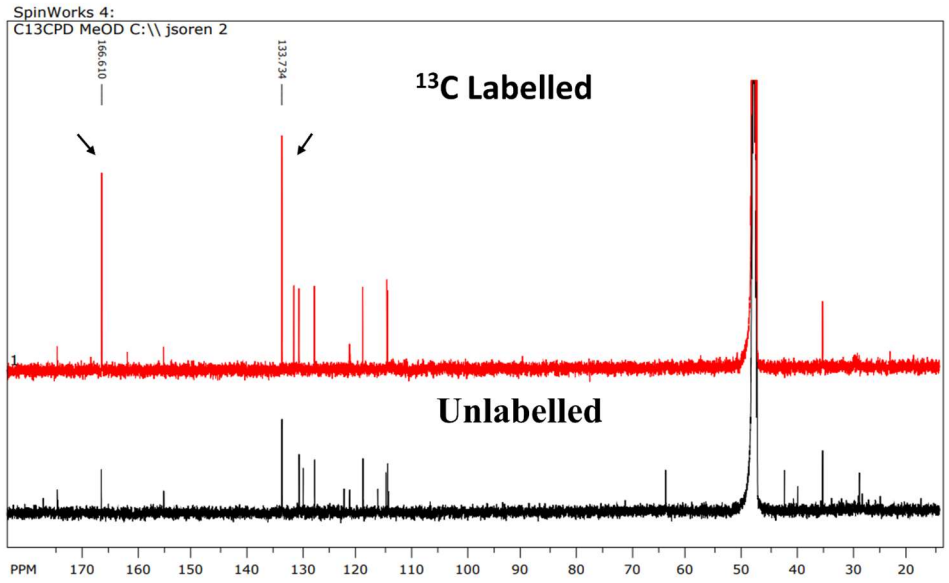

Figure 66: Comparison of ^{13}CNMR spectra from cultures extracted after 7 days of incubation. The top spectrum (in red) represents the culture fed with ^{13}C-labeled sodium acetate, while the bottom spectrum (in black) corresponds to the culture fed with unlabeled sodium acetate. Differences in spectral peaks, indicated by arrows, illustrate the incorporation of the ^{13}C isotope into the metabolite profiles of the cultures.

7.7 Discussion

In this chapter, the results provide significant insights into the *Cu*-OMT, O-methyl transferase enzyme from *C. uncialis*. Bioinformatics analyses confirmed its classification within the AdoMet_MTases superfamily, supporting its role in the transfer of methyl groups. Methyl orsellinate is formed by methylating the phenolic hydroxyl group of orsellinic acid. This modification significantly increases lipophilicity, enhancing the ability of the molecule to permeate biological membranes. Research indicates that lipophilic compounds integrate more efficiently into cell membranes, which is crucial for cellular uptake and increased bioactivity (Bogo et al., 2010; Ingólfsdóttir et al., 2002; Lopes et al., 2008). For instance, one study synthesized a series of 2,4-dihydroxy-6-methylbenzoates (ranging from methyl to hexyl

orsellinates) via the alcoholysis of lecanoric acid to assess their cytotoxic activity against *Artemia salina*. All derivatives exhibited cytotoxic activity against *A. salina*, with *n*-pentyl orsellinate and *n*-hexyl orsellinate demonstrating particularly strong effects, which were even greater than those of well-known cytotoxic agents like podophyllotoxin and emetine (Bogo et al., 2010). The methyl orsellinate experiments yielded compound **10**. Here we propose that methyl orsellinate reacts with acetate from *A. oryzae*, forming an intermediate compound through nucleophilic attack. This intermediate undergoes reduction and cyclization to produce 6-hydroxymellein. An O-methyltransferase enzyme then methylates specific positions on the aromatic ring, resulting in the formation of the final product, 6,8-dimethoxy-3-methyl-3,4-dihydro-1H-isochromen-1-one (compound **10**).

Moreover, isotope labeling experiments indicated the integration of ^{13}C-labeled sodium acetate into metabolites, but the newly synthesized compound remained uncharacterized due to insufficient yield.

7.8 Conclusion

This chapter highlights the role of the *Cu*-OMT enzyme from *cu-pks-4* gene cluster of *C. uncialis*. Bioinformatics analyses confirm that *Cu*-OMT belongs to the AdoMet_MTases superfamily. Preliminary results suggest that methyl orsellinate is converted to compound **10** when fed with *Cu*-OMT *A. oryzae* transformants. Although isotope labeling experiments confirmed the incorporation of labeled sodium acetate, the low yield hindered the full characterization of the final compound (that was different than compound **10**). Further research and optimization are required to fully elucidate the catalytic mechanism and substrate specificity of *Cu*-OMT.

Chapter 8

Conclusions and Future Prospectives

8.1 What was the understanding of *Cladonia uncialis* secondary metabolite biosynthesis in 2019?

When I began my PhD program in September 2019, our research group had already identified and annotated 48 BGCs within the genome of *C. uncialis*. We first attempted heterologous expression of two polyketide synthases (PKSs), methylsalicylic acid synthase (MSAS) and orsellinic acid synthase (OAS) from *C. uncialis* in *Aspergillus oryzae* NSAR1. Although these genes were transcribed in *A. oryzae*, they failed at the translational level. As controls, we successfully expressed methylsalicylic acid synthase and orsellinic acid synthase from non-lichen fungi (*Penicillium spp*. and *Fusarium spp*., respectively) in *A. oryzae* NSAR1, resulting in the production of 6-methylsalicylic acid and orsellinic acid respectively.

This led to the conclusion that, for reasons yet unknown, these expression systems can functionally express PKS from non-lichenized fungi but fail to do so for lichen PKS. A possible explanation for this discrepancy could be codon bias in *A. oryzae* NSAR1 host may hinder the efficient translation of lichen PKS genes.

8.2 Rationale behind the objectives of my thesis (2019 to 2024)

To address the challenge of expressing lichen PKS genes in *A. oryzae* NSAR1, we proposed codon-optimizing these genes to enhance their expression in the *A. oryzae*. At the onset of my PhD program in Fall of 2019, the Sorensen group established a collaboration with Dr. Jerome Collemare at the Westerdijk Fungal Biodiversity Institute in the Netherlands. Through this

collaboration, we secured approximately 635 kb of gene synthesis from the Joint Genome Institute (JGI) in Berkeley, California, to obtain codon-optimized fungal plasmids.

The first delivery of codon-optimized plasmids was anticipated in March 2020. However, around the same time, the COVID-19 pandemic was declared, and on March 11, 2020, we were asked to leave the laboratory. The Joint Genome Institute (JGI) also suspended work on non-COVID-related projects, redirecting their focus towards COVID-19 research, which caused substantial delays. During the six-month lockdown, in addition to completing coursework, I contributed to a book chapter (Gill, Sorensen, et al., 2023). After nearly two years, in March 2021, we received the first shipment of codon-optimized plasmids with tailoring genes from JGI. By September 2022, after three years, we finally obtained the complete collection of biosynthetic gene clusters (BGCs), including the PKSs from JGI.

While waiting for plasmids, I initiated two bridging projects to explore the chemical diversity of fungal natural products. These projects aligned with my first thesis objectives and involved the isolation, characterization, and profiling of bioactive secondary metabolites produced by *Aspergillus fumigatus* and *Penicillium sanguifluum*.

8.3 Chemical Diversity of Fungal Natural Products from *A. fumigatus* and *P. sanguifluum.*

In Chapter 3, we successfully identified and characterized bioactive secondary metabolites from a strain of *Aspergillus fumigatus* SL-2203 isolated from soil beneath a lichen thallus. Through bioassay-guided fractionation, two compounds were isolated: N-formyl-4-hydroxyphenyl-acetamide (**1**) and atraric acid (**2**). Compound **1** displayed moderate antifungal activity and selective inhibition against the efflux pump-deficient bacterial strain *Acinetobacter baumannii*

AB258, whereas compound **2** exhibited significant antifungal potency, particularly against *Pleurotus ostreatus* and other fungal species.

This study highlights the ecological significance of secondary fungal metabolites in competitive environments, suggesting that both compounds contribute to resource competition in soil and lichen ecosystems. The unusually high production levels (~ **120 mg/L)** of compound **1**, especially compared with previous reports (**1 -3 mg/L**), could indicate ecological adaptations linked to the strain's unique environment. Atraric acid **2** has been previously only reported in lichen fungi (Mun et al., 2020). It has exhibited various bioactivities such as, anti-cancer activity against prostate cancer by acting as an antagonist of androgen receptors (Hessenkemper et al., 2014), as well as antioxidant and antimicrobial (Güvenç et al., 2012) activities against Gram (+) microorganisms and *Candida dubliniensis* and *Candida krusei*. The identification of atraric acid **(2)** in a non-lichen fungus suggests horizontal gene transfer between lichen-associated and non-lichen fungi, although this hypothesis remains speculative. This report represents the first observation of atraric acid **(2)** production in a non-lichen fungus.

In future research, studies should focus on optimizing the production of these bioactive compounds and further explore their mechanisms of action. Additionally, investigating the possibility of horizontal gene transfer between lichen and non-lichen fungi could provide insights into the evolution of metabolite biosynthesis in fungi. Such research could open new avenues for biotechnological applications, including the development of novel antimicrobial agents.

Antimicrobial resistance is a critical global issue, particularly for *A. baumannii* and methicillin-resistant *S. aureus* MRSA. In **chapter 4**, we identified the fungus *P. sanguifluum* as a potent source of two bioactive compounds, dehydrocurvularin (**3**) and 11-hydroxycurvularin

(**4**). These compounds (**3** and **4**) exhibit antibacterial activity against resistant bacterial strains and showed synergy with antibiotics like meropenem and ampicillin, potentially reducing the required doses to combat disease. Additionally, they possess antifungal properties, particularly dehydrocurvularin, against pathogens causing Dutch Elm Disease and Chestnut Blight.

Genomic analysis of *P. sanguifluum* revealed 42 BGCs involved in secondary metabolite production, suggesting their potential for producing diverse bioactive compounds. This study underscores the importance of exploring fungal-derived compounds as potential solutions to the growing problem of antibiotic resistance. **Future research** should focus on optimizing the production of these compounds, elucidating their mechanisms of action, and exploring their clinical applications.

8.4 Unveiling the Biosynthetic Potential of BGCs in *C. uncialis*

There has been a lot of recent interest in the biosynthesis of lichen natural products. However, only two studies have successfully demonstrated the heterologous expression of depside polyketide synthases (PKSs). One study demonstrated the heterologous expression of a codon-optimized gene, PFUR17_02294, from the perfume lichen *Pseudevernia furfuracea* in *Saccharomyces cerevisiae* (Kealey et al., 2021). Another report by Kim et al., 2021 showed the functional heterologous expression of a novel lichen polyketide biosynthetic gene cluster (BGC) from the lichen mycobiont *Stereocaulon alpinium* in a plant pathogenic fungus, *Ascochyta rabiei*.

Despite challenges in assigning putative gene functions *in Aspergillus spp.*, successful expression of PKSs in different microbial systems opens the possibilities for us to further investigate the cryptic genes in the lichen genome. I initiated my second objective by focusing

on a gene cluster, *cu-nr-pks-5*, consisting primarily of two genes: a gene that encodes for a polyketide synthase (PKS) and an accessory gene that encodes for a decarboxylase (**Figure 36**). The PKS gene *cu-nr-pks-5* (AUW31139) appears to be a type I non-reducing polyketide synthase to produce orsellinic acid. The tailoring gene was annotated as encoding for a decarboxylase enzyme that was predicted to convert orsellinic acid to orcinol (Bertrand et al., 2018a). Homology mapping indicated the possibility for the reversible role of the decarboxylase gene based on a comparison with a previously reported enzyme identified in a species of *Rhizobium* Gram-negative bacteria (Yoshida et al., 2007).

Building upon previous work in the Sorensen lab, I aimed to heterologously express this PKS (orsellinic acid synthase) in *A. oryzae* NSAR1. My results have corroborated our previous observations, where I demonstrated that *A. oryzae* could produce orsellinic acid from non-lichen fungi (e.g., *Fusarium spp.*), but not from the lichen-forming *C. uncialis*. This was done to gain hands-on training with *A. oryzae* NSAR1 system and assess the reproducibility of earlier findings.

Then, we decided to focus on the heterologous expression of a decarboxylase gene from the same gene cluster. In **Chapter 5**, we report the successful expression of this decarboxylase in *E. coli* and demonstrate the reversible carboxylation of aromatic phenols. To the best of our knowledge, this is the first report of the successful functional heterologous expression of a native lichen gene in *E. coli* and the production of a catalytically active protein.

In summary, Chapter **5** details the following results:

1. The heterologous expression of a PKS from a non-lichen fungus (*Fusarium spp*) was observed in *A. oryzae.*

2. A 963 bp gene was cloned from *C. uncialis* and expressed in *Escherichia coli* (BL21(DE3) cells using the pQE80L expression vector. The resulting 35 kDa protein was purified by applying a Ni^{+}-NTA column using an FPLC system.

3. The 3D protein structure was predicted based on sequence similarity with a known decarboxylase from *Rhizobium sp.* and revealed the importance of a zinc cofactor for the catalytic activity of the enzyme.

4. Functional activity assays revealed the decarboxylation and reversible carboxylation of resorcinol to 2,4-dihydroxybenzoic acid and orcinol to orsellinic acid. This suggests a potential role for this decarboxylase in SM biosynthesis.

The implications of this discovery are significant because they hold promise for enhancing reaction efficiency and facilitating the synthesis of valuable phenolic compounds. Notably, while orcinol costs only 0.355 CAD for 25 mg, orsellinic acid is substantially more expensive at 207 CAD for the same quantity. **In future**, the optimization of the reaction conditions, particularly for orsellinic acid production from orcinol, may enhance conversion rates and offer a viable route for industrial-scale production of bioactive compounds.

8.5 Collection of codon-optimized BGCs from JGI

After 2.5 years, we received a library of codon-optimized plasmids for *A. oryzae* from the JGI, including all genes for the halogenated isocoumarin (*cu-pks-4*) BGC **(Figure 49)**.

I then began working on the final objective of my thesis i.e heterologous expression of halogenated isocoumarin (*cu-pks-4*) BGC in *A. oryzae* NSAR1. This gene cluster comprises five genes, (1) *Cu*-A, (2) *Cu*-B, (3) *Cu*-D, (4) *Cu*-OMT, and (5) *Cu*-halo. Three of these genes (*Cu*-

A, *Cu*-D, *Cu*-OMT) share significant genetic similarity with genes in the terrein BGC of *A. terreus*. However, the *C. uncialis* cluster uniquely contains a halogenase (*Cu*-halo) and an O-methyltransferase (*Cu*-OMT), which are absent in the terrein BGC of *A. terrus*. Based on the known biosynthetic role of the core polyketide synthase (PKS) TerA in the terrein pathway of *A. terreus* and the similarity between TerA and *Cu*-A, it is proposed that *Cu*-A catalyzes similar condensation reactions, leading to the formation of a pentaketide scaffold, 2,3 dihydro,6-hydroxymellein **(Figure 49)**. The addition of *Cu*-halo and *Cu*-OMT genes in *cu-pks-4* BGC of *C. uncialis*, which are absent in the terrein pathway of *A. terrus*, suggests that the intermediate undergoes additional modifications, specifically O-methylation and halogenation. This hypothesis is supported by the isolation of molecules from lichens with structures similar to the predicted end-product (Takenaka et al., 2011) **(Figure 50).**

In Chapter 6, we confirmed the successful integration of the entire five gene BGC into the genome of the *A. oryzae* NSAR1 transformant. Genomic DNA extraction and PCR amplification, followed by agarose gel electrophoresis, revealed bands corresponding to the expected sizes of the *Cu*-A, *Cu*-B, *Cu*-D, *Cu*-OMT, and *Cu*-halo genes. This indicates the presence of all five genes within the transformed genome (**Figure 55**).

To further assess the gene expression, we performed RT-qPCR analysis. The results showed that three genes within the isocoumarin BGC (*Cu*-A, *Cu*-OMT, and *Cu*-D) were significantly expressed in the transformed *A. oryzae* NSAR1, with Ct values around 20 cycles compared to Ct values greater than 30 in untransformed samples **(Figure 56)**. This suggests transcription of these genes in the *A. oryzae* transformant. While *Cu*-B and *Cu*-halo exhibited minimal or undetectable expression levels **(Figure 56)**. There could be several reasons for the limited expression of *Cu*-

B and *Cu*-halo. One possibility is that these genes were integrated into a silent chromosomal region, future studies should consider again transformation experiments to increase the likelihood of integrating the gene cluster into an active chromosomal region.

Fermentation of the transformants with plasmids containing: (1) *Cu*-A, (2) *Cu*-B, *Cu*-D, *Cu*-OMT and (3) five genes, resulting in the production of compound **5**, which is characterized as a pyrone **(Figure 54)**. The structure of this pyrone is an isomer of kojic acid, which is naturally produced by *A. oryzae*. In the literate its reported that sugar-fermenting fungi, *A. flavus* and *A. oryzae* converts glucose to kojic acid via gluconic acid (Ola et al., 2019; Rasmey & Abdel-Kareem, 2021). However, we confirmed that compound **5** is different from kojic acid **(Figure 60)**, which is produced in the *Cu-A* gene containing *A. oryzae* transformants. In our transformants, since all of them carried *Cu*-A gene, we observed compound **5**. In control experiments in which untransformed *A. oryzae* was grown under the same conditions, compound **5** was not detected. Structural elucidation of compound **5** was performed using 1D and 2D NMR. HMBC analysis revealed a strong correlation between C-5 and H-7, indicating a three-bond relationship characteristic of pyrone. In contrast, this correlation in kojic acid involves a five-bond relationship, which typically results in a weak or absent signal, confirming that compound **5** is distinct from kojic acid **Figure 60**.

LC-MS analysis of crude extracts from *A. oryzae* NSAR1 transformants containing the single (*Cu-A*), triple (*Cu-A*, *Cu-D*, *Cu-OMT*), and five gene BGC did not detect 6-hydroxymellein (m/z 193.05, negative ion mode). However, a distinct peak was observed at a retention time of approximately 5.4 minutes in the triple transformant (*Cu*-A, *Cu*-D, and *Cu*-OMT), with a corresponding mass $[M-H]^-$ at 367.35 (-ve ion mode) **(Figure 58)**. This molecular weight

suggests the production of a compound **9**, glycosylated isocoumarin. Further characterization, such as NMR spectroscopy, is required to confirm the structure of this compound.

The absence of 6-hydroxymellein in the transformants may be attributed to the minimal expression of *Cu-B*. It has been reported in the literature that genes homologous to *Cu*-A and *Cu*-B, such as TerA and TerB, are essential for the reduction of 2,3-dehydro-6-hydroxymellein to 6-hydroxymellein (Kahlert, Villanueva, et al., 2021). The limited expression of *Cu*-B likely hindered the completion of the biosynthetic pathway, resulting in the absence of 6-hydroxymellein.

Bioinformatics analysis revealed homology between the *Roussoella* genes rslA and rslB and the TerA and TerB genes involved in terrein biosynthesis. Heterologous expression confirmed the functional similarity between these gene pairs and the possibility of gene swapping between cross-species (rslA + TerB and TerA + rslB) for 6-hydroxymellein production (Kahlert, Bernardi, et al., 2021).

In the future, the following approaches could be considered to investigate the expression of all genes of isocoumarin BGC:

1. **Chromosomal Integration:** The lack of transcriptional activity for *Cu*-B and *Cu*-halo may be due to their integration into a transcriptionally silent region of the chromosome. To address this, future experiments could involve repeated transformation attempts to increase the likelihood of integrating these genes into active chromosomal regions, potentially leading to enhanced expression.

2. **Plasmid Construction:** Currently, *Cu*-A and *Cu*-B are located on separate plasmids. To increase the likelihood of co-expression of *Cu*-A and *Cu*-B, constructing a new plasmid containing both genes could be a promising approach. This strategy would ensure that both genes are integrated into the genome together, potentially leading to more coordinated expression and increased production of 6-hydroxymellein.

3. **Cross-Species Gene Expression:** Recent studies have demonstrated the potential for gene swapping between species to produce 6-hydroxymellein (Kahlert, Bernardi, et al., 2021). To explore this further in *C. uncialis*, we could combine *Cu*-A with TerB or TerA with *Cu*-B to potentially enhance the expression of *Cu*-B and facilitate the production of 6-hydroxymellein.

4. **Host System Modification:** Another option is to test the same plasmid in a yeast system, *S. cerevisiae,* to see if the change in host enhances gene expression and may produce fortunate outcomes.

Previous studies demonstrated that heterologous expression of TerA in *A. oryzae* led to the production of triketide lactone, 6,7-dihydroxymellein, and orsellinic acid. However, the heterologous expression of *Cu*-A in *A. oryzae* did not yield similar compounds, suggesting a distinct role for the PKS in *C. uncialis*. To explore the role of another gene, *Cu*-OMT from same BGC, in **chapter 7**, O-methyl transferase (*Cu*-OMT) activity was examined by feeding a *Cu*-OMT transformant of *A. oryzae* with orsellinic acid and methyl orsellinate.

Interestingly, the results showed the formation of 6,8-dimethoxy-3-methyl-3,4-dihydro-1H-isochromen-1-one, methylated 6-hydroxymellein (compound **10**) when feeding with methyl orsellinate. These results were confirmed by NMR. We also conducted isotope labeling experiments, which suggested the incorporation of labeled sodium acetate; however, due to low

yields, the final product was not characterized. Future research could focus on optimizing expression conditions and increasing yield to fully characterize the newly synthesized compounds.

8.6 Summary

In this study, we isolated and characterized four secondary metabolites from *Aspergillus fumigatus* (**1**, **2**) and *Penicillium sanguifluum* (**3**, **4**) and did bioactivity profiling. We found that Compound **1** was produced in significant amounts (~120 mg/L) by *A. fumigatus* SL-2203. This is the first report of these metabolites from *A. fumigatus*, and particularly compound **2** is the first reported instance from a non-lichen fungus.

This study also achieved the successful cloning, expression, and characterization of a native decarboxylase gene from *C. uncialis* in *E. coli*. These results suggest a role for this enzyme in natural product biosynthesis in lichen fungi. The full biotechnological potential of this enzyme as a biocatalyst has yet to be fully realized. To our knowledge, this is the first successful expression of a native lichen gene in *E. coli*, yielding a catalytically active protein.

Although this research provided valuable insights into the biosynthesis of halogenated isocoumarin (*cu-pks-5*) BGC in *C. uncialis*, we were unable to fully achieve our goal of expressing the entire BGC (*cu-pks-5*) in *A. oryzae*. Thanks to JGI, we obtained a collection of codon-optimized plasmids, including those containing genes from the *cu-pks-5* gene cluster. While we could not fully express the entire BGC in *A. oryzae* yet, we succeeded in expressing a partial gene cluster comprising three out of the five genes from *C. uncialis*, which led to the production of new compounds. These early results lay the groundwork for further exploration of lichen secondary metabolism.

References

Abdel-Hameed, M., Bertrand, R. L., Piercey-Normore, M. D., & Sorensen, J. L. (2016a). Identification of 6-Hydroxymellein Synthase and Accessory Genes in the Lichen Cladonia uncialis. *Journal of Natural Products*, *79*(6), 1645–1650. https://doi.org/10.1021/acs.jnatprod.6b00257

Abdel-Hameed, M., Bertrand, R. L., Piercey-Normore, M. D., & Sorensen, J. L. (2016b). Putative identification of the usnic acid biosynthetic gene cluster by *de novo* whole-genome sequencing of a lichen-forming fungus. *Fungal Biology*, *120*(3), 306–316. https://doi.org/10.1016/j.funbio.2015.10.009

Abdel-Hameed, M. E., Bertrand, R. L., Donald, L. J., & Sorensen, J. L. (2018). Lichen ketosynthase domains are not responsible for inoperative polyketide synthases in *Ascomycota* hosts. *Biochemical and Biophysical Research Communications*, *503*(3), 1228–1234. https://doi.org/10.1016/j.bbrc.2018.07.029

Akey, D. L., Razelun, J. R., Tehranisa, J., Sherman, D. H., Gerwick, W. H., & Smith, J. L. (2010). Crystal Structures of Dehydratase Domains from the Curacin Polyketide Biosynthetic Pathway. *Structure*, *18*(1), 94–105. https://doi.org/10.1016/j.str.2009.10.018

Alberts, A. W. (1988). Discovery, biochemistry and biology of lovastatin. *The American Journal of Cardiology*, *62*(15), J10–J15. https://doi.org/10.1016/0002-9149(88)90002-1

Ames, B. D., Nguyen, C., Bruegger, J., Smith, P., Xu, W., Ma, S., Wong, E., Wong, S., Xie, X., Li, J. W.-H., Vederas, J. C., Tang, Y., & Tsai, S.-C. (2012). Crystal structure and biochemical studies of the trans-acting polyketide enoyl reductase LovC from lovastatin

biosynthesis. *Proceedings of the National Academy of Sciences of the United States of America*, *109*(28), 11144–11149. https://doi.org/10.1073/pnas.1113029109

An, C.-Y., Li, X.-M., Li, C.-S., Gao, S.-S., Shang, Z., & Wang, B.-G. (2013). Triazoles and Other N-Containing Metabolites from the Marine-Derived Endophytic Fungus Penicillium chrysogenum EN-118. *Helvetica Chimica Acta*, *96*(4), 682–687. https://doi-org.uml.idm.oclc.org/10.1002/hlca.201200433

Araújo, H. D. A. de, Silva, H. A. M. F., Silva Júnior, J. G. da, Albuquerque, M. C. P. de A., Coelho, L. C. B. B., & Aires, A. de L. (2021). The natural compound hydrophobic usnic acid and hydrophilic potassium usnate derivative: Applications and comparisons. *Molecules*, *26*(19), 5995. https://doi.org/10.3390/molecules26195995

Arcamone, F. (1981). *Doxorubicin: Anticancer Antibiotics*. Academic Press. No doi

Armaleo, D., Sun, X., & Culberson, C. (2011b). Insights from the first putative biosynthetic gene cluster for a lichen depside and depsidone. *Mycologia*, *103*(4), 741–754. https://doi.org/10.3852/10-335

Arnold, K. E., Laing, G., McMahon, B. J., Fanning, S., Stekel, D. J., Pahl, O., Coyne, L., Latham, S. M., & McIntyre, K. M. (2024). The need for One Health systems-thinking approaches to understand multiscale dissemination of antimicrobial resistance. *The Lancet Planetary Health*, *8*(2), e124–e133. https://doi.org/10.1016/S2542-5196(23)00278-4

Bačkor, M., & Loppi, S. (2009). Interactions of lichens with heavy metals. *Biologia Plantarum*, *53*(2), 214–222. https://doi.org/10.1007/s10535-009-0042-y

Bahram, M., & Netherway, T. (2022). Fungi as mediators linking organisms and ecosystems. *FEMS Microbiology Reviews*, *46*(2), fuab058. https://doi.org/10.1093/femsre/fuab058

Barker, K. F. (1999). Antibiotic resistance: A current perspective. *British Journal of Clinical Pharmacology*, *48*(2), 109–124. https://doi.org/10.1046/j.1365-2125.1999.00997.x

Bates, S. T., Cropsey, G. W. G., Caporaso, J. G., Knight, R., & Fierer, N. (2011). Bacterial Communities Associated with the Lichen Symbiosis. *Applied and Environmental Microbiology*, *77*(4), 1309–1314. https://doi.org/10.1128/AEM.02257-10

Bauri, A. K., Dionicio, I. C., Arellano, E. S., Jeyaraj, J. G., Foro, S., & Carcache de Blanco, E. J. (2024). A New Rare Halogenated Depside from Lichen and Study of its Anti-Proliferative Activity. *Chemistry & Biodiversity*, *21*(6), e202301874. https://doi.org/10.1002/cbdv.202301874

Bérdy, J. (2005). Bioactive Microbial Metabolites: A Personal View. *The Journal of Antibiotics*, *58*(1), 1–26. https://doi.org/10.1038/ja.2005.1

Bertrand, R. L., Abdel-Hameed, M., & Sorensen, J. L. (2015). Limitations of the 'ambush hypothesis' at the single-gene scale: What codon biases are to blame? *Molecular Genetics and Genomics*, *290*(2), 493–504. https://doi.org/10.1007/s00438-014-0937-y

Bertrand, R. L., Abdel-Hameed, M., & Sorensen, J. L. (2018a). Lichen Biosynthetic Gene Clusters. Part I. Genome Sequencing Reveals a Rich Biosynthetic Potential. *Journal of Natural Products*, *81*(4), 723–731. https://doi.org/10.1021/acs.jnatprod.7b00769

Bertrand, R. L., Abdel-Hameed, M., & Sorensen, J. L. (2018b). Lichen Biosynthetic Gene Clusters. Part I. Genome Sequencing Reveals a Rich Biosynthetic Potential. *Journal of Natural Products*, *81*(4), 723–731. https://doi.org/10.1021/acs.jnatprod.7b00769

Bertrand, R. L., & Sorensen, J. L. (2019). Lost in Translation: Challenges with Heterologous Expression of Lichen Polyketide Synthases. *ChemistrySelect*, *4*(21), 6473–6483. https://doi.org/10.1002/slct.201901762

Bierbaumer, S., Nattermann, M., Schulz, L., Zschoche, R., Erb, T. J., Winkler, C. K., Tinzl, M., & Glueck, S. M. (2023). Enzymatic Conversion of CO2: From Natural to Artificial Utilization. *Chemical Reviews*. https://doi.org/10.1021/acs.chemrev.2c00581

Bignell, E., Cairns, T. C., Throckmorton, K., Nierman, W. C., & Keller, N. P. (2016). Secondary metabolite arsenal of an opportunistic pathogenic fungus. *Philosophical Transactions of the Royal Society B: Biological Sciences*, *371*(1709), 20160023. https://doi.org/10.1098/rstb.2016.0023

Blachowicz, A., Chiang, A. J., Romsdahl, J., Kalkum, M., Wang, C. C. C., & Venkateswaran, K. (2019). Proteomic characterization of Aspergillus fumigatus isolated from air and surfaces of the International Space Station. *Fungal Genetics and Biology*, *124*, 39–46. https://doi.org/10.1016/j.fgb.2019.01.001

Blackwell, M. (2011). The Fungi: 1, 2, 3 … 5.1 million species? *American Journal of Botany*, *98*(3), 426–438. https://doi.org/10.3732/ajb.1000298

Blin, K., Shaw, S., Augustijn, H. E., Reitz, Z. L., Biermann, F., Alanjary, M., Fetter, A., Terlouw, B. R., Metcalf, W. W., Helfrich, E. J. N., van Wezel, G. P., Medema, M. H., & Weber, T. (2023). antiSMASH 7.0: New and improved predictions for detection, regulation, chemical structures and visualisation. *Nucleic Acids Research*, *51*(W1), W46–W50. https://doi.org/10.1093/nar/gkad344

Bogo, D., de Matos, M. F. C., Honda, N. K., Pontes, E. C., Oguma, P. M., da Santos, E. C. S., de Carvalho, J. E., & Nomizo, A. (2010). In vitro antitumour activity of orsellinates. *Zeitschrift Fur Naturforschung. C, Journal of Biosciences*, *65*(1–2), 43–48. https://doi.org/10.1515/znc-2010-1-208

Borchardt, J. K. (2002). The Beginnings of Drug Therapy: Ancient Mesopotamian Medicine. *Drug News & Perspectives*, *15*(3), 187–192. https://doi.org/10.1358/dnp.2002.15.3.840015

Boruta, T., & Bizukojc, M. (2017). Production of lovastatin and itaconic acid by Aspergillus terreus: A comparative perspective. *World Journal of Microbiology and Biotechnology*, *33*(2), 34. https://doi.org/10.1007/s11274-017-2206-9

Bradford, M. M. (1976). A rapid and sensitive method for the quantitation of microgram quantities of protein utilizing the principle of protein-dye binding. *Analytical Biochemistry*, *72*, 248–254. https://doi.org/10.1006/abio.1976.9999

Brown, N. M., Goodman, A. L., Horner, C., Jenkins, A., & Brown, E. M. (2021). Treatment of methicillin-resistant *Staphylococcus aureus* (MRSA): Updated guidelines from the UK. *JAC-Antimicrobial Resistance*, *3*(1), dlaa114. https://doi.org/10.1093/jacamr/dlaa114

Calchera, A., Dal Grande, F., Bode, H. B., & Schmitt, I. (2019). Biosynthetic Gene Content of the 'Perfume Lichens' Evernia prunastri and Pseudevernia furfuracea. *Molecules*, *24*(1), Article 1. https://doi.org/10.3390/molecules24010203

Cazar, M. E., Schmeda-Hirschmann, G., & Astudillo, L. (2005). Antimicrobial Butyrolactone I Derivatives from the Ecuadorian Soil Fungus Aspergillus terreus Thorn. Var terreus. *World Journal of Microbiology and Biotechnology*, *21*(6), 1067–1075. https://doi.org/10.1007/s11274-004-8150-5

Chooi, Y.-H., Stalker, D. M., Davis, M. A., Fujii, I., Elix, J. A., Louwhoff, S. H., & Lawrie, A. C. (2008). Cloning and sequence characterization of a non-reducing polyketide synthase gene from the lichen Xanthoparmelia semiviridis. *Mycological Research*, *112*(2), 147–161. https://doi.org/10.1016/j.mycres.2007.08.022

Cohen, P. A., & Neil Towers, G. H. (1996). Biosynthetic studies on chlorinated anthraquinones in the lichen *Nephroma laevigatum*. *Phytochemistry*, *42*(5), 1325–1329. https://doi.org/10.1016/0031-9422(96)00148-3

Correche, E., Carrasco, M., Giannini, F., Piovano, M., Garbarino, J., & Enriz, D. (2002). Cytotoxic Screening Activity of Secondary Lichen Metabolites. *Acta Farmacéutica Bonaerense*, *21*. No doi

Correché, E., Enriz, R., Piovano, M., Garbarino, J., & Gómez-Lechón, M. J. (2005). Cytotoxic and Apoptotic Effects on Hepatocytes of Secondary Metabolites Obtained from Lichens. *Alternatives to Laboratory Animals : ATLA*, *32*, 605–615. https://doi.org/10.1177/026119290403200611

Cox, R. J., & Skellam, E. J. (2020). 1.09-Fungal non-reducing polyketide synthases. *Comprehensive Natural Products III: Chemistry and Biology,* 266-309. Elsevier. https://doi.org/10.1016/b978-0-12-409547-2.14780-8

Cox, R. J., Skellam, E., & Williams, K. (2018). Biosynthesis of Fungal Polyketides. In T. Anke & A. Schüffler (Eds.), *Physiology and Genetics: Selected Basic and Applied Aspects* (pp. 385–412). Springer International Publishing. https://doi.org/10.1007/978-3-319-71740-1_13

Czeczuga, B., & Czeczuga-Semeniuk, E. (2003). Effect of light quality on the size of phyco- and photobiont cells of some lichen species from the Knyszyńska Forest (NE Poland). *The Journal of the Hattori Botanical Laboratory*, *93*, 189–200. https://doi.org/10.18968/jhbl.93.0_189

Dagenais, T. R. T., & Keller, N. P. (2009). Pathogenesis of Aspergillus fumigatus in Invasive Aspergillosis. *Clinical Microbiology Reviews*, *22*(3), 447–465. https://doi.org/10.1128/CMR.00055-08

Devi, R., Kaur, T., Guleria, G., Rana, K. L., Kour, D., Yadav, N., Yadav, A. N., & Saxena, A. K. (2020). Chapter 9—Fungal secondary metabolites and their biotechnological applications for human health. In A. A. Rastegari, A. N. Yadav, & N. Yadav (Eds.), *New and Future Developments in Microbial Biotechnology and Bioengineering* (pp. 147–161). Elsevier. https://doi.org/10.1016/B978-0-12-820528-0.00010-7

Diederich, P., Lawrey, J. D., & Ertz, D. (2018). The 2018 classification and checklist of lichenicolous fungi, with 2000 non-lichenized, obligately lichenicolous taxa. *The Bryologist*, *121*(3), 340–425. https://doi.org/10.1639/0007-2745-121.3.340

Domalaon, R., De Silva, P. M., Kumar, A., Zhanel, G. G., & Schweizer, F. (2019). The Anthelmintic Drug Niclosamide Synergizes with Colistin and Reverses Colistin Resistance in Gram-Negative Bacilli. *Antimicrobial Agents and Chemotherapy*, *63*(4), 10.1128/aac.02574-18. https://doi.org/10.1128/aac.02574-18

Dopazo, J. (1994). Estimating errors and confidence intervals for branch lengths in phylogenetic trees by a bootstrap approach. *Journal of Molecular Evolution*, *38*(3), 300–304. https://doi.org/10.1007/BF00176092

Du, L., & Lou, L. (2010). PKS and NRPS release mechanisms. *Natural Product Reports*, *27*(2), 255–278. https://doi.org/10.1039/B912037H

Endo, A. (2002, May 1). *Compactin (ML-236B) and related compounds as potential cholesterol-lowering agents that inhibit HMG-CoA reductase* (world). ACS Publications; American Chemical Society. https://doi.org/10.1021/jm00382a001

Fan, J., Ran, H., Wei, P.-L., Li, Y., Liu, H., Li, S.-M., Hu, Y., & Yin, W.-B. (2023). Pretrichodermamide A Biosynthesis Reveals the Hidden Diversity of Epidithiodiketopiperazines. *Angewandte Chemie*, *135*(18), e202217212. https://doi.org/10.1002/ange.202217212

Farnsworth, N. R., Akerele, O., Bingel, A. S., Soejarto, D. D., & Guo, Z. (1985). Medicinal plants in therapy. *Bulletin of the World Health Organization*, *63*(6), 965–981. No doi

Farzam, K., Nessel, T. A., & Quick, J. (2024). Erythromycin. In *StatPearls*. StatPearls Publishing. http://www.ncbi.nlm.nih.gov/books/NBK532249/

Felix, S., Sandjo, L. P., Opatz, T., & Erkel, G. (2013). SF002-96-1, a new drimane sesquiterpene lactone from an Aspergillus species, inhibits survivin expression. *Beilstein Journal of Organic Chemistry*, *9*(1), 2866–2876. https://doi.org/10.3762/bjoc.9.323

Feng, J., Hauser, M., Cox, R. J., & Skellam, E. (2021). Engineering Aspergillus oryzae for the Heterologous Expression of a Bacterial Modular Polyketide Synthase. *Journal of Fungi*, *7*(12), Article 12. https://doi.org/10.3390/jof7121085

Fischbach, M. A., & Clardy, J. (2007). One pathway, many products. *Nature Chemical Biology*, *3*(7), Article 7. https://doi.org/10.1038/nchembio0707-353

Frisvad, J. C., Rank, C., Nielsen, K. F., & Larsen, T. O. (2009). Metabolomics of Aspergillus fumigatus. *Medical Mycology*, *47*(sup1), S53–S71. https://doi.org/10.1080/13693780802307720

Gadea, A., Charrier, M., Fanuel, M., Clerc, P., Daugan, C., Sauvager, A., Rogniaux, H., Boustie, J., Le Lamer, A.-C., & Lohézic-Le Devehat, F. (2019). Overcoming deterrent

metabolites by gaining essential nutrients: A lichen/snail case study. *Phytochemistry*, *164*, 86–93. https://doi.org/10.1016/j.phytochem.2019.04.019

Gagunashvili, A. N., Davíðsson, S. P., Jónsson, Z. O., & Andrésson, Ó. S. (2009). Cloning and heterologous transcription of a polyketide synthase gene from the lichen Solorina crocea. *Mycological Research*, *113*(3), 354–363. https://doi.org/10.1016/j.mycres.2008.11.011

Galanty, A., Popiół, J., Paczkowska-Walendowska, M., Studzińska-Sroka, E., Paśko, P., Cielecka-Piontek, J., Pękala, E., & Podolak, I. (2021). (+)-Usnic Acid as a Promising Candidate for a Safe and Stable Topical Photoprotective Agent. *Molecules*, *26*(17), 5224. https://doi.org/10.3390/molecules26175224

Gao, S.-S., Duan, A., Xu, W., Yu, P., Hang, L., Houk, K. N., & Tang, Y. (2016). Phenalenone Polyketide Cyclization Catalyzed by Fungal Polyketide Synthase and Flavin-Dependent Monooxygenase. *Journal of the American Chemical Society*, *138*(12), 4249–4259. https://doi.org/10.1021/jacs.6b01528

Garg, N., Zeng, Y., Edlund, A., Melnik, A. V., Sanchez, L. M., Mohimani, H., Gurevich, A., Miao, V., Schiffler, S., Lim, Y. W., Luzzatto-Knaan, T., Cai, S., Rohwer, F., Pevzner, P. A., Cichewicz, R. H., Alexandrov, T., & Dorrestein, P. C. (2016). Spatial Molecular Architecture of the Microbial Community of a *Peltigera* Lichen. *mSystems*, *1*(6), e00139-16. https://doi.org/10.1128/mSystems.00139-16

Gauslaa, Y. (2005). Lichen palatability depends on investments in herbivore defence. *Oecologia*, *143*(1), 94–105. https://doi.org/10.1007/s00442-004-1768-z

Gill, H., Sorensen, J. L., & Collemare, J. (2023). Lichen Fungal Secondary Metabolites: Progress in the Genomic Era Toward Ecological Roles in the Interaction. In B. Scott &

C. Mesarich (Eds.), *Plant Relationships: Fungal-Plant Interactions* (pp. 185–208). Springer International Publishing. https://doi.org/10.1007/978-3-031-16503-0_7

Gill, H., Sykes, E. M. E., Kumar, A., & Sorensen, J. L. (2023). Isolation of Bioactive Metabolites from Soil Derived Fungus-Aspergillus fumigatus. *Microorganisms*, *11*(3), Article 3. https://doi.org/10.3390/microorganisms11030590

Gilman, H., Willis, H. B., Cook, T. H., Webb, F. J., & Meals, R. N. (1940). Dibenzofuran. XVIII. Isomeric Metalation Products of Some Phenols and their Methyl Ethers1. *Journal of the American Chemical Society*, *62*(3), 667–669. No doi

Glueck, S. M., Gümüs, S., Fabian, W. M., & Faber, K. (2010). Biocatalytic carboxylation. *Chemical Society Reviews*, *39*(1), 313–328. https://doi.org/10.1039/B807875K

Goga, M., Antreich, S. J., Bačkor, M., Weckwerth, W., & Lang, I. (2017). Lichen secondary metabolites affect growth of Physcomitrella patens by allelopathy. *Protoplasma*, *254*(3), 1307–1315. https://doi.org/10.1007/s00709-016-1022-7

Goga, M., Elečko, J., Marcinčinová, M., Ručová, D., Bačkorová, M., & Bačkor, M. (2018). Lichen Metabolites: An Overview of Some Secondary Metabolites and Their Biological Potential. In J.-M. Mérillon & K. G. Ramawat (Eds.), *Bioactive Molecules in Food* (pp. 1–36). Springer International Publishing. https://doi.org/10.1007/978-3-319-76887-8_57-1

Goto, M., Hayashi, H., Miyahara, I., Hirotsu, K., Yoshida, M., & Oikawa, T. (2006). Crystal Structures of Nonoxidative Zinc-dependent 2,6-Dihydroxybenzoate (γ-Resorcylate) Decarboxylase from Rhizobium sp. Strain MTP-10005. *Journal of Biological Chemistry*, *281*(45), 34365–34373. https://doi.org/10.1074/jbc.M607270200

Greve, H., Schupp, P. J., Eguereva, E., Kehraus, S., Kelter, G., Maier, A., Fiebig, H.-H., & König, G. M. (2008). Apralactone A and a New Stereochemical Class of Curvularins from the Marine-Derived Fungus Curvularia sp. *European Journal of Organic Chemistry*, *2008*(30), 10.1002/ejoc.200800522. https://doi.org/10.1002/ejoc.200800522

Grimm, M., Grube, M., Schiefelbein, U., Zühlke, D., Bernhardt, J., & Riedel, K. (2021). The Lichens' Microbiota, Still a Mystery? *Frontiers in Microbiology*, *12*, 623839. https://doi.org/10.3389/fmicb.2021.623839

Grube, M., Cardinale, M., De Castro, J. V., Müller, H., & Berg, G. (2009). Species-specific structural and functional diversity of bacterial communities in lichen symbioses. *The ISME Journal*, *3*(9), 1105–1115. https://doi.org/10.1038/ismej.2009.63

Grube, M., Cernava, T., Soh, J., Fuchs, S., Aschenbrenner, I., Lassek, C., Wegner, U., Becher, D., Riedel, K., Sensen, C. W., & Berg, G. (2015). Exploring functional contexts of symbiotic sustain within lichen-associated bacteria by comparative omics. *The ISME Journal*, *9*(2), 412–424. https://doi.org/10.1038/ismej.2014.138

Güvenç, A., Küpeli Akkol, E., Süntar, İ., Keleş, H., Yıldız, S., & Çalış, İ. (2012). Biological activities of Pseudevernia furfuracea (L.) Zopf extracts and isolation of the active compounds. *Journal of Ethnopharmacology*, *144*(3), 726–734. https://doi.org/10.1016/j.jep.2012.10.021

Hale, M. E. (1973). Chapter 14—GROWTH. In V. Ahmadjian & M. E. Hale (Eds.), *The Lichens* (pp. 473–492). Academic Press. https://doi.org/10.1016/B978-0-12-044950-7.50019-2

Hanson, G., & Coller, J. (2018). Codon optimality, bias and usage in translation and mRNA decay. *Nature Reviews Molecular Cell Biology*, *19*(1), 20–30. https://doi.org/10.1038/nrm.2017.91

Harvey, C. J. B., Tang, M., Schlecht, U., Horecka, J., Fischer, C. R., Lin, H.-C., Li, J., Naughton, B., Cherry, J., Miranda, M., Li, Y. F., Chu, A. M., Hennessy, J. R., Vandova, G. A., Inglis, D., Aiyar, R. S., Steinmetz, L. M., Davis, R. W., Medema, M. H., … Hillenmeyer, M. E. (2018). HEx: A heterologous expression platform for the discovery of fungal natural products. *SCIENCE ADVANCES*, 15. https://doi.org/10.1126/sciadv.aar5459

Hawksworth, D. L., & Lücking, R. (2017). Fungal Diversity Revisited: 2.2 to 3.8 Million Species. *Microbiology Spectrum*, *5*(4), 10.1128/microbiolspec.funk-0052–2016. https://doi.org/10.1128/microbiolspec.funk-0052-2016

Hertweck, C. (2009). The Biosynthetic Logic of Polyketide Diversity. *Angewandte Chemie International Edition*, *48*(26), 4688–4716. https://doi.org/10.1002/anie.200806121

Hertweck, C., Luzhetskyy, A., Rebets, Y., & Bechthold, A. (2007). Type II polyketide synthases: Gaining a deeper insight into enzymatic teamwork. *Natural Product Reports*, *24*(1), 162–190. https://doi.org/10.1039/B507395M

Hessenkemper, W., Roediger, J., Bartsch, S., Houtsmuller, A. B., van Royen, M. E., Petersen, I., Grimm, M.-O., & Baniahmad, A. (2014). A Natural Androgen Receptor Antagonist Induces Cellular Senescence in Prostate Cancer Cells. *Molecular Endocrinology*, *28*(11), 1831–1840. https://doi.org/10.1210/me.2014-1170

Honegger, R. (1997). Metabolic Interactions at the Mycobiont-Photobiont Interface in Lichens. In G. C. Carroll & P. Tudzynski (Eds.), *Plant Relationships: Part A* (pp. 209–221). Springer. https://doi.org/10.1007/978-3-662-10370-8_12

Houbraken, J. A. M. P., Frisvad, J. C., & Samson, R. A. (2010). Taxonomy of Penicillium citrinum and related species. *Fungal Diversity*, *44*(1), 117–133. https://doi.org/10.1007/s13225-010-0047-z

Houbraken, J., Frisvad, J. C., & Samson, R. A. (2011). Taxonomy of Penicillium section Citrina. *Studies in Mycology*, *70*, 53–138. https://doi.org/10.3114/sim.2011.70.02

Huneck, S. (1973). NATURE OF LICHEN SUBSTANCES. In *The Lichens* (pp. 495–522). Elsevier. https://doi.org/10.1016/B978-0-12-044950-7.50020-9

Ingólfsdóttir, K., Gudmundsdóttir, G. F., Ögmundsdóttir, H. M., Paulus, K., Haraldsdóttir, S., Kristinsson, H., & Bauer, R. (2002). Effects of tenuiorin and methyl orsellinate from the lichen *Peltigera leucophlebia* on 5-/15-lipoxygenases and proliferation of malignant cell lines *in vitro*. *Phytomedicine*, *9*(7), 654–658. https://doi.org/10.1078/094471102321616481

Ishii, Y., Narimatsu, Y., Iwasaki, Y., Arai, N., Kino, K., & Kirimura, K. (2004). Reversible and nonoxidative γ-resorcylic acid decarboxylase: Characterization and gene cloning of a novel enzyme catalyzing carboxylation of resorcinol, 1, 3-dihydroxybenzene, from Rhizobium radiobacter. *Biochemical and Biophysical Research Communications*, *324*(2), 611–620. https://doi.org/10.1016/j.bbrc.2004.09.091

Jeandet, P., Douillet-Breuil, A.-C., Bessis, R., Debord, S., Sbaghi, M., & Adrian, M. (2002). Phytoalexins from the Vitaceae: Biosynthesis, Phytoalexin Gene Expression in

Transgenic Plants, Antifungal Activity, and Metabolism. *Journal of Agricultural and Food Chemistry*, *50*(10), 2731–2741. https://doi.org/10.1021/jf011429s

Jeon, Y.-T. (2009). Alternariol Monomethyl Ether and α, β-Dehydrocurvularin from Endophytic Fungi Alternaria spp. Inhibit Appressorium Formation of Magnaporthe grisea. *Journal of the Korean Society for Applied Biological Chemistry*, *53*(1), 39–42. https://doi.org/10.3839/jksabc.2010.007

Jeong, M.-H., Park, C.-H., Kim, J. A., Choi, E. D., Kim, S., Hur, J.-S., & Park, S.-Y. (2021). Production and activity of cristazarin in the lichen-forming fungus Cladonia metacorallifera. *Journal of Fungi*, *7*(8), 601. https://doi.org/10.3390/jof7080601

Jin, F. J., Watanabe, T., Juvvadi, P. R., Maruyama, J., Arioka, M., & Kitamoto, K. (2007). Double disruption of the proteinase genes, tppA and pepE, increases the production level of human lysozyme by Aspergillus oryzae. *Applied Microbiology and Biotechnology*, *76*(5), 1059–1068. https://doi.org/10.1007/s00253-007-1088-4

Jones, D. T., Taylor, W. R., & Thornton, J. M. (1992). The rapid generation of mutation data matrices from protein sequences. *Bioinformatics*, *8*(3), 275–282. https://doi.org/10.1093/bioinformatics/8.3.275

Kahlert, L., Bernardi, D., Hauser, M., Ióca, L. P., Berlinck, R. G. S., Skellam, E. J., & Cox, R. J. (2021). Early Oxidative Transformations During the Biosynthesis of Terrein and Related Natural Products. *Chemistry – A European Journal*, *27*(46), 11895–11903. https://doi.org/10.1002/chem.202101447

Kahlert, L., Villanueva, M., Cox, R. J., & Skellam, E. J. (2021). Biosynthesis of 6-Hydroxymellein Requires a Collaborating Polyketide Synthase-like Enzyme.

Angewandte Chemie International Edition, *60*(20), 11423–11429. https://doi.org/10.1002/anie.202100969

Kahriman, N., Yazici, K., Arslan, T., Aslan, A., Karaoglu, Ş., & Yayli, N. (2011). Chemical Composition and Antimicrobial Activity of the Essential Oils from Evernia prunastri and Evernia divaricata (L.) Ach.. *ASIAN JOURNAL OF CHEMISTRY* , vol.23, no.5, 1937-1939. No doi

Kamauchi, H., Furukawa, M., Kiba, Y., Kitamura, M., Usui, K., Katakura, M., Takao, K., & Sugita, Y. (2022). Antifungal activity of dehydrocurvularin for Candida spp. Through the inhibition of adhesion to human adenocarcinoma cells. *The Journal of Antibiotics*, *75*(9), 530–533. https://doi.org/10.1038/s41429-022-00543-5

Kealey, J. T., Craig, J. P., & Barr, P. J. (2021). Identification of a lichen depside polyketide synthase gene by heterologous expression in Saccharomyces cerevisiae. *Metabolic Engineering Communications*, *13*, e00172. https://doi.org/10.1016/j.mec.2021.e00172

Keating, T. A., & Walsh, C. T. (1999). Initiation, elongation, and termination strategies in polyketide and polypeptide antibiotic biosynthesis. *Current Opinion in Chemical Biology*, *3*(5), 598–606. https://doi.org/10.1016/S1367-5931(99)00015-0

Keatinge-Clay, A. T., & Stroud, R. M. (2006). The structure of a ketoreductase determines the organization of the beta-carbon processing enzymes of modular polyketide synthases. *Structure (London, England: 1993)*, *14*(4), 737–748. https://doi.org/10.1016/j.str.2006.01.009

Keller, N. P. (2019). Fungal secondary metabolism: Regulation, function and drug discovery. *Nature Reviews Microbiology*, *17*(3), 167–180. https://doi.org/10.1038/s41579-018-0121-1

Kelley, L. A., Mezulis, S., Yates, C. M., Wass, M. N., & Sternberg, M. J. E. (2015). The Phyre2 web portal for protein modeling, prediction and analysis. *Nature Protocols*, *10*(6), 845–858. https://doi.org/10.1038/nprot.2015.053

Kibwage, I. O., Hoogmartens, J., Roets, E., Vanderhaeghe, H., Verbist, L., Dubost, M., Pascal, C., Petitjean, P., & Levol, G. (1985). Antibacterial activities of erythromycins A, B, C, and D and some of their derivatives. *Antimicrobial Agents and Chemotherapy*, *28*(5), 630–633. https://doi.org/10.1128/AAC.28.5.630

Kim, W., Jeong, M.-H., Yun, S.-H., & Hur, J.-S. (2021). Transcriptome analysis identifies a gene cluster for the biosynthesis of biruloquinone, a rare phenanthraquinone, in a lichen-forming fungus Cladonia macilenta. *Journal of Fungi*, *7*(5), 398. https://doi.org/10.3390/jof7050398

Kim, W., Liu, R., Woo, S., Kang, K. B., Park, H., Yu, Y. H., Ha, H.-H., Oh, S.-Y., Yang, J. H., Kim, H., Yun, S.-H., & Hur, J.-S. (2021). Linking a Gene Cluster to Atranorin, a Major Cortical Substance of Lichens, through Genetic Dereplication and Heterologous Expression. *mBio*, *12*(3). https://doi.org/10.1128/mBio.01111-21

Kino, K., Hirokawa, Y., Gawasawa, R., Murase, R., Tsuchihashi, R., & Hara, R. (2020). Screening, gene cloning, and characterization of orsellinic acid decarboxylase from Arthrobacter sp. K8 for regio-selective carboxylation of resorcinol derivatives. *Journal of Biotechnology*, *323*, 128–135. https://doi.org/10.1016/j.jbiotec.2020.08.011

Kirimura, K., Gunji, H., Wakayama, R., Hattori, T., & Ishii, Y. (2010). Enzymatic Kolbe–Schmitt reaction to form salicylic acid from phenol: Enzymatic characterization and gene identification of a novel enzyme, Trichosporon moniliiforme salicylic acid

decarboxylase. *Biochemical and Biophysical Research Communications*, *394*(2), 279–284. https://doi.org/10.1016/j.bbrc.2010.02.154

Knox, B. P., Blachowicz, A., Palmer, J. M., Romsdahl, J., Huttenlocher, A., Wang, C. C. C., Keller, N. P., & Venkateswaran, K. (2016). Characterization of Aspergillus fumigatus Isolates from Air and Surfaces of the International Space Station. *mSphere*, *1*(5), e00227-16. https://doi.org/10.1128/mSphere.00227-16

Korman, T. P., Crawford, J. M., Labonte, J. W., Newman, A. G., Wong, J., Townsend, C. A., & Tsai, S.-C. (2010). Structure and function of an iterative polyketide synthase thioesterase domain catalyzing Claisen cyclization in aflatoxin biosynthesis. *Proceedings of the National Academy of Sciences*, *107*(14), 6246–6251. https://doi.org/10.1073/pnas.0913531107

Kornsakulkarn, J., Thongpanchang, C., Lapanun, S., & Srichomthong, K. (2009). Isocoumarin Glucosides from the Scale Insect Fungus Torrubiella tenuis BCC 12732. *Journal of Natural Products*, *72*(7), 1341–1343. https://doi.org/10.1021/np900082h

Kowalska-Krochmal, B., & Dudek-Wicher, R. (2021). The Minimum Inhibitory Concentration of Antibiotics: Methods, Interpretation, Clinical Relevance. *Pathogens*, *10*(2), 165. https://doi.org/10.3390/pathogens10020165

Kramer, C. L., & Pady, S. M. (1961). Inhibition of Growth of Fungi on Rose Bengal Media by Light. *Transactions of the Kansas Academy of Science (1903-)*, *64*(2), 110–116. https://doi.org/10.2307/3626929

Kumar, S., Stecher, G., & Tamura, K. (2016). MEGA7: Molecular Evolutionary Genetics Analysis Version 7.0 for Bigger Datasets. *Molecular Biology and Evolution*, *33*(7), 1870–1874. https://doi.org/10.1093/molbev/msw054

Le Pogam, P., Legouin, B., Geairon, A., Rogniaux, H., Lohézic-Le Dévéhat, F., Obermayer, W., Boustie, J., & Le Lamer, A.-C. (2016). Spatial mapping of lichen specialized metabolites using LDI-MSI: Chemical ecology issues for Ophioparma ventosa. *Scientific Reports*, *6*(1), 37807. https://doi.org/10.1038/srep37807

Lee, I.-S., Ryoo, I.-J., Kwon, K.-Y., Ahn, J. S., & Yoo, I.-D. (2011). Pleurone, a novel human neutrophil elastase inhibitor from the fruiting bodies of the mushroom Pleurotus eryngii var. Ferulae. *The Journal of Antibiotics*, *64*(8), 587–589. https://doi.org/10.1038/ja.2011.47

Legouin, B., Lohézic-Le Dévéhat, F., Ferron, S., Rouaud, I., Le Pogam, P., Cornevin, L., Bertrand, M., & Boustie, J. (2017). Specialized metabolites of the lichen Vulpicida pinastri act as photoprotective agents. *Molecules*, *22*(7), 1162. https://doi.org/10.3390/molecules22071162

Li, D.-H., Han, T., Guan, L.-P., Bai, J., Zhao, N., Li, Z.-L., Wu, X., & Hua, H.-M. (2016). New naphthopyrones from marine-derived fungus Aspergillus niger 2HL-M-8 and their in vitro antiproliferative activity. *Natural Product Research*, *30*(10), 1116–1122. https://doi.org/10.1080/14786419.2015.1043553

Li, T., Iwaki, H., Fu, R., Hasegawa, Y., Zhang, H., & Liu, A. (2006). α-Amino-β-carboxymuconic-ε-semialdehyde Decarboxylase (ACMSD) Is a New Member of the Amidohydrolase Superfamily. *Biochemistry*, *45*(21), 6628–6634. https://doi.org/10.1021/bi060108c

Li, X., Kim, S. K., Kang, J. S., Choi, H. D., & Son, B. W. (2006). Radical Scavenging Hydroxyphenyl Ethanoic Acid Derivatives from a Marine-Derived Fungus. *Journal of Microbiology and Biotechnology*,*16* (4), 637-638. No doi

Li, Y., Chooi, Y.-H., Sheng, Y., Valentine, J. S., & Tang, Y. (2011). Comparative Characterization of Fungal Anthracenone and Naphthacenedione Biosynthetic Pathways Reveals an α-Hydroxylation-Dependent Claisen-like Cyclization Catalyzed by a Dimanganese Thioesterase. *Journal of the American Chemical Society*, *133*(39), 15773–15785. https://doi.org/10.1021/ja206906d

Lind, A. L., Wisecaver, J. H., Lameiras, C., Wiemann, P., Palmer, J. M., Keller, N. P., Rodrigues, F., Goldman, G. H., & Rokas, A. (2017). Drivers of genetic diversity in secondary metabolic gene clusters within a fungal species. *PLOS Biology*, *15*(11), e2003583. https://doi.org/10.1371/journal.pbio.2003583

Liscombe, D. K., Louie, G. V., & Noel, J. P. (2012). Architectures, mechanisms and molecular evolution of natural product methyltransferases. *Natural Product Reports*, *29*(10), 1238–1250. https://doi.org/10.1039/C2NP20029E

Liu, M., Zhou, Q., Wang, J., Liu, J., Qi, C., Lai, Y., Zhu, H., Xue, Y., Hu, Z., & Zhang, Y. (2018). Anti-inflammatory butenolide derivatives from the coral-derived fungus Aspergillus terreus and structure revisions of aspernolides D and G, butyrolactone VI and 4′, 8′′-diacetoxy butyrolactone VI. *RSC Advances*, *8*(23), 13040–13047. https://doi.org/10.1039/C8RA01840E

Liu, Y., Fernie, A. R., & Tohge, T. (2022). Diversification of Chemical Structures of Methoxylated Flavonoids and Genes Encoding Flavonoid-O-Methyltransferases. *Plants*, *11*(4), Article 4. https://doi.org/10.3390/plants11040564

Lopes, T. I. B., Coelho, R. G., Yoshida, N. C., & Honda, N. K. (2008). Radical-Scavenging Activity of Orsellinates. *Chemical and Pharmaceutical Bulletin*, *56*(11), 1551–1554. https://doi.org/10.1248/cpb.56.1551

Lutzoni, F., & Miadlikowska, J. (2009). Lichens. *Current Biology: CB*, *19*(13), R502-503. https://doi.org/10.1016/j.cub.2009.04.034

Magaldi, S., Mata-Essayag, S., Hartung de Capriles, C., Perez, C., Colella, M. T., Olaizola, C., & Ontiveros, Y. (2004). Well diffusion for antifungal susceptibility testing. *International Journal of Infectious Diseases*, *8*(1), 39–45. https://doi.org/10.1016/j.ijid.2003.03.002

Mahajan, G., & Balachandran, L. (2015). Biodiversity in production of antibiotics and other bioactive compounds. *Advances in Biochemical Engineering/Biotechnology*, *147*, 37–58. https://doi.org/10.1007/10_2014_268

Manganyi, M. C., & Ateba, C. N. (2020). Untapped potentials of endophytic fungi: A review of novel bioactive compounds with biological applications. *Microorganisms*, *8*(12), 1934. https://doi.org/10.3390/microorganisms8121934

Maragakis, L. L., & Perl, T. M. (2008). Antimicrobial Resistance: *Acinetobacter baumannii:* Epidemiology, Antimicrobial Resistance, and Treatment Options. *Clinical Infectious Diseases*, *46*(8), 1254–1263. https://doi.org/10.1086/529198

Martinet, L., Naômé, A., Deflandre, B., Maciejewska, M., Tellatin, D., Tenconi, E., Smargiasso, N., de Pauw, E., van Wezel, G. P., & Rigali, S. (2019). A Single Biosynthetic Gene Cluster Is Responsible for the Production of Bagremycin Antibiotics and Ferroverdin Iron Chelators. *mBio*, *10*(4), e01230-19. https://doi.org/10.1128/mBio.01230-19

Matos, P., Pinho, P., Aragón, G., Martínez, I., Nunes, A., Soares, A. M. V. M., & Branquinho, C. (2015). Lichen traits responding to aridity. *Journal of Ecology*, *103*(2), 451–458. https://doi.org/10.1111/1365-2745.12364

McEvoy, M., Gauslaa, Y., & Solhaug, K. A. (2007). Changes in pools of depsidones and melanins, and their function, during growth and acclimation under contrasting natural light in the lichen *Lobaria pulmonaria*. *New Phytologist*, *175*(2), 271–282. https://doi.org/10.1111/j.1469-8137.2007.02096.x

Medema, M. H., Blin, K., Cimermancic, P., de Jager, V., Zakrzewski, P., Fischbach, M. A., Weber, T., Takano, E., & Breitling, R. (2011). antiSMASH: Rapid identification, annotation and analysis of secondary metabolite biosynthesis gene clusters in bacterial and fungal genome sequences. *Nucleic Acids Research*, *39*(suppl_2), W339–W346. https://doi.org/10.1093/nar/gkr466

Meepagala, K. M., Johnson, R. D., & Duke, S. O. (2016). Curvularin and Dehydrocurvularin as Phytotoxic Constituents from <i>Curvularia intermedia</i> Infecting <i>Pandanus amaryllifolius</i> *Journal of Agricultural Chemistry and Environment*, *05*(01), 12–22. https://doi.org/10.4236/jacen.2016.51002

Merinero, S., & Gauslaa, Y. (2018). Specialized fungal parasites reduce fitness of their lichen hosts. *Annals of Botany*, *121*(1), 175–182. https://doi.org/10.1093/aob/mcx124

Michel, G. W. (1977). Nystatin. In K. Florey (Ed.), *Analytical Profiles of Drug Substances* (Vol. 6, pp. 341–421). Academic Press. https://doi.org/10.1016/S0099-5428(08)60349-4

Millot, M., Tomasi, S., Studzinska, E., Rouaud, I., & Boustie, J. (2009). Cytotoxic Constituents of the Lichen *Diploicia canescens*. *Journal of Natural Products*, *72*(12), 2177–2180. https://doi.org/10.1021/np9003728

Molnár, K., & Farkas, E. (2010). Current results on biological activities of lichen secondary metabolites: A review. *Zeitschrift Fur Naturforschung. C, Journal of Biosciences*, *65*(3–4), 157–173. https://doi.org/10.1515/znc-2010-3-401

Mosbach, K. (1969). Biosynthesis of Lichen Substances, Products of a Symbiotic Association. *Angewandte Chemie International Edition in English*, *8*(4), 240–250. https://doi.org/10.1002/anie.196902401

Mosunova, O. V., Navarro-Muñoz, J. C., Haksar, D., van Neer, J., Hoeksma, J., den Hertog, J., & Collemare, J. (2022). Evolution-Informed Discovery of the Naphthalenone Biosynthetic Pathway in Fungi. *mBio*, e00223-22. https://doi.org/10.1128/mbio.00223-22

Mun, S.-K., Kang, K.-Y., Jang, H.-Y., Hwang, Y.-H., Hong, S.-G., Kim, S.-J., Cho, H.-W., Chang, D.-J., Hur, J.-S., & Yee, S.-T. (2020). Atraric Acid Exhibits Anti-Inflammatory Effect in Lipopolysaccharide-Stimulated RAW264.7 Cells and Mouse Models. *International Journal of Molecular Sciences*, *21*(19), 7070. https://doi.org/10.3390/ijms21197070

Mushegian, A. A., Peterson, C. N., Baker, C. C. M., & Pringle, A. (2011). Bacterial Diversity across Individual Lichens. *Applied and Environmental Microbiology*, *77*(12), 4249–4252. https://doi.org/10.1128/AEM.02850-10

Nayaka, S., & Haridas, B. (2020). Bioactive Secondary Metabolites from Lichens. In S. T. Sukumaran, S. Sugathan, & S. Abdulhameed (Eds.), *Plant Metabolites: Methods, Applications and Prospects* (pp. 255–290). Springer Singapore. https://doi.org/10.1007/978-981-15-5136-9_12

Neamati, N., Hong, H., Mazumder, A., Wang, S., Sunder, S., Nicklaus, M. C., Milne, G. W., Proksa, B., & Pommier, Y. (1997). Depsides and depsidones as inhibitors of HIV-1 integrase: Discovery of novel inhibitors through 3D database searching. *Journal of Medicinal Chemistry*, *40*(6), 942–951. https://doi.org/10.1021/jm960759e

Newman, D. J., & Cragg, G. M. (2020). Natural Products as Sources of New Drugs over the Nearly Four Decades from 01/1981 to 09/2019. *Journal of Natural Products*, *83*(3), 770–803. https://doi.org/10.1021/acs.jnatprod.9b01285

Nguyen, K.-H., Chollet-Krugler, M., Gouault, N., & Tomasi, S. (2013). UV-protectant metabolites from lichens and their symbiotic partners. *Natural Product Reports*, *30*(12), 1490–1508. https://doi.org/10.1039/C3NP70064J

Noh, H.-J., Lee, Y. M., Park, C. H., Lee, H. K., Cho, J.-C., & Hong, S. G. (2020). Microbiome in Cladonia squamosa Is Vertically Stratified According to Microclimatic Conditions. *Frontiers in Microbiology*, *11*. https://doi.org/10.3389/fmicb.2020.00268

Ohmura, Y., Hosaka, K., Kasuya, T., Abe, J. P., & Kakishima, M. (2013). Activity concentrations of radionuclides in lichens following the Fukushima nuclear accident. *The Lichenologist*, *45*(5), 685–689. https://doi.org/10.1017/S0024282913000431

Ola, A. R. B., Metboki, G., Lay, C. S., Sugi, Y., Rozari, P. D., Darmakusuma, D., & Hakim, E. H. (2019). Single Production of Kojic Acid by Aspergillus flavus and the Revision of Flufuran. *Molecules*, *24*(22), Article 22. https://doi.org/10.3390/molecules24224200

O'Neill, J. (2016). *Tackling drug-resistant infections globally: Final report and recommendations.* https://www.cabidigitallibrary.org/doi/full/10.5555/20173071720

Özgür, Ö., & Aksaray, N. (2014). Acinetobacter Infections and Treatment. *Journal of Pediatric Infection*, *8*(1), 28–32. https://doi.org/10.5152/ced.2013.38

Pangging, M., Nguyen, T. T. T., & Lee, H. B. (2019). New Records of Four Species Belonging to Eurotiales from Soil and Freshwater in Korea. *Mycobiology*, *47*(2), 154–164. https://doi.org/10.1080/12298093.2018.1554777

Papadopoulou, P., Tzakou, O., Vagias, C., Kefalas, P., & Roussis, V. (2007). β-Orcinol Metabolites from the Lichen Hypotrachyna revoluta. *Molecules*, *12*(5), Article 5. https://doi.org/10.3390/12050997

Park, Choi, J., Kim, J. A., Jeong, M.-H., Kim, S., Lee, Y.-H., & Hur, J.-S. (2013). Draft Genome Sequence of *Cladonia macilenta* KoLRI003786, a Lichen-Forming Fungus Producing Biruloquinone. *Genome Announcements*, *1*(5), e00695-13. https://doi.org/10.1128/genomeA.00695-13

Park, H., Kevany, B. M., Dyer, D. H., Thomas, M. G., & Forest, K. T. (2014). A Polyketide Synthase Acyltransferase Domain Structure Suggests a Recognition Mechanism for Its Hydroxymalonyl-Acyl Carrier Protein Substrate. *PLoS ONE*, *9*(10), e110965. https://doi.org/10.1371/journal.pone.0110965

Park, S.-Y., Choi, J., Lee, G.-W., Kim, J. A., Oh, S.-O., Jeong, M.-H., Yu, N.-H., Kim, S., Lee, Y.-H., & Hur, J.-S. (2014). Draft Genome Sequence of Lichen-Forming Fungus *Cladonia metacorallifera* Strain KoLRI002260. *Genome Announcements*, *2*(1), e01065-13. https://doi.org/10.1128/genomeA.01065-13

Parker, E. M., Ballash, G. A., Mollenkopf, D. F., & Wittum, T. E. (2024). A complex cyclical One Health pathway drives the emergence and dissemination of antimicrobial resistance. *American Journal of Veterinary Research*, 1–9. https://doi.org/10.2460/ajvr.24.01.0014

Paysan-Lafosse, T., Blum, M., Chuguransky, S., Grego, T., Pinto, B. L., Salazar, G. A., Bileschi, M. L., Bork, P., Bridge, A., Colwell, L., Gough, J., Haft, D. H., Letunić, I., Marchler-Bauer, A., Mi, H., Natale, D. A., Orengo, C. A., Pandurangan, A. P., Rivoire,

C., … Bateman, A. (2023). InterPro in 2022. *Nucleic Acids Research*, *51*(D1), D418–D427. https://doi.org/10.1093/nar/gkac993

Perrone, G., & Gallo, A. (2017). Aspergillus Species and Their Associated Mycotoxins. In A. Moretti & A. Susca (Eds.), *Mycotoxigenic Fungi: Methods and Protocols* (pp. 33–49). Springer. https://doi.org/10.1007/978-1-4939-6707-0_3

Pescott, O. L., Simkin, J. M., August, T. A., Randle, Z., Dore, A. J., & Botham, M. S. (2015). Air pollution and its effects on lichens, bryophytes, and lichen-feeding Lepidoptera: Review and evidence from biological records: Lichens, Bryophytes, Moths and Air Quality. *Biological Journal of the Linnean Society*, *115*(3), 611–635. https://doi.org/10.1111/bij.12541

Pettersen, E. F., Goddard, T. D., Huang, C. C., Couch, G. S., Greenblatt, D. M., Meng, E. C., & Ferrin, T. E. (2004). UCSF Chimera—A visualization system for exploratory research and analysis. *Journal of Computational Chemistry*, *25*(13), 1605–1612. https://doi.org/10.1002/jcc.20084

Phinney, N. H., Gauslaa, Y., & Solhaug, K. A. (2019). Why chartreuse? The pigment vulpinic acid screens blue light in the lichen Letharia vulpina. *Planta*, *249*(3), 709–718. https://doi.org/10.1007/s00425-018-3034-3

Pizarro, D., Divakar, P. K., Grewe, F., Crespo, A., Dal Grande, F., & Lumbsch, H. T. (2020). Genome-wide analysis of biosynthetic gene cluster reveals correlated gene loss with absence of usnic acid in lichen-forming fungi. *Genome Biology and Evolution*, *12*(10), 1858–1868. https://doi.org/10.1093/gbe/evaa189

Pöykkö, H., Hyvärinen, M., & Bačkor, M. (2005). Removal of lichen secondary metabolites affects food choice and survival of lichenivorous moth larvae. *Ecology*, *86*(10), 2623–2632. https://doi.org/10.1890/04-1632

Quax, T. E. F., Claassens, N. J., Söll, D., & van der Oost, J. (2015). Codon Bias as a Means to Fine-Tune Gene Expression. *Molecular Cell*, *59*(2), 149–161. https://doi.org/10.1016/j.molcel.2015.05.035

Rajab, M. S., Cantrell, C. L., Franzblau, S. G., & Fischer, N. H. (1998). Antimycobacterial activity of (E)-phytol and derivatives: A preliminary structure-activity study. *Planta Medica*, *64*(01), 2–4. https://doi.org/10.1055/s-2006-957354

Ranković, B. (Ed.). (2019). *Lichen Secondary Metabolites: Bioactive Properties and Pharmaceutical Potential*. Springer International Publishing. https://doi.org/10.1007/978-3-030-16814-8

Rasmey, A.-H. M., & Abdel-Kareem, M. (2021). Optimization of culture conditions for kojic acid production in surface fermentation by aspergillus oryzae isolated from wheat grains. *Bulletin of Pharmaceutical Sciences Assiut University*, *44*(1), 201–211. https://doi.org/10.21608/bfsa.2021.174146

Rice, L. B. (2008). Federal Funding for the Study of Antimicrobial Resistance in Nosocomial Pathogens: No ESKAPE. *The Journal of Infectious Diseases*, *197*(8), 1079–1081. https://doi.org/10.1086/533452

Ristić, S., Ranković, B., Kosanić, M., Stanojković, T., Stamenković, S., Vasiljević, P., Manojlović, I., & Manojlović, N. (2016). Phytochemical study and antioxidant, antimicrobial and anticancer activities of Melanelia subaurifera and Melanelia

fuliginosa lichens. *Journal of Food Science and Technology*, *53*(6), 2804–2816. https://doi.org/10.1007/s13197-016-2255-3

Robey, M. T., Caesar, L. K., Drott, M. T., Keller, N. P., & Kelleher, N. L. (2021). An interpreted atlas of biosynthetic gene clusters from 1,000 fungal genomes. *Proceedings of the National Academy of Sciences*, *118*(19), e2020230118. https://doi.org/10.1073/pnas.2020230118

Rzhetsky, A., & Nei, M. (1992). Statistical properties of the ordinary least-squares, generalized least-squares, and minimum-evolution methods of phylogenetic inference. *Journal of Molecular Evolution*, *35*(4), 367–375. https://doi.org/10.1007/BF00161174

Sadeghian, M., Shahidi Bonjar, G. H., & Sharifi Sirchi, G. R. (2016). Post harvest biological control of apple bitter rot by soil-borne Actinomycetes and molecular identification of the active antagonist. *Postharvest Biology and Technology*, *112*, 46–54. https://doi.org/10.1016/j.postharvbio.2015.09.035

Safe, S., Safe, L. M., & Maass, W. S. G. (1975). Sterols of three lichen species: Lobaria pulmonaria, Lobaria Scrobiculata and Usnea Longissima. *Phytochemistry*, *14*(8), 1821–1823. https://doi.org/10.1016/0031-9422(75)85302-7

Scott, A. I., Phillips, G. T., & Kircheis, U. (1971). Biosynthesis of polyketides the synthesis of 6-methylsalicylic acid and triacetic acid lactone in *Penicillium patulum*. *Bioorganic Chemistry*, *1*(4), 380–399. https://doi.org/10.1016/0045-2068(71)90041-1

Seneviratne, G., & Indrasena, I. K. (2006). Nitrogen fixation in lichens is important for improved rock weathering. *Journal of Biosciences*, *31*(5), 639–643. https://doi.org/10.1007/BF02708416

Shi, Y.-S., Zhang, Y., Chen, X.-Z., Zhang, N., & Liu, Y.-B. (2015). Metabolites Produced by the Endophytic Fungus Aspergillus fumigatus from the Stem of Erythrophloeum fordii Oliv. *Molecules*, *20*(6), 10793–10799. https://doi.org/10.3390/molecules200610793

Shrestha, G., & St. Clair, L. L. (2013). Lichens: A promising source of antibiotic and anticancer drugs. *Phytochemistry Reviews*, *12*(1), 229–244. https://doi.org/10.1007/s11101-013-9283-7

Sierra, M. A., Danko, D. C., Sandoval, T. A., Pishchany, G., Moncada, B., Kolter, R., Mason, C. E., & Zambrano, M. M. (2020). The Microbiomes of Seven Lichen Genera Reveal Host Specificity, a Reduced Core Community and Potential as Source of Antimicrobials. *Frontiers in Microbiology*, *11*. https://doi.org/10.3389/fmicb.2020.00398

Sigurbjörnsdóttir, M. A., Andrésson, Ó. S., & Vilhelmsson, O. (2015). Analysis of the Peltigera membranacea metagenome indicates that lichen-associated bacteria are involved in phosphate solubilization. *Microbiology*, *161*(5), 989–996. https://doi.org/10.1099/mic.0.000069

Singh, G., Armaleo, D., Dal Grande, F., & Schmitt, I. (2021). Depside and depsidone synthesis in lichenized fungi comes into focus through a genome-wide comparison of the olivetoric acid and physodic acid chemotypes of Pseudevernia furfuracea. *Biomolecules*, *11*(10), 1445. https://doi.org/10.3390/biom11101445

Sinnemann, S. J., Andrésson, Ó. S., Brown, D. W., & Miao, V. P. (2000). Cloning and heterologous expression of Solorina crocea pyrG. *Current Genetics*, *37*(5), 333–338. https://doi.org/10.1007/s002940050536

Skiba, M. A., Sikkema, A. P., Fiers, W. D., Gerwick, W. H., Sherman, D. H., Aldrich, C. C., & Smith, J. L. (2016). Domain Organization and Active Site Architecture of a Polyketide Synthase C-methyltransferase. *ACS Chemical Biology*, *11*(12), 3319–3327. https://doi.org/10.1021/acschembio.6b00759

Solhaug, K. A., Larsson, P., & Gauslaa, Y. (2010). Light screening in lichen cortices can be quantified by chlorophyll fluorescence techniques for both reflecting and absorbing pigments. *Planta*, *231*(5), 1003–1011. https://doi.org/10.1007/s00425-010-1103-3

Song, F., Liu, X., Guo, H., Ren, B., Chen, C., Piggott, A. M., Yu, K., Gao, H., Wang, Q., & Liu, M. (2012). Brevianamides with antitubercular potential from a marine-derived isolate of Aspergillus versicolor. *Organic Letters*, *14*(18), 4770–4773. https://doi-org.uml.idm.oclc.org/10.1021/ol302051x

Song, F., Ren, B., Chen, C., Yu, K., Liu, X., Zhang, Y., Yang, N., He, H., Liu, X., & Dai, H. (2014). Three new sterigmatocystin analogues from marine-derived fungus Aspergillus versicolor MF359. *Applied Microbiology and Biotechnology*, *98*(8), 3753–3758. https://doi.org/10.1007/s00253-013-5409-5

Spribille, T., Tuovinen, V., Resl, P., Vanderpool, D., Wolinski, H., Aime, M. C., Schneider, K., Stabentheiner, E., Toome-Heller, M., Thor, G., Mayrhofer, H., Johannesson, H., & McCutcheon, J. P. (2016). Basidiomycete yeasts in the cortex of ascomycete macrolichens. *Science (New York, N.Y.)*, *353*(6298), 488–492. https://doi.org/10.1126/science.aaf8287

Stadler, M., & Anke, H. (1995). Metabolites with nematicidal and antimicrobial activities from the ascomycete Lachnum papyraceum (Karst.) Karst. III. Production of novel

isocoumarin derivatives, isolation, and biological activities. *Journal of Antibiotics, 48*(3), 261-266. https://doi.org/10.7164/antibiotics.48.149

Staunton, J., & Weissman, K. J. (2001). Polyketide biosynthesis: A millennium review. *Natural Product Reports*, *18*(4), 380–416. https://doi.org/10.1039/A909079G

Struck, A.-W., Thompson, M. L., Wong, L. S., & Micklefield, J. (2012). S-Adenosyl-Methionine-Dependent Methyltransferases: Highly Versatile Enzymes in Biocatalysis, Biosynthesis and Other Biotechnological Applications. *ChemBioChem*, *13*(18), 2642–2655. https://doi.org/10.1002/cbic.201200556

Takenaka, Y., Hamada, N., & Tanahashi, T. (2011). Aromatic compounds from cultured lichen mycobionts of three Graphis species. *Heterocycles, 83*(9), 2011-2018. https://doi.org/10.3987/com-11-12270

Tamura, K., Stecher, G., & Kumar, S. (2021). MEGA11: Molecular Evolutionary Genetics Analysis Version 11. *Molecular Biology and Evolution*, *38*(7), 3022–3027. https://doi.org/10.1093/molbev/msab120

Tang, K. W. K., Millar, B. C., & Moore, J. E. (2023). Antimicrobial Resistance (AMR). *British Journal of Biomedical Science*, *80*, 11387. https://doi.org/10.3389/bjbs.2023.11387

Tekaia, F., & Latgé, J.-P. (2005). Aspergillus fumigatus: Saprophyte or pathogen? *Current Opinion in Microbiology*, *8*(4), 385–392. https://doi.org/10.1016/j.mib.2005.06.017

The Galaxy Community, Afgan, E., Nekrutenko, A., Grüning, B. A., Blankenberg, D., Goecks, J., Schatz, M. C., Ostrovsky, A. E., Mahmoud, A., Lonie, A. J., Syme, A., Fouilloux, A., Bretaudeau, A., Nekrutenko, A., Kumar, A., Eschenlauer, A. C., DeSanto, A. D., Guerler, A., Serrano-Solano, B., … Briggs, P. J. (2022). The Galaxy platform for

accessible, reproducible and collaborative biomedical analyses: 2022 update. *Nucleic Acids Research*, *50*(W1), W345–W351. https://doi.org/10.1093/nar/gkac247

Türk, H., Yılmaz, M., Tay, T., Türk, A. Ö., & Kıvanç, M. (2006). Antimicrobial Activity of Extracts of Chemical Races of the Lichen Pseudevernia furfuracea and their Physodic Acid, Chloroatranorin, Atranorin, and Olivetoric Acid Constituents. *Zeitschrift Für Naturforschung C*, *61*(7–8), 499–507. https://doi.org/10.1515/znc-2006-7-806

Uzma, F., & Chowdappa, S. (2017). Antimicrobial and Antioxidant Potential of Endophytic Fungi Isolated from Ethnomedicinal Plants of Western Ghats, Karnataka. *Journal of Pure and Applied Microbiology*, *11*(2), 1009–1025. https://doi.org/10.22207/JPAM.11.2.43

van Otterlo, W. A. L., Michael, J. P., & de Koning, C. B. (2007). Alternatives to N,N-Diethyl-2,4-dimethoxybenzamide as a Precursor for the Synthesis of 6,8-Dimethoxy-3-methyl-3,4-dihydro-1H-isochromen-1-one. *Synthetic Communications*, *37*(20), 3611–3621. https://doi.org/10.1080/00397910701557655

Visagie, C. M., Seifert, K. A., Houbraken, J., Samson, R. A., & Jacobs, K. (2014). Diversity of *Penicillium* section *Citrina* within the fynbos biome of South Africa, including a new species from a *Protea repens* infructescence. *Mycologia*, *106*(3), 537–552. https://doi.org/10.3852/13-256

Wai, A., & Hausner, G. (2021). The mitochondrial genome of *Ophiostoma himal-ulmi* and comparison with other fungi causing Dutch elm disease. *Canadian Journal of Microbiology*, *67*(8), 584–598. https://doi.org/10.1139/cjm-2020-0589

Walle, T. (2007). Methylation of Dietary Flavones Greatly Improves Their Hepatic Metabolic Stability and Intestinal Absorption. *Molecular Pharmaceutics*, *4*(6), 826–832. https://doi.org/10.1021/mp700071d

Wang, B., Lei, X., Chen, J., Li, W., Long, Y., & Wang, W. (2022). Antifungal Activities of Bacillus mojavensis BQ-33 towards the Kiwifruit Black Spot Disease Caused by the Fungal Pathogen Didymella glomerata. *Microorganisms*, *10*(10), Article 10. https://doi.org/10.3390/microorganisms10102085

Wang, Y., Geng, C., Yuan, X., Hua, M., Tian, F., & Li, C. (2018). Identification of a putative polyketide synthase gene involved in usnic acid biosynthesis in the lichen Nephromopsis pallescens. *PLoS One*, *13*(7), e0199110. https://doi.org/10.1371/journal.pone.0199110

Wayne, P. A. (2010). Clinical and Laboratory Standards Institute: Performance standards for antimicrobial susceptibility testing: 20th informational supplement. *CLSI Document M100-S20*. No doi

Weber, G., Schörgendorfer, K., Schneider-Scherzer, E., & Leitner, E. (1994). The peptide synthetase catalyzing cyclosporine production in Tolypocladium niveum is encoded by a giant 45.8-kilobase open reading frame. *Current Genetics*, *26*(2), 120–125. https://doi.org/10.1007/BF00313798

Weber, T., Blin, K., Duddela, S., Krug, D., Kim, H. U., Bruccoleri, R., Lee, S. Y., Fischbach, M. A., Müller, R., Wohlleben, W., Breitling, R., Takano, E., & Medema, M. H. (2015). antiSMASH 3.0—A comprehensive resource for the genome mining of biosynthetic gene clusters. *Nucleic Acids Research*, *43*(W1), W237–W243. https://doi.org/10.1093/nar/gkv437

Weissman, K. J. (2009). Chapter 1 Introduction to Polyketide Biosynthesis. In *Methods in Enzymology* (Vol. 459, pp. 3–16). Academic Press. https://doi.org/10.1016/S0076-6879(09)04601-1

Wiemann, P., Guo, C.-J., Palmer, J. M., Sekonyela, R., Wang, C. C. C., & Keller, N. P. (2013). Prototype of an intertwined secondary-metabolite supercluster. *Proceedings of the National Academy of Sciences*, *110*(42), 17065–17070. https://doi.org/10.1073/pnas.1313258110

Williams, D. E., Davies, J., Patrick, B. O., Bottriell, H., Tarling, T., Roberge, M., & Andersen, R. J. (2008). Cladoniamides A−G, Tryptophan-Derived Alkaloids Produced in Culture by *Streptomyces uncialis*. *Organic Letters*, *10*(16), 3501–3504. https://doi.org/10.1021/ol801274c

Wuensch, C., Gross, J., Steinkellner, G., Lyskowski, A., Gruber, K., Glueck, S. M., & Faber, K. (2014). Regioselective ortho-carboxylation of phenols catalyzed by benzoic acid decarboxylases: A biocatalytic equivalent to the Kolbe–Schmitt reaction. *RSC Advances*, *4*(19), 9673–9679. https://doi.org/10.1039/C3RA47719C

Wuensch, C., Pavkov-Keller, T., Steinkellner, G., Gross, J., Fuchs, M., Hromic, A., Lyskowski, A., Fauland, K., Gruber, K., & Glueck, S. M. (2015). Regioselective Enzymatic β-Carboxylation of para-Hydroxy-styrene Derivatives Catalyzed by Phenolic Acid Decarboxylases. *Advanced Synthesis & Catalysis*, *357*(8), 1909–1918. https://doi-org.uml.idm.oclc.org/10.1002/adsc.201401028

Xiang, C., Liu, Y., Liu, S.-M., Huang, Y.-F., Kong, L.-A., Peng, H., Liu, M.-Y., Liu, J., Peng, D.-L., & Huang, W.-K. (2020). Aβ-Dehydrocurvularin isolated from the fungus Aspergillus welwitschiae effectively inhibited the behaviour and development of the

root-knot nematode Meloidogyne graminicola in rice roots. *BMC Microbiology*, *20*(1), 48. https://doi.org/10.1186/s12866-020-01738-2

Xu, Y., Espinosa-Artiles, P., Schubert, V., Xu, Y., Zhang, W., Lin, M., Gunatilaka, A. A. L., Sï¿½ssmuth, R., & Molnï¿½r, I. (2013). Characterization of the Biosynthetic Genes for 10,11-Dehydrocurvularin, a Heat Shock Response-Modulating Anticancer Fungal Polyketide from Aspergillus terreus. *Applied and Environmental Microbiology*, *79*(6), 2038–2047. https://doi.org/10.1128/AEM.03334-12

Yang, K., Tian, J., & Keller, N. P. (2022). Post-translational modifications drive secondary metabolite biosynthesis in Aspergillus: A review. *Environmental Microbiology*, *24*(7), 2857–2881. https://doi.org/10.1111/1462-2920.16034

Yi, W., Neng, Z., Xiaolong, Y., Mei, H., Jae-Seoun, H., Yuming, Y., & Juan, W. (2016). Heterologous transcription of a polyketide synthase gene from the lichen forming fungi Usnea longissima. *Research Journal of Biotechnology*, *11*(10), 16–21. No doi

Yoshida, M., Fukuhara, N., & Oikawa, T. (2004). Thermophilic, Reversible γ-Resorcylate Decarboxylase from Rhizobium sp. Strain MTP-10005: Purification, Molecular Characterization, and Expression. *Journal of Bacteriology*, *186*(20), 6855–6863. https://doi.org/10.1128/JB.186.20.6855-6863.2004

Yoshida, M., Oikawa, T., Obata, H., Abe, K., Mihara, H., & Esaki, N. (2007). Biochemical and genetic analysis of the γ-resorcylate (2, 6-dihydroxybenzoate) catabolic pathway in Rhizobium sp. strain MTP-10005: Identification and functional analysis of its gene cluster. *Journal of Bacteriology*, *189*(5), 1573–1581. https://doi.org/10.1128/jb.01675-06

Yu, D., Xu, F., Zeng, J., & Zhan, J. (2012). Type III polyketide synthases in natural product biosynthesis. *IUBMB Life*, *64*(4), 285–295. https://doi.org/10.1002/iub.1005

Zhang, X., Li, Z., & Gao, J. (2018). Chemistry and biology of secondary metabolites from Aspergillus genus. *The Natural Products Journal*, *8*(4), 275–304. https://doi.org/10.2174/2210315508666180501154759

Zhang, X., Ren, J., Yao, P., Gong, R., Wang, M., Wu, Q., & Zhu, D. (2018). Biochemical characterization and substrate profiling of a reversible 2,3-dihydroxybenzoic acid decarboxylase for biocatalytic Kolbe-Schmitt reaction. *Enzyme and Microbial Technology*, *113*, 37–43. https://doi.org/10.1016/j.enzmictec.2018.02.008

Zhang, Y., Li, X.-M., & Wang, B.-G. (2012). Anthraquinone derivatives produced by marine-derived fungus Aspergillus versicolor EN-7. *Bioscience, Biotechnology, and Biochemistry*, *76*(9), 1774–1776. https://doi.org/10.1271/bbb.120047

Zhao, W. Y., Zhu, T. J., Fan, G. T., Liu, H. B., Fang, Y. C., Gu, Q. Q., & Zhu, W. M. (2010). Three new dioxopiperazine metabolites from a marine-derived fungus Aspergillus fumigatus Fres. *Natural Product Research*, *24*(10), 953–957. https://doi.org/10.1080/14786410902726134

Zhao, W.-Y., Yi, J., Chang, Y.-B., Sun, C.-P., & Ma, X.-C. (2022). Recent studies on terpenoids in Aspergillus fungi: Chemical diversity, biosynthesis, and bioactivity. *Phytochemistry*, *193*, 113011. https://doi.org/10.1016/j.phytochem.2021.113011.

Zhgun, A. A. (2023). Fungal BGCs for Production of Secondary Metabolites: Main Types, Central Roles in Strain Improvement, and Regulation According to the Piano Principle. *International Journal of Molecular Sciences*, *24*(13), Article 13. https://doi.org/10.3390/ijms241311184

Supplementary Information

Chapter 1: *Not applicable*

Chapter 2

Table S1: List of Primers

Primer	Sequence (5′-3′)	Description
ITS1 F	TCC GTA GGT GAA CCT GCG G	Amplifies the internal transcribed spacer (ITS) region of fungal DNA, forward primer
ITS4 R	TCC TCC GCT TAT TGA TAT GC	Amplifies the internal transcribed spacer (ITS) region of fungal DNA, reverse primer
deCO2 Gib F. Primer	atcacggatccgagaacctgtacttccaaggtacc ATGATTACGCTCGAAG	Amplifies the deco2 gene from pUSA plasmid, The plasmid is designed for Gibson assembly, the lower-case alphabet represent the pQE plasmid sequence , and uppercase represent gene sequence.
deCO2 Gib R. Primer	aggagtccaagctcagctaattATCGAAGCTTTTAT CAAACAGCCGGCATATTTATTTTCAG	Amplifies the deco2 gene from pUSA plasmid, The plasmid is designed for Gibson assembly, the lower-case alphabet represents the pQE plasmid, and uppercase represent gene sequence.

Amy-For	GTCCCTTGTCGATGCGATGTATC	Amplifies the segment of the amylase promoter that is adjacent to *Cu*-A region, forward primer
Cu-A-rev *(TerA rev)**	GATGGACGCCTCTTTCTGGGC	Amplifies the segment of *Cu*-A, reverse primer
padh-for	CCTTTCCTTTCCCTCTCTCCGG	Amplifies the segment of the padh promoter which is adjacent to *Cu*-MO (monooxygenase) gene, forward primer
Cu-MO-rev *(TerD-rev)**	ATACTTGGCCTCGAATGTTTCCTCC	Amplifies the portion of *Cu*-MO (monooxygenase) gene, reverse primer
pgpd-for	AATATCGTGCCTCTCCTGCTTTGC	Amplifies the segment of the pgpd promoter, which is adjacent to *Cu*-OMT gene, forward primer
Cu-OMT *(OMT-rev)**	CCACTCTGAAATTTCGTTCGATTTGTACGTG	Amplifies the segment *Cu*-OMT gene, reverse primer
Cu-B-rev *(TerB-rev)**	CTAACACATCGTACCAATAAGCTCGCG	Amplifies the *Cu*-B gene, reverse primer, padh-for primer was used as forward primer.
Cu-halo *(Halo-rev)**	CGATTGACTCGACTCTGACGCC	Amplifies the *Cu*-halogenase gene, reverse primer. pgpd-for primer was used as forward primer

*Names written under the primary name in brackets and italics *(abc)* indicate the name listed on the vials stored at -20°C.

All primers used throughout this study were procured from IDT (Integrated DNA Technologies). Each primer (100μM) was diluted with sterile H_2O at a ratio of 1:10, to obtain a concentration of 10 μM, and was stored at -20°C.

Table S2: List of Media Components

Media	Components
Czapek-Dox	3 g/L $NaNO_3$, 2 g/L KCl, 10 g/L peptone, 0.5 g/L $MgSO_4 \cdot 7H_2O$, 1 g/L KH_2PO_4, 0.02 g/L $FeSO_4$, 20 g/L starch, 0.1 g adenine, pH 5.5
DPY	20 g/L dextrose, 10 g/L peptone, 5 g/L yeast extract, 0.5 g/L $MgSO_4 \cdot 7H_2O$, 5 g/L KH_2PO_4; pH 5.5
MEA	30 g/L of Malt extract, 20 g/L of Agar, 1 g/L of yeast extract
MEA + Rose Bengal	30 g/L of Malt extract, 20 g/L of Agar, 1 g/L of yeast extract, 3.3 g/L Rose Bengal
PYG Broth	1 g/L peptone, 1 g/L yeast extract, 3 g/L glucose
TF1	0.058 g maleic acid, 0.79 g $(NH_4)_2SO_4$, 0.1 g yatalase (*Clontech*); pH adjusted to 5.5; recipe per 10 mL of water.
TF2	218.5 g/L sorbitol, 10.95 g/L $CaCl_2 \cdot 6H_2O$, 2.05 g/L NaCl, 1.21 g/L Tris, pH 7.5
TF3	600 g/L Polyethylene glycol, 10.95 g/L CaCl2•6H2O, 1.21 g/L Tris, pH 7.5
Two- layer agar • **bottom layer**	2 g/L NH_4Cl, 1 g/L $(NH_4)_2SO_4$, 0.5 g/L KCl, 0.5 g/L NaCl, 1 g/L KH_2PO_4, 0.5 g/L $MgSO_4 \cdot 7H_2O$, 0.02 g/L $FeSO_4$, 218.6 g/L sorbitol, 15 g/L agar. Depending on the selection markers used, the amino acids: add 1 g arginine, 1.5 g methionine and/or 0.1 g adenine were added, pH 5.5
• **top layer**	2 g/L NH_4Cl, 1 g/L $(NH_4)_2SO_4$, 0.5 g/L KCl, 0.5 g/L NaCl, 1 g/L KH_2PO_4, 0.5 g/L $MgSO_4 \cdot 7H_2O$, 0.02 g/L $FeSO_4$, 218.6 g/L sorbitol, 8 g/L agar. Depending on the

	selection markers used, the amino acids: add 1 g arginine, 1.5 g methionine and/or 0.1 g adenine were added, pH 5.5

Milli-Q water was used to prepare all microbial media throughout this study. All media was sterilized by autoclaving for 15 min at 121°C prior to use.

Chapter 3

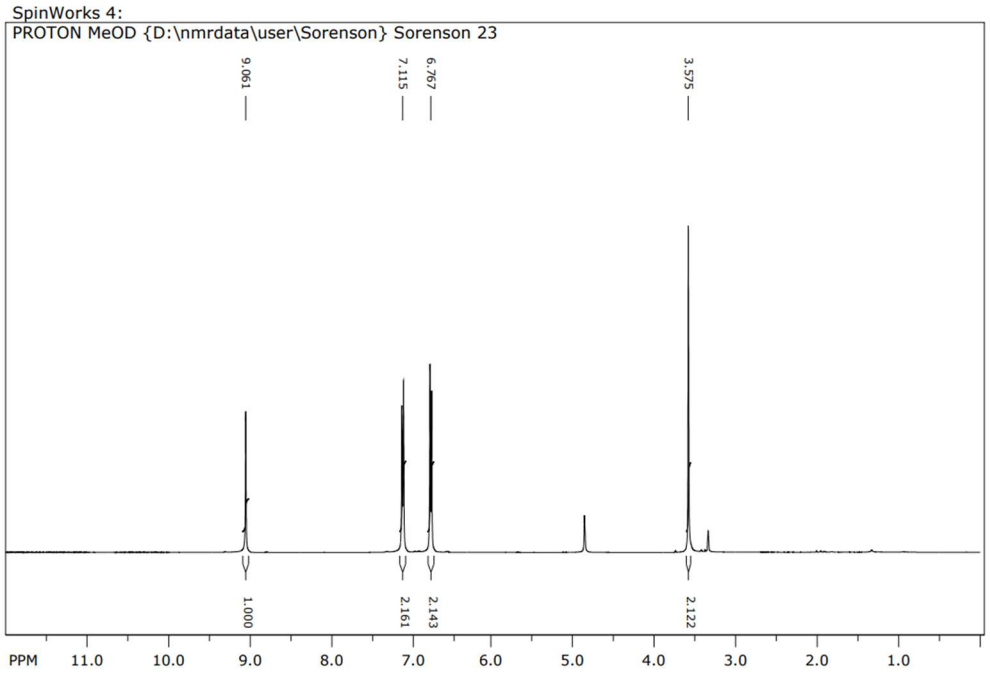

Figure S 1: [1]HNMR spectrum of compound **1** dissolved in MeOD at 500 MHz.

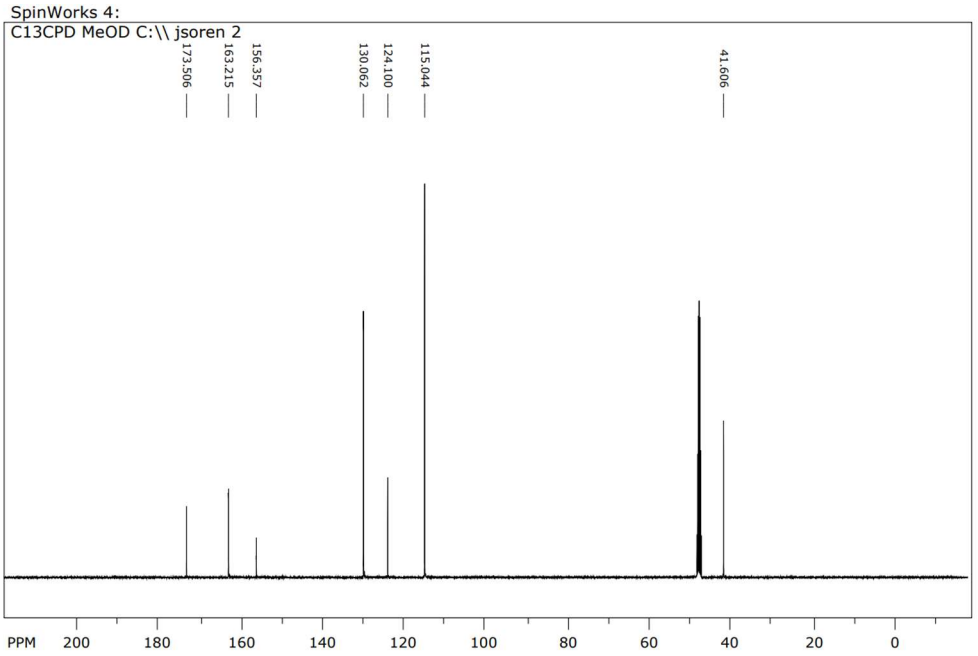

Figure S 2: ^{13}C NMR spectrum of compound **1** dissolved in MeOD at 500 MHz.

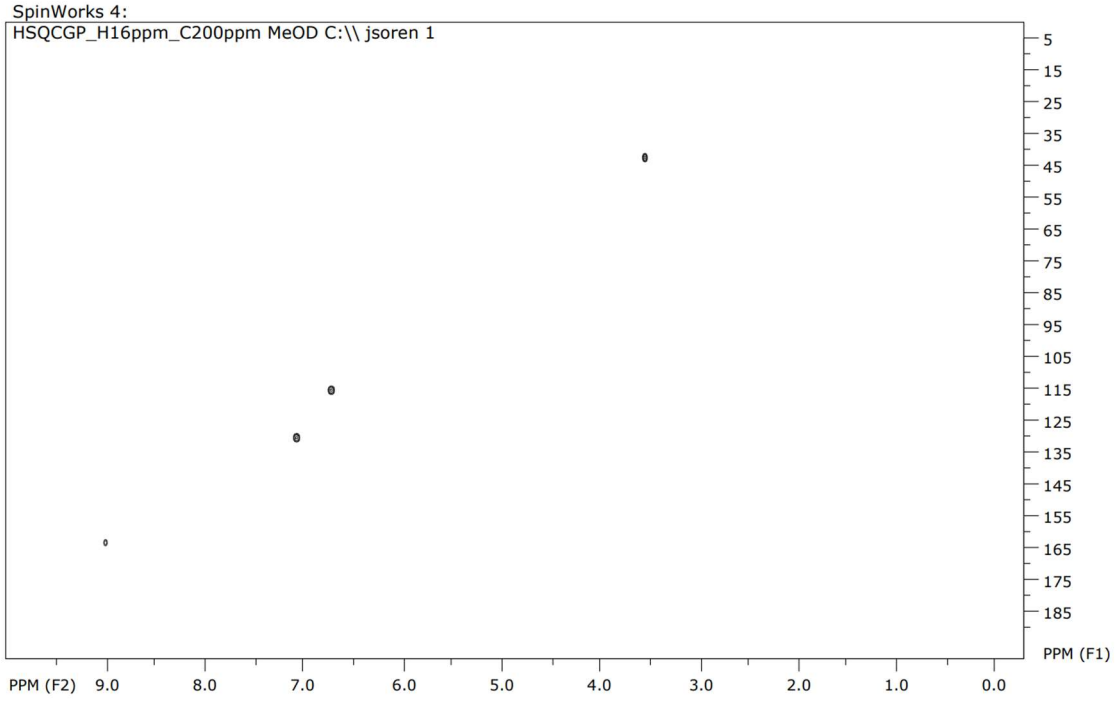

Figure S 3: HSQC spectrum of compound **1** dissolved in MeOD at 500 MHz.

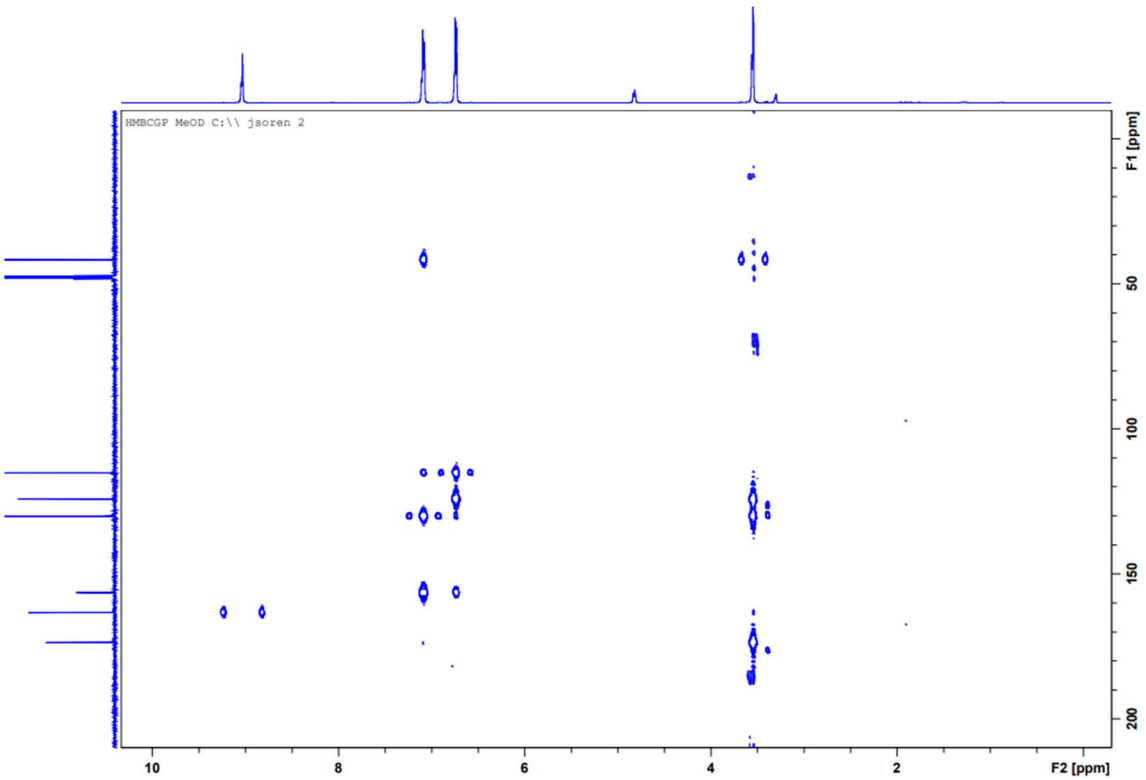

Figure S 4: ^{1}H-^{13}C HMBC spectrum of compound **1** dissolved in MeOD at 500 MHz.

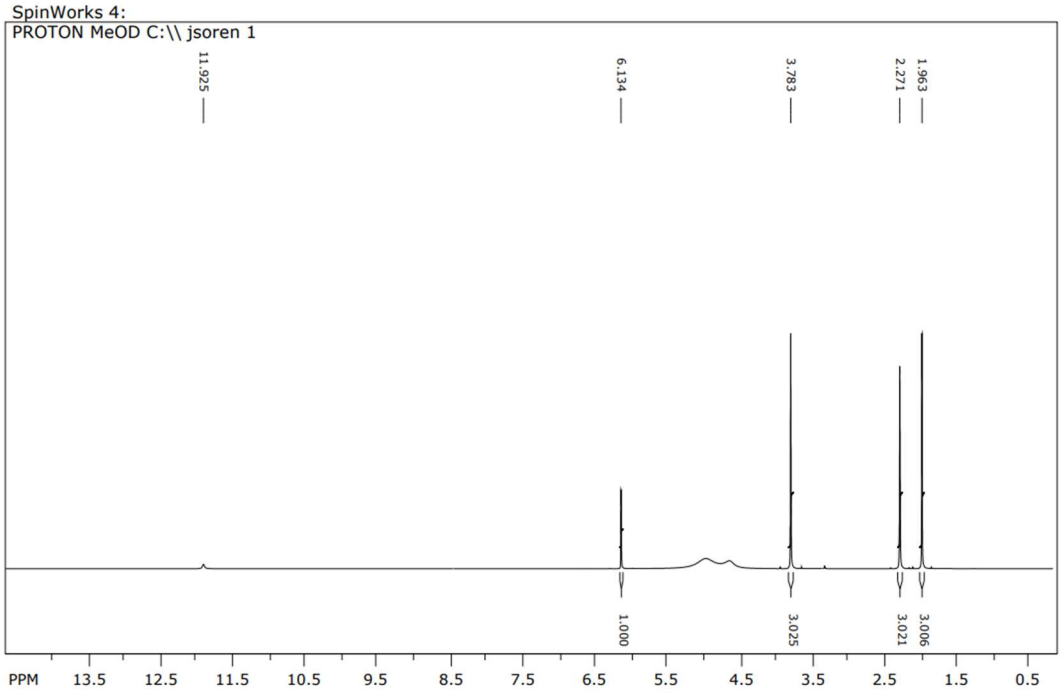

Figure S 5: ^{1}H NMR spectrum of compound **2** dissolved in MeOD at 500 MHz.

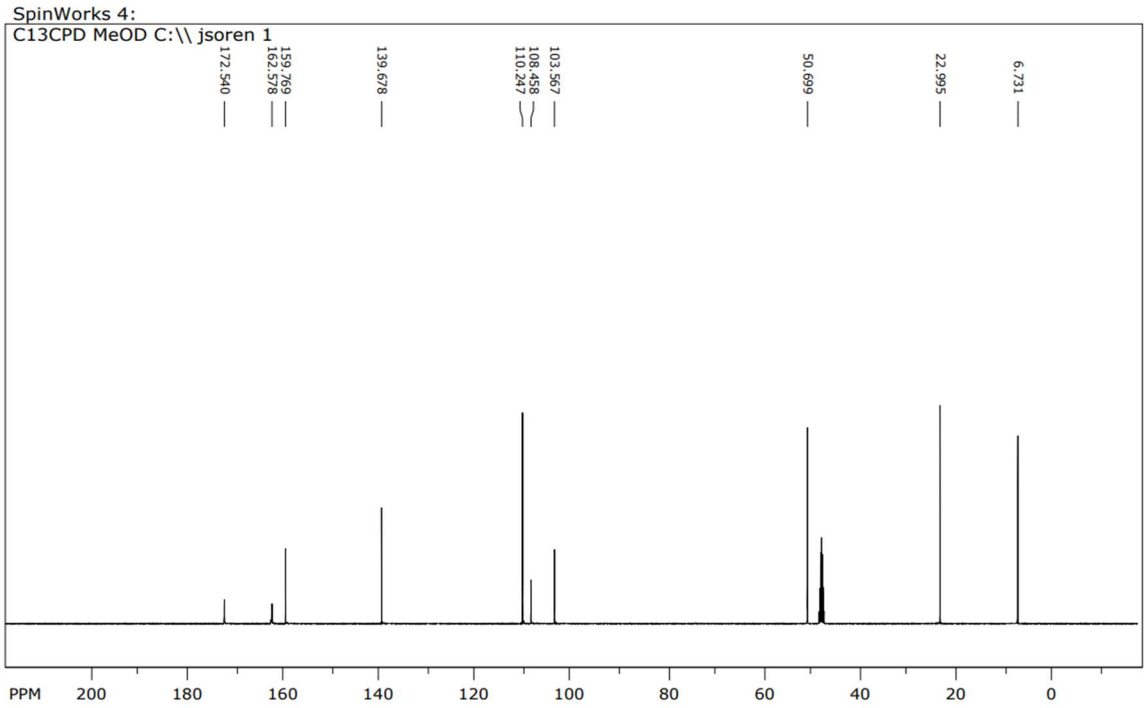

Figure S 6: ^{13}C NMR spectrum of compound **2** dissolved in MeOD at 500 MHz.

	Description	Scientific Name	Max Score	Total Score	Query Cover	E value	Per. Ident	Acc. Len	Accession
☑	Aspergillus fumigatus clone EF_482 small subunit ribosomal RNA gene, partial sequence; internal tra...	Aspergillus fum...	473	473	99%	5e-129	98.51%	616	gi|1846267941|MT529131.1
☑	Aspergillus fumigatus isolate RRF06 small subunit ribosomal RNA gene, partial sequence; internal tra...	Aspergillus fum...	473	473	99%	5e-129	98.51%	564	gi|1818779557|MT152189.1
☑	Aspergillus sp. strain ZMXR29 small subunit ribosomal RNA gene, partial sequence; internal transcrib...	Aspergillus sp.	472	472	99%	2e-128	98.51%	637	gi|1839354992|MT446134.1

Figure S 7: Blastn search of S4, showed 99% query coverage and 98.51% with known *A. fumigatus* strain SL-2203.

Chapter 4

Table S 3: Nucleotide sequences of four markers (ITS, Beta tubulin, Calmodulin, and RNA polymerase gene (RPB2) of *Penicillium sanguifluum.*

Markers	Nucleotide Sequences
Internal Transcribed Spacer (ITS)	ATTACCGAGTGAGGGCCCTCTGGGTCCAACCTCCCACCCGTGTTTAACGAACCTTGTTGC TTCGGCGGGCCCGCCTCACGGCCGCCGGGGGGCATCCGCCCCCGGGCCCGCGCCCGCCG AAGACACCTGTGAACACTGTCTGAAGTTGCAGTCTGAGAAACTAGCTAAATTAGTTAAA ACTTTCAACAACGGATCTCTTGGTTCCGGCATCGATGAAGAACGCAGCGAAATGCGATA AATAATGTGAATTGCAGAATTCAGTGAATCATCGAGTCTTTGAACGCACATTGCGCCCTC TGGTATTCCGGAGGGCATGCCTGTCCGAGCGTCATTGCTGCCCTCAAGCACGGCTTGTGT GTTGGGCCCCCGTCCCCCCCCACCGGGGGGACGGGCCCGAAAGGCAGCGGCGGCACCG CGTCCGGTCCTCGAGCGTATGGGGCTCTGTCACCCGCTCTTGTAGGCCCGGCCGGCGCCA GCCGACCCCCCTCAATCTATTTTTTCAGGTTGACCTCGGATCAGGTAGGGATACCCGCTG AACTTAAGCATATCAATAA
Beta tubulin (BT)	CAATTGTTGGGTATGTGAGGCATTATACTAACCAATTCAATAGGCAAACCATTGCTGGTG AGCACGGCCTTGACGGCGATGGCCAGTGAGTTCTCCCATTCCGACGTACTGGGACTTTCG AGAATGGCGGTCTGATATTTTTGGGCAGGTACAATGGTGCTTCCGACCTCCAGCTGGAGC GCATGAACGTCTACTTCACCCACGTAAGTGATACCGGCCTCACTAATAACTGCAACCATT TTTCTCATAACTTTTTCTTTTCTTTCAAATAGGCTTCCGGTGACAAGTATGTTCCCCGTGC CGTTCTGGTCGACCTGGAGCCTGGTACCATGGATGCTGTCCGGGCCGGTCCCTTCGGCAA GCTTTTCCGTCCCGACAACTTCGTCTTCGGTCAGTCTGGTGCTGGTAACAACTGGGCTAA GGGTCA
Calmodulin	TGTTTGTGAGTGATTTGATCCCAGCATTGACGTTGTGAGTGTGGAGCATTTGGACTAACG GGGCATCTTGTGATCGACAGGACAAGGATGGCGATGGTGAGTGCGGTCTTCCAACAACA ATCCGTAACCTTTTCACGGGCGGCGTTTCCCCCGCGATTGGACTCTATGCAACCATGTTT GAACCGTGCTGAGATATCTGTGATCAATAGGCCAGATCACCACCAAGGAGCTGGGTACC GTCATGCGCTCCCTGGGCCAGAACCCCTCCGAGTCCGAGCTGCAGGATATGATCAACGA GGTCGACGCCGACAACAACGGCACCATTGACTTCCCCGGTACGATGCCACACCACATGC CATGCCATCCCATCATATATCATAGTAAACATCCGTATTGACTTACGCCCGCAGAGTTCT TGACCATGATGGCCCGCAAGATGAAGGACACCGACTCCGAGGAGGAGATCCGCGAAGC GTTCAAGGTGTTTGATCGCGACAACAACGGCTTCATCTCCGCCGCCGAGCTGCG
RNA polymerase gene (RPB2)	CCTCTTCTGGCAAACCTTTTCCGCGTCCTTTTCACTCGTGTCACTCGTGACCTGCAGCGTT ATGTGCAGCGCTGCGTTGAAACCAACCGTGAGATCTACCTTAACATTGGTCTCGCTGCCA CCTTGACTGGTGGTCTGAAATATGCCCTTGCCACTGGTAACTGGGGTGAACAAAAGAAG GCGGCGAGCGCCAAGGCTGGTGTCTCGCAAGTGTTGAGTAGATACACATTCGCTTCTTCG CTGTCTCATTTGCGCCGGACCAACACGCCTATTGGTCGTGACGGCAAGATTGCCAAACCG CGTCAGCTTCACAACACCCACTGGGGCCTCGTGTGTCCCGCAGAAACACCAGAAGGACA GGCTTGTGGTCTCGTCAAGAACTTGGCACTCATGTGCTACATCACTGTTGGTACTCCTAG CGAGCCCATCATCGACTTCATGATTCAGCGAAATATGGAAGTCCTGGAGGAGTTTGAGC CTCAAGTCACGCCAAATGCCACCAAGGTCTTTGTCAACGGTGTCTGGGTTGGTATCCACC GCGATCCGTCCCATCTGGTTAACACCATGCAATCCCTGCGTCGACGAAACATGATTTCCC ACGAAGTCAGTTTGATTCGGGATATCCGTGAGCGAGAGTTCAAGATCTTCACCGATACT GGACGTGTCTGCCGGCCATTGTTCGTGGTTGACAATGACCCCAAGAGCGACAATGCTGG GTCCTTGATTCTTAACAAGGAACATATTCACAAGCTTGAGCAGGACAAGGACCTGCCGC CTAATATGGATGTGGAGGAGCGCCGGGAGCGTTACTTCGGATGGGATGGCTTGGTCCGA TCAGGAGCCGTTGAATACGTCGACGCGGAGGAAGAAGAGACTATTATGATTGTCATGAC GCCCGAAGATTTGGAGATTTCCAAGCAACTCCAGGCTGGTTATGCACTGCCCGAGGAGG AGACTAGTGACCCGAACAAGCGAGTCCGCTCGATTCTGAGCCAGCGCGCTCACACCTGG

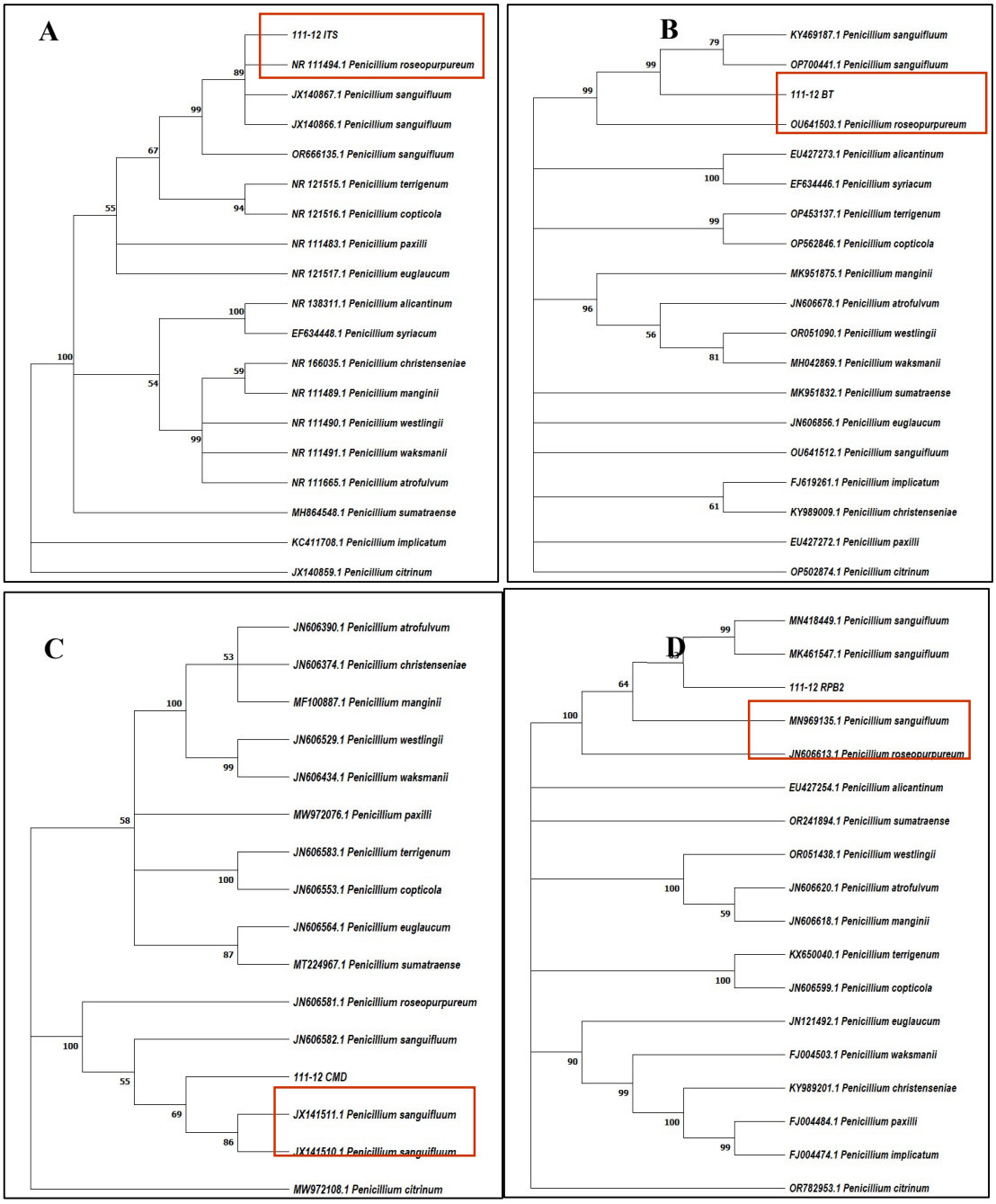

Figure S 8: Phylogenetic majority rule consensus tree inferred using the maximum likelihood method for *Penicillium sanguilluum* (111-12) (A) ITS, (B) beta-tublin, (C) Calmodulin, and (D) RNA polymerase gene sequence comparison with other *Penicillium spp*. Bootstrap percentages based on 1000 replicates are indicated at the nodes.

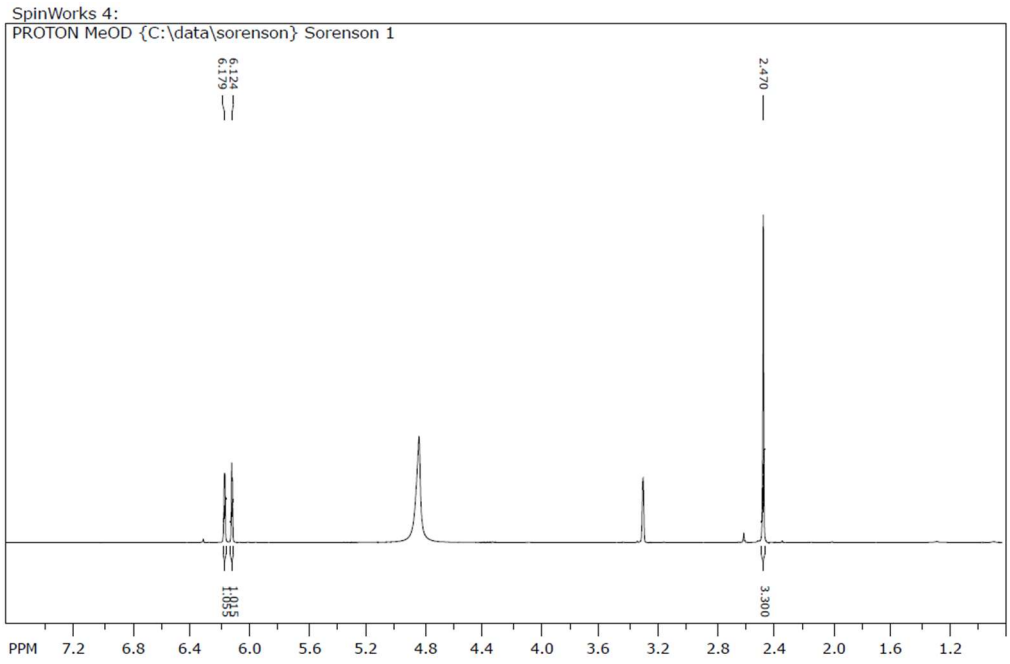

Figure S 9: [1]HNMR spectrum of orsellinic acid standard dissolved in MeOD at 500 MHz.

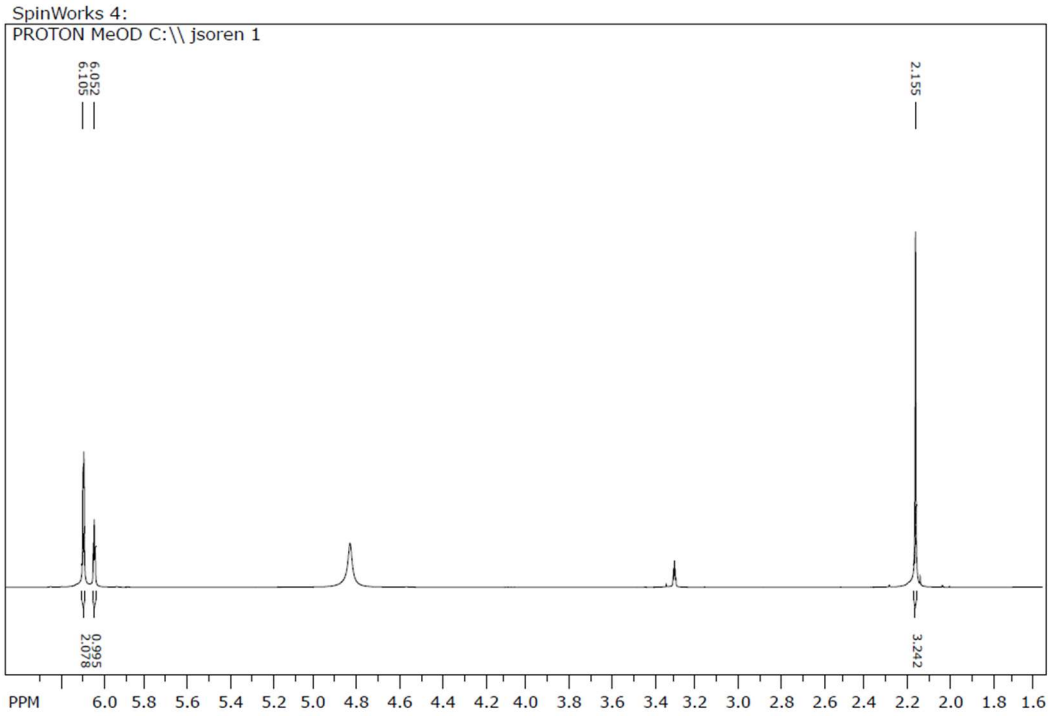

Figure S 10: [1]HNMR spectrum of orcinol dissolved in MeOD at 500 MHz.

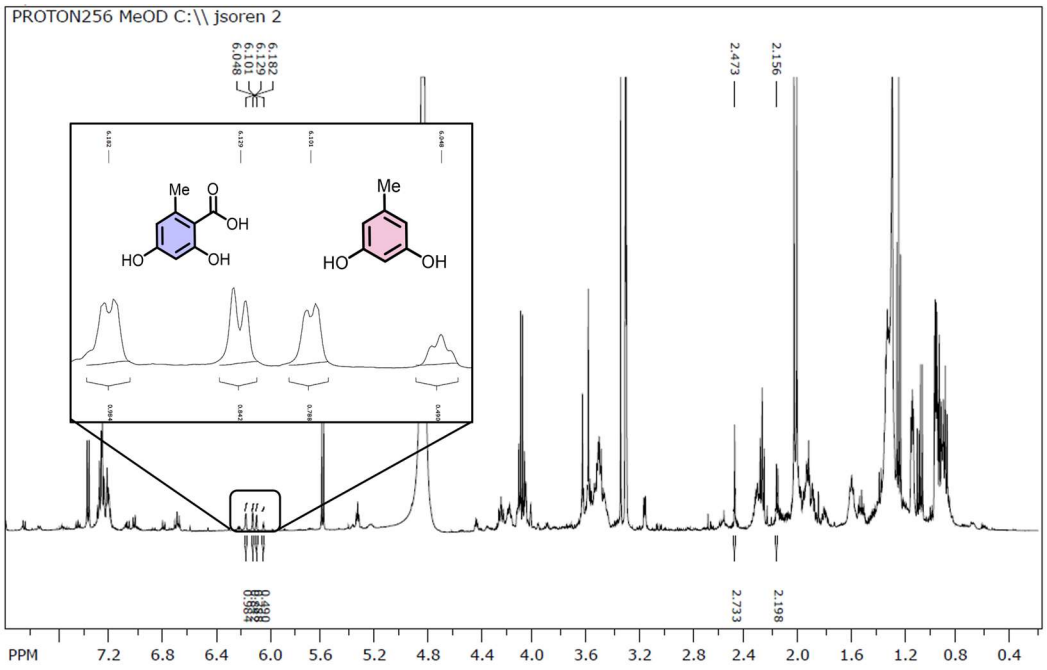

Figure S 11: [1]HNMR spectrum of crude extract from uninduced decarboxylase *A. oryzae* transformants recorded in MeOD at 500 MHz.

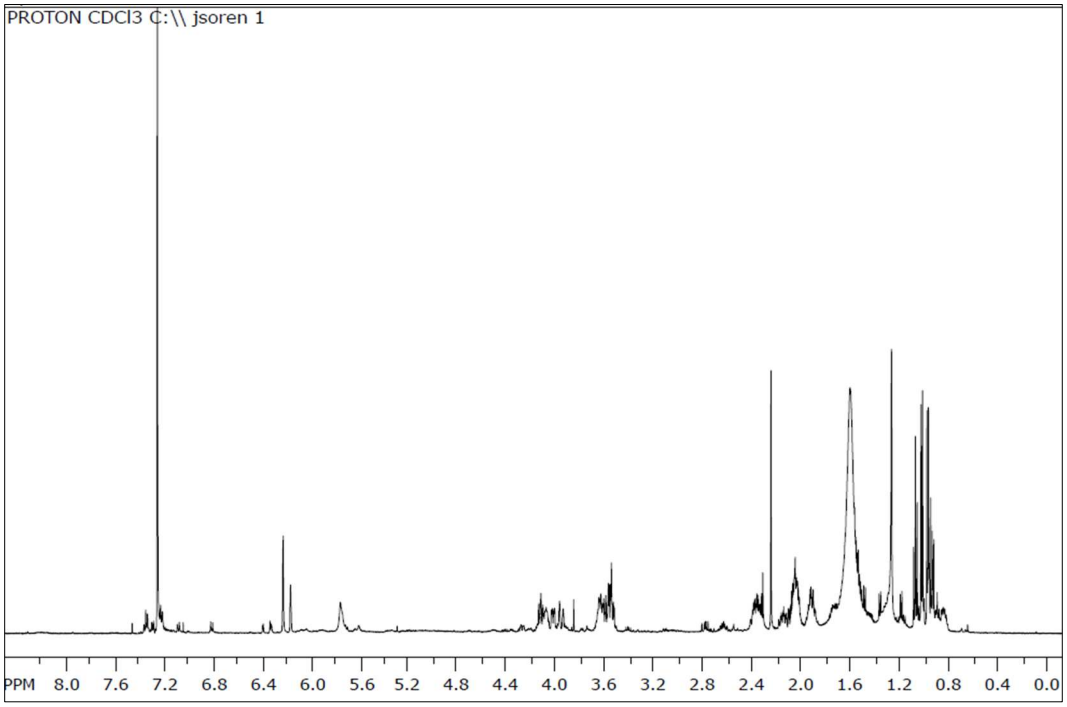

Figure S 12: [1]HNMR spectrum of crude extract from *A. oryzae* NSAR1 native recorded in $CDCl_3$ at 500 MHz.

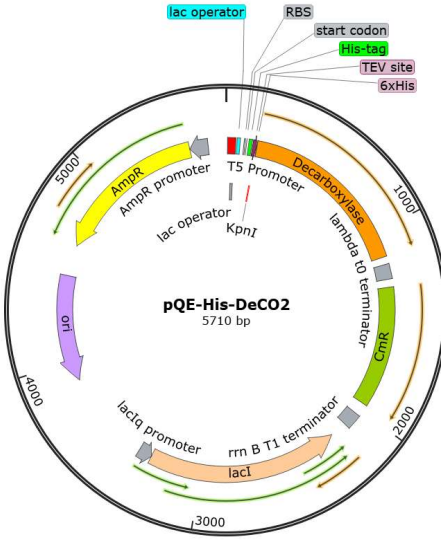

Figure S 13: Map of the pQE3080L plasmid visualized using SnapGene software.

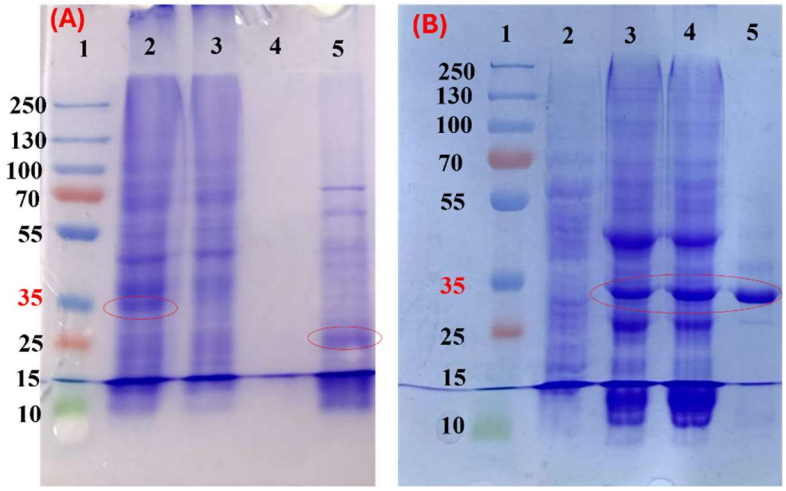

Figure S 14: SDS gel post-purification using AKTA pure.

(A) Protein purification performed at 30°C, featuring lane 1: protein ladder (kDa); lane 2: soluble fraction; lane 3: flow-through; lane 4: empty; lane 5: eluted fraction (~20kDa) showing degraded protein. (B) Fractions obtained after washing with imidazole, including lane 1: protein ladder (kDa); lane 2: wash-through (with 50mM); lanes 3 & 4: partially purified fractions collected post-elution (with 500mM) of imidazole; lane 5: purified fraction.

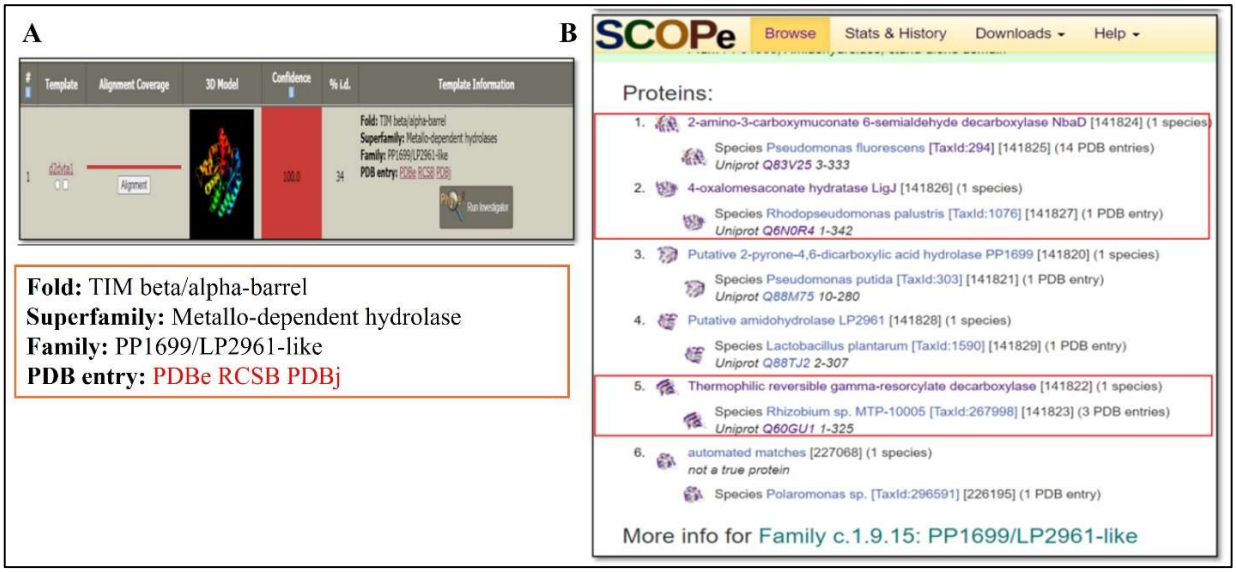

Figure S 15: (A) Homology results of the decarboxylase (B) PP1699/LP2961-like homology results through SCOPe- Structural Classification of Proteins.

Decarboxylation

Please disregard the letters (A, B, C, D, E) on the chromatogram images of the carboxylation and decarboxylation reactions. They were labeled according to the manuscript. However, I used numerical numbers for each image in this instance.

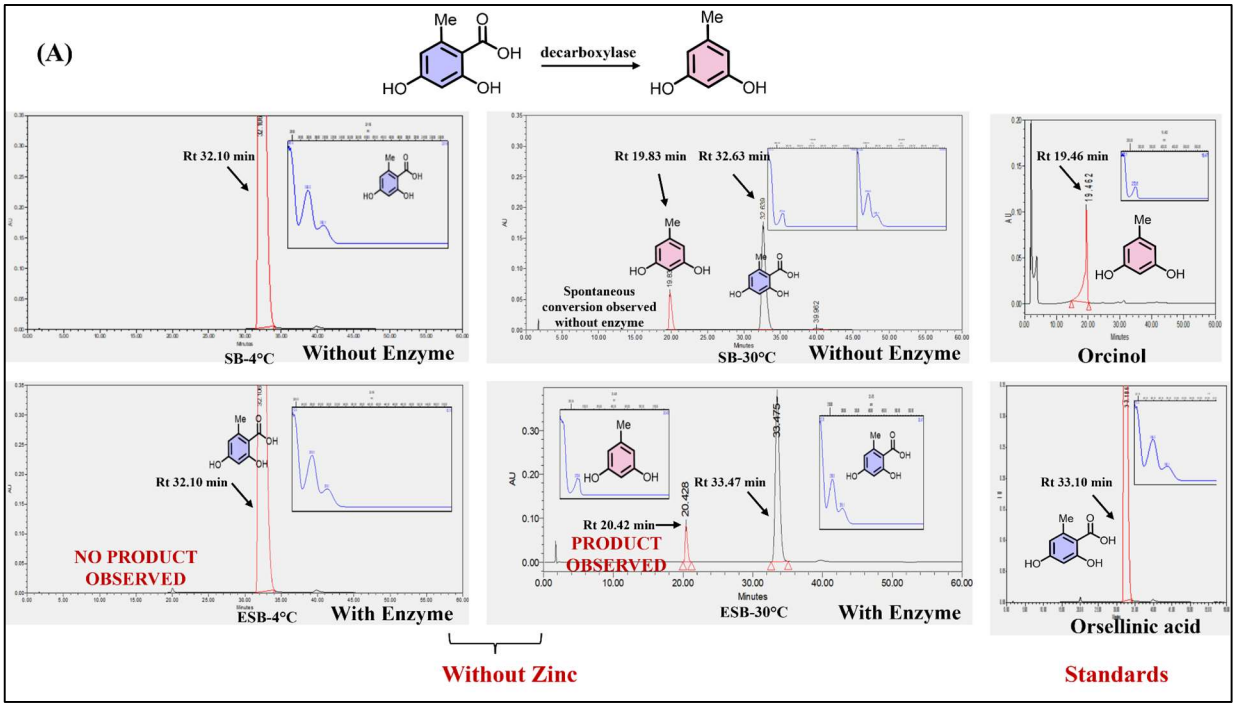

Figure S 16: HPLC chromatograms alongside UV spectra at 250 nm for the enzyme catalyzed decarboxylation reaction. The conversion of orsellinic acid to orcinol both with and without the enzyme in the reaction, and in the absence of zinc.

In this figure **(Figure S 16)** , ESB indicates Enzyme, Substrate, and Buffer, while SB denotes Substrate and Buffer. The reactions were performed at two temperatures: 30°C and 4°C. The top rows display control chromatograms without enzyme addition, while the bottom rows show results with enzyme added. The rightmost images in both rows represent the chromatograms of standards. Notably, the conversion of orsellinic acid to orcinol was observed at a retention time (Rt) of 20.42 min with enzyme addition at 30°C. We also observed the spontaneous conversion of orsellinic acid to orcinol in the absence of enzyme but at lesser rate as compared with enzyme.

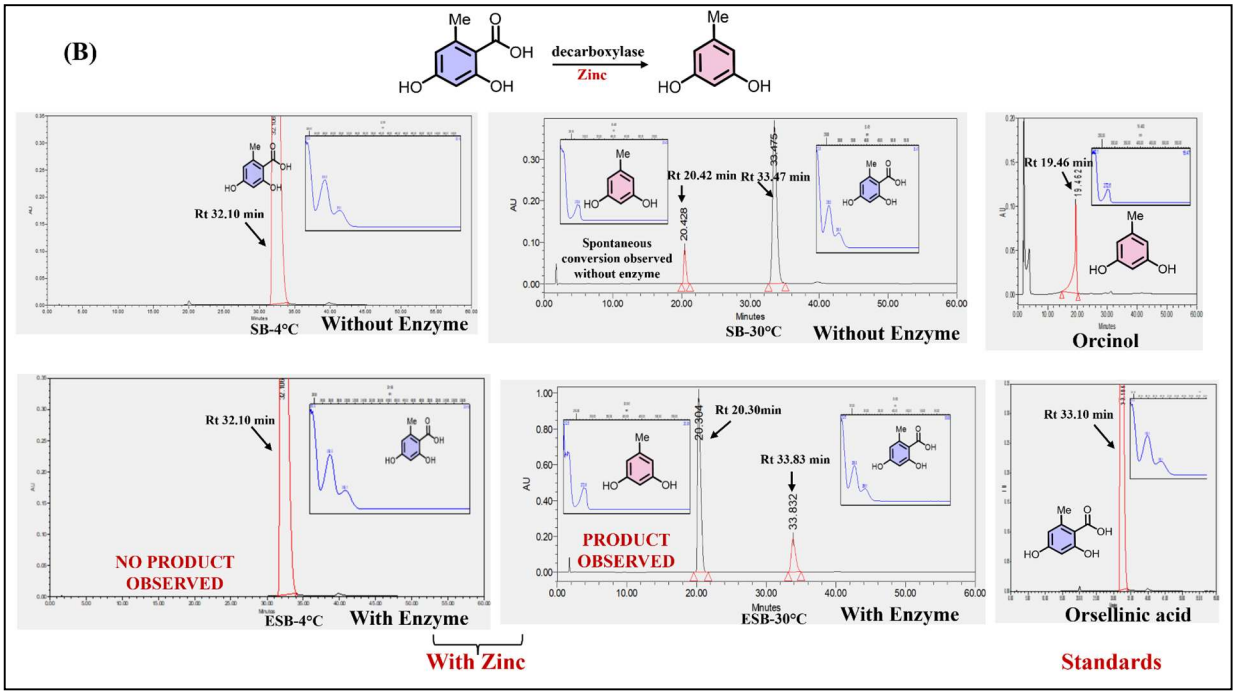

Figure S 17: The conversion of orsellinic acid to orcinol both with and without the addition of the decarboxylase enzyme, and in the **presence** of zinc.

In this figure **(Figure S 17)**, ESB indicates Enzyme, Substrate, and Buffer, while SB denotes Substrate and Buffer. The reactions were performed at two temperatures: 30°C and 4°C. The top rows display control chromatograms without enzyme addition, while the bottom rows show results with enzyme and zinc added. The rightmost images in both rows represent the chromatograms of standards. Notably, the conversion of orsellinic acid to orcinol was observed at a retention time (Rt) of 20.30 min with the addition of enzyme and zinc at 30°C. The UV max (272 nm) was identical to the standard orcinol was observed.

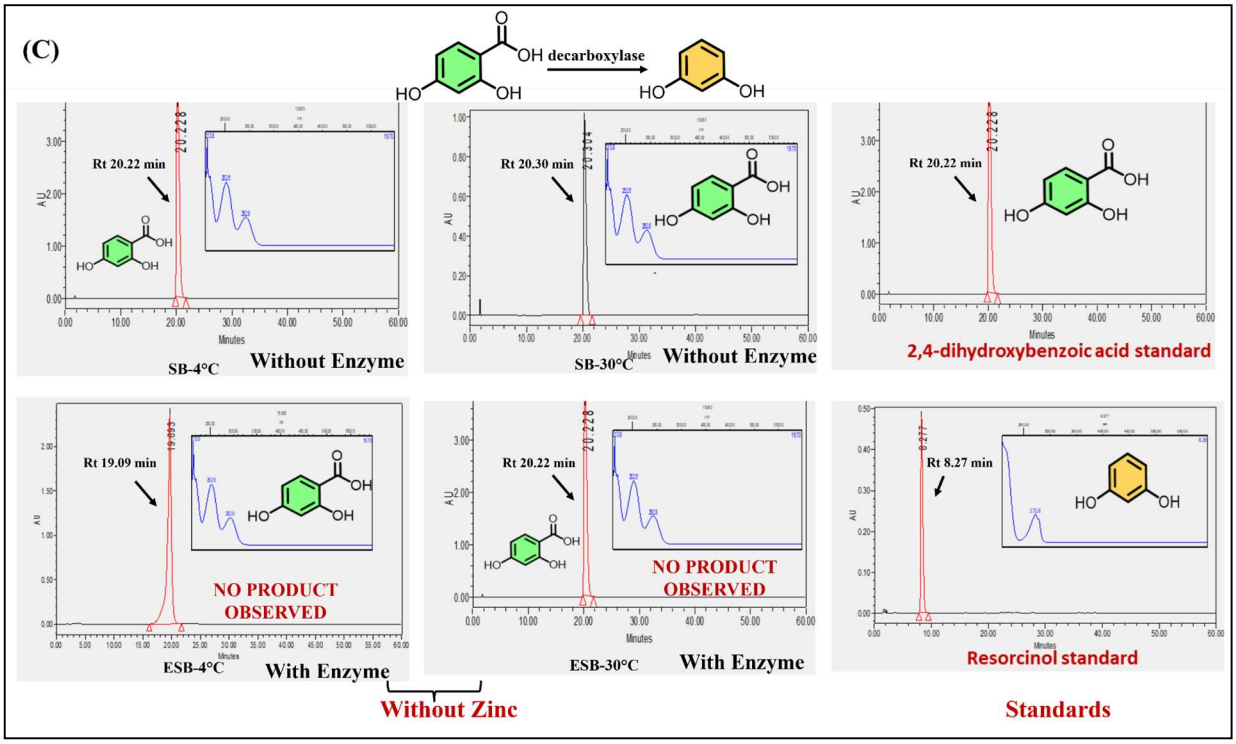

Figure S 18 : The conversion of 2,4-dihydroxybenzoic acid to resorcinol with and without the addition of the decarboxylase enzyme, and in the **absence** of zinc.

In this figure **(Figure S 18)**, ESB indicates Enzyme, Substrate, and Buffer, while SB denotes Substrate and Buffer. The reactions were performed at two temperatures: 30°C and 4°C. The top rows display control chromatograms without enzyme addition, while the bottom rows show results with enzyme. The rightmost images in both rows represent the chromatograms of 2,4-dihydroxybenzoic acid and resorcinol standards. No conversion was observed in at both temperatures.

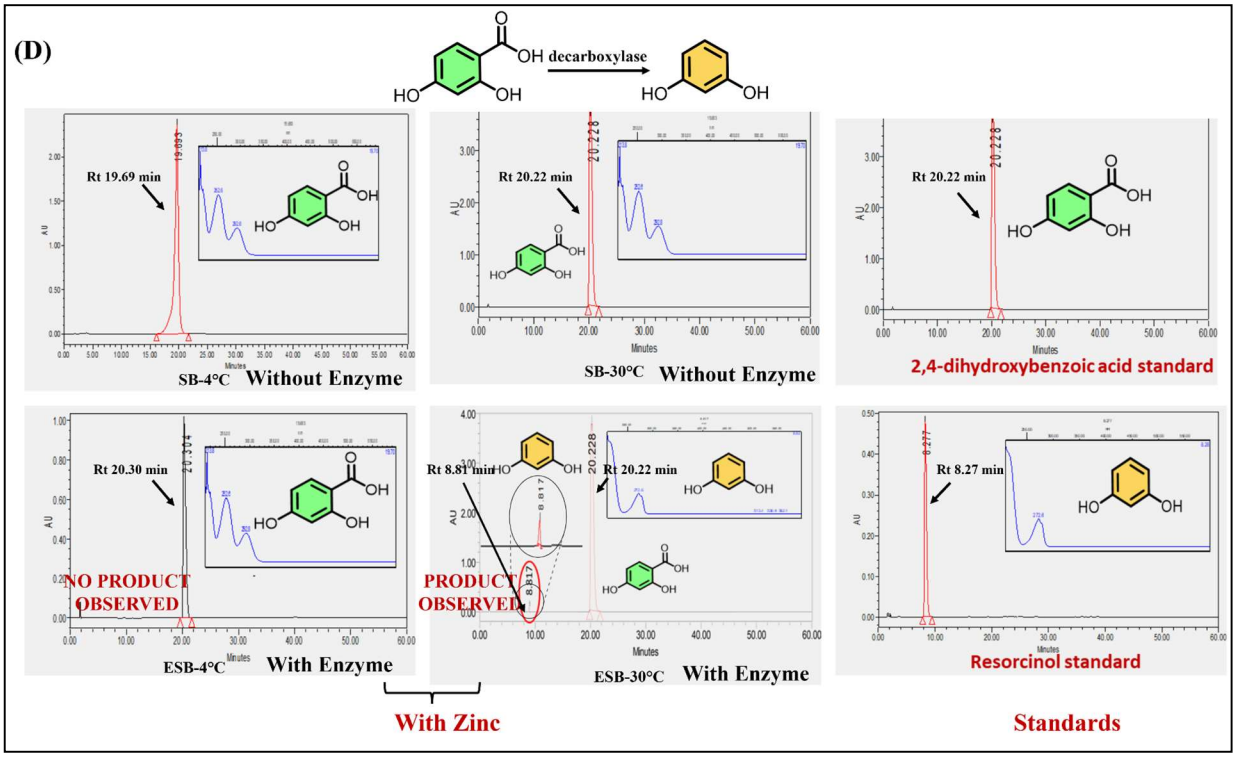

Figure S 19: The conversion of 2,4-dihydroxybenzoic acid to resorcinol with and without the addition of the decarboxylase enzyme, and in the **presence** of zinc.

In this figure **(Figure S 19)**, ESB refers to Enzyme, Substrate, and Buffer, while SB denotes Substrate and Buffer. The reactions were performed at two temperatures: 30°C and 4°C. The top rows illustrate control chromatograms without enzyme addition, whereas the bottom rows show results with enzyme and zinc. The rightmost images in both rows represent the chromatograms of 2,4-dihydroxybenzoic acid and resorcinol standards. A conversion from 2,4-dihydroxybenzoic acid to resorcinol, was detected at retention time (Rt) 8.81 minutes in ESB with zinc at 30°C. The UV spectrum at (Rt) 8.81was identical to standard of resorcinol, UV max 272.6 nm.

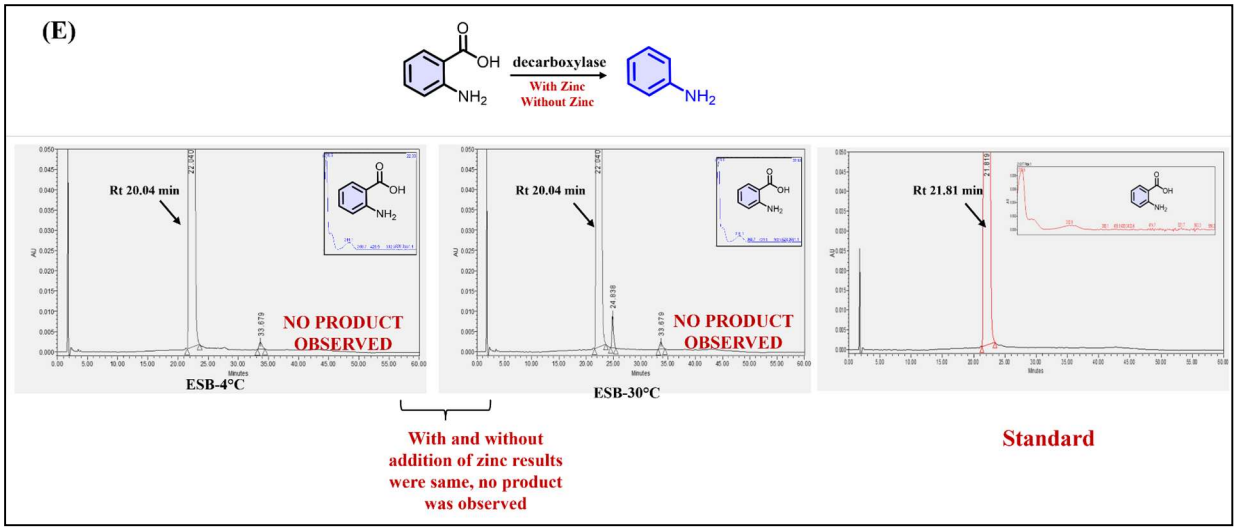

Figure S 20: The enzymatic conversion of anthranilic acid to aniline with and without the addition of zinc.

In this figure **(Figure S 20)**, ESB refers to Enzyme, Substrate, and Buffer. The reactions were carried out at two temperatures: 30°C and 4°C. The rightmost image shows the chromatogram of anthranilic acid standard. These experiments were conducted both with and without the addition of zinc, but the results remained the same. No conversion of anthranilic acid to aniline was observed under either condition.

Carboxylation Reactions

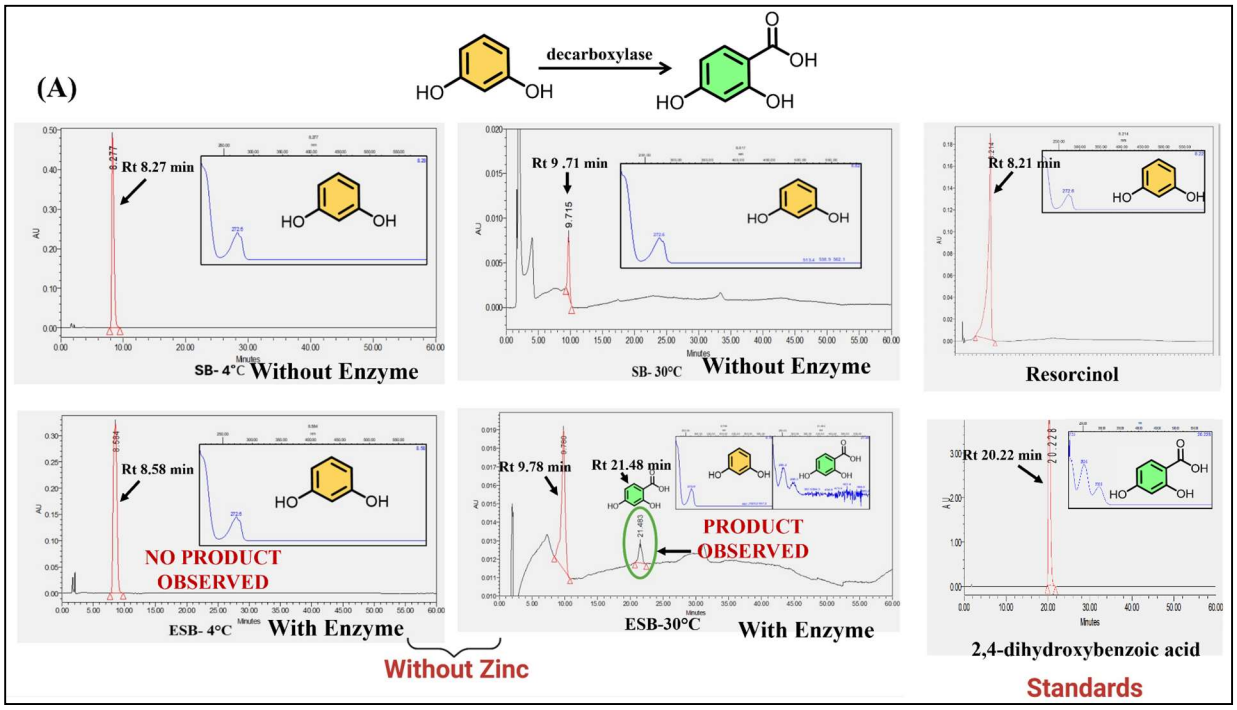

Figure S 21: HPLC chromatograms alongside UV spectra at 250 nm for the enzyme catalyzed carboxylation reaction.

(A) The conversion of resorcinol to 2,4-dihydroxybenzoic acid both with and without the enzyme in the reaction, and in the **absence** of zinc.

In this figure **(Figure S 21)**, ESB refers to Enzyme, Substrate, and Buffer, while SB denotes Substrate and Buffer. The reactions were performed at two temperatures: 30°C and 4°C. The top rows illustrate control chromatograms without enzyme addition, whereas the bottom rows show results with enzyme. The rightmost images in both rows represent the chromatograms of 2,4-dihydroxybenzoic acid and resorcinol standards. A conversion from resorcinol to 2,4-dihydroxybenzoic acid was detected at retention time (Rt) 21.48 minutes in ESB at 30°C. The UV spectrum at (Rt) 21.48 was identical to standard of resorcinol, UV max 252.6 and 292.8 nm.

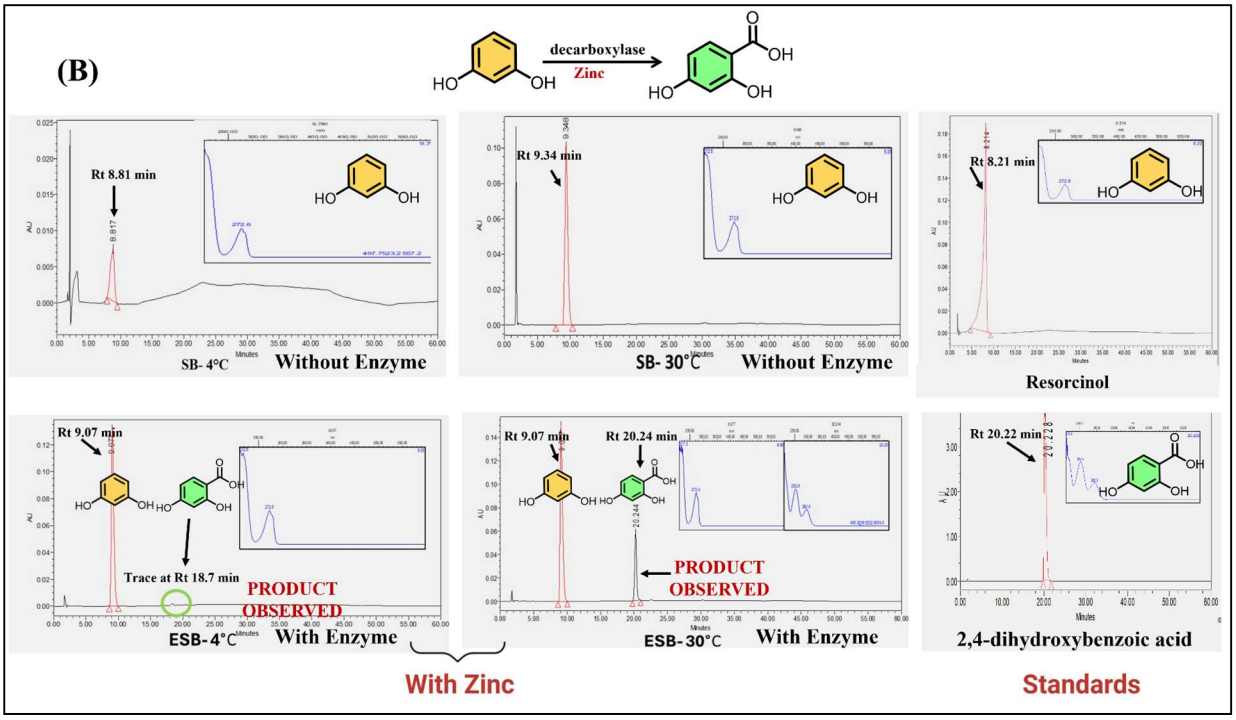

Figure S 22: The conversion of resorcinol to 2,4-dihydroxybenzoic acid both with and without the enzyme in the reaction, and in the **presence** of zinc.

In this figure **Figure S 22** ESB refers to Enzyme, Substrate, and Buffer, while SB denotes Substrate and Buffer. The reactions were performed at two temperatures: 30°C and 4°C. The top rows illustrate control chromatograms without enzyme addition, whereas the bottom rows show results with enzyme. The rightmost images in both rows represent the chromatograms of 2,4-dihydroxybenzoic acid and resorcinol standards. A conversion from resorcinol to 2,4-dihydroxybenzoic acid was detected at retention time (Rt) 20.24 minutes in ESB and zinc at 30°C. The UV spectrum at (Rt) 20.24 was identical to standard of resorcinol, UV max 252.6 and 292.8 nm .

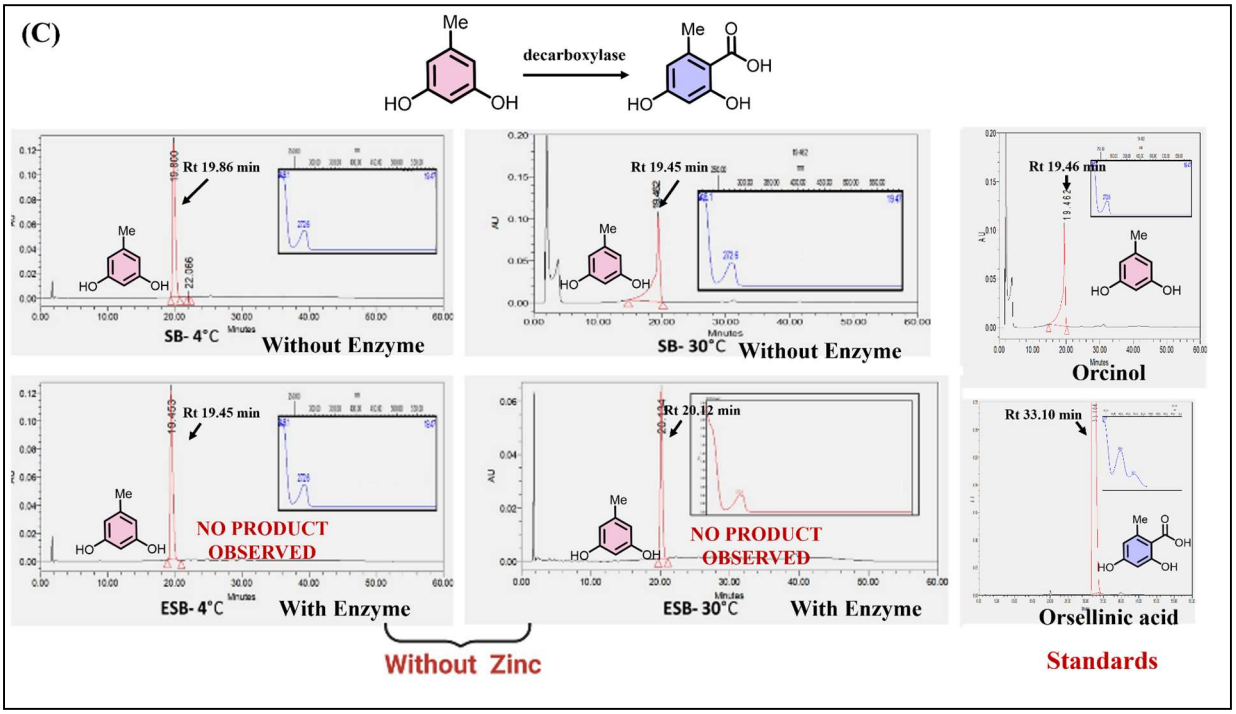

Figure S 23: The conversion of orcinol to orsellinic acid both with and without the addition of the decarboxylase enzyme, and in the **absence** of zinc.

In this figure **(Figure S 23)**, ESB refers to Enzyme, Substrate, and Buffer, while SB denotes Substrate and Buffer. The reactions were performed at two temperatures: 30°C and 4°C. The top rows illustrate control chromatograms without enzyme addition, whereas the bottom rows show results with enzyme. The rightmost images in both rows represent the chromatograms of orsellinic acid and orcinol standards. No conversion from orcinol to orsellinic acid was detected.

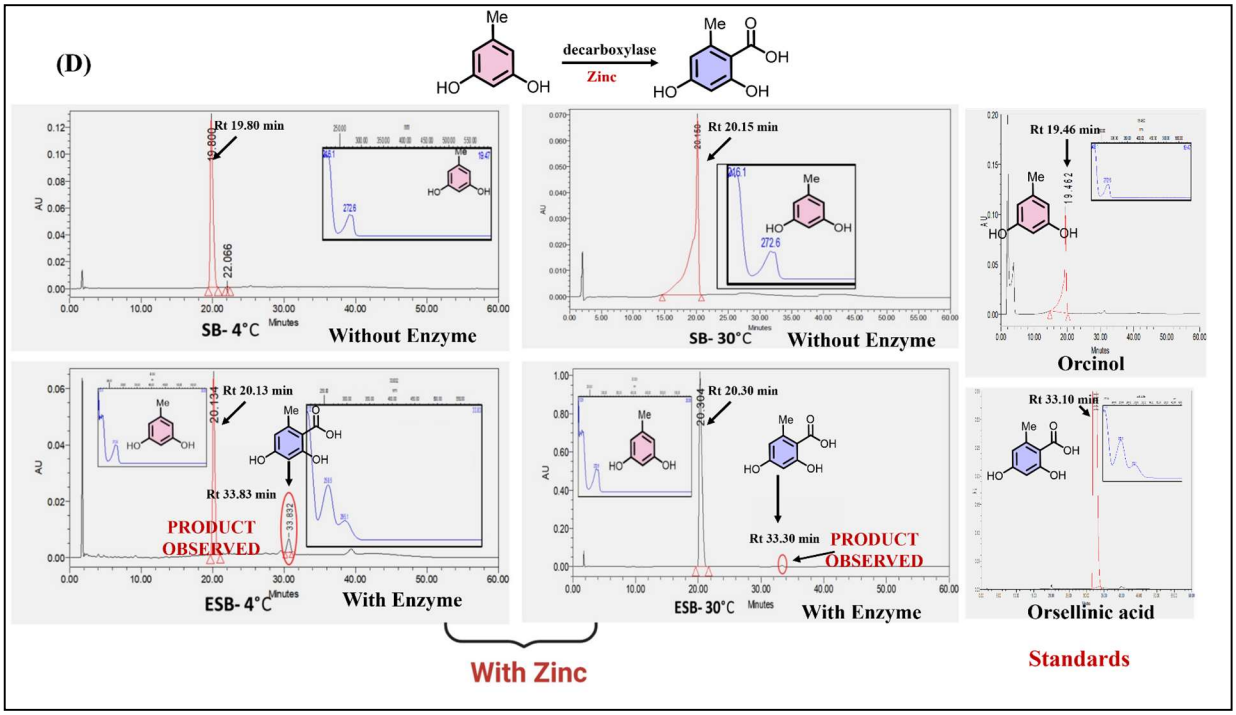

Figure S 24: The conversion of orcinol to orsellinic acid both with and without the addition of the decarboxylase enzyme, and in the **presence** of zinc.

In this figure **(Figure S 24)**, ESB refers to Enzyme, Substrate, and Buffer, while SB denotes Substrate and Buffer. The reactions were performed at two temperatures: 30°C and 4°C. The top rows illustrate control chromatograms without enzyme addition, whereas the bottom rows show results with enzyme. The rightmost images in both rows represent the chromatograms of orsellinic acid and orcinol standards. The conversion from orcinol to orsellinic acid was detected at retention time (Rt) 33.83 minutes in ESB and zinc at 4°C. The UV spectrum at (Rt) 33.83 was identical to standard orsellinic acid, UV max 212, 258 and 295 nm.

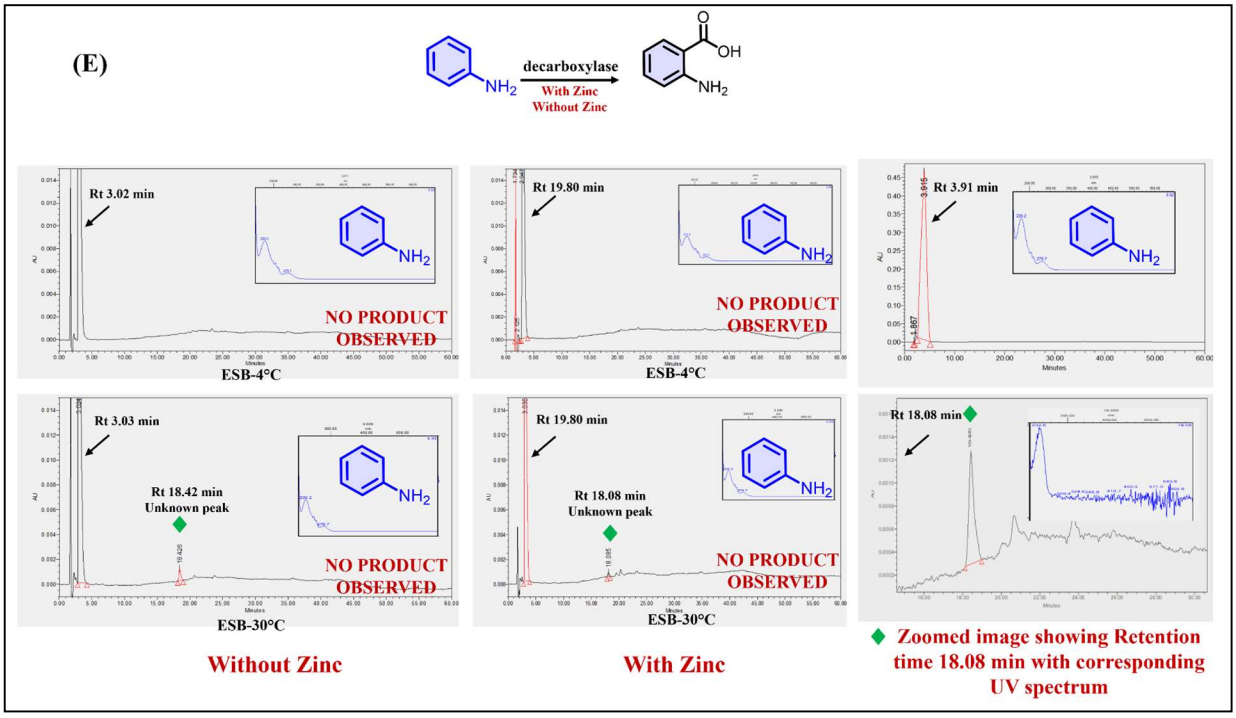

Figure S 25: The enzymatic conversion of aniline to anthranilic acid with and without the addition of zinc.

In this figure **Figure S 25**, ESB refers to Enzyme, Substrate, and Buffer. The reactions were carried out at two temperatures: 30°C and 4°C. The rightmost image shows the chromatogram of aniline standard. These experiments were conducted with and without the addition of zinc. No conversion of aniline to anthranilic acid was detected in either case.

A single peak with a retention time (Rt) of approximately 18 minutes was observed in the ESB samples at 30°C, both with and without zinc. The UV spectrum associated with this peak does not correspond to anthranilic acid. The peak was very small, and we were unable to identify this unknown substance.

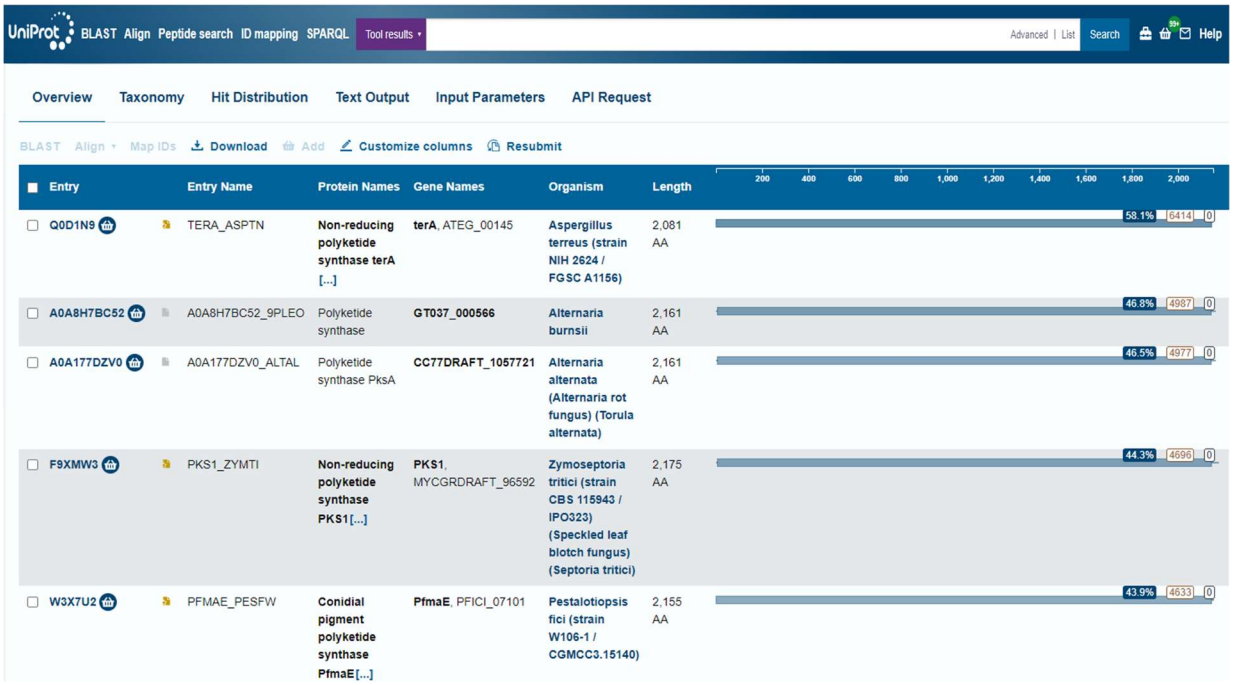

Figure S 26: UniProt BLAST analysis of the *Cu*-A amino acid sequence with PKS from other fungal species. The highest identity was observed with *A. terreus* (58.1%), followed by *A. burnsii* (48.6%).

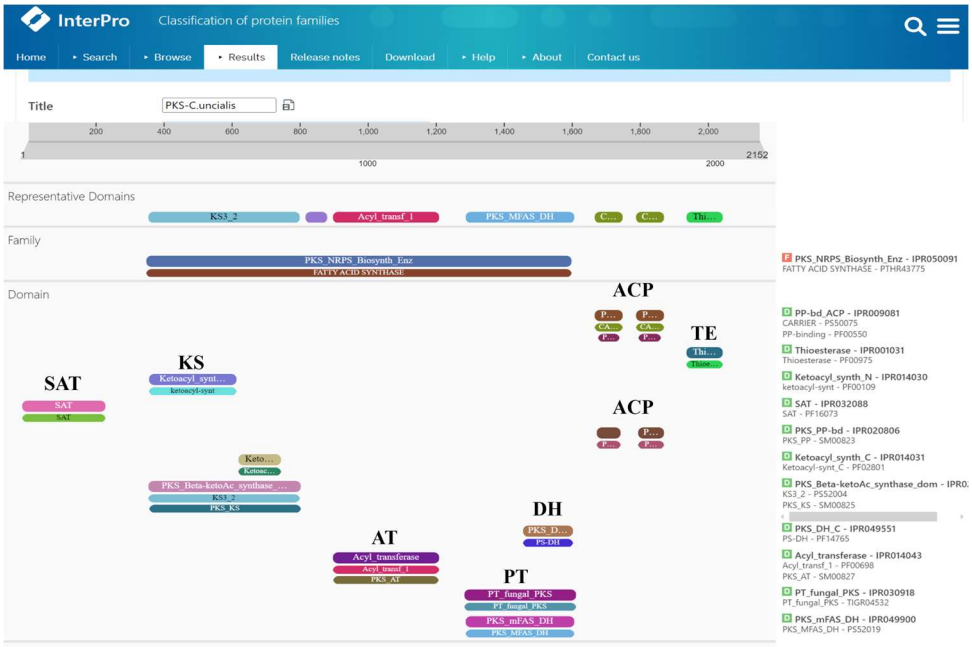

Figure S 27: InterPro analysis of *Cu*-A from *C. uncialis*. SAT, KS, AT, PT, DH, ACP, ACP, TE. Labels were added manually. Corresponding InterPro identifier codes are shown on the right side.

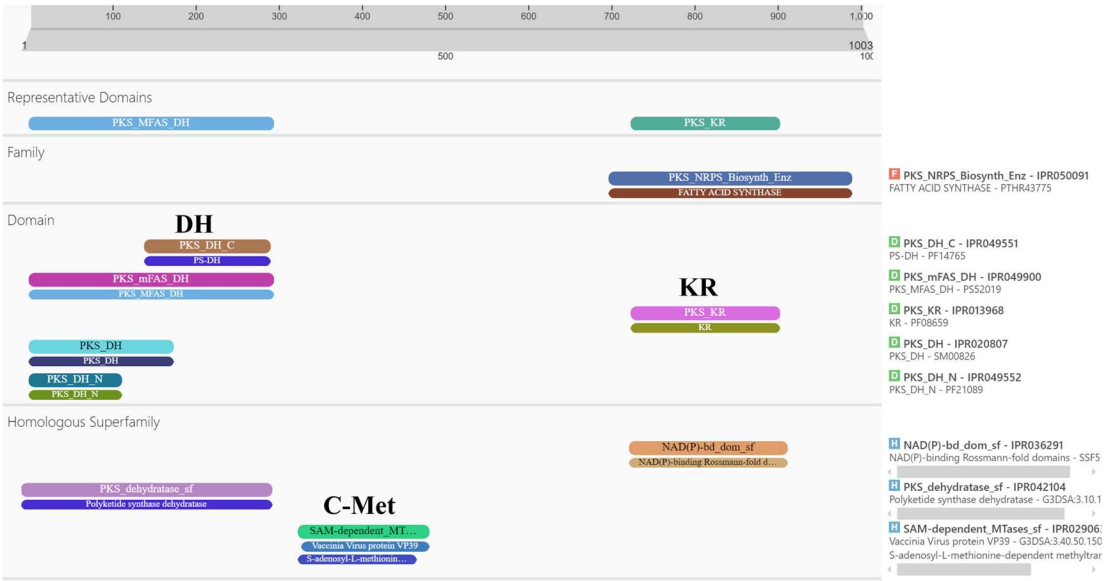

Figure S 28: InterPro analysis of *Cu*-B from *C. uncialis*. Presence of DH,C-Met and KR domains. Labels were added manually. Corresponding InterPro identifier codes are shown on the right side.

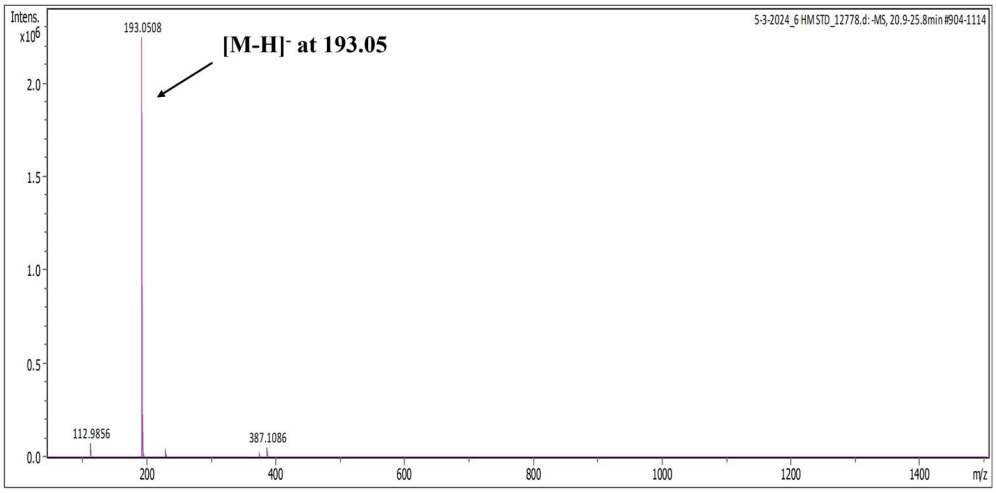

Figure S 29: Mass spectrum of 6-hydroxymellein (m/z = 193). Spectra was acquired in the negative ion mode.

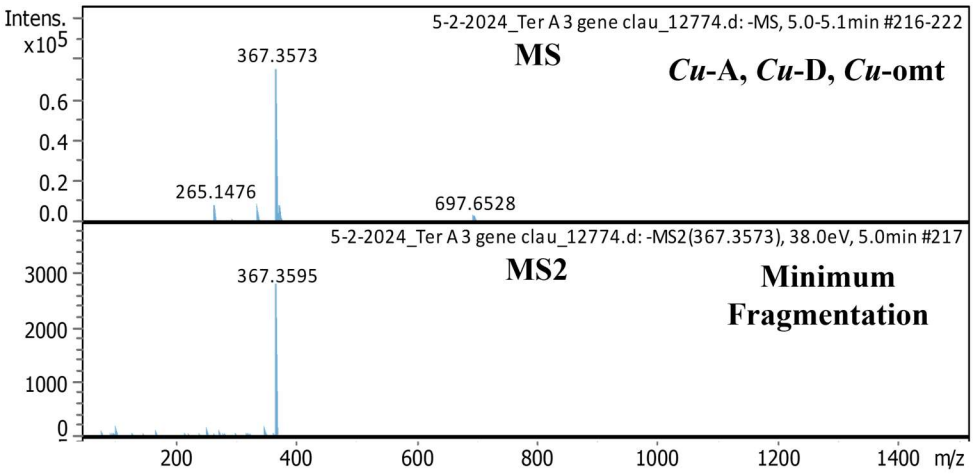

Figure S 30: Mass spectra (MS) with a base peak (on the top) and the fragmentation pattern/ product ion (MS2) spectra (on the bottom) of the peak at retention time (RT) ~5.4 minutes from the crude extracts of *A. oryzae* NSAR1 transformants with *Cu*-A, *Cu*-D, and *Cu*-OMT genes. Spectra was acquired in the negative ion mode.

Chapter 7

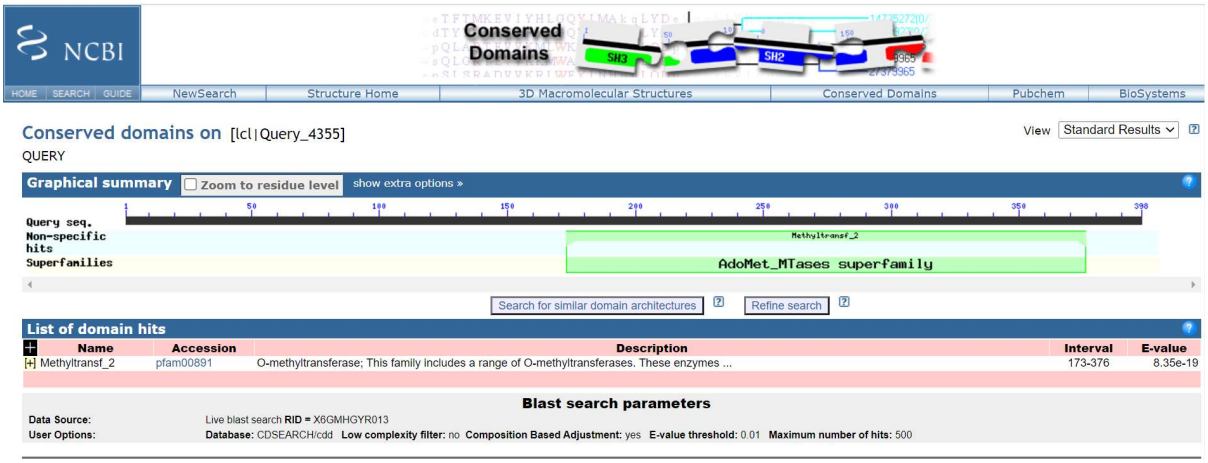

Figure S 31: Identification of domains through Conserved Domain software.

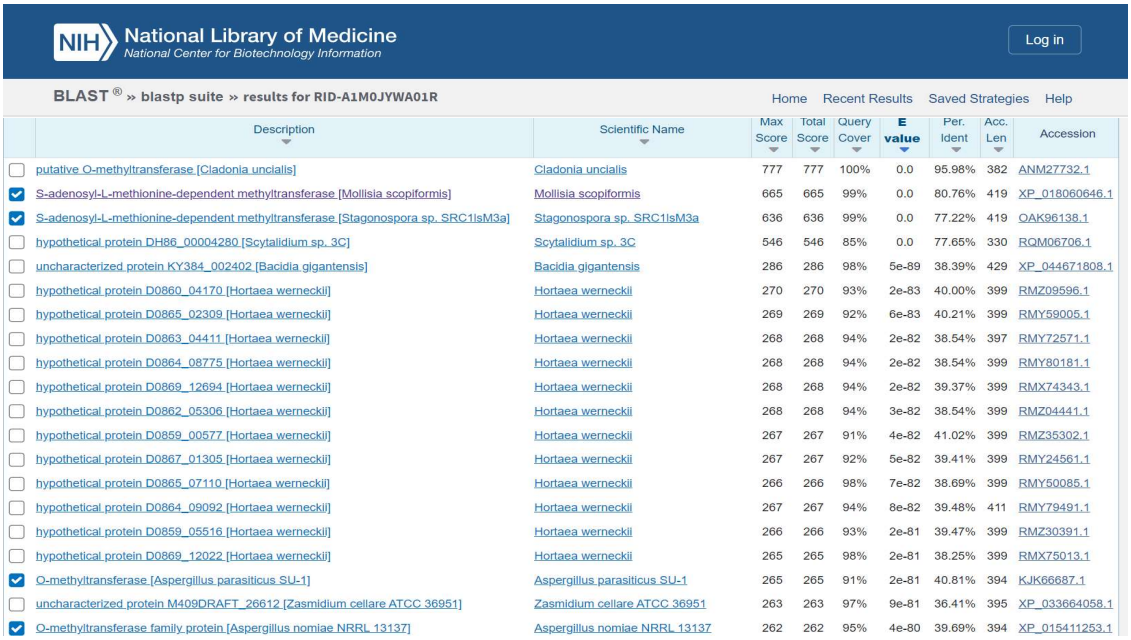

Figure S 32: NCBI blastp results for codon-optimized O-methyltransferase from *C. uncialis*.

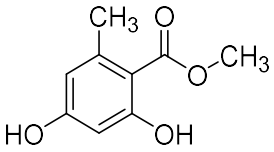

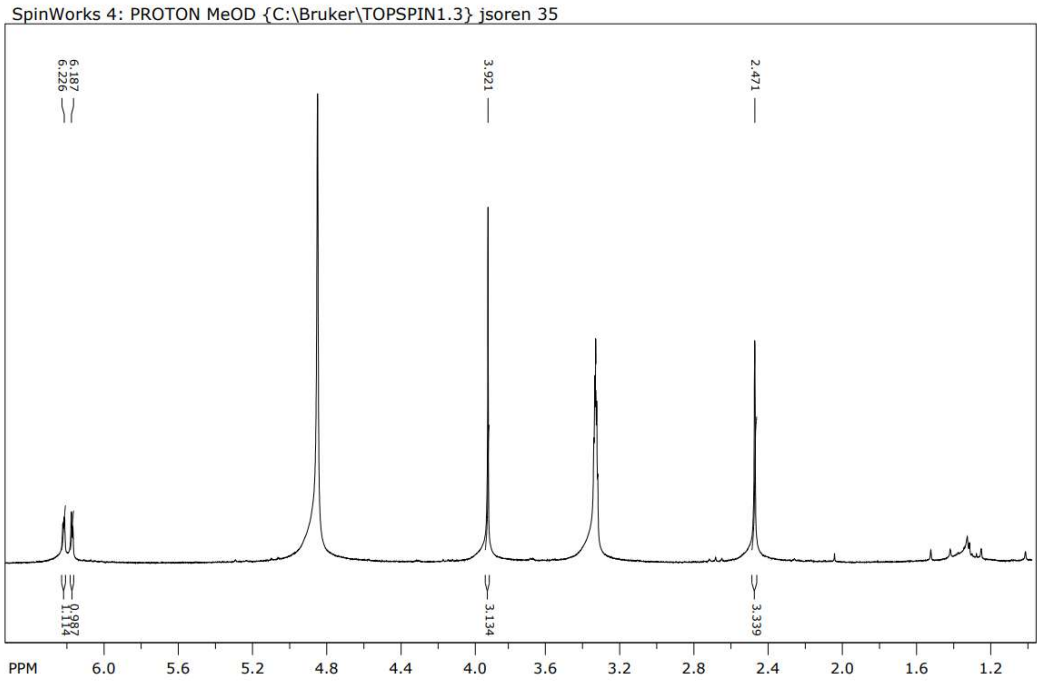

Figure S 33: [1]HNMR spectrum of methyl orsellinate standard dissolved in MeOD at 500 MHz.

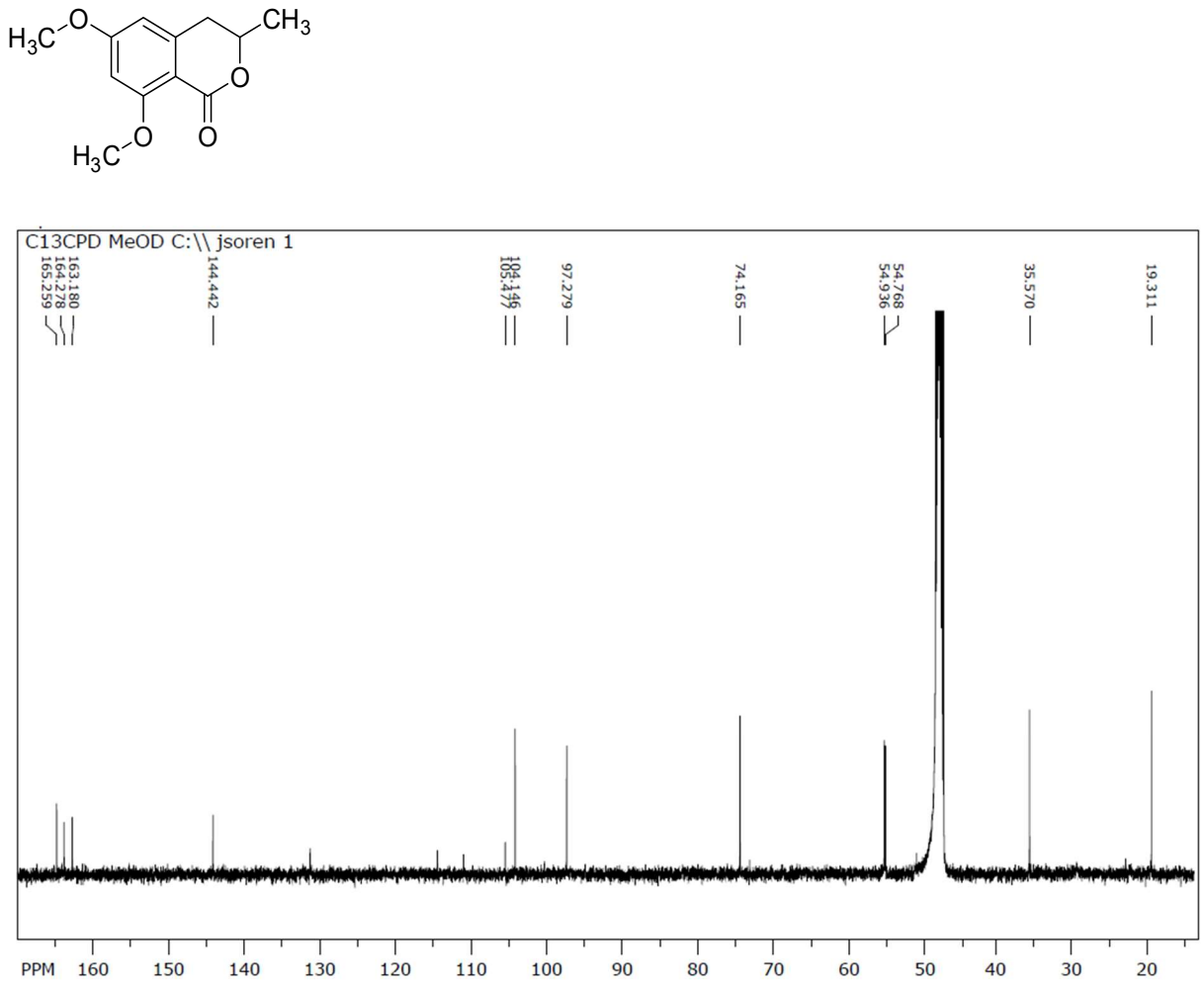

Figure S 34: ^{13}CNMR spectrum of compound **10** dissolved in MeOD at 500 MHz.

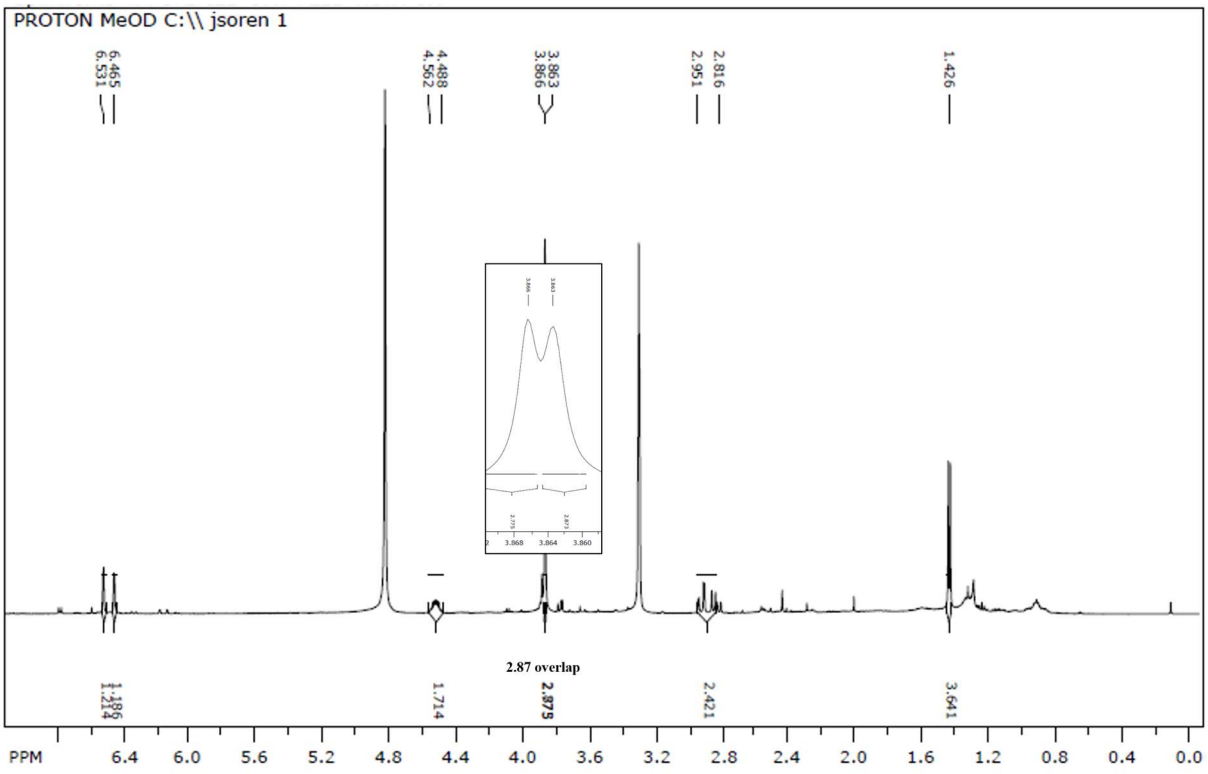

Figure S 35: [1]HNMR spectrum of compound **10** dissolved in MeOD at 500 MHz.

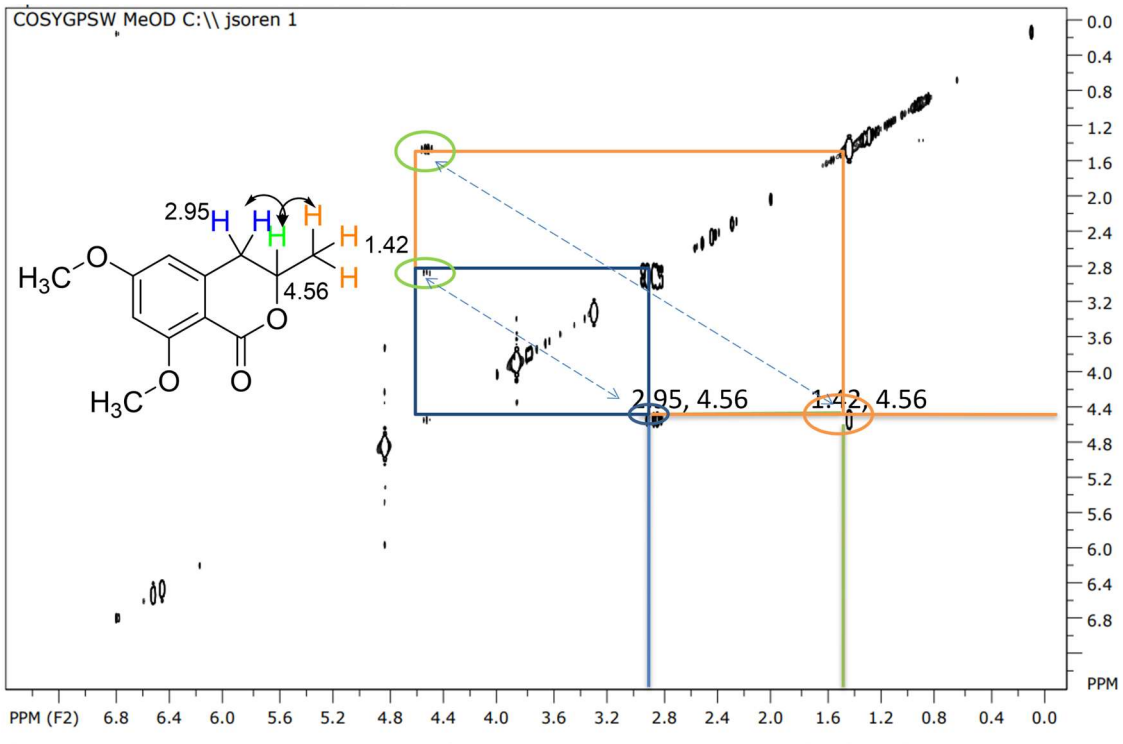

Figure S 36: ^{1}H-^{1}H COSY spectrum of compound **10** dissolved in MeOD at 500 MHz.

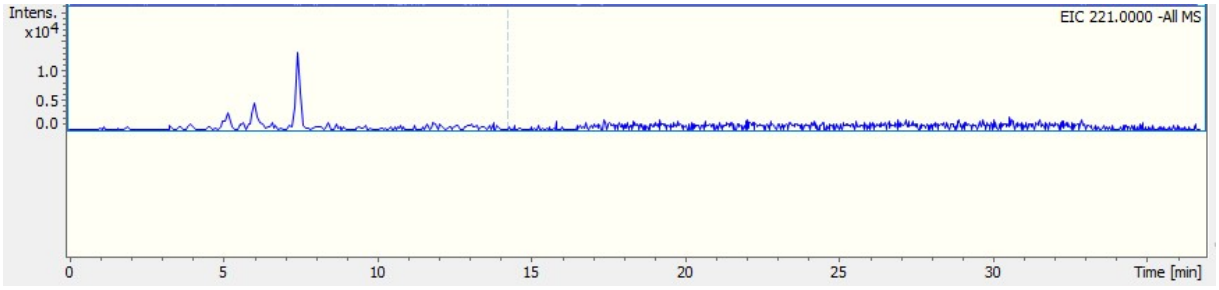

Figure S 37: The extracted ion chromatogram (EIC) at m/z 221 from the liquid chromatography-mass spectrometry (LC-MS) analysis of compound **10**.

The observed m/z of compound **10** is 221. The calculation of the expected mass is as follows:

- Mass of 6-hydroxymellein: 194.18
- Mass of 2 methyl groups: 30
- Removal of 2 protons: -2

This gives an expected mass of 222. Since the analysis is in the $[M-H]^-$ ionization mode, one proton is removed, resulting in an observed m/z of 221, which matches the expected value.

Permission Documents

This Agreement between Harman Gill ("You") and Springer Nature ("Springer Nature") consists of your license details and the terms and conditions provided by Springer Nature and Copyright Clearance Center.

License Number	5806540098165
License date	Jun 12, 2024
Licensed Content Publisher	Springer Nature
Licensed Content Publication	Springer eBook
Licensed Content Title	Lichen Fungal Secondary Metabolites: Progress in the Genomic Era Toward Ecological Roles in the Interaction
Licensed Content Author	Harman Gill, John L. Sorensen, Jérôme Collemare
Licensed Content Date	Jan 1, 2023
Type of Use	Thesis/Dissertation
Requestor type	academic/university or research institute
Format	electronic
Portion	full article/chapter

Pertains to: Gill, H., Sorensen, J.L., Collemare, J. (2023). Lichen Fungal Secondary Metabolites: Progress in the Genomic Era Toward Ecological Roles in the Interaction. The Mycota, vol 5. Springer, Cham. https://doi-org.uml.idm.oclc.org/10.1007/978-3-031-16503-0_7

Dear Authors,

Thank you very much for your email. Please note that Journal Microorganisms is an open access journal and we follow the conditions of the Creative Commons Attribution license (http://creativecommons.org/licenses/by/4.0/), which provides that published material can be re-used without obtaining permission as long as a correct citation to the original publication is given.

We hope this offers some clarity. Please feel free to let me know if you have any other questions.

A short note: the CiteScore of Microorganisms increased to 7.4!
45/140 (Q2) in the category "Microbiology (medical) ";
56/182 (Q2) in the category "Microbiology";
25/80 (Q2) in the category "Virology"
https://www.scopus.com/sourceid/21100933947

Best,
Kind Regards,
/Microorganisms/ Editorial Office

Pertains to: Gill H, Sykes EME, Kumar A, Sorensen JL. Isolation of Bioactive Metabolites from Soil Derived Fungus-*Aspergillus fumigatus*. *Microorganisms*. 2023; 11(3):590. https://doi.org/10.3390/microorganisms11030590